Methods for identification of biochemical network models

Sara Berthoumieux

▶ To cite this version:

Sara Berthoumieux. Methods for identification of biochemical network models. Quantitative Methods [q-bio.QM]. Université Claude Bernard - Lyon I, 2012. English. NNT : . tel-00768731v1

HAL Id: tel-00768731
https://theses.hal.science/tel-00768731v1

Submitted on 23 Dec 2012 (v1), last revised 3 Oct 2014 (v2)

HAL is a multi-disciplinary open access archive for the deposit and dissemination of scientific research documents, whether they are published or not. The documents may come from teaching and research institutions in France or abroad, or from public or private research centers.

L'archive ouverte pluridisciplinaire **HAL**, est destinée au dépôt et à la diffusion de documents scientifiques de niveau recherche, publiés ou non, émanant des établissements d'enseignement et de recherche français ou étrangers, des laboratoires publics ou privés.

Université Claude Bernard Lyon 1

THÈSE

Pour obtenir le grade de

DOCTEUR DE L'UNIVERSITE CLAUDE BERNARD LYON 1

Spécialité : Biologie des systèmes et microbiologie

Arrêté ministériel : 7 août 2006

Présentée par

Sara BERTHOUMIEUX

Thèse dirigée par Hidde DE JONG et Daniel KAHN

préparée au sein de l'équipe-projet IBIS, INRIA Grenoble - Rhône - Alpes
et de l'Ecole Doctorale E2M2

Méthodes pour l'identification des modèles de réseaux biochimiques

Thèse soutenue publiquement le 13/06/2012,
devant le jury composé de :

Dr. Joseph J. HEIJNEN
Professeur, Université Technique de Delft, Rapporteur
Dr. Béatrice LAROCHE
Directrice de recherche, INRA Jouy, Rapporteur
Dr. Johannes GEISELMANN
Professeur, Université Joseph Fourier de Grenoble, Examinateur
Dr. Sandrine CHARLES
Maître de conférence universitaire, Université Claude Bernard Lyon 1, Examinatrice
Dr. Madalena CHAVES
Chargée de recherche, INRIA Sophia-Antipolis, Examinatrice
Dr. Hidde DE JONG
Directeur de recherche, INRIA Grenoble-Rhône-Alpes, Directeur de thèse
Dr. Daniel KAHN
Directeur de recherche, INRA, Université Claude Bernard Lyon 1, Directeur de thèse

ACKNOLEDGEMENTS

First of all, I present my deepest acknowledgements to Hidde DE JONG, my PhD advisor. Without his involvment in my PhD, his availability at any moment of the day (and night) to discuss anything and his constant trust and support, the work presented here would have never been possible.

I would also like to thank Daniel KAHN, my other PhD advisor, for his involvement in my work despite the distance between our two laboratories and for showing understanding during the difficult times of this PhD.

My deepest thanks go to Eugenio CINQUEMANI, with whom I had a great time working and whose arrival in the team had a key impact on my work.

I would like to thank Delphine ROPERS for all the many useful discussions and advices and for being present and understanding when necessary.

I present my acknowledgements to Hans GEISELMANN, Guillaume BAPTIST, Matteo BRILLI, Corinne PINEL, Caroline RANQUET, Jérôme IZARD, Alain VIARI, François RECHENMANN and Françoise DE CONINCK for always being available to answer my numerous questions and for doing it with so much kindness and clarity.

I also thank all the students and trainees of the IBIS team during the 4 years of my PhD as well as the engineers of GENOSTAR for the friendly work atmosphere and the breaks, also numerous.

Last but not least, I thank all my friends that endured my constant complaining during these last 4 years and specially Anna, Aurore and Magali for their determining support during the writing of this manuscript.

RÉSUMÉ en français

Les bactéries ajustent constamment leur composition moléculaire pour répondre à des changements environnementaux. Nous nous intéressons aux systèmes de régulation métabolique et génique permettant une telle adaptation, notamment dans le contexte de la diauxie chez *Escherichia coli* lors de la transition de croissance sur une source de carbone riche, le glucose, à une source plus pauvre, l'acétate. Afin de modéliser de tels réseaux métaboliques, nous utilisons un formalisme cinétique approché appelé linlog et abordons les problèmes rencontrés lors de l'estimation de paramètres. Ainsi, nous proposons une méthode d'estimation de paramètres à partir de jeux de données incomplets basée sur l'algorithme EM ("Expectation Maximization") et l'appliquons au modèle linlog du métabolisme central du carbone. Nous proposons également une méthode d'analyse d'identifiabilité et de réduction de modèles non identifiables que nous appliquons ensuite sur des jeux de données simulés ou obtenus expérimentalement. Par ailleurs, nous mesurons des profils temporels d'expression de gènes impliqués dans le contrôle de la diauxie et mettons en évidence, à l'aide de modèles cinétiques développés dans ces travaux, l'importance de la contribution de l'état physiologique de la cellule dans la régulation génique. En se confrontant aux défis méthodologiques rencontrés lors du développement de modèles de réseaux métabolique et génique, cette thèse contribue aux efforts futurs portant sur l'intégration de ces deux types de réseaux dans des modèles quantitatifs.

TITRE en anglais

METHODS FOR IDENTIFICATION OF BIOCHEMICAL NETWORK MODELS

RÉSUMÉ en anglais

Bacteria manage to constantly adapt their molecular composition to respond to environmental changes. We focus on systems of both metabolic and gene regulation that enable such type of adaptation, notably in the context of diauxic growth of *Escherichia coli*, when it shifts from glucose to acetate as a carbon source. To model a metabolic network, we use an approximate kinetic formalism called linlog and address methodological issues encountered when performing parameter estimation. We propose a maximum-likelihood method based on Expectation Maximization for parameter estimation from incomplete datasets. We then apply it to the linlog model of central carbon metabolism. We also propose a method for identifiability analysis and reduction of nonidentifiable models that we then apply to both simulated and experimental datasets. Moreover, we monitored gene expression patterns for a gene network involved in the control of diauxie and highlight, by means of kinetic models developed in this study, the role of the global physiological state of the cell in regulation of gene expression. By addressing methodological challenges encountered with models of metabolic and gene networks, this thesis contributes to future efforts integrating both types of networks into quantitative models.

DISCIPLINE

Biologie des systèmes et microbiologie

MOTS CLÉS

Estimation de paramètres, identifiabilité, métabolisme, réseau génique, modélisation quantitative, microbiologie, régulation

INTITULÉ ET ADRESSE DU LABORATOIRE

Equipe IBIS, INRIA Grenoble-Rhône-Alpes
655 avenue de l'Europe
38330 Montbonnot-Saint-Martin

RÉSUMÉ SUBSTANTIEL EN FRANÇAIS

Les bactéries maintiennent en permanence une coordination cellulaire complexe qui leur permet de croître et de se diviser, ceci même au sein d'environnements en constante évolution. Une telle adaptation aux aléas exterieurs implique des changements rapides et globaux dans la composition moléculaire des cellules, comme les pools métaboliques ou la machinerie d'expression génique, ainsi que des changements plus spécifiques dans les profils d'expression génique. Nous nous intéressons aux comportements dynamiques de tels systèmes, et plus précisément aux réseaux de régulation métabolique et génique dans le contexte de la diauxie chez *Escherichia coli*, c'est-à-dire lors de la transition de croissance sur une source de carbone riche (glucose) à une source pauvre (acétate). Un grand nombre de données moléculaires sur ce type de réseaux a été accumulé ces dernières années grâce au développement de techniques expérimentales adaptées. La présence de telles données permet l'étude dynamique des réseaux de régulation et pour cela, nous développons des modèles quantitatifs de deux sous-réseaux d'intérêt: le réseau métabolique qui englobe le métabolisme central du carbone, présenté Fig. 1, et un réseau génique impliqué dans le contrôle de la diauxie, présenté Fig. 2.

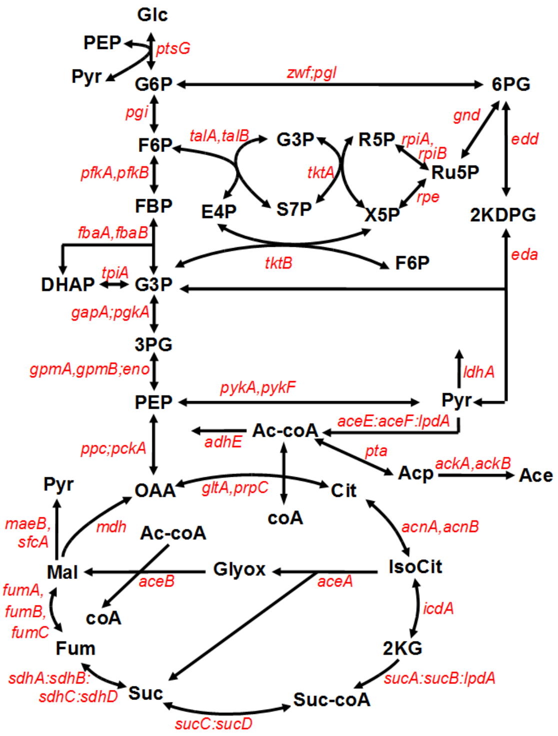

Figure 1: Réseau du métabolisme central du carbone chez *E. coli*

Pour le modèle du réseau métabolique, nous utilisons un formalisme cinétique approché et nous focalisons sur certaines complications rencontrées en pratique lors de l'estimation de paramètres de ces modèles, appelés linlogs. Premièrement, à cause de limitations expérimentales ou de défaillances instrumentales, les jeux de données disponibles contiennent une quantité importante de valeurs manquantes. Face à de telles données, les méthodes d'estimation linéaires standards sont peu efficaces. Nous proposons une méthode de maximisation de la vraisemblance basée sur l'algorithme EM ("Expectation Maximization") pour l'estimation de paramètres à partir de jeux de données incomplets. Nous montrons à l'aide d'expériences simulées que notre approche donne de meilleurs résultats que la régression linéaire et que l'imputation multiple, une méthode standard en cas de données manquantes. Nous l'appliquons ensuite à un modèle linlog du métabolisme central chez *E. coli*, ce qui nous permet d'obtenir des estimations raisonnables pour la plupart des paramètres identifiables du modèle, même lorsque la régression ne peut donner de résultats.

Deuxièmement, selon le jeu de données disponible pour l'estimation de paramètres, un modèle peut s'avérer non identifiable, c'est-à-dire que les valeurs de paramètres ne peuvent être reconstituées de manière unique à partir des données. Nous traitons cette problématique en discutant de manière théorique l'identifiabilité de modèles cinétiques approchés du métabolisme. Nous proposons des définitions rigoureuses de l'identifiabilité structurelle et l'identifiabilité pratique de ces modèles, ainsi qu'un cadre théorique reliant ces deux notions. Par ailleurs, nous décrivons une méthode de réduction de modèles, lorsque ceux-ci sont détectés comme non identifiables, basée sur la décomposition en valeurs singulières. Nous discutons l'adaptation de cette méthode dans les cas où les effets du bruit, du biais d'échantillonnage et des données manquantes sont explicitement pris en compte et l'appliquons ensuite à des jeux de données simulés ou obtenus expérimentalement.

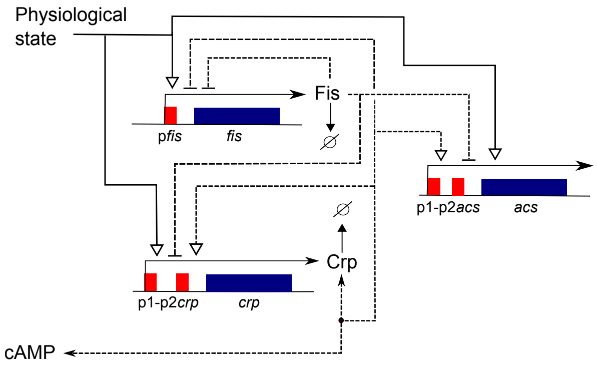

Figure 2: Réseau de régulation de l'expression d'*acs* chez *E. coli*.

En ce qui concerne le réseau génique, nous examinons les contributions respectives des facteurs de transcriptions et de l'état physiologique global de la bactérie à la régulation de l'expression génique. Nous nous focalisons sur deux facteurs de transcription pléiotropiques, Fis et Crp, ainsi que sur le gène *acs* qui code pour l'enzyme clé de l'assimilation d'acétate. Nous enregistrons *in vivo*, sous différentes conditions physiologiques et pour différents contextes génétiques, les profils temporels d'expression de ces gènes à l'aide de plasmides rapporteurs . Nous déduisons des données ainsi obtenues que les changements dans l'expression de *fis* et *crp* au cours de la transition de croissance sont principalement expliqués par des changements de l'état physiologique global de la bactérie alors que l'induction d'*acs* est principalement contrôlée par Crp et le métabolite cAMP. Nous approfondissons l'étude de la distribution des rôles dans la régulation génique avec un modèle d'équations différentielles ordinaires (EDO). La régulation par les facteurs de transcription est modélisée par des cinétiques de Hill alors que l'activité de l'état physiologique global de la bactérie est représentée par une fonction phénoménologique. Les paramètres sont estimés à l'aide d'un sous-ensemble des données enregistrées et le modèle est validé sur le reste du jeu de données.

En se confrontant aux défis méthodologiques rencontrés lors du développement de modèles de réseaux métaboliques et géniques, cette thèse contribue aux efforts futurs portant sur l'intégration de ces deux types de réseaux au sein de modèles quantitatifs.

Contents

Chapter 1

Introduction

1.1 Context

Microbes, organisms not visible with the human eye, are very ancient and the first living cells on Earth. They are essential for human life, *e.g.,* as part of the microbial flora or as the main source of nitrogen for plants. Microbes grow everywhere even in extreme environments with extreme temperatures, pH, hydrostatic or osmotic pressures, where humans would not be able to survive. In one sentence, “Where there is life, there are microbes” [Schaechter et al., 2006].

An important property of microbes is that they can grow when subject to continuous environmental changes in nutrient availability, temperature, pH or pressure, alteration of the physical properties of the niche, or exposition to various radiation or toxic factors. As an example of the sudden changes microbes have to cope with, imagine a gut bacterium expelled from animal intestine [Schaechter et al., 2006]. Despite all these stresses and changes, microbial organisms manage to maintain the complex coordination of the cell enabling cell growth and division. How does a living organism first sense and then adapt to such environmental alterations ? Which dynamical changes appear in the internal behavior of the cell during this adaptation to the environment ?

We will explore these questions by means of the example of the enterobacterium *Escherichia coli* during its adaptation to the exhaustion of one nutrient and the consequent transition to the uptake and assimilation of another nutrient. The switch of one growth substrate to another by a bacterial population is called a diauxie. Consider the example of a glucose/acetate diauxie shown Fig. 1.1. In a glucose-rich environment, the bacterial population grows exponentially, and the cells produce and excrete acetate into the growth medium. When the glucose level drops, the excreted acetate can be utilized as a carbon source, leading to a much lower growth rate [Wolfe, 2005]. Growth in the presence of acetate is interesting for biotechnology as a high concentration of acetate in the medium has a negative effect on bacterial growth [Luli and Strohl, 1990].

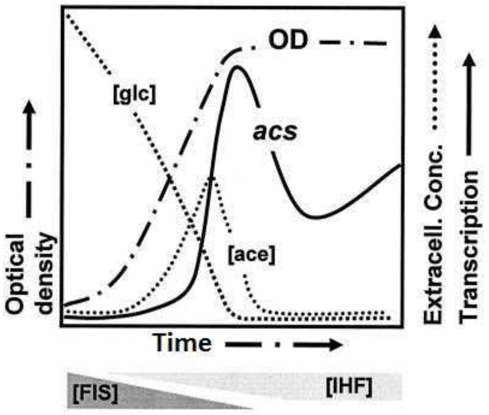

Figure 1.1: Transcription (or, equivalently, promoter activity) of *acs* (solid line) during growth on glucose and glucose/acetate diauxie taken from [Wolfe, 2005]. Bacteria grow in a minimal medium supplemented with glucose. The population growth is represented by the optical density (OD) curve (semi-dotted line). The extracellular concentrations of glucose (glc) and acetate (ace) are shown in dotted lines. The relative change of the intracellular concentrations of proteins Fis and IHF over the bacterial growth phase is represented below the figure.

As a consequence of the diauxie, morphological changes are observed concerning among other things the cell membrane and cell volume. Moreover, the molecular composition of the cell changes: DNA concentration, ribosome concentration, RNA polymerase concentration, enzyme and transcription factor concentrations, metabolic fluxes and metabolic pools [Bremer and Dennis, 1996]. Below, we briefly discuss the extent of these changes.

The contents of the cellular machinery, including DNA, RNA and protein, depends on the growth rate of the bacterial population [Schaechter et al., 2006, §4] [Bremer and Dennis, 1996]. Indeed, these macromolecular quantities decrease in the cell when the growth rate decreases during diauxie [Neidhardt and Fraenkel, 1961]. Moreover, not only the quantities in the cell vary with the growth rate but also the relative proportions compared to cell mass: the ratio of the amounts of DNA and protein per cell mass increases, while the ratio of RNA per cell mass decreases.

The central carbon metabolism of *E. coli* degrades, via a network of metabolic reactions, the external carbon source to several intermediate metabolites to produce the energy (ATP) and to synthesize the precursors of macromolecules (amino acids) necessary for the development and growth of the cell. Fig. 1.2 shows the network of central carbon metabolism of *E. coli*. When growing on glucose, the substrate is imported into the cell by the phosphotransferase system (PTS) and converted it to glucose-6-phosphate (G6P) [Görke and Stülke, 2008, Saier Jr et al., 1996]. G6P is then metabolized through glycolysis to phosphoenolpyruvate (PEP). Mostly, PEP is used to produce energy and precursors. At high carbon fluxes, acetate is produced and excreted from the cell. Once glucose is exhausted and no other carbon source is present in the medium, acetate is imported back into the cell and converted to

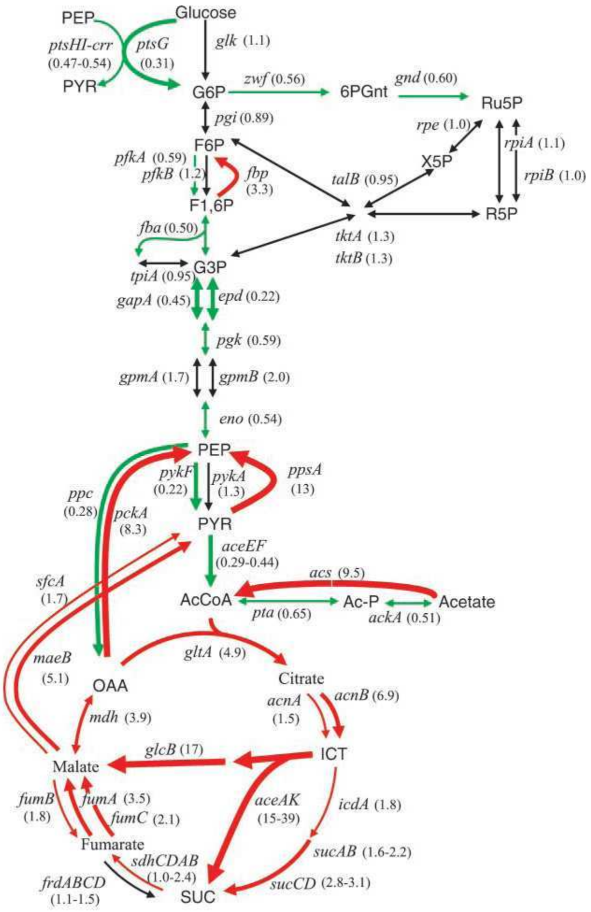

Figure 1.2: Expression levels of genes encoding enzymes of central carbon metabolism in *E. coli* for growth on acetate as compared to growth on glucose [Oh et al., 2002]. The numbers represent the fold-changes of expression levels. The red arrows represent the induced genes, while the green arrows represent the repressed genes during growth on acetate as compared to growth on glucose (¿ 95% confidence). The thicker the arrows, the higher the genes were regulated.

acetyl-CoA. Acetyl-CoA is then converted to malate through the glyoxylate shunt (reactions catalyzed by AceA, AceK and GlcB in Fig. 1.2) and metabolized via the tricarboxylic acid cycle (TCA) [Oh et al., 2002]. Then carbon flux is delivered from TCA to the gluconeogenic pathway by metabolizing PEP through reactions catalyzed by *ppsA* and *pckA* [Oh et al., 2002, Saier Jr et al., 1996]. This flux inversion during the glucose/acetate diauxie illustrates that the flux distribution in carbon metabolism significantly differs with the carbon source used [Zhao et al., 2004].

The expression of genes involved in carbon, nitrogen and oxygen availability also changes during a glucose/acetate diauxie [Zhao et al., 2004]. One of the most striking examples is *acs*, the gene coding for the enzyme catalyzing the degradation of acetate to acetyl-CoA. Fig. 1.1

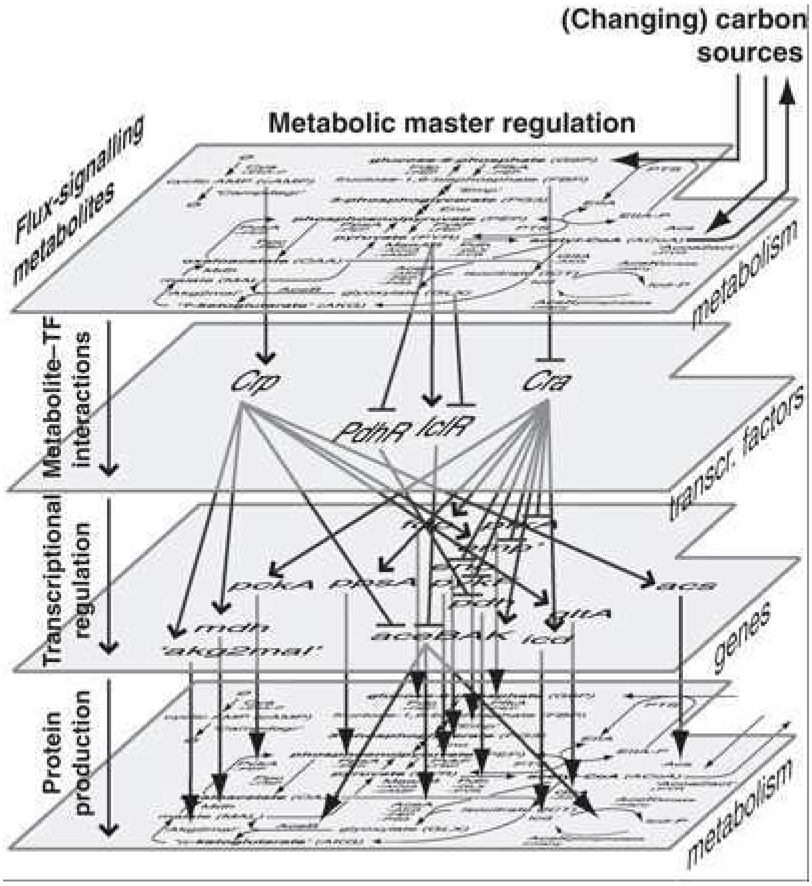
(Changing) carbon sources
Metabolic master regulation
Flux-signalling metabolites
metabolism
Metabolite–TF interactions
Crp
Cra
PdhR
IclR
transcr. factors
Transcriptional regulation
pckA
ppsA
mdh
'akg2mal'
aceBAK
icd
gltA
acs
genes
Protein production
metabolism

Figure 1.3: Different levels of regulation involved in the molecular adaptation of *E. coli* during the glucose/acetate diauxie [Kotte et al., 2010]. The scheme is centered around the gene-metabolite interactions and establishes a feedback loop from the metabolic layer through the transcriptional regulation layer and the gene expression layer back to the metabolic layer.

shows the gene expression pattern of *acs* during subsequent growth on glucose and acetate. As we can see, there is a significant increase in *acs* expression when glucose is exhausted. In addition, the relative amounts of the proteins Fis and IHF differ with the carbon source used for cell metabolism.

How are the gene expression changes coordinated and controlled to allow a coherent functioning of the bacterial cell ? Fig. 1.3 shows a scheme of the different regulation levels of the cell involved in the glucose/acetate diauxie [Kotte et al., 2010]. Let us explore the internal regulatory behavior of the bacterium following this scheme.

Responding to environmental changes necessitates a sensory mechanism to monitor the state of the environment. In the case of growth on glucose, the flux through the PTS system is sensed by the cell. The import and degradation of glucose leads to catabolite repression, *i.e.,* the prevention of the import of other carbon sources [Kremling et al., 2009, Bettenbrock et al., 2006, Görke and Stülke, 2008]. Catabolite repression operates when glucose is in the medium and inactivates adenylate cyclase, thus preventing the formation of the small metabolite cyclic AMP (cAMP). When glucose is exhausted, catabolite repression is lifted, leading to activation of adenylate cyclase which causes accumulation of cAMP, derepression of other import pathways and consumption of acetate.

In microbes, an important control process of the metabolic flux distribution, though not the only one, is the regulation of the concentrations of enzymes catalyzing metabolic reactions [Schaechter et al., 2006, §12]. Indeed, Fig. 1.2, taken from Oh et al. [2002], shows the difference in gene expression for enzymes catalyzing reactions of central carbon metabolism in *E. coli* in conditions of growth on glucose and growth on acetate. As an example, consider the reversible metabolic reaction converting PEP to oxaloacetate (OAA). Each direction is catalyzed by a different enzyme. During growth on glucose, Ppc is more expressed than growth on acetate, which favors the conversion of PEP to OAA. On the contrary, when acetate is the carbon source, PckA is more highly expressed than growth on glucose and leads to flux inversion, thus favoring the conversion of OAA to PEP.

Metabolic fluxes are indirectly regulated via the control of the expression of enzymes. Gene expression is mainly controlled by regulatory proteins, called transcription factors, that bind to the promoter region of a gene and activate or repress transcription. We can distinguish between transcription factors that are specific to a given promoter, and thus only impact the transcription of genes inside one operon, and transcription factors that have a more global regulatory role in that they can bind to a larger number of promoters and thus impact the transcription of an entire group of genes. Regulatory proteins falling in this latter category, called global regulators, are key components of the cell regulation process, notably when adaptation to environmental changes imposes a major re-organization of the protein composition of the cell. For example, the catabolite repression system is driven by the complex Crp.cAMP which regulates many genes related to substrate utilization by the cell [Schaechter et al., 2006, §12]. Fig. 1.4 shows the global transcriptional regulatory network of *E. coli*. Seven proteins (ArcA, FNR, Fis, Crp, IHF, Lrp and Hns) have been detected as global regulators, as they directly regulate expression of more than half of the genes in *E. coli* [Martinez-Antonio and Collado-Vides, 2003]. Some of them are of major importance during the glucose/acetate diauxie. For instance, Crp, when bound to the small metabolite cAMP, regulates catabolite repression. Moreover, Fis, IHF and Hns bind to DNA and regulate gene transcription by altering DNA topology according to the energy levels in the cell [Martinez-Antonio and Collado-Vides, 2003].

Global regulators involved in environmental adaptation need to get information about external changes from molecules involved in signaling pathways. Indeed, half of the known transcription factors have known binding sites for small metabolites, so they can achieve activation or repression according to metabolic changes [Martinez-Antonio and Collado-Vides, 2003]. Four transcription factors have been identified as playing a key role in the glucose/acetate diauxie and being active regulators when bound to intermediates of cen-

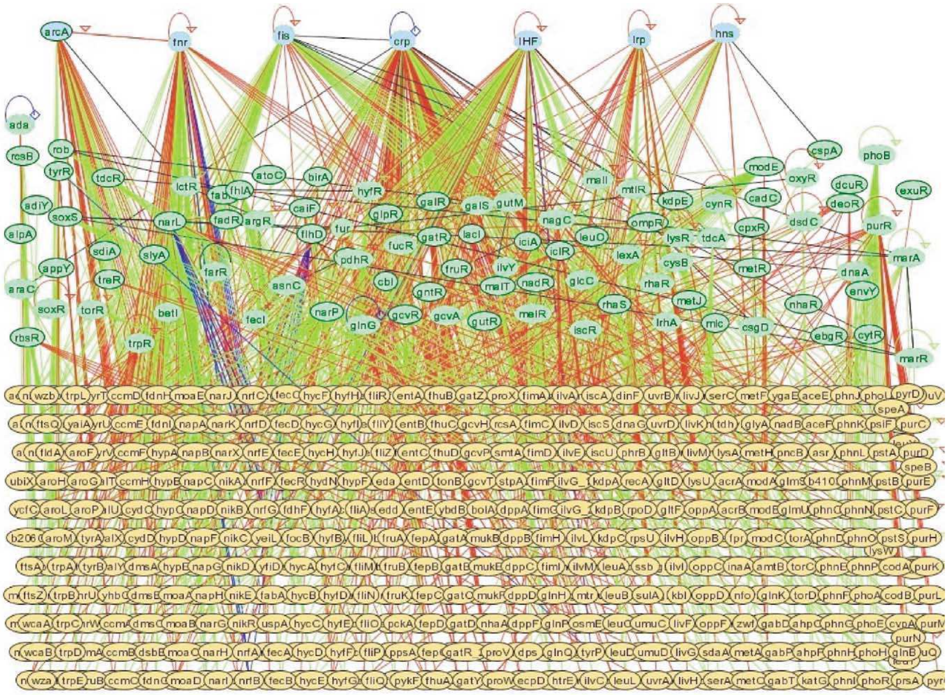

Figure 1.4: Overview of the transcriptional regulatory network in *E. coli* [Martinez-Antonio and Collado-Vides, 2003]. Regulated genes are shown as yellow ovals, transcription factors are shown as green ovals and global regulators are shown as blue ovals. The green lines indicate activation, red lines indicate repression, and dark blue lines indicate dual regulation (activation and repression).

tral metabolism (Crp.cAMP, Cra.FBP, IclR-GLX, IclR-PYR and PdhR-PYR) [Kotte et al., 2010]. Cra, when forming a complex with fructose-biphosphate (FBP), also regulates catabolite repression. IclR, when bound to glyoxylate or pyruvate, regulates the enzymes catalyzing glyoxylate shunt [Lorca et al., 2007] and PdhR regulates *aceEF* [Quail and Guest, 1995].

In summary, the metabolic flux distribution is controlled by the activities of metabolic enzymes and the environment. Those activities depend on enzyme concentrations, while the expression levels of enzyme-coding genes is regulated by transcription factors, so indirectly, metabolism is regulated by transcriptional regulation. Moreover, some transcription factors are only active when forming a complex with a metabolite (Cra, Crp, IclR, PdhR [Kotte et al., 2010]). Thus gene regulation is controlled by metabolism. Metabolic and gene regulations are connected to form a complex and heterogeneous regulatory network (Fig. 1.3).

Finally, the adaptation of the cell to external changes also involves regulation by the gene expression machinery, which includes all molecules necessary for gene expression, notably as transcription and translation (ribosomes, amino acids, RNA polymerase). Changes in the growth rate impact the synthesis rate of all cellular proteins (translation and transcription mechanisms) via the resulting change in concentration and activity of ribosomes and RNA polymerase [Bremer and Dennis, 1996, Tadmor and Tlusty, 2008]. Thus the cell has one more level of regulation: global regulation of gene expression by the growth rate [Scott et al., 2010]. This impacts the overall functioning of the cell, including gene regulation (proteins binding to gene promoters) and metabolic regulation (enzyme activities and concentrations).

In summary, *E. coli* reacts to environmental changes with a coordinated response between different levels of molecular processes and it is necessary to consider a global system involving all these regulation levels.

Recent developments of high-throughput techniques for obtaining experimental data of internal molecules of *E. coli* have led to massive accumulation of information on such mechanisms [Oh et al., 2002, Kao et al., 2004, Ishii et al., 2007]. Since the integrated system we are interested in involves complex feedback loops between its molecular elements, it is very difficult to have an intuitive understanding of its dynamical behavior. Mathematical models are useful tools to deduce dynamical information from mechanistic biological knowledge and the available experimental data. Indeed, the modeler translates his knowledge of regulatory mechanisms into an unambiguous system structure, chooses mathematical formalisms to describe the molecular kinetics involved and uses simulation methods and computer tools to make predictions of the dynamical behavior of the system.

In the past decades, mathematical formalisms for modeling the kinetics of metabolic reactions [Heijnen, 2005, Chen et al., 2010, Heinrich and Schuster, 1996] and gene regulatory networks [de Jong, 2002] have been developed. Models focusing on the dynamical behavior of metabolic or gene regulatory networks intervening in diauxic behavior in *E. coli* have been developed ([Ropers et al., 2006, Bettenbrock et al., 2006], see [Kremling et al., 2009] for a review, [Hardiman et al., 2009, Chassagnole et al., 2002]). However, models of networks integrating both regulation levels have been little studied so far [Kotte et al., 2010, Baldazzi et al., 2010, Tenazinha and Vinga, 2011]. One of the reason is that integrated networks are large and heterogeneous, so they imply the development of complex models with many parameters, which raises a number of methodological challenges. Another reason is that the amount of data necessary for model development is huge.

In order to understand the dynamics of such complicated networks, quantitative modeling and data are necessary. Indeed, quantitative measurements of the outputs of the model under various conditions are required for the calibration of the model on the wild-type dataset and the validation of the model predictions in the other conditions by means of other datasets.

In all the steps for system modeling enumerated above, the current bottleneck is the calibration of the model [Ashyraliyev et al., 2009]. In quantitative modeling, it boils down to the estimation of the kinetic parameters of the system. These parameters need to be estimated as the majority of them can not be measured experimentally. Moreover, some of them may not have a physical interpretation, in case of phenomenological models. "The parameter estimation problem can be formulated from the mathematical viewpoint as a constrained optimization problem where the goal is to minimize the objective function, defined as the error between model predictions and real data." [Marucci et al., 2011] Parameter estimation is a difficult task as models contain a large number of variables, whose dynamics evolve on different time-scales and are described by complex, nonlinear rate equations. Thus, these models also contain a large number of parameters and their nonlinearity implies complex objective functions for parameter estimation. Moreover, identification requires a large quantity of experimental data of good quality. These data, in practice, are noisy, partial and they are obtained with heterogeneous techniques and experimental conditions.

1.2 Problem statement

How can we build a quantitative model of complex biological systems, and particularly networks involving regulation on multiple levels? As we investigate dynamical molecular processes of integrated networks, mathematical models may grow very quickly in terms of number of parameters and variables involved and the complexity of the nonlinear rate equations. Such models usually generate analytical and numerical problems. Moreover, the fact that the model has many parameters, given an available dataset whose size and accuracy are limited by experimental considerations in many cases, renders the model nonidentifiable. This means that it is not possible to distinguish between different sets of parameters, as they all lead to the same dynamical behavior of the model. Model identifiability has been well-studied in control theory and applied mathematics [Walter and Pronzato, 1997] and nonidentifiability is a problem commonly encountered in the field of systems biology [Ashyraliyev et al., 2009, Gutenkunst et al., 2007]. In the case where, given the available information on a biological system, it is not possible to distinguish between different kinetic models having the same outputs, the model with the simplest formalism and the lowest number of variables should be considered. A standard strategy to tackle this difficulty when working with complex systems of all kinds (may they be electronic, physical or social) is to reduce the model. There are several methods available for reducing the complexity and the size of a model, depending on the systemic properties of interest and of the initial model complexity. Below, we highlight some of the most commonly-used methods.

First of all, when modeling large systems of heterogeneous elements, time-scale discrepancies between the dynamics of the variables frequently occur. Depending on the time-scale of interest, the kinetic rates can be simplified [Okino and Mavrovouniotis, 1998]. At the time-scale of the fast processes, slow processes can be neglected or the concentrations of the substances involved can be treated as parameters. At the time-scale of the slow processes, using the quasi steady-state approximation (QSSA), fast processes can be assumed to instantaneously adapt to slow processes and give rise to a reduced model with algebraic equations [Heinrich and Schuster, 1996]. For example, in the context of regulatory networks developed in Sec. 1.1, metabolites have a time-response in the order of seconds [Ishii et al., 2007] while for proteins, the response is in the order of hours [de Jong et al., 2010]. In the above cases, the dynamics of different time-scales can be decoupled based on time-scale separation and subsystems of interest can be defined.

Secondly, a detailed mechanistic description of molecular processes leads to highly nonlinear models. Simpler mathematical formalisms can in many cases be developed. Indeed, lumping model parameters, variables or processes is a classical reduction method [Okino and Mavrovouniotis, 1998]: some parameters and variables may not bring anything to the model as no information about them is contained in available data. Moreover, regular approximated mathematical formulations, obtained for example from Taylor series approximation, allow optimization problems, such as model identification, to be solved with less difficulty and may provide a systematic way of automatically building models [Heijnen, 2005, Alves et al., 2008]. For example, in the context of Sec. 1.1, one might ask if a model investigating multi-level regulation needs to consider translational and transcriptional dynamics of gene regulation separately. And within the range of metabolite concentrations allowed by the physiology of a bacterial cell, the dynamics of metabolic reactions may be obtained with simpler formalisms than Michaelis-Menten.

Finally, with interest growing in the dynamical analysis of large biological networks, methods for decomposing a large system into functional subsystems have been developed, such as decomposition based on elementary flux modes [Klamt and Stelling, 2003, Schuster et al., 1993] or modularization based on absence of retroactivity [Saez-Rodriguez et al., 2005, Del Vecchio et al., 2008]. Getting inspiration from such formal methods of system decomposition, one can define subsystems by measuring some internal variables and considering them as entries of smaller systems. Thus, models for such subsystems are not required to predict the dynamics of the measured variables and subsystems can be detached from the global network and analyzed separately without losing information or introducing bias.

Back to our original problematic, the aim of my thesis is to develop a quantitative model investigating the dynamics of interconnection of metabolic, gene and cellular machinery regulations during the glucose/acetate diauxie of *E. coli.* As the dynamics of the large and embedded system of interest cannot be analyzed simultaneously, we will decompose the system and its dynamics inspired by the reduction methods described above. For each of the subsystems obtained in this way, a model will be developed using approximate kinetic equations and calibrated using parameter estimation approaches and appropriate experimental datasets. Most of the work consists of computational and mathematical issues, but there is also some effort spent on obtaining experimental data for parameter estimation.

1.3 Questions and approaches

We are interested in the dynamical behavior of the system integrating regulation by metabolites, transcription factors and the gene expression machinery during the glucose/acetate diauxie in *E. coli.* The network involved is extremely large and complex. Thus, to efficiently address the question, we need to decompose the original system and isolate subsystems of interest based on biological considerations taking inspiration from the reduction methods described in Sec. 1.2.

As mentioned in the previous section, several orders of magnitude separate the time-scales of metabolic and gene expression processes. So we can separate the variables of the global system into slow variables (mRNA and protein concentrations) and fast variables (metabolite concentrations) [Baldazzi et al., 2010]. Then, depending on the time scale of interest, dynamical processes can be simplified. In this chapter, we carry out these simplifications for the development of reduced models of the two following subsystems: the central carbon metabolism and a gene regulatory network involved in the glucose/acetate diauxie of *E. coli.*

1.3.1 Development of a simplified kinetic model for central carbon metabolism of *E. coli*

The network of central carbon metabolism, introduced in the previous sections, can be decomposed into 5 subnetworks: glycolysis/gluconeogenesis, pentose-phosphate pathway, Krebs cycle, EDD pathway and glyoxylate shunt, as shown Fig. 1.5.

As mentioned previously during a glucose/acetate diauxie, metabolic fluxes in central carbon metabolism are reorganized [Zhao et al., 2004]. But before even adapting to a new

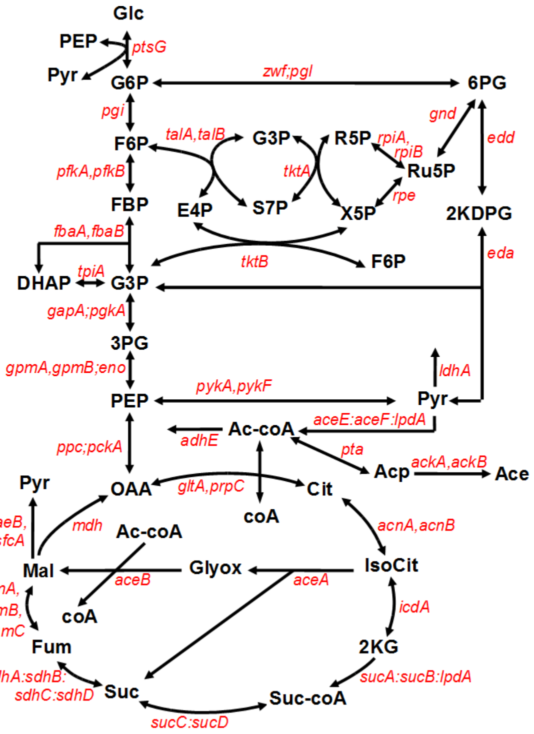

Figure 1.5: Schematic representation of central carbon metabolism of *E. coli*

carbon source, how do the kinetics of central carbon metabolism of *E. coli* function under growth on glucose and respond to changes in enzyme concentrations?

The model of central carbon metabolism of *E. coli* explores the network shown in Fig. 1.5 and takes intracellular metabolite concentrations as dynamical variables. Concentrations of extracellular metabolites, in this case glucose and acetate, are considered as model inputs. Due to time-scale separation, concentrations of the catabolic enzymes are considered constant and treated as inputs of the model.

The development of a quantitative model of central carbon metabolism is a challenge and raises methodological issues, especially for parameter estimation. Indeed, the standard Michaelis-Menten formalism used to model unimolecular enzymatic reaction kinetics and variations for multimolecular processes [Heinrich and Schuster, 1996], are strongly non linear and contain a lot of parameters, which makes the analysis of the model very difficult. Moreover, we might encounter identifiability issues arising from the large number of parameters. Simplified kinetic modeling frameworks have been proposed for metabolic kinetics including linlog [Visser and Heijnen, 2003], loglin [Hatzimanikatis and Bailey, 1997] and power-law kinetics [Savageau, 1976]. Particularly, linlog formalism have shown to produce the same dynamical behaviour as Michaelis-Menten under some range of metabolic concentrations consistent with the conditions inside the bacterium [Heijnen, 2005]. Consequently, we develop a model of the catabolic network of *E. coli* using linlog kinetics.

As mentioned before, the most sensitive step of modeling is parameter estimation. Experimental data for inputs and outputs of the model are needed. Large-scale and high-throughput techniques for measuring metabolite concentration [Vemuri and Aristidou, 2005] and gene expression data [Dharmadi and Gonzalez, 2004], respectively, have been developed and large-scale datasets comprising simultaneous measurements of metabolism (fluxes, metabolite concentrations) and gene expression (protein and mRNA concentrations) have become available. Notwithstanding these experimental advances, parameter estimation remains a particularly challenging problem, among other things due to noisy and partial observations and heterogeneous experimental methods and conditions. We focus on two principal complications encountered in practice when performing model calibration.

First of all, the large-scale datasets contain a substantial amount of missing values, due to experimental limitations or instrument failures. Standard linear estimation methods perform poorly in that case. We develop an estimation method adapted to incomplete datasets. We then apply this method for calibrating the model of central carbon metabolism of *E. coli* using the largest dataset available in the literature [Ishii et al., 2007].

Secondly, given an experimental dataset, a model may be nonidentifiable, *i.e.*, the parameter values cannot be uniquely reconstructed from the data. We address this issue by defining a theoretical background for both structural and practical identifiability and by describing a model reduction method to resolve identifiability issues. We then discuss the practical application of this reduction method depending on the properties of the experimental dataset available for parameter estimation.

1.3.2 Interplay between specific regulators and global cell physiology in the dynamic adaptation of gene expression in bacteria

Gene expression is regulated by transcription factors via gene regulatory networks that have been widely studied. However during growth transitions, such as the glucose/acetate diauxie, major changes in the physiological state of the cell occur, which also affect gene expression, as described in Sec. 1.1. Which part of the dynamics of gene expression is due to gene regulation and which part to changes in the macromolecular composition of the cell? We tackle this problem by producing time-series data of the expression of transcription factors during the exhaustion of glucose and by developing a quantitative model describing the dynamics of the network of transcription factors.

In order to study the impact of gene regulation and the global physiological state on gene expression during the glucose/acetate diauxie in *E. coli*, we focus on the network shown in

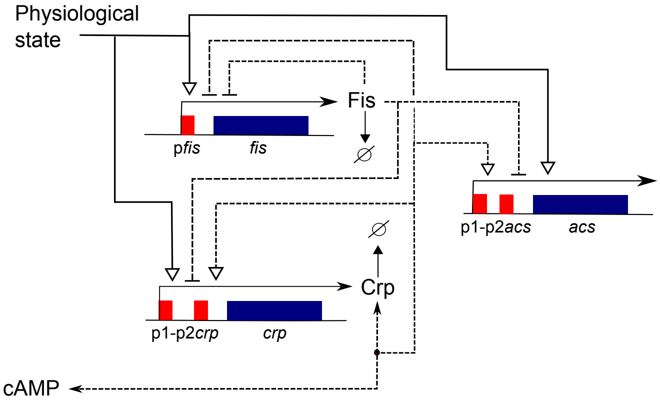

Figure 1.6: Reciprocal regulation of global regulators Crp and Fis and regulation of *acs*.

Fig. 1.6. The network includes two global regulators, Crp and Fis, which regulate each other [Martinez-Antonio and Collado-Vides, 2003]. The network of interest also embraces the most characteristic expression pattern of diauxic change, *acs*, the gene coding for the enzyme catalyzing the degradation of acetate into acetyl-CoA, which is regulated by Crp, when forming a complex with the small metabolite cAMP, and Fis [Wolfe, 2005].

We monitored in real time and *in vivo*, by means of GFP reporters, the expression of the genes in the network in response to glucose depletion. In parallel, we also measured the time-varying concentration of extracellular cAMP and computed from these data intracellular cAMP dynamic behaviors. GFP reporter driven by a non-regulated, constitutive phage promoter was used to assay the time-varying physiological state. The above experiments were repeated when the network was submitted to various physiological and genetic perturbations, such as shifting the cell to a low-glucose medium or deleting the genes *fis* and *crp*.

We first use a simple, parameterless mathematical model that can be used to analyze the roles of global physiological control and transcription regulation in the variation of the promoter activity of the genes of the network in Fig. 1.6. Additionally, we investigate the roles of the different regulatory mechanisms by developing and analyzing a quantitative ODE model of the network. The model takes the protein concentrations of Crp and Fis as dynamical variables and returns the promoter activity of *acs*. At the time-scale of gene regulation, the metabolite concentration can be considered as adapting instantaneously to changes in gene expression using the quasi-steady-state approximation [Heinrich and Schuster, 1996]. Thus, the dynamical evolution of intracellular cAMP concentration is considered as a model input. Gene regulation kinetics are modeled by Hill formalisms and the translational and transcriptional dynamics are merged. The parameters are estimated using heuristic methods and the gene expression data. The predictions of the model are compared to experimental data on *fis* and *crp* mutant strains.

1.4 Thesis overview

This thesis is organized as follows:

Chapter 2 introduces fundamental notions of ODE models of metabolism and gene expression as well as the estimation of model parameters and reduction methods based on time-scale discrepancies and approximate kinetic formalisms. The chapter also lists the experimental techniques and datasets that can be used for the investigation of cellular adaptation processes during growth transitions. Finally, quantitative models of metabolism and gene regulation of *E. coli* during growth transitions are reviewed.

Chapter 3 describes a method for estimating parameters of linlog models from high-throughput incomplete datasets. The method is applied to experimental data to identify the linlog model of central carbon metabolism of *E. coli* and returns reasonable estimates for most of the identifiable model parameters. The results of this chapter were presented in the ISMB/ECCB conference in 2011 and published in *Bioinformatics* [Berthoumieux et al., 2011].

Chapter 4 investigates the identifiability of metabolic network models by presenting precise definitions of structural and practical identifiability and clarifying the fundamental relations between these concepts. This work will be presented at the SYSID conference in 2012 and published in the proceedings of the conference [Berthoumieux et al., 2012b].

Moreover, the chapter describes a method based on Singular Value Decomposition (SVD) to detect identifiability problems and to reduce the model to an identifiable approximation. Moreover, it discusses the application of this method to scarce, incomplete and noisy data. The identifiability analysis of the linlog model of central carbon metabolism of *E. coli* revealed that very few parameters are identifiable from currently available, state-of-the-art datasets. These results were submitted for publication [Berthoumieux et al., 2012a].

Chapter 5 presents results of the investigation of the relative contributions of transcription factors and the global physiological state of the cell to the regulation of gene expression. By means of gene expression measurements and development of kinetic models, this chapter highlights the importance of the global physiological state of the cell in gene expression regulation during the glucose/acetate diauxie. This work forms the basis for a paper currently in preparation.

Chapter 2

State of the art

In this chapter, we develop the different steps encountered when quantitatively modeling a biological regulatory system. First, a mathematical formulation has to be defined and in Sec. 2.1, we present some standard kinetic models in the formalism of ordinary differential equations for regulatory networks. It is also important to investigate the possibility to reduce the complexity and dimension of a model by looking at mathematical and biological properties of the system. In Sec. 2.2, we briefly describe reduction approaches for biological network models. Once the equations of the model are defined, the calibration of the model, *i.e.,* the estimation of its parameters, requires experimental data on the outputs of the system. In Sec. 2.3 we introduce common experimental techniques that allow measurement of high-throughput datasets for different biochemical species. In Sec. 2.4, we address the challenge of defining the parameter estimation problem and solving it using the best adapted algorithm. Finally, we present in Sec. 2.5 the state of the art of quantitative modeling of regulatory networks in *E. coli* during growth transitions.

2.1 Kinetic modeling of biochemical reaction systems

Being the most widespread formalism to model dynamical systems in science and engineering, ordinary differential equations (ODEs) have been widely used to analyze biochemical reaction networks. The ODE formalism models the concentrations of proteins, metabolites and other molecules by time-dependent variables which are real and positive. Biochemical reactions take the form of functional and differential relations between the concentration species.

More specifically, biochemical reactions are modeled by the following mathematical equation

$$\frac{dx}{dt} = N \cdot v(x, p, u) \tag{2.1}$$

with $x \in \mathbb{R}_+^n$ the vector of concentration variables of the system, $N \in \mathbb{Z}^{n \times m}$ a stoichiometry matrix describing the network structure, $v \in \mathbb{R}^m$ rate functions, $p \in \mathbb{R}^{n_p}$ the vector of model

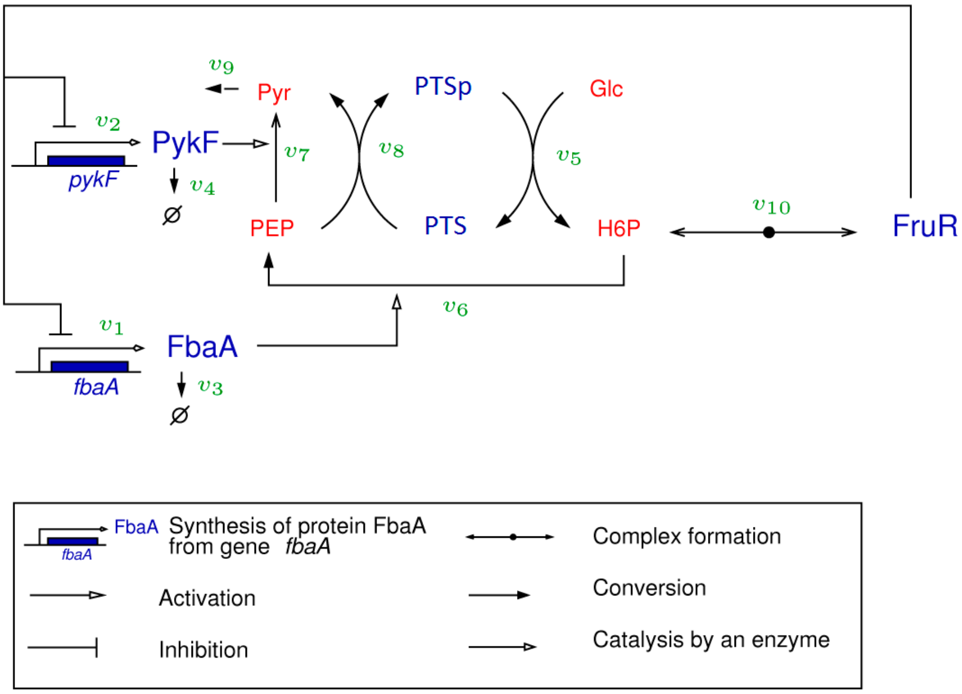

Figure 2.1: Simplified network of glycolysis taken from [Baldazzi et al., 2010]. The metabolites are written in red, the genes and proteins in blue, and reactions rates in green.

parameters and $u \in \mathbb{R}^z$ the vector of input signals, with $n, m, n_p, z \in \mathbb{N}$.

Depending on the nature of the system variables, the dependence of the kinetic rate v on the elements x and inputs u differs. In this section, we discuss the different forms that v can take in the case where the variables are metabolites, proteins or metabolite-protein complexes.

We will illustrate this discussion with the simplified network of glycolysis in *E. coli* developed by Baldazzi et al. [2010] (following [Kremling et al., 2008]), which is shown Fig. 2.1. This network describes the main reactions involved in the control of the glycolytic pathway during growth on glucose. It accounts for the sensing and uptake of glucose via the phospho-transferase system (PTS) which is described in a simplified way by considering the phosphorylated (PTSp) and non-phosphorylated (PTS) form of its proteins. Glucose is converted to a generic hexose-6-phosphate (H6P), whose conversion to PEP is schematized as a single reaction catalyzed by FbaA, taken as a representative of all glycolytic enzymes. The network also considers genetic regulation of enzyme expression by FruR, which is an inactive regulator when bound to fructose-1,6-biphosphate, here represented by H6P.

The corresponding ODE system takes as variables the metabolite concentrations of PEP, Pyr and H6P, the protein concentrations of PTS, PTSp and free FruR (not bound to H6P), the concentration of the protein-metabolite complex FruR·H6P and the concentrations of FbaA and PykF. As we assume the concentrations of total PTS and total FruR to be constant, the algebraic equations of Eq. (2.2) derived from mass conservation enable us to reduce the number of dynamical variables of the model.

$$\begin{cases} x_{PTS_T} = x_{PTS} + x_{PTSp} \\ x_{FruR_T} = x_{FruR\cdot H6P} + x_{FruR\cdot free} \end{cases} \tag{2.2}$$

with x_{PTS_T} and x_{FruR_T} the total concentrations of PTS and FruR, respectively. Thus, the kinetic model of this network in the form of Eq. (2.1) becomes

$$\begin{bmatrix} \dot{x}_{H6P} \\ \dot{x}_{PEP} \\ \dot{x}_{Pyr} \\ \dot{x}_{PTSp} \\ \dot{x}_{FruR\cdot free} \\ \dot{x}_{FbaA} \\ \dot{x}_{PykF} \end{bmatrix} = \begin{bmatrix} 0 & 0 & 0 & 0 & 1 & -1 & 0 & 0 & 0 & -1 \\ 0 & 0 & 0 & 0 & 0 & 2 & -1 & -1 & 0 & 0 \\ 0 & 0 & 0 & 0 & 0 & 0 & 1 & 1 & -1 & 0 \\ 0 & 0 & 0 & 0 & -1 & 0 & 0 & 1 & 0 & 0 \\ 0 & 0 & 0 & 0 & 0 & 0 & 0 & 0 & 0 & -1 \\ 1 & 0 & -1 & 0 & 0 & 0 & 0 & 0 & 0 & 0 \\ 0 & 1 & 0 & -1 & 0 & 0 & 0 & 0 & 0 & 0 \end{bmatrix} \begin{bmatrix} v_1 \\ v_2 \\ v_3 \\ v_4 \\ v_5 \\ v_6 \\ v_7 \\ v_8 \\ v_9 \\ v_{10} \end{bmatrix}. \tag{2.3}$$

2.1.1 Metabolic reactions

In metabolic models, v in Eq. (2.1) represents the metabolic reaction rates. Kinetic modeling of metabolism has been widely studied and a huge dedicated literature is available. The aim of this section is not to provide an exhaustive list of models of metabolic reactions but to discuss different types of kinetic equations.

First of all, the mass action rate law, a fundamental kinetic function, states that the reaction velocity v is proportional to each substrate concentration raised to the power of its respective molecularity, represented by its stoichiometric coefficient [Heinrich and Schuster, 1996].

For enzymatic reactions, the fundamental kinetic function is the Michaelis-Menten equation, which was first derived for unimolecular irreversible reactions [Michaelis and Menten, 1913, Michaelis et al., 2011]. The generalization to reversible reactions introduces the product concentration in the kinetic rate equation [Haldane, 1930], taking into account competitive product inhibition.

To model kinetic rates of a reaction subject to an inhibitor, it is crucial to distinguish between different inhibition mechanisms. Competitive inhibition occurs when substrate and inhibitor compete for the same enzyme binding site. Uncompetitive inhibition takes place when the inhibitor only binds to the complex formed by the enzyme and the substrate. Finally, an inhibitor binding to all forms of the enzyme is performing mixed inhibition.

Each of these inhibition mechanisms are modeled using different kinetic expressions [Cornish-Bowden, 1995].

The models listed above, however, are not able to reproduce the sigmoidal shape of the dependence of enzymatic activity on substrate concentrations that has sometimes been observed experimentally [Heinrich and Schuster, 1996]. Models accounting for enzyme cooperativity and allosteric interactions have been developed. Commonly encountered models are the phenomenological Hill function [Hill, 1910], the Monod-Wyman-Changeux rate law [Monod et al., 1965] and the sequential model of Koshland, Nemethy and Filmer [Koshland et al., 1966].

In the case of multimolecular reactions, kinetic modeling gets more difficult and kinetic rate laws quickly become complex non linear equations with a lot of parameters [Cornish-Bowden, 1995, Liebermeister and Klipp, 2006].

We illustrate some of the kinetic models just described on reactions of the network shown Fig. 2.1. We notice that reaction 8 operates without any enzymatic catalyzer. The kinetic rate of this reversible reaction can thus be modeled using mass-action kinetics,

$$v_8 = k_8^+ \cdot x_{PEP} \cdot x_{PTS} - k_8^- \cdot x_{Pyr} \cdot x_{PTSp} \tag{2.4}$$

with $k_8^+, k_8^- \in \mathbb{R}_+$ the forward and reverse rate constants, respectively.

Alternatively, reaction 6 of Fig. 2.1 is a reaction catalyzed by the enzyme FbaA. In order to account for product inhibition, we model this reaction velocity by reversible Michaelis-Menten kinetics

$$v_6 = x_{FbaA} \cdot \frac{k_{cat}^+ \cdot \frac{x_{H6P}}{K_{m,H6P}} - k_{cat}^- \cdot \frac{x_{PEP}}{K_{m,PEP}}}{1 + \frac{x_{H6P}}{K_{m,H6P}} + \frac{x_{PEP}}{K_{m,PEP}}}, \tag{2.5}$$

where $k_{cat}^+, k_{cat}^- \in \mathbb{R}_+$ are the catalytic constants of the forward and reverse reaction, respectively, and $K_{m,H6P}, K_{m,PEP} \in \mathbb{R}_+$ the Michaelis constants of H6P and PEP, respectively.

As mentioned before, alternative kinetics accounting for cooperativity or allosteric interactions can be encountered. The Hill function models the kinetic rate as a function of the concentrations of substrates to the power of the enzyme cooperativity, called Hill coefficient. In the case of irreversible reaction 6, the kinetic rate v_6 can be modeled as follows

$$v_6 = k_6 \cdot x_{FbaA} \cdot \frac{x_{H6P}^h}{K_{0.5}^h + x_{H6P}^h} \tag{2.6}$$

with k_6 the rate constant, $K_{0.5}$ the phenomenological constant defined as the substrate concentration for which the velocity reaches half its maximum value and h the Hill coefficient.

2.1.2 Gene expression

In gene expression models, v can represent either the synthesis rate of a protein or its degradation rate. Gene expression is a very complex process that can be regulated at several stages of mRNA and protein synthesis [Schaechter et al., 2006]. Although it is possible to develop mechanistic models of gene expression taking all steps into account ([Kremling, 2007] and references therein), in practice, the lack of quantitative biological knowledge about these processes and the complexity of the mathematical equations obtained render those models very difficult to properly develop and analyze. Usually, phenomenological functions are used to describe gene expression kinetics. Gene regulation modeling has been widely studied and a variety of different modeling formalisms have been developed (see [de Jong, 2002] for a review).

In the context of continuous ODE models, a common formalism uses Hill functions to describe gene expression rate laws. The activation of gene expression by a transcription factor is modeled by a Hill function whereas inhibition is modeled by an inverse Hill function. When several transcription factors act on the same promoter, the Hill functions can form complex expressions, whose structures are inspired from Boolean networks [de Jong, 2002].

In the simplified glycolytic network shown Fig. 2.1, the enzyme FbaA is negatively regulated by the transcription factor FruR, when the latter is not bound to H6P. We can therefore model the synthesis rate of FbaA using the Hill formalism, which gives

$$v_1 = \kappa_b + \kappa_r \cdot \left(1 - \frac{x^h_{FruR\cdot free}}{\theta^h + x^h_{FruR\cdot free}}\right) = \kappa_b + \kappa_r \cdot \frac{\theta^h}{\theta^h + x^h_{FruR\cdot free}} \tag{2.7}$$

with $\kappa_b \in \mathbb{R}_+$ the basal synthesis rate of FbaA, $\kappa_r \in \mathbb{R}_+$ the regulated synthesis rate of FbaA and $h, \theta \in \mathbb{R}_+$ the Hill coefficient and threshold for regulation of FbaA by FruR, respectively.

As for the degradation rate of FbaA, which is not regulated according to Fig. 2.1, we can model its rate by a first-order rate law. v_3 is then defined by

$$v_3 = \gamma_{FbaA} \cdot x_{FbaA} \tag{2.8}$$

with $\gamma_{FbaA} \in \mathbb{R}_+$ the protein degradation constant.

Usually the degradation rate is extended in order to account for the dilution of protein concentration due to bacterial growth as well. The degradation rate still depends linearly on the protein concentration, but the proportionality coefficient changes. This gives rise to

$$v_3 = (\gamma_{FbaA} + \mu) \cdot x_{FbaA} \tag{2.9}$$

with $\mu \in \mathbb{R}_+$ the bacterial growth rate.

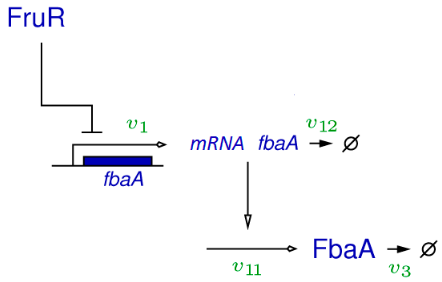

Figure 2.2: Network of FbaA synthesis when transcription and translation processes are considered separately.

A more detailed representation of gene expression kinetics is obtained by considering protein synthesis as a two-step process, transcription leading to mRNA and translation to protein. In that case, mRNA concentration can be treated as another system variable. In the example of FbaA synthesis, as shown Fig. 2.2, reaction 1 now produces mRNA and the new reaction 11 produces the protein. A reaction for mRNA degradation should also be considered (v_{12}).

When the transcription process is considered explicitly, reaction 1 becomes the synthesis of *fbaA* mRNA and the protein synthesis reaction is no longer directly regulated by FruR. Its kinetic rate can be modeled using first-order rate laws giving rise to the following model for the reactions of Fig. 2.2

$$\begin{cases} v_1 = \kappa_b + \kappa_r \cdot \frac{\theta^h}{\theta^h + x^h_{FruR \cdot free}} \\ v_3 = (\gamma_{FbaA} + \mu) \cdot x_{FbaA} \\ v_{11} = \kappa_p \cdot m_{FbaA} \\ v_{12} = (\gamma_{fbaA} + \mu) \cdot m_{FbaA} \end{cases} \tag{2.10}$$

with κ_b, κ_r the basal and regulated synthesis constant of *fbaA* mRNA, $m_{FbaA} \in \mathbb{R}_+$ the concentration of *fbaA* mRNA, $\kappa_p \in \mathbb{R}_+$ the synthesis constant of FbaA and $\gamma_{fbaA} \in \mathbb{R}_+$ the degradation constant of *fbaA* mRNA.

2.1.3 Protein-metabolite complexes

We can see that a complex formed of the metabolite H6P and the protein FruR is involved in the network of Fig. 2.1. The reaction of complex formation, shown in Eq. (2.11), is not catalyzed and can be modeled using mass-action kinetics.

$$\text{FruR} + \text{H6P} \rightleftharpoons \text{FruR}\cdot \text{H6P} \tag{2.11}$$

The dynamics of the complex concentration can be written in the following way:

$$\dot{x}_{FruR\cdot H6P} = k_{on} \cdot x_{FruR\cdot free} \cdot x_{H6P} - k_{off} \cdot x_{FruR\cdot H6P} \tag{2.12}$$

with k_{on} and k_{off} the rate constants for complex association and dissociation, respectively.

With mass conservation Eq. (2.2), we can reformulate Eq. (2.12) in terms of the concentrations of total FruR and FruR·H6P.

$$\dot{x}_{FruR\cdot H6P} = k_{on} \cdot (x_{FruR} - x_{FruR\cdot H6P}) \cdot x_{H6P} - k_{off} \cdot x_{FruR\cdot H6P} \tag{2.13}$$

2.2 Approximate kinetic models and model reduction

As mentioned in Sec. 1.2, quantitative models of biochemical kinetics can be difficult to handle and model simplifications appear to be helpful, if not necessary. In this chapter, we briefly present some approaches for reducing a model based on time-scale discrepancies (quasi-steady-state approximation) or based on linearization of local behaviours (approximated kinetic formats).

2.2.1 Reduction based on time-scale discrepancies

To a first approximation, three different classes of biological processes in a network can be distinguished based on their time scale. The main class is the class of processes which operate on the time-scale of interest. The second and third classes comprise processes that move much slower and much faster than the time-scale of interest, respectively.

When the time scale of interest is the time scale of a metabolic reaction, typical slow processes are, for example, changes in enzyme concentrations due to gene regulation and, in the case of excess substrate levels, changes in external metabolite concentrations. Examples of fast processes would be the association and dissociation of protein-metabolite complexes, either composed of a substrate and the enzyme catalyzing its consumption or complexes such as FruR·H6P in Fig. 2.1. When the time-scale of interest is the time-scale of gene expression, the third class of fast reactions comprises for example metabolic reactions or metabolite-protein complex formation.

The processes of the second class of slow reactions can be neglected or the concentrations of the substances involved can be treated as parameters of the model. As for the processes of the third class, their time-scale is so fast that after a rapid transient phase, they reach a quasi-stationary state in which their concentrations follow changes in the slow processes. This is the rationale behind the quasi-steady-state approximation, abbreviated to QSSA [Heinrich and Schuster, 1996], which states that the fast processes can be assumed to be at quasi-steady state, instantly adapting to the dynamics of variables of the main class. This approximation only applies if some conditions on system stability and steady-state uniqueness are satisfied.

These conditions are given by the Tikhonov theorem, which imposes exponential stability of the processes in the third class [Heinrich and Schuster, 1996].

A tremendous literature is dedicated to the mathematical analysis of the QSSA and its application to the modeling of biological systems. It has notably been applied to the dynamics of enzyme-substrate complexes to derive the Michaelis-Menten kinetics presented in Sec. 2.1. It can also be applied to reduce a model integrating both metabolic and gene regulation [Baldazzi et al., 2010, Roussel and Fraser, 2001].

Let us illustrate the possible model simplifications of the subnetwork composed of reactions 5, 6 and 10 of the network presented in Fig. 2.1, depending on which time-scale we are interested in. The variables of the submodel of these 3 equations are the concentrations of H6P and FruR·H6P and their dynamics are described by the following system of differential equations:

$$\begin{cases} \dot{x}_{H6P} & = & v_5(x_{PTS}, x_{PTSp}, x_{H6P}) - v_6(x_{H6P}, x_{PEP}, x_{FbaA}) \\ & & -v_{10}(x_{H6P}, x_{FruR\cdot H6P}, x_{FruR}) \\ \dot{x}_{FruR\cdot H6P} & = & v_{10}(x_{H6P}, x_{FruR\cdot H6P}, x_{FruR}) \\ & = & k_{on} \cdot (x_{FruR} - x_{FruR\cdot H6P}) \cdot x_{H6P} - k_{off} \cdot x_{FruR\cdot H6P} \end{cases} \tag{2.14}$$

We first consider the reactions on the time-scale of metabolism. Gene expression dynamics become a slow process and the concentrations of FruR and FbaA are treated as parameters: $C_{FruR} = x_{FruR}$, $C_{FbaA} = x_{FbaA} \in \mathbb{R}_+$. The formation of the complex FruR·H6P becomes a fast process and the QSSA can be applied. The complex concentration $x_{FruR\cdot H6P}$ is obtained by solving $\dot{x}_{FruR\cdot H6P} = 0$. Thus, the differential equation for FruR·H6P reduces to an algebraic equation from which the concentration of FruR·H6P can be directly computed given the concentration of H6P and the parameter accounting C_{FruR}. The model of Eq. (2.14) is then simplified so as to consider a single dynamical variable:

$$\begin{cases} \dot{x}_{H6P} = v_5(x_{PTS}, x_{PTSp}, x_{H6P}) - v_6(x_{H6P}, x_{PEP}, C_{FbaA}) \\ x_{FruR\cdot H6P} = C_{FruR} \cdot \frac{x_{H6P}}{\frac{k_{off}}{k_{on}} + x_{H6P}} \end{cases} \tag{2.15}$$

Now, if we consider the reaction on the time-scale of complex formation, gene expression and metabolism both become slow processes. We can define the parameters C_{FruR} and C_{H6P} as accounting for the constant concentrations of FruR and H6P, respectively. The model of Eq. (2.14) then becomes a system with one dynamical variable defined as follows

$$\begin{cases} \dot{x}_{FruR\cdot H6P} = \alpha x_{FruR\cdot H6P}) + \beta \\ x_{H6P} = C_{H6P} \end{cases} \tag{2.16}$$

with $\alpha = -(k_{off} + k_{on} C_{H6P})$ and $\beta = k_{on} C_{FruR} \cdot C_{H6P}$. The solution of this linear differential equation is an exponential relaxation to the steady-state value $x^0_{FruR\cdot H6P}$ given by

$$x^0_{FruR \cdot H6P} = -\frac{\beta}{\alpha} = C_{FruR} \cdot \frac{C_{H6P}}{\frac{k_{off}}{k_{on}} + C_{H6P}} \tag{2.17}$$

Notice that this value is the same as Eq. (2.15). Therefore, the definition of the time-scale of interest, and the resulting simplifications, do not alter the reduced model of the system in this case.

2.2.2 Approximate kinetic models

The reaction rates v are nonlinear and generally complex functions of x, u, and e, with many kinetic parameters that are difficult to reliably estimate from the data. This has motivated the use of approximate rate functions, which can be obtained from mathematical approximation techniques, such as the Taylor series expansion [Alves et al., 2008]. We will present two approximated representations of metabolic kinetics obtained in this way.

The first approximated model for v is the power-law formalism [Savageau, 1976]. This formalism is a consequence of approximating the rate equation in logarithmic space using a first-order Taylor series and then returning to Cartesian coordinates. For a metabolic reaction of the form

$$X_1 + \cdots + X_s \xrightarrow{E} X_{s+1} + \cdots + X_{s+p} \ , \tag{2.18}$$

the power-law model of the kinetic rate boils down to

$$v = k \cdot e \cdot \prod_{i=1}^{s} x_i^{b_i^0} \tag{2.19}$$

with k a rate constant, e the concentration of enzyme E, x_i the concentration of substrate X_i with $i = 1, \cdots, s$, and b_i^0 the local sensitivity of v to changes in X_i at a given operating point (x_i^0, v^0), defined by

$$b_i^0 = \left(\frac{\partial v}{\partial x_i}\right)_0 \cdot \frac{x_i^0}{v^0} \tag{2.20}$$

In case that reaction (2.18) is reversible, the same approximation can be applied to the reverse reaction and the rate v has the following form

$$v = k_+ \cdot e \cdot \prod_{i=1}^{s} x_i^{b_i^0} - k_- \cdot e \cdot \prod_{j=s+1}^{s+p} x_j^{c_j^0} \tag{2.21}$$

with k_+, k_- rate constants of the forward and reverse reactions, x_j the concentration of product X_j with $j = s+1, \cdots, s+p$ and c_j^0 the local sensitivity of the reverse rate v_- to changes in X_j at a given operating point (x_j^0, v_-^0).

Other approximated formalisms have been derived using the Taylor series approximation. For example the linlog model introduced by Heijnen [2005] expresses the reaction rates as proportional to the enzyme concentrations and to a linear function of the logarithms of metabolite concentrations around an operating point (x^0, v^0, e^0). Its expression of the kinetic rate of reaction (2.18) is given by

$$\frac{v}{v^0} = \frac{e}{e^0} \cdot \left[1 + \sum_{i=1}^{s+p} b_i^0 \ln \left(\frac{x_i}{x_i^0} \right) \right] \tag{2.22}$$

The linlog model can also be encountered in its non-relative form, *i.e.,* without the operating point apparent in the kinetic expression. Thus the kinetic rate v is expressed as

$$v = e \cdot (a + \sum_{i=1}^{s+p} b_i \ln x_i) \tag{2.23}$$

with $a \in \mathbb{R}$ and $b = (b_1, \cdots, b_{n+p}) \in \mathbb{R}^{s+p}$ parameters. An in-depth discussion of linlog models and comparison with other approximative rate functions can be found in the reviews by Heijnen [2005] and Alves et al. [2008].

As for gene regulation models, the use of formal methods to study regulatory networks is subject to two major constraints. First, as mentioned before, an incomplete knowledge of biochemical reaction mechanisms underlying these interactions prevents the development of detailed kinetic models. Second, the general absence of quantitative information on kinetic parameters and molecular concentrations renders the quantitative analysis of the model difficult. Thus, a model formalism called piecewise-linear has been developed that approximates Hill dynamics by step functions [Glass and Kauffman, 1973]. The piecewise-linear models have mathematical properties that allow qualitative predictions to be made on the steady-states and transient behaviors of the system [de Jong et al., 2004]. Other modeling frameworks enable coarse-grained qualitative analysis of gene regulatory networks when no quantitative information is available (see [de Jong, 2002] for a review).

2.3 Measurements of gene expression and metabolism

The development of quantitative models of integrated networks of gene and metabolic regulation requires the access to measurements of different biochemical species such as mRNA, protein and metabolites as well as of metabolic fluxes. Large efforts have been made to develop experimental methods allowing the production of such datasets. The aim of this section is not to present an exhaustive list of all methods available but to quickly introduce the methods that have produced the data we will work with in the following chapters.

First of all, both in the case of metabolic and gene regulatory networks, we are interested in gene expression data, either mRNA concentrations or protein concentrations. DNA microarrays are the most widely adopted technology for high-throughput measurements of gene expression. The underlying principle of DNA microarrays is the complementary binding property of mRNA. In a microarray, single-stranded DNA, acting as probes, are arrayed on a solid substrate. RNA is extracted from a sample, fluorescently labeled, reverse-transcribed and hybridized on the microarray, where the probes will capture their complementary labeled cDNAs. Thereby, the probes act as molecular sensors for quantitative measurements and the intensity of fluorescence is a measure of the expression level of its targeted gene [Dharmadi and Gonzalez, 2004, Crampin, 2006]. Many choices of DNA microarray platforms and physical formats are available, such as cDNA microarrays or oligonucleotide microarrays [Schena et al., 1995, Lockhart et al., 1996]. This approach enables the characterization of gene expression at a genomic scale.

Microarrays have been extensively used to produce high-throughput datasets for the study of bacterial systems, including *E. coli.* Notably, they have been used to report gene expression changes in response to specific stimuli from the environment, to provide insights into specific transcriptional events and for genetic and metabolic engineering (see [Dharmadi and Gonzalez, 2004] for a review). Oh et al. [2002] characterized the transcript profile of *E. coli* in acetate cultures using DNA microarray on glass slides. As for using microarrays to look for transcriptional regulation, reviews of microarray datasets for *E. coli* can be found in [Faith et al., 2007, Park et al., 2005].

However DNA microarrays only return relative RNA concentration values computed from a comparison with a control experiment. Other techniques have been developed to measure absolute mRNA concentrations, such as quantitative PCR, but they do not generally allow high-throughput measurements [Crampin, 2006] (see [White et al., 2011] for an exception). Moreover, even if DNA microarray is the most used technology for gene expression measurements (see [Meloni et al., 2004] and references therein), heterogeneity of experimental designs, target preparation protocols and data analysis methods prevents a reliable comparison between available microarray data. [Dharmadi and Gonzalez, 2004]. Moreover, as microarray technology necessitates to extract mRNA from a bacterial sample, measurements cannot be made *in vivo* or used to assess individual cells.

The use of reporter genes for the measurement of gene expression allows the measurement of promoter activity *in vivo* at high-temporal resolution. The technology is based on the fusion of the promoter region of a gene of interest to a fluorescent or luminescent reporter gene. The expression of the reporter gene generates a visible fluorescent or luminescent signal that is easy to capture and reflects the expression of the gene of interest. These constructions enable single-cell measurements, which helps probing key biological phenomena in individual living cells [Longo and Hasty, 2006]. Moreover, the GFP protein has been modified to produce blue, cyan, yellow and red fluorescent proteins, making it possible to study the expression of multiple genes in the same cell.

Data analysis requires precise information on half life of signal proteins, be it fluorescent or luminescent, and plasmids used [de Jong et al., 2010]. The reporter gene can be expressed from a (low-copy) plasmid or integrated into the chromosome. Using a plasmid enables an easier construction and emphasizes the signal intensity, which can be very close to background when reporter genes are placed on the chromosome. However, reporter plasmids can introduce bias in the signal as their copy number in the cell can vary depending on experimental conditions [Lin-Chao and Bremer, 1986]. This bias can be quantitatively monitored by measuring the copy number of reporter plasmids using qRT-PCR technology [Lee et al., 2004, Chen et al., 2005].

Several examples of the real-time quantification of gene expression in *E. coli* using reporter genes have been reported in the literature. For example, Ronen et al. [2002] and Dyk et al. [2001] used fluorescent and luminescent reporter genes to investigate the DNA damage response. Kalir et al. [2005] analyzed the feed-forward loop motif of flagella gene-regulation network, the system that allows the bacteria to swim. And recently, a high-throughput library of fluorescent reporter genes has been constructed for *E. coli* and enabled the discovery of new transcription units [Zaslaver et al., 2006].

Although transcription profiling by microarrays or reporter genes delivers valuable mRNA concentration patterns, a systematic post-genomic approach which describes the overall state of a biological system is an important supplement to transcriptome analysis. Methods for high-throughput measurement of protein abundance such as liquid chromatography tandem mass spectrometry (LC-MS/MS) and 2D fluorescence difference gel electrophoresis have been developed [Gstaiger and Aebersold, 2009, Marouga et al., 2005]. These methods have been widely applied to study the proteome of *E. coli.* For example, combined analyses of transcriptome and proteome were performed to investigate the effects of recombinant protein production on metabolic enzymes [Dürrschmid et al., 2008] and to understand metabolic and physiological changes during high cell-density cultivation [Yoon et al., 2003].

The measurement of changes in intracellular metabolite concentrations reveals an aspect of regulation that cannot be studied by measuring changes in mRNA or protein concentrations only [Vemuri and Aristidou, 2005]. Metabolomics draws on a range of analytical platforms including mass spectrometry (MS) and chromatography- and electrophoresis-based separation methods. The popular technologies for the identification and quantification of metabolites are a combination of gas (or liquid) chromatography and mass spectrometry called GC-MS (or LC-MS) or capillary electrophoresis and mass spectrometry called CE-MS (see [Villas-Boas et al., 2005, Monton and Soga, 2007] for reviews).

It is not currently possible to quantify all intracellular metabolites in a cell due to the lack of a robust, automated and reproducible analytical technique. Thus, metabolomics, in the strictest sense, is practically impossible, and the term is used broadly to cover approaches concerned with investigating subsets of the metabolome.

These methods have been applied to the metabolome analysis of *E. coli.* Examples include the profiling of bacterial metabolites [Jia et al., 2005], the quantification of changes in central carbon metabolism under different growth conditions and for different mutant strains [Ishii et al., 2007] or the effect of the *lpdA* gene knockout on metabolism [Li et al., 2006]. More recently, the LC-MS/MS method was used to compute absolute metabolite concentrations during growth on glucose [Bennett et al., 2009] and a combination of transcriptomic and metabolomic data was analyzed to investigate gene and metabolic regulatory interactions during stress response [Jozefczuk et al., 2010].

When it comes to the study of dynamics of a complex network, genomic or proteomic data are not sufficient as they do not contain full information on the functional behaviour of the network. The network response is also characterized by changing metabolic fluxes through the network, which can be computed with ^{13}C-based flux analysis. ^{13}C-labeled substrates are introduced into the growing medium and metabolized by the cell population until the isotope label is distributed throughout the network. Then mass spectrometry detects the isotopic carbon in amino acids and from those data and a stoichiometric model of metabolic network, the flux distribution is computed [Sauer, 2006].

^{13}C-labeled flux analysis has been intensively applied to microbes, and to *E. coli* in particular, to determine the phenotypic effects of structural changes in the metabolic network, providing direct evidence for the nature and extent of the mechanisms that compensate the effects of perturbations. For example, Nicolas et al. [2007] studied the redistribution of central metabolic fluxes when the *zwf* gene, which codes the enzyme catalyzing the production of 6PG from G6P, was deleted. To study the consequences of *lpdA* gene knockout on the metabolism, Li et al. [2006] used both metabolite concentration measurements and flux analysis. More recently, van Rijsewijk et al. [2011] provided insights in the transcriptional control of carbon metabolism when bacteria grow on glucose and on galactose using GC-MS-detected mass isotope partitioning.

2.4 Parameter estimation of kinetic models

Parameter estimation is an important step in the process of developing data-driven models for biological systems with a predicted value. To compare a model with experimental data, the mathematical model has to be simulated. Then, model parameters can be estimated from measured observations [Ashyraliyev et al., 2009]. Typically, parameter estimation starts with a guess about parameter values and then changes them to minimize an objective function, defined by the modeler. A usual objective function is the discrepancy between model and data using a particular metric. To estimate these parameters, optimization methods have been developed, depending on the nature of the estimation problem.

Here, we focus on parameter estimation in the case of dynamical ODE models of biochemical species discussed in Sec. 2.1. Recall that these models have the following form:

$$\frac{dx}{dt} = N \cdot v(x(t), p, u(t)) \tag{2.24}$$

with $x \in \mathbb{R}^n_+$ the vector of variables of the system (usually, a concentration of biochemical species), $N \in \mathbb{R}^{n \times m}$ the stoichiometry matrix, $v \in \mathbb{R}^m$ rate functions, $p \in \mathbb{R}^{n_p}$ the vector of model parameters and $u \in \mathbb{R}^z$ the vector of input signals, with $n, m, n_p, z \in \mathbb{N}$. We define a vector of observables $y \in \mathbb{R}^r$ in the following way

$$y(t) = g(x(t), p, u(t)) \tag{2.25}$$

with $g : \mathbb{R}^{n+n_p+z} \mapsto \mathbb{R}^r$. y is a vector of quantities in the model that can be experimentally measured. Let us assume that q measurements $(y^1, \cdots, y^q)$, corresponding to q input measurements $(u^1, \cdots, u^q)$, are available for the estimation of p with $q \in \mathbb{N}$. Corresponding values of state variables $(x^1, \cdots, x^q)$, given a specific parameter vector $\hat{p}$, are computed by numerical integration of Eq. (2.24) and values of observable function are obtained by computing $\hat{g_i} = g(x_i, \hat{p}, u)$. We want to find a parameterization p that minimizes discrepancies between model predictions and experimental values. So parameter estimation boils down to the optimization problem of minimizing a function $F : \mathbb{R}^{n_p} \mapsto \mathbb{R}_+$ that is a measure of these discrepancies. The definition of F, called objective function, depends on the properties of the model formalism and available data. Most of the time, F is defined as the squared error between model and data:

$$F(p) = \sum_{k=1}^{q} ((g(x_k, p, u_k)) - y_k)^2 \tag{2.26}$$

The aim of this chapter is not to make an exhaustive list of all methods and algorithms available for parameter estimation (see Walter and Pronzato [1997], Ljung [1999] for reviews) but rather to review options in solving the parameter estimation problem according to the situation faced. In particular, only one or two methods will be briefly explained, as they will be used in the following chapters.

2.4.1 Defining the objective function

Parameter estimation depends on the available experimental data and therefore the problem of calibrating the model, *i.e.,* defining the objective function, is formulated differently depending on the situation. We enumerate two possible situations faced for such models when performing parameter estimation.

1. A case commonly encountered is when the observables are composed of the state variables x, the inputs u and the kinetic rates v under q different experimental conditions. For metabolic networks, it would imply possessing measures of metabolite concentrations, enzyme concentrations and reaction fluxes. Such a dataset has been obtained for the central carbon metabolism of *E. coli* [Ishii et al., 2007]. For gene regulatory

networks, measurements of growth rate, protein concentrations and promoter activities would be available, for instance as time series of fluorescent signal. With an appropriate data analysis, data about protein concentrations and promoter activities (synthesis rates of mRNA) can be computed [de Jong et al., 2010].

Let us call $x^k \in \mathbb{R}^n_+$, $u^k \in \mathbb{R}^z_+$ and $v^k \in \mathbb{R}^m$, with $k = 1, \cdots, q$, the measurements of variables, inputs and kinetic rates. The experimental conditions for the production of the q datapoints may vary. Datasets may be composed of steady-state or time-series measurements. In the first case, each datapoint k is obtained for different genetic backgrounds or under different environmental conditions. In the second case, each measurement k is associated to t_k, the timepoint at which the measurement was taken.

Regardless of the experimental conditions, the parameter estimation problem is formulated as finding a solution in p for an algebraic system composed of the following equations

$$v^k = v(x^k, u^k, p) \tag{2.27}$$

with $k = 1, \cdots, q$. Thus, by defining the observables of the system as the kinetic rates ($y = g(x, p, u) = v(x, p, u)$), the objective function of this parameter estimation problem becomes

$$F(p) = \sum_{k=1}^{q} (v_k - v(x_k, p, u_k))^2. \tag{2.28}$$

2. We also face situations where only data about the variables of the system and the inputs are available. In that case, we can define the vector of observables as the vector of variables, $y = x$ and the objective function becomes

$$F(p) = \sum_{k=1}^{q} (x^k - x(u^k, p))^2. \tag{2.29}$$

The computation of F for a given parameter vector p requires the integration of the ODE system (2.24) in order to calculate x given p and the input u^k.

2.4.2 Minimizing the objective function

The optimization problem of minimizing F depends on the form of the observable function $g(x, p, u)$. In case that g is linear in the parameters, one can use linear regression to find the optimal p. Indeed, the observable $g(x, p, u)$ can be reformulated as

$$g(x, p, u) = a(x, u) + b_1(x, u) \cdot p_1 + \cdots + b_{n_p}(x, u) \cdot p_{n_p} \tag{2.30}$$

with $a : \mathbb{R}^{n+z} \mapsto \mathbb{R}^r$ and $b_\ell : \mathbb{R}^{n+z} \mapsto \mathbb{R}^r$ with $\ell = 1, \cdots, n_p$. Let us define the data matrices $W = (W_{ik}) \in \mathbb{R}^{r\times q}$ and $B^\ell = (B^\ell_{ik}) \in \mathbb{R}^{r\times q}$ such that

$$W_{.k} = y_k - a(x_k, u_k) \quad ; \quad B^\ell_{.k} = b_\ell(x_k, u_k) \tag{2.31}$$

with $k = 1, \cdots, q$ and $\ell = 1, \cdots, n_p$. The parameter estimation problem then becomes

$$W = B^1 \cdot p_1 + \cdots + B^{n_p} \cdot p_{n_p} + \varepsilon \tag{2.32}$$

with ε the modeling error and the objective function can be written as follows.

$$F(p) = ||W - B^1 \cdot p_1 - \cdots - B^{n_p} \cdot p_{n_p}||^2 \tag{2.33}$$

The optimal parameter vector is then given by the following expression [Hamilton, 1992]:

$$\hat{p_\ell} = [B^{\ell^T} \Sigma_\varepsilon^{-1} B^{\ell^T}]^{-1} B^{\ell^T} \Sigma_\varepsilon^{-1} W \tag{2.34}$$

with Σ_ε the covariance matrix of the error ε.

In case where g is nonlinear in the parameters, the regression problem becomes a nonlinear problem and most of the time, there is no theoretical framework giving the solution minimizing F. Thus, heuristic methods are used that randomly search over a range of parameter values to find the minimum. A variety of optimization algorithms have been developed for this purpose ([Ljung, 1999], see [Chou and Voit, 2009, Ashyraliyev et al., 2009] for reviews in systems biology) and some of them have been applied to biological models [Moles et al., 2003]. Among them, we can distinguish two classes: local-search methods and global-search methods.

Local search methods converge fast to a minimum, as the parameter space scanned is reduced to local values around the initial parameter guess. They are able to perform a precise scan of a centered parameter space. However, the algorithm can easily be stuck in a local minimum, since the method has no possibility to escape from this minimum and find the global minimum. For such an algorithm, assuming the initial guess is sufficiently close to a minimum (may it be local or global), there is a theoretical framework to prove convergence of the method [Ashyraliyev et al., 2009].

Some of the commonly encountered local-search algorithms that are included in all major software packages are gradient-based methods such the Gauss-Network and Levenberg-Marquardt algorithms and direct-search methods such as the Nelder-Mead simplex approach. The latter has been implemented in MATLAB for the function `fminsearch` [Nelder and Mead, 1965]. This algorithm is based on the idea of a simplex, *i.e.,* a polyhedron without specific properties of $d + 1$ vertices in a space of d dimensions, with $d \in \mathbb{N}$, that adapts at each iteration and wanders the parameter space to find the optimal vector. At each iteration, the objective function is evaluated at each vertex and the one giving the highest objective function, *i.e.,* the worst one, is deleted. Its replacement is searched on the line formed by this former vertex and the center of the remaining vertices.

To avoid the problem of being stuck in a local minimum, global-search methods that search over the entire parameter space to find increasingly smaller values for F have been developed. In general, there is no proof of convergence for these methods [Ashyraliyev et al., 2009]. Several search strategies have been developed, taking inspiration from other scientific domains.

For example, simulated annealing is inspired by the physical process of heating up a solid until it melts and slowly cooling it down until the molecules are aligned in a crystalline structure corresponding to the minimum energy state [Kirkpatrick et al., 1983]. Evolutionary algorithms, such as genetic algorithms or evolutionary strategies, are inspired by concepts of biological evolution such as reproduction, mutation and selection, to produce an optimized parameter vector [Beyer and Schwefel, 2002]. First, an initial population of possible parameter vectors, whose size is specified by the modeler, is defined. Part of the population is selected to form the parents of a new generation. A population of children, whose values are computed from recombination of values of random parents, is created. Each child can be mutated, *i.e.,* its values can be altered based on mutation strategies. Finally, the parameter vectors that return the lowest objective function values are selected among the old and new generations to create the next generation. This process is iterated until some convergence criterion, defined by the modeler and usually based on the change of objective function between estimates, is reached.

One major drawback of global-search algorithms is their convergence speed, which is in general much lower than for local-search methods. Usually, users define a time limit when they run these algorithms. Another strategy is to combine both types of optimization algorithms and use hybrid methods. Indeed, first a global-search algorithm can be used to scan efficiently the range of possible parameter values to find the area with the global minimum. Then, a local-search algorithm can be applied with the parameter vector obtained by the global-search method as initial vector to perform a more precise scan of the promising area. These hybrid methods have shown better results than global- or local-search methods alone and faster computation [Rodriguez-Fernandez et al., 2006].

In the case where the computation of F requires integration of the ODE system, the optimization procedure of minimizing Eq. (2.29) is very demanding on the computational level, as at each iteration of the optimization algorithm, an ODE system has to be solved. One may thus encounter extreme computational lengths or numerical issues that practically prevent the parameter estimation to be performed.

Another situation not yet mentioned is the case where not all observables have been measured for all experimental conditions. Due to this lack of data, parameter estimation problem gets trickier as the objective function defined as in Eq. (2.28) or Eq. (2.29) cannot be computed. One way to overcome this difficulty is to estimate the missing values of the dataset. Some methods for missing data imputation have been developed [Oba et al., 2003, Scholz et al., 2005, Rubin, 1976], enabling the computation of the objective function as defined in the previous section and the use of optimization algorithms just described. Alternatively, Expectation-Maximization is an iterative method that minimizes the least-square error by maximizing an intermediary function which is recomputed at each iteration [Dempster et al., 1977]. This method does not require values for missing data. We will present it in detail in Chap. 3.

2.5 Quantitative modeling of growth transitions in *E. coli*

In this section, we list quantitative models of growth transitions in *E. coli* published in the literature. We will mainly talk about continuous models, but other types of modeling frameworks such as logic-based or flux balance analysis are reviewed in [Tenazinha and Vinga, 2011, Bulik et al., 2011].

Central carbon metabolism of *E. coli* has been extensively studied. More particularly, several quantitative models of this network using kinetic formalisms such as those described in Sec. 2.1 have been developed. Chassagnole et al. [2002] have first developed a quantitative dynamical model of glycolysis and the pentose-phosphate pathway. They validated this model with metabolite concentrations that they measured at transient conditions and showed, using metabolic control analysis, that the flux control during glucose uptake was shared by the PTS system and enzymes degrading PTS inhibitors. Bettenbrock et al. [2006] investigated this question and modeled dynamically the uptake of glucose, lactose, glycerol, sucrose and galactose. They quantitatively predicted the behaviour of catabolite repression, *i.e,* the system that prevents uptake of other carbon sources when glucose is available, and validated it on metabolite and enzyme concentrations that they measured in different growth situations. Moreover, Kremling et al. [2007] highlighted, by means of a quantitative model of the PTS, the relationship between the bacterial growth rate and the phosphorylation state of an element of the PTS. Both in the last two examples, the authors estimated the parameters and discussed the choices of kinetic formalisms. The systems of carbohydrate uptake involve signalling metabolites as well as enzymes and regulation by transcription factors, such as Crp. Thus, the models of this system, which are reviewed in [Kremling et al., 2009] combine metabolic and gene regulations.

More recently, Kotte et al. [2010] have considered a simplified network of glycolysis and the Krebs cycle and extended it to take gene regulation of metabolic enzymes into account. They developed a quantitative model with Monod-Wyman-Changeux, Hill and Michaelis-Menten kinetics and estimated the parameters from published steady-state data. With their model, they were able to reproduce the flux inversion between glycolysis and gluconeogenesis that occurs during the glucose/acetate diauxie. Usuda et al. [2010] also looked at an integrated network by considering glycolysis, the pentose-phosphate pathway, the Krebs cycle, the glyoxylate shunt and anaplerotic pathways as well as transcription factors involved in the regulation of catabolic enzymes. Their model used Michaelis-Menten kinetics, was calibrated with parameter estimation and was validated on metabolite concentrations that they measured on wild-type and glutamate-producing strains. Note that in these last two examples, gene regulation kinetics were described as being dependent to the bacterial growth rate.

There exists also quantitative models of such networks that were developed using the approximate kinetic formalisms introduced in Sec. 2.2.2. For the linlog formalism, simulation studies on the level of both individual enzymatic reactions [Heijnen, 2005] and metabolic networks [Hadlich et al., 2009] have shown that they provide reasonable approximations of classical enzymatic rate laws. Moreover, Visser et al. [2004] developed a linlog model of glycolysis and validated the dynamical predictions by comparing them to a complete mechanistic model. With the help of a recent genome-scale linlog model of yeast metabolism, parametrized using previously-published kinetic models, it has been possible to identify key steps in the network, that is, reactions exerting most control over glucose transport and biomass production [Smallbone et al., 2010]. Moreover, Hardiman et al. [2009] have presented a model of a network combining metabolism and gene regulation with linlog kinetics. As for other approximate formalisms, models of metabolic networks using power-law kinetics mixed with Petri Nets have also been developed [Wu and Voit, 2009].

It is also possible to mix different kinetic formalisms in quantitative modeling. Costa et al. [2010] studied the predictive performances of a model of the central carbon metabolism using a mix of Michaelis-Menten and approximate kinetics. They found out that the linlog model, combined with Michaelis-Menten, was the most efficient. A review of models with hybrid kinetics of regulatory networks from other organisms than *E. coli* can be found in [Bulik et al., 2009].

Finally, we mention the existence of qualitative studies of the dynamics of the metabolic and gene regulation networks during growth transitions. Ropers et al. [2006] developed a piecewise-linear model to investigate the dynamics of the network formed by the global regulators of *E. coli* during glucose exhaustion. Baldazzi et al. [2012] extended the network of global regulators so as to consider the glycolytic pathway as well. They show, by the comparison of predictions of different piecewise-linear models to steady-state data of enzyme and metabolite concentrations under growth on glucose and acetate, that interactions between metabolism and gene regulation are essential to describe the adaptation of gene expression during diauxie. Other examples of gene regulatory models can be found in the review by Karlebach and Shamir [2008].

Chapter 3

Parameter estimation of linlog metabolic models

We focus in this chapter on the modeling of central carbon metabolism of *E. coli* shown in Fig. 1.5 and described in Sec. 1.3.1. This network has been studied for a long time from different perspectives. A rather precise idea of the structure of the network exists and several kinetic models of the network dynamics are available ([Bettenbrock et al., 2006, Kotte et al., 2010] and references therein). Moreover, a high-throughput dataset gathering required information for parameter estimation has recently been published [Ishii et al., 2007].

The usefulness of approximate kinetic laws for the mathematical formalism of the metabolic model has been presented before in Chaps. 1 and 2. Linlog models are a particularly interesting choice for modeling metabolism [Heijnen, 2005, Visser and Heijnen, 2003]. A major advantage of linlog models is that, when measurements of fluxes, enzyme concentrations, and metabolite concentrations are available, the parameter estimation problem reduces to multiple linear regression [Nikerel et al., 2006]. Power-law models, up to a logarithmic transformation, and loglin models also have this convenient property. However, in all of the above formalisms, the performance of regression approaches quickly degrades in the presence of missing data, as is often the case in high-throughput datasets due to experimental limitations or instrument failures.

In order to deal with this problem, we propose in this chapter a maximum-likelihood method for the identification of linlog models of metabolism from incomplete datasets.

3.1 Parameter estimation in linlog models

We recall that the dynamics of metabolic networks are described by kinetic models having the form of systems of ordinary differential equations (ODEs) [Heinrich and Schuster, 1996]:

$$\dot{x} = N \cdot v(x, u, e) \tag{3.1}$$

where $x \in \mathbb{R}_+^{n_x}$ denotes the vector of (nonnegative) internal metabolite concentrations, $u \in \mathbb{R}_+^{n_u}$ the vector of external metabolite concentrations, $e \in \mathbb{R}_+^m$ the vector of enzyme concentrations, and $v : \mathbb{R}_+^{n_x+n_u+m} \to \mathbb{R}^m$ the vector of reaction rate functions. $N \in \mathbb{Z}^{n_x \times m}$ is a stoichiometry matrix. As mentioned in Sec. 2.2.2, the complexity and non-linearity of v stimulate the use of approximate kinetic laws. The linlog approximation leads to the rate equation

$$v(x, u, e) = \operatorname{diag}(e) \cdot \big(a + B^x \cdot \ln x + B^u \cdot \ln u\big) \tag{3.2}$$

where $\operatorname{diag}(e)$ is the square diagonal matrix with the elements of e on the diagonal, and the logarithm of a vector means the vector of logarithms of its elements. For conciseness, in the sequel we shall drop the dependence of v on (x, u, e) from the notation.

The identification of metabolic networks in the linlog formalism amounts to estimating the (generally unknown) parameters $a \in \mathbb{R}^m$, $B^x \in \mathbb{R}^{m \times n_x}$ and $B^u \in \mathbb{R}^{m \times n_u}$ from q experimental datapoints (v^k, x^k, u^k, e^k), $k = 1, \dots, q$. That is, the data used for parameter estimation are parallel measurements of enzyme and metabolite levels as well as metabolic fluxes. The datapoints (v^k, x^k, u^k, e^k) are obtained under different experimental conditions, for instance different dilution rates in continuous cultures or different mutant strains. Notice that in practice reaction rates are most of the time measured at (quasi-)steady state (see also Sec. 3.5). That is, on the time-scale of interest the derivatives of metabolite concentrations vanish and Eq. (3.1) can be rewritten as $N \cdot v = 0$.

For the purpose of parameter estimation, it is convenient to rewrite (3.2) in the form of a regression model:

$$\left(\frac{v}{e}\right)^T = [1 \;\ln x^T \;\ln u^T] \cdot \begin{bmatrix} a^T \\ (B^x)^T \\ (B^u)^T \end{bmatrix} \tag{3.3}$$

where the ratio of two vectors (here v/e) denotes element-wise division. Let us use an upperbar to denote the mean of a quantity over its q experimental observations, for instance: $\overline{v/e} = (1/q) \sum_{k=1}^q v^k/e^k$. By the linearity of (3.3), it holds that

$$\overline{\left(\frac{v}{e}\right)} = [1 \;\overline{\ln x}^T \;\overline{\ln u}^T] \cdot \begin{bmatrix} a^T \\ (B^x)^T \\ (B^u)^T \end{bmatrix}. \tag{3.4}$$

This allows (3.3) to be reformulated as a mean-removed model

$$\left(\frac{v}{e} - \overline{\left(\frac{v}{e}\right)}\right)^T = \begin{bmatrix} \ln x - \overline{\ln x} \\ \ln u - \overline{\ln u} \end{bmatrix}^T \cdot \begin{bmatrix} (B^x)^T \\ (B^u)^T \end{bmatrix} \tag{3.5}$$

and we obtain the following parameter estimation problem:

Problem 1. *Given the data matrices*

$$\underbrace{\begin{bmatrix} \left(\frac{v^1}{e^1} - \overline{\left(\frac{v}{e}\right)}\right)^T \\ \vdots \\ \left(\frac{v^q}{e^q} - \overline{\left(\frac{v}{e}\right)}\right)^T \end{bmatrix}}_{\triangleq W}, \quad \underbrace{\begin{bmatrix} \left(\ln(x^1) - \overline{\ln x}\right)^T & \left(\ln(u^1) - \overline{\ln u}\right)^T \\ \vdots & \vdots \\ \left(\ln(x^q) - \overline{\ln x}\right)^T & \left(\ln(u^q) - \overline{\ln u}\right)^T \end{bmatrix}}_{\triangleq Y}$$

find parameters $B \triangleq \begin{bmatrix} B^x & B^u \end{bmatrix}^T$ *solving the regression problem*

$$W = Y \cdot B + \varepsilon \tag{3.6}$$

where $\varepsilon \in \mathbb{R}^{q \times m}$ *is measurement noise on* W*.*

Notice that the parameter vector a no longer appears in the regression problem, but an estimate of it can be recovered from estimates of $B = \begin{bmatrix} B^x & B^u \end{bmatrix}^T$ by way of Eq. (3.4).

In the remainder of the chapter, we make the assumption that each column $\varepsilon_{\cdot i}$ of ε follows a Gaussian distribution, indicated by $\varepsilon_{\cdot i} \sim \mathcal{N}(0, \Sigma_{\varepsilon_i})$, where Σ_{ε_i} is diagonal, *i.e.,* the measurement errors in different experiments are mutually uncorrelated. We further assume that $\varepsilon_{\cdot i}$ is independent of $\varepsilon_{\cdot j}$ for $i \neq j$. Then, Problem 1 can be subdivided into m independent subproblems, one for each reaction i:

$$w_{\cdot i} = Y \cdot b_{\cdot i} + \varepsilon_{\cdot i} \tag{3.7}$$

where $w_{\cdot i}$ and $b_{\cdot i}$ are the ith columns of W and B, respectively.

The values of the parameter matrices B^x and B^u admit an interesting biological interpretation. Notice that one can immediately find values $x_0 \in \mathbb{R}_+^{n_x}$, $u_0 \in \mathbb{R}_+^{n_u}$, $e_0 \in \mathbb{R}_+^m$ and $v_0 \in \mathbb{R}^m$ such that $v_0/e_0 = \overline{v/e}$, $\ln x_0 = \overline{\ln x}$, and $\ln u_0 = \overline{\ln u}$. As a consequence, Eq. (3.5) can be rearranged into the common relative formulation of linlog models,

$$\frac{v}{e} = \operatorname{diag}\left(\frac{v_0}{e_0}\right)\left[\mathbb{1} + B_0^x \ln \frac{x}{x_0} + B_0^u \ln \frac{u}{u_0}\right] \tag{3.8}$$

where $\mathbb{1}$ is an $m \times 1$ vector of ones, (v_0, x_0, u_0, e_0) is a so-called reference state [Heijnen, 2005] and B_0^x, B_0^u are matrices of elasticity constants, where

$$B_0^x = \operatorname{diag}\left(\frac{e_0}{v_0}\right) \cdot B^x, \quad B_0^u = \operatorname{diag}\left(\frac{e_0}{v_0}\right) \cdot B^u. \tag{3.9}$$

The elasticities, introduced in the context of Metabolic Control Analysis (MCA) [Heinrich and Schuster, 1996], describe the normalized local response of the reaction rates to changes in metabolite concentrations. The interest is that they can thus be immediately computed from the values of B^x and B^u found by the solution of Problem 1, and the equality $e_0/v_0 = 1/(\overline{v/e})$.

Although straightforward in theory, solving the regression problem (3.6) encounters two complications in practice.

1. Since the measurements are carried out at (quasi-)steady state, we have $N \cdot v(x, u, e) = 0$. This introduces dependencies among the data and thus reduces the information content of the data matrix Y, in the sense that Y becomes rank deficient. Like in earlier work [Nikerel et al., 2009], we use standard approaches to solve this problem. We notably rely on Principal Component Analysis (PCA) [Jolliffe, 1986, Nikerel et al., 2009] applied to the data matrix Y to reduce the model order, *i.e.*, the number of independent parameters, and ensure well-posedness of the regression problem. Identifiability analysis will be discussed in detail in Chap. 4.

   Briefly, we use Singular Value Decomposition (SVD), a technique decomposing the data matrix into dominant and marginal components according to a variance criterion. For the purpose of linear regression, this corresponds to decomposing the parameter vector into a reduced number of components that can be determined with certainty based on the data, while the remaining components are poorly determined, *i.e.*, they are 'non-identifiable', and are discarded with negligible effect on the fit. We note in passing that the columns of W and Y are zero-mean, an important requirement for the correctness of the outlined analysis.

2. The high-throughput datasets contain a substantial amount of missing values, due to experimental limitations or instrument failures. If, for any given reaction, we only used the datapoints in which all relevant metabolite concentrations, enzyme concentrations, and metabolic fluxes playing a role in that reaction are available, then a large amount of data would have to be thrown away. In practice, we would run the risk that the parameters cannot be reliably identified. The development of a method that is capable of maximally exploiting the information contained in incomplete datasets for solving Problem 1 is the main subject of this chapter and will be fully developed in the later sections.

3.2 Likelihood-based identification of linlog models from missing data

For every reaction i, we are concerned with the problem of estimating the unknown parameters $b_{\cdot i}$ of the model given in (3.7) in the case where some entries of Y are unknown. We address the estimation problem by a likelihood-maximization approach, which is known to yield optimal (unbiased and minimum variance) estimates for our problem setting in the case where Y is fully known. As the problem is identical for all reactions i, in the remainder of the section we will drop for simplicity index $\cdot i$ from the notation.

Let $\mathscr{I}$ be the set of indices (row, column) corresponding to the known entries of Y, *i.e.*, $(j, k) \in \mathscr{I}$ if and only if $Y_{j,k}$ is available. It is convenient to introduce the decomposition

$Y = \check{Y} + \grave{Y}$, where

$$\check{Y}_{j,k} = \begin{cases} Y_{j,k}, & \text{if } (j,k) \in \mathscr{I}, \\ 0, & \text{otherwise;} \end{cases} \qquad \grave{Y}_{j,k} = \begin{cases} 0, & \text{if } (j,k) \in \mathscr{I}, \\ Y_{j,k}, & \text{otherwise.} \end{cases}$$

Matrix $\check{Y}$ is fully determined: Once measurements $\check{y}$ of $\check{Y}$ are collected, we treat $\check{Y} = \check{y}$ as fixed parameters of the regression problem. Matrix $\grave{Y}$ collects the unknown entries of Y. We model these missing data as unobserved independent random variables, whose prior distributions encode our generic knowledge about them. Assuming that the *a-priori* distributions are not known (worst case), we define a Gaussian prior for each quantity that is missing in an experiment based on the measurements of the same quantity available from other experiments. For every $(j,k) \notin \mathscr{I}$ and $\mathscr{Y}_{j,k} = \{Y_{j',k} : \ (j',k) \in \mathscr{I}\}$ (assumed nonempty), we let

$$\begin{cases} \grave{Y}_{j,k} \sim \mathscr{N}(\mu_{j,k}, \sigma_{j,k}^2), \\ \mu_{j,k} = \text{mean}(\mathscr{Y}_{j,k}), \\ \sigma_{j,k} = \text{std}(\mathscr{Y}_{j,k}). \end{cases} \tag{3.10}$$

We can now formulate the estimation problem.

Problem 2. *Given measurements* $W = w$ *and* $\check{Y} = \check{y}$*, compute the estimate* $\hat{b} = \arg\max_b \log \mathscr{L}(b)$*, with* $\mathscr{L}(b) = f_{W|\check{y},b}(w)$*, where, for any* b*,* $f_{W|\check{y},b}(\cdot)$ *is the probability density function of* W *given* $\check{Y} = \check{y}$ *corresponding to model* (3.7)–(3.10)*.*

Note that $\mathscr{L}(b)$ is a likelihood function for a linear model with missing data, in the sense that it is defined with respect to available data $\check{Y}$ only. One can express $\mathscr{L}(b)$ by marginalization,

$$\log \mathscr{L}(b) = \log \int f_{W|\check{y},\grave{y},b}(w) f_{\grave{Y}|\check{y},b}(\grave{y}) d\grave{y} \tag{3.11}$$

where $f_{W|\check{y},\grave{y},b}(\cdot)$ is the standard likelihood function for model (3.7) given $\check{Y} = \check{y}$ and $\grave{y}$, with $\grave{y}$ varying over all possible values of $\grave{Y}$, and $f_{\grave{Y}|\check{y},b}$ is determined by the prior (3.10). The explicit solution to the integral and the technical details of its computation are reported in Appendix A.1. A direct approach to solving Problem 2 is to maximize (3.11) by numerical optimization. However, the function is not convex in b, whence its direct optimization is prone to end up in local minima and the use of global optimization strategies is required.

Alternatively, we propose to tackle Problem 2 by an Expectation-Maximization (EM) algorithm [Dempster et al., 1977]. EM provides a general methodology for the optimization of a likelihood function with missing information. It is based on an iterative two-step procedure that, for the problem at hand, we implement as follows. Let us define the random variable $Z = \grave{Y} \cdot b$, so that model (3.7) becomes $W = \check{Y} \cdot b + Z + \varepsilon$. Note that $Z \sim \mathscr{N}(\mu_{\check{y},b}, \Sigma_{\check{y},b})$, where for any given b, mean and variance can be derived from (3.10). Let $\hat{b}^0$ be an initial guess of b. At every iteration $\ell = 1, 2, 3, \ldots$, compute an updated estimate $\hat{b}^\ell$ from the estimate $\hat{b}^{\ell-1}$ at the previous iteration by performing the following EM steps:

Expectation: Compute

$$\begin{aligned} Q(b|\hat{b}^{\ell-1}) &= \mathbb{E}[\log f_{Z,W|\check{y},b}(Z,w)|\check{y},\hat{b}^{\ell-1},w] \\ &= \int \log f_{Z,W|\check{y},b}(z,w) f_{Z|\check{y},\hat{b}^{\ell-1},w}(z)dz. \end{aligned} \tag{3.12}$$

Maximization: Solve

$$\hat{b}^{\ell} = \arg\max_{b} Q(b|\hat{b}^{\ell-1}). \tag{3.13}$$

In (3.12), $f_{Z,W|\check{y},b}$ is the joint probability density function of Z and W given $\check{Y} = \check{y}$ and b, while $f_{Z|\check{y},\hat{b}^{\ell-1},w}$ is the probability density function of Z given $\check{Y} = \check{y}$, $W = w$ and $\hat{b}^{\ell-1}$. In fact, this quantity is independent of w and can be computed by our definition (3.10).

It can be proven that, at every iteration ℓ, the EM algorithm increases the value of $\mathscr{L}(\hat{b}^{\ell})$, and eventually converges to a maximum of $\mathscr{L}$ [Little and Rubin, 2002]. While this is not necessarily a global maximum, EM has proven effective in many applications [Graham, 2009, Horton and Kleinman, 2007]. A key property is that convergence to a maximum is achieved even if (3.13) is not solved exactly: It suffices that $\hat{b}^{\ell}$ is such that $Q(\hat{b}^{\ell}|\hat{b}^{\ell-1}) \geq Q(\hat{b}^{\ell-1}|\hat{b}^{\ell-1})$, which is easily achieved even by a local optimization algorithm. In practice, we can use the explicit expression of $\mathscr{L}$ in Problem 2 for stopping the iterations, *e.g.*, when the relative improvement on $\mathscr{L}$ falls below a specified threshold $\tau > 0$:

$$|\mathscr{L}(\hat{b}^{\ell}) - \mathscr{L}(\hat{b}^{\ell-1})|/|\mathscr{L}(\hat{b}^{\ell})| \leq \tau.$$

To complete the implementation of the algorithm, one must express $Q(b|\hat{b}^{\ell-1})$ in a form convenient for maximization. One can express (3.12) as an explicit function of b for any given $\hat{b}^{\ell-1}$. The explanation of how to compute this function can be found in Appendix A.1. In compact form:

$$Q(b|\hat{b}^{\ell-1}) \propto -KL(f_b||f_{\hat{b}^{\ell-1}}) - H(f_{\hat{b}^{\ell-1}}) + \log(\kappa_{f_b}) \tag{3.14}$$

where f_b stands for a Gaussian distribution with variance $\Sigma_{f_b} = [\Sigma_{\varepsilon}^{-1} + \Sigma_{\check{y},b}^{-1}]^{-1}$ and mean $\mu_{f_b} = \Sigma_{f_b} \cdot (\Sigma_{\varepsilon}^{-1} \cdot (w - \check{y} \cdot b) + \Sigma_{\check{y},b}^{-1} \cdot \mu_{\check{y},b})$, κ_{f_b} is a function depending on b via μ_{f_b} and Σ_{f_b}, and the proportionality factor that we dropped (indicated by the presence of $\propto$ in place of $=$) depends on $\hat{b}^{\ell-1}$ but not on b. Finally, $KL(\cdot||\cdot)$ and $H(\cdot)$ are the Kullback-Leibler distance between distributions and the entropy of a distribution, respectively, for which, in the Gaussian case at hand, explicit formulas are available [Cover and Thomas, 2006, Stoorvogel and van Schuppen, 1996]. A slight technical complicacy is needed in case $\Sigma_{\check{y},b}$ is singular. One can refer to Appendix A.1 for all the mathematical details.

The availability of the closed-form expression (3.14) allows us to implement EM efficiently, *i.e.*, with an explicit maximization problem that is solved numerically at all iterations. Once the parameter estimates are obtained, several methods from the literature can be used to assess the accuracy of the results by inferring confidence intervals. Examples are randomized methods such as bootstrapping [Manly, 1997] and the profile likelihood method by Raue et al.

[2009]. This method derives confidence intervals using a threshold on a function called the profile likelihood. In our application, this is obtained separately for each parameter b_j by re-maximization of (3.11) with respect to all parameters $b_{k \neq j}$, for all values b_j in a neighborhood of $\hat{b}_j$.

3.3 Validation on simulated data

Before applying the EM algorithm to actual biological identification problems, we test the performance of the method on simulated data. For this purpose, a synthetic model has been developed, a simplified variant of the linlog model of *E. coli* central metabolism studied in Sec. 3.4 below. The model, in the form (3.2), contains 17 variables, representing internal and external metabolites involved in 25 reactions, and 78 parameters. The model equations are presented in Appendix A.2. We generate data matrices Y from this model by means of simulation, for different percentages of missing data and experimental noise. Using the model structure and the simulated data, we solve Problem 1 for each reaction independently, as described in Sec. 3.2.

In order to assess the added value of our specific implementation of likelihood optimization, we first compare the performance of the EM algorithm of Sec. 3.2 with the direct maximization of the loglikelihood (3.11) implemented with a general-purpose MATLAB optimization routine. This method will be referred to as MaxLL in the sequel.

Second, we compare the likelihood-based identification approaches with standard methods, notably linear regression (referred to as Rg) and the commonly-used multiple imputation (MI) method [Rubin, 1976, 1996]. Regression is performed based on full datasets only, *i.e.*, it does not consider an experimentally-determined datapoint (v^k, x^k, u^k, e^k) when at least one of the measurements is missing. MI is based on imputation of missing data by random draws of the missing values, *i.e.*, non-zero elements of $\grave{Y}$, from the *a-priori* distribution defined in (3.10). Both methods thus exploit only part of the information contained in an incomplete dataset and provide a lower limit for quantifying the performance of the methods proposed in Sec. 3.2.

Third, we compare the results of EM with the least-squares identification of the model on complete datasets (a method referred to as RgF, where F stands for Full datasets). Though inapplicable to real data with missing measurements, the method is statistically optimal. Hence, it provides us an upper performance bound that can be used to assess the role of missing data in performance degradation, separately from the role of noise.

Most of the high-throughput datasets available in the literature have been obtained when metabolism is at (quasi-)steady-state (Sec. 3.1). In order to mimic available experimental data as closely as possible, simulated data obtained from the synthetic model should therefore be steady-state data. We generated steady states of (3.1)-(3.2), and recorded the corresponding metabolite concentrations and metabolic flux values for 30 different conditions, each consisting of a random change in the enzyme concentration with respect to a reference value.

We compared performance of the five methods described above (EM, MaxLL, MI, Rg, RgF) on datasets with different amounts of missing data (40% and 75%) for the metabolite concentrations and noise levels (10% and 20%) for w. The only difference with the dataset used for the reference method RgF is that the latter has no missing data. A noise level of 10% means that the distribution used to generate the noise has a standard deviation equal to 10% of the values in w. The percentages of missing data in the simulation study are comparable to those observed in practice (Sec. 3.4 and [Ishii et al., 2007]). For every different combination of missing data percentage and noise level, a dataset was generated by homogeneously distributing missing data among columns of Y, the indices for each column being chosen at random. For every simulated scenario, randomly generated noise was added to w in the dataset.

For all of the above scenarios, identification of each reaction was addressed separately, in accordance with the discussion of Sec. 3.1. For every reaction, we first tested the identifiability of the synthetic linlog model by PCA of the full data matrix Y. In our simulation, 9 reactions out of the 25 composing the model were detected as having nonidentifiable parameters. For those reactions, identification of a reduced-order model

$$w = \breve{Y} \cdot \breve{b} + \varepsilon \tag{3.15}$$

was performed in place of the identification of the original model. $\breve{Y} \in \mathbb{R}^{q \times r}$, with $r \leq n_x + n_u$, is a reduced-order data matrix obtained by linear transformation of Y, and $\breve{b} \in \mathbb{R}^r$ is a parameter vector, smaller than b, that is ‘identifiable’, in the sense that it is well determined by the data (see Appendix A.2).

We implemented the different parameter estimation algorithms in Matlab, using the `lscov` function for the regression-based methods and `fminsearch` for global optimization in MaxLL and the maximization step in EM. Both EM and MaxLL require an initial guess of the parameters to be specified. We proposed 10 different initial parameter vectors, including the estimation obtained with the baseline method Rg where available. In order to draw statistics for the estimation performance, each of the five algorithms was applied on 100 Monte-Carlo repetitions of the identification problem. The complete performance test over all methods, conditions and 100 repetitions took about 7 h 40 min in Matlab 7.4.0 on a Linux PC workstation (1862 MhZ, 2 Gb RAM).

The most informative results from all identification methods are summarized by boxplots of the ratio of the estimated parameter values b over the reference parameter values b_{ref} used to simulate the data. The closer the ratio to 1, the better the estimates. Ensemble statistics are drawn for all parameters corresponding to the same reaction. Fig. 3.1 is dedicated to the scenario with 40% missing data and 10% noise, whereas Fig. 3.2 reports on 75% missing data and 20% noise. Complete results for all reactions under all conditions are reported in

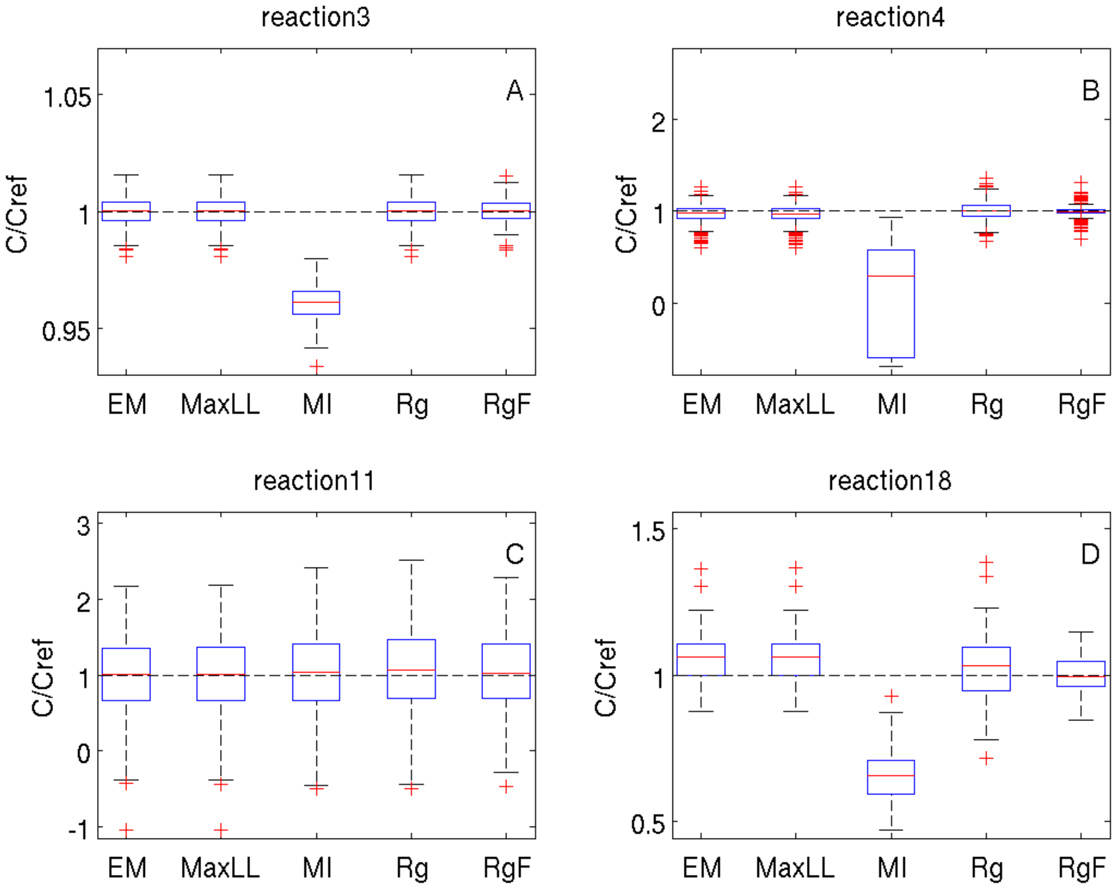

Figure 3.1: Statistics of estimated parameter values for datasets with 40% of missing data and 10% noise. The results are shown as boxplots of the ratio of the estimated parameter values b and reference parameter values b_{ref}. Statistics have been computed for each of the 5 methods from 100 datasets. For each method, the red line displays the median and the lower and upper blue lines represent the lower and upper quartile values, respectively. Whiskers extend from each end of the box to the most extreme values within 1.5 times the interquartile range from the ends of the box and outliers are shown with red crosses. The tested algorithms are Expectation Maximization (EM), direct optimization of loglikelihood (MaxLL), multiple imputation (MI), regression on incomplete datasets (Rg) and regression on complete datasets (RgF). (A–D) Boxplots for reactions 3, 4, 11 and 18 of the network, respectively.

Appendix A.2.

Since the individual reactions of the model involve only a small subset of metabolites, each of the m identification subproblems consists of the estimation of a limited number of parameters, mostly 2 or 3. For the case with 40% missing data, Rg can therefore be performed in all runs for every reaction of the model. On the contrary, with 75% missing data, regression

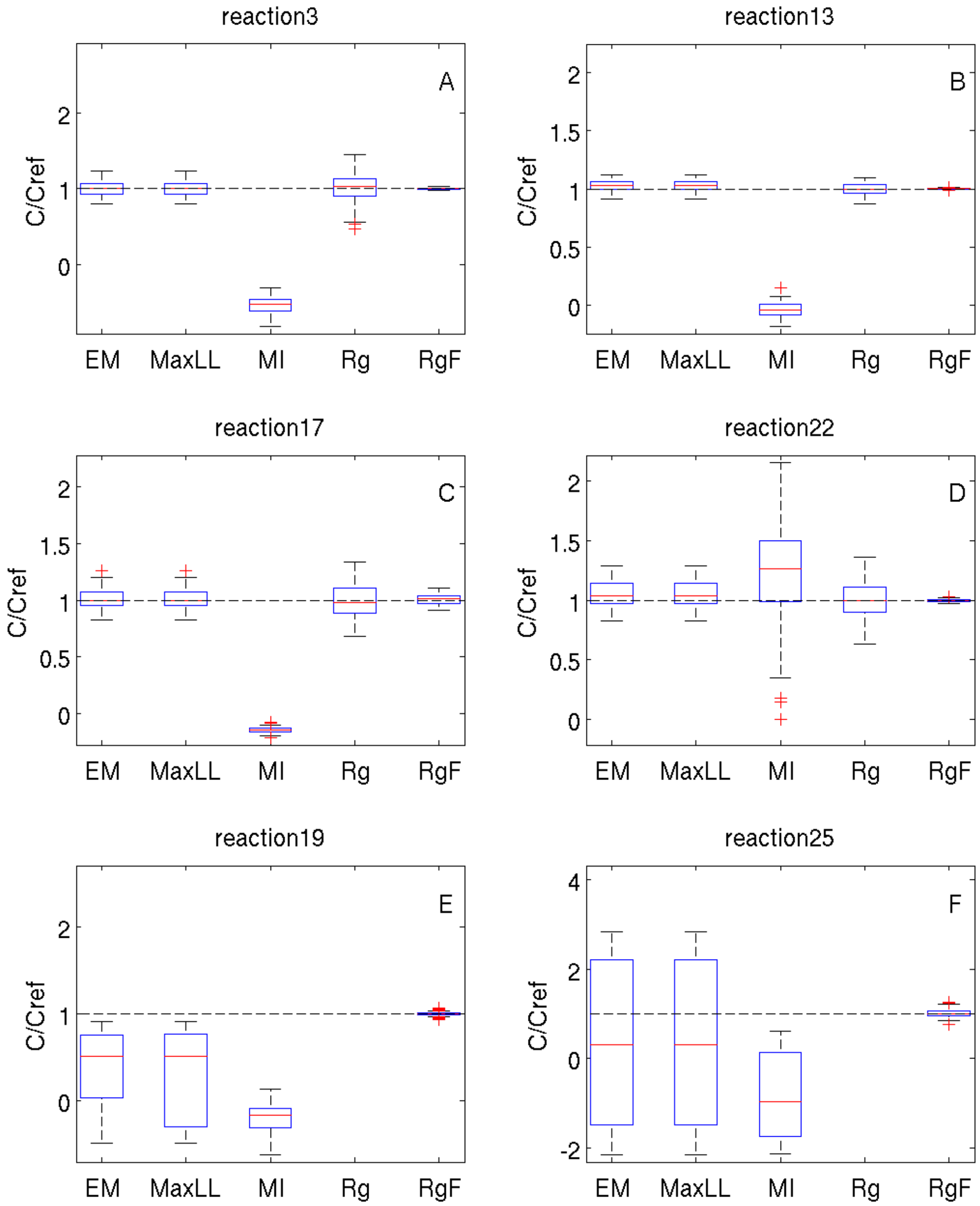

Figure 3.2: Statistics of estimated parameter values for datasets with 75% of missing data and 20% noise. The graphical notations are the same as for Fig. 3.1. (A–F) Boxplots for reactions 3, 13, 17, 22, 19 and 25 of the network, respectively.

cannot be applied to 6 reactions which is apparent from the absence of the Rg statistics for 2 reactions in Fig. 3.2.

In comparison with the other methods, multiple imputation (MI) gives the worst results (largest bias) in 3 out of the 4 reactions shown in Fig. 3.1, and in 5 out of 6 reactions in Fig. 3.2. In reactions 11 of Fig. 3.1 and 22 of Fig. 3.2, the relatively small biases are accompanied by an estimation uncertainty wider than for EM and MaxLL. This could be explained by a restricted use of information contained in the distribution of missing data. Indeed, MI only considers random draws from the distribution while EM and MaxLL are based on all possible values taken by missing data through integration of the distribution.

Analysis of Fig. 3.1 reveals that, for 40% missing data and 10% noise, the performance of EM and MaxLL is almost identical and similar to that of regression (Rg and RgF), with limited improvements on Rg, *i.e.*, slightly smaller variability. In some cases, such as for reactions 11 and 18, their performance approaches the optimal, unattainable bound provided by RgF, *i.e.*, they have similar bias and variability.

Performance improvements of likelihood-based methods over Rg become more significant when identification is performed on the dataset with higher percentage of missing data and larger noise. Fig. 3.2A-D show results for reactions where Rg was applicable. Both EM and MaxLL substantially reduce estimation variability in reactions 3, 17 and 22. At the same time, due to the larger amount of missing data, performance loss with respect to RgF is more significant. Turned another way, this shows the accuracy that could be recovered were all datasets complete.

Fig. 3.2E-F show the results when Rg fails to produce estimates and cannot be used to initialize EM and MaxLL optimization. Still, EM provides estimates of the right order of magnitude and, for the case of Fig. 3.2E, of the right sign in at least 75% of the runs (box entirely above 0), while the median has the right sign and is reasonably close to 1. The estimation of the sign provided by MaxLL is less reliable (box crossing 0).

Overall, we conclude that the EM-based approach provides the most accurate estimates under all simulated conditions. We will therefore apply this method to the identification of the linlog model of an actual metabolic network from a published high-throughput dataset.

3.4 Application to central metabolism in *E. coli*

The network we consider here gathers enzymes, metabolites and reactions that make up the bulk of *E. coli* central carbon metabolism, including glycolysis, the pentose-phosphate pathway, the tricarboxylic acid cycle and anaplerotic reactions such as glyoxylate shunt and PEP-carboxylase (Fig. 3.3).

The dataset used for identification of this network was obtained by experiments with 24 single-gene mutants that were grown at a fixed dilution rate of 0.2 h^{-1} in a glucose-limited chemostat, and with wild-type cells at 5 different dilution rates [Ishii et al., 2007]. The

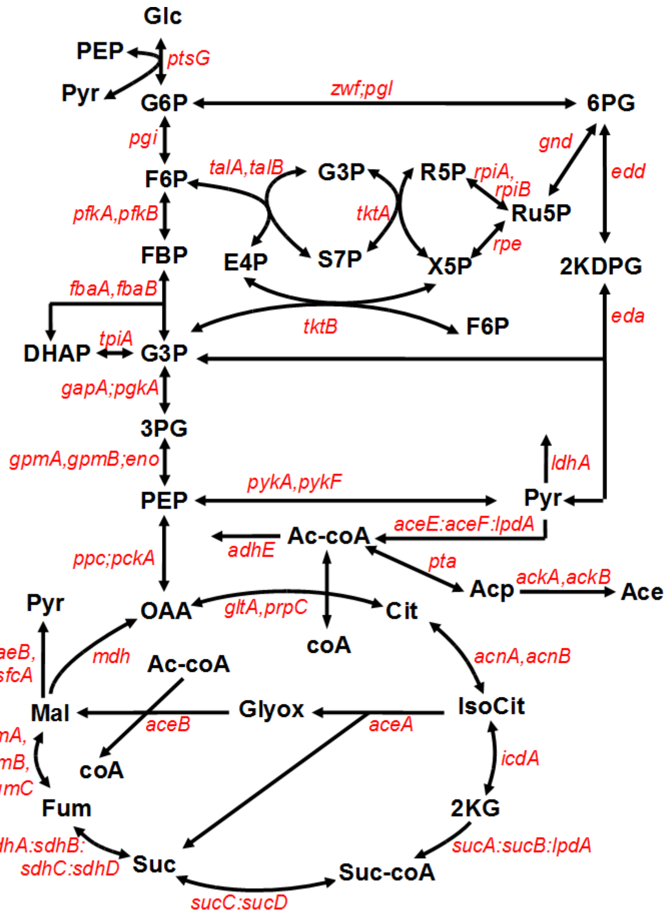

Figure 3.3: Scheme of *Escherichia coli* central carbon metabolism. This map, showing metabolites (bold fonts) and genes (italic) is adapted from [Ishii et al., 2007]. Abbreviations of metabolites are glucose (Glc), glucose 6-phosphate (G6P), fructose 6-phosphate (F6P), fructose 1-6-biphosphate (FBP), dihydroxyacetone phosphate (DHAP), glyceraldehyde 3-phosphate (G3P), 3-phosphoglycerate (3PG), phosphoenolpyruvate (PEP), pyruvate (Pyr), 6-phosphogluconate (6PG), 2-keto-3-deoxy-6-phosphogluconate (2KDPG), ribulose 5-phosphate (Ru5P), ribose 5-phosphate (R5P), xylulose 5-phosphate (X5P), sedoheptulose 7-phosphate (S7P), erythrose 4-phosphate (E4P), oxaloacetate (OAA), citrate (Cit), isocitrate (IsoCit), 2-keto-glutarate (2KG), succinate-CoA (SuccoA), succinate (Suc), fumarate (Fum), malate (Mal), glyoxylate (Glyox), acetyl-CoA (Ac-coA), acetylphosphate (Acp) and acetate (Ace). Cofactors impacting the reactions are not shown. The gene names are separated by a comma in the case of isoenzymes, by a colon for enzyme complexes, and by a semicolon when the enzymes catalyze reactions that have been lumped together in the model.

authors collected data using multiple high-throughput techniques, in particular DNA microarray analysis and two-dimensional differential gel electrophoresis (2D-DIGE) for genes and proteins, capillary electrophoresis time-of-flight mass spectrometry (CE-TOFMS) for metabolites, and metabolic flux analysis. They thus obtained a dataset consisting of metabolite concentrations, mRNA and protein concentrations for the enzymes, and metabolic fluxes under 29 different experimental conditions. A large number of different metabolites were measured in the experiments, with missing data in varying amounts, from 0 to 80% of the observations, 28% on average for the metabolites considered below.

From the reactions listed in [Ishii et al., 2007], we have constructed a linlog model of the form (3.2). The (simplified) network of central carbon metabolism in *E. coli* shown Fig. 3.3 could not be directly transformed into a linlog model of the form (3.1)-(3.2), since metabolites G3P, E4P, X5P, 2KDPG, OAA, IsoCit, SuccoA, Acp and Glyox were not measured by Ishii et al. [2007]. This precludes estimation of the corresponding elements in the parameter matrices B^x and B^u and thus, their inclusion in the model. We overcome this limitation by simplifying or lumping reactions when a shared metabolite has not been measured by Ishii et al. [2007]. Each of the reactions is catalyzed by a single enzyme, which may actually stand for several enzymes in the case of isoenzymes, enzyme complexes, or lumped reactions. In addition to these simplifications imposed by the available dataset, we added a phenomenological reaction μ to model biomass production. The reaction involves 11 metabolites, its reaction flux is equal to the dilution rate under the experimental conditions of Ishii et al. [2007] and the enzyme concentration is set to 1.

The linlog model thus obtained contains $n_x = 16$ internal metabolites, $n_u = 7$ external metabolites or cofactors, listed in Table 3.1, and $m = 31$ reactions, listed in Table 3.2. In comparison with an earlier linlog model of *E. coli* central carbon metabolism [Visser et al., 2004], we extended the scope to include the tricarboxylic acid cycle and the glyoxylate shunt, but due to the above-mentioned simplifications our model is more coarse-grained.

An identifiability analysis was performed by several rounds of missing data imputation using the *a-priori* distribution defined in Eq. (3.10) and PCA, which led in each case to the same result: 7 out of 31 reactions were detected as having nonidentifiable parameters. For those reactions, the model has been reduced as described in Eq. (3.15) using a data matrix Y completed by the means $\mu_{j,k}$ of the *a-priori* distributions. For every individual reaction, the reduced model has a parameter vector $\breve{b}$ that is now entirely identifiable.

Apart from the distribution of the *a-priori* missing data, given by Eq. (3.10), application of EM requires information about the distribution of ε, the error on the ratios of fluxes and enzyme concentrations. The Ishii dataset provides several replica measurements for a reference experimental condition: wild-type cells grown in a glucose-limited chemostat with a dilution rate of 0.2 h^{-1}. These data were used for the computation of the variance of ε. In order to assess the accuracy of the estimated B^x and B^u, we computed for each

Internal metabolites			
Index	Symbol	Index	Symbol
1	PEP	9	Ru5P
2	G6P	10	R5P
3	Pyr	11	S7P
4	F6P	12	2KG
5	FBP	13	Suc
6	DHAP	14	Fum
7	3PG	15	Mal
8	6PG	16	Cit

Index	External metabolites or cofactors
17	Glc
18	Ac-coA/coA
19	ATP/ADP
20	NADPH/NADP
21	NADH/NAD
22	FAD
23	Ace

Table 3.1: Internal and external metabolites and cofactors of the linlog model of carbon metabolism in *E. coli.* Some of the cofactors are modeled as ratios of metabolite concentrations, *e.g.,* ATP/ADP.

parameter a 95% confidence interval, by means of the profile likelihood method outlined in Sec. 3.2. Running the EM method on the model and the data took about 220 s using the implementation of Sec. 3.3. The computation of the confidence intervals for all parameters required about 23 min.

Contrary to the simulation studies reported in Sec. 3.3, a reference or 'real' model for the evaluation of the results does not exist in this case. However, *a-priori* biochemical knowledge on the signs of the elasticities is available, *i.e.*, elasticities are positive for substrates and negative for products. This information can be compared with the estimated signs of the elasticities, and their confidence intervals, computed from the parameter matrices using the relations in Eq. (3.9). The results are shown in Table 3.3. Similar unshown results are obtained by means of the MaxLL method.

We observe that the EM method obtains estimates for all reactions, including the 7 cases where the insufficient amount of data made regression not applicable. However, 26 of the 100 non-zero elasticities of the model are not identifiable from this dataset. Moreover, out of the remaining 74 elasticity estimates, more than half of them have signs that are not statistically significant, in the sense that the 95% confidence interval straddles 0. This is most likely due to the fact that the magnitude of noise in metabolite concentrations is comparable to the magnitude of relevant information. For example, for PEP the standard deviation over all experimental conditions equals the standard deviation of the replicates in a single condition (0.06 mM vs 0.05 mM). This precludes the estimation of an unambiguous sign.

Of the elasticities with statistically significant signs, 20 out of 34 are correct, in the sense that they have the expected positive or negative sign. The remaining elasticities, distributed over 9 reactions, are incorrectly estimated. Let us now discuss what we believe are potential sources of these errors, giving information that could be used to single out erroneous estimates

Index	Reaction
1	Glc + PEP $\xleftrightarrow{ptsG}$ Pyr+G6P
2	G6P $\xleftrightarrow{pgi}$ F6P
3	F6P + ATP/ADP $\xleftrightarrow{pfkA,pfkB}$ FBP $[\text{PEP}]_{in}$
4	FBP $\xleftrightarrow{fbaA,fbaB}$ DHAP
5	DHAP $\xleftrightarrow{tpiA}$ 3PG
6	FBP + ATP/ADP $\xleftrightarrow{gapA;pgk}$ 3PG + NADH/NAD
7	3PG $\xleftrightarrow{gpmA,gpmB;eno}$ PEP
8	PEP + ATP/ADP $\xleftrightarrow{pykA,pykF}$ Pyr $[\text{FBP}]_{act}$
9	Pyr $\xleftrightarrow{aceE:aceF:lpdA}$ Ac-coA/coA + NADH/NAD
10	G6P $\xleftrightarrow{zwf;pgl}$ 6PG + NADPH/NADP
11	6PG $\xleftrightarrow{gnd}$ Ru5P + NADPH/NADP
12	Ru5P $\xleftrightarrow{rpe}$ S7P
13	Ru5P $\xleftrightarrow{rpiA,rpiB}$ R5P $[\text{G6P}]_{in}$
14	R5P $\xleftrightarrow{tktA}$ S7P
15	S7P $\xleftrightarrow{talA,talB}$ F6P
16	Ru5P $\xleftrightarrow{tktB}$ F6P
17	Ac-coA/coA $\xleftrightarrow{gltA,prpC}$ Cit $[\text{2KG}]_{in}$ $[\text{NADH/NAD}]_{act}$
18	Cit $\xleftrightarrow{acnA,acnB}$ 2KG
19	Ac-coA/coA $\xleftrightarrow{icdA}$ 2KG + NADPH/NADP
20	2KG $\xleftrightarrow{sucA:sucB:lpdA;sucC:sucD}$ Suc + NADH/NAD
21	Suc + FAD $\xleftrightarrow{sdhA:sdhB:sdhC:sdhD}$ Fum
22	Fum $\xleftrightarrow{fumA,fumB,fumC}$ Mal
23	Mal + PEP $\xleftrightarrow{mdh}$ Cit +NADH/NAD
24	PEP $\xleftrightarrow{ppc;pckA}$ Mal + Cit + ATP/ADP $[\text{FBP}]_{act}$
25	Mal $\xleftrightarrow{maeB,sfcA}$ Pyr + NADPH/NADP $[\text{Ac-coA/coA}]_{in}$ $[\text{NADH/NAD}]_{act}$
26	Ac-coA/coA $\xleftrightarrow{aceA;aceB}$ Suc + Mal
27	PEP+G6P+Pyr+F6P+3PG+Ac-coA/coA+R5P+2KG+ATP/ADP $\xrightarrow{\mu}$NADPH/NADP+NADH/NAD
28	6PG $\xleftrightarrow{edd;eda}$ Pyr
29	Ac-coA/coA $\xleftrightarrow{pta;ackA,ackB}$ Ace+ATP/ADP $[\text{Pyr}]_{act}$ $[\text{NADPH/NADP}]_{in}$ $[\text{NADH/NAD}]_{in}$
30	Pyr + NADH/NAD $\xrightarrow{ldhA}$
31	Ac-coA/coA $\xrightarrow{adhE}$

Table 3.2: Reactions of the linlog model of carbon metabolism in *E. coli.* Activators and inhibitors of the reaction are shown with $[\cdot]_{act}$ and $[\cdot]_{in}$, respectively. Reaction 27, labeled μ, is a phenomenological reaction for biomass production. The enzyme names are separated by a comma in the case of isoenzymes, by a colon for enzyme complexes, and by a semicolon when the enzymes catalyze reactions that have been lumped together in the model. Reactions 20, 26, 28 and 29 result from the merging of reactions due to the absence of measurements of SuccoA, Glyox, 2KDPG and Acp, respectively, in the dataset of Ishii et al. [2007].

Table 3.3: Elasticity matrix $[B_0^x \;\; B_0^u]$ estimated by EM from the data of [Ishii et al., 2007] for the linlog model of *E. coli* central carbon metabolism (the columns of the matrix have been permuted for readability). Unidentifiable elasticities are shown in gray, uncertain elasticities (*i.e.*, having a sign that is not significant with 95% confidence) in yellow, and correctly/incorrectly identified elasticities (*i.e.*, having a sign that is significant with 95% confidence) in green/red. Abbreviations are as in Fig. 3.3. Some of the cofactors are modeled as ratios of metabolite concentrations, *e.g.* ATP/ADP. Reaction 27, labeled μ, is a phenomenological reaction for biomass production. The last row indicates the percentage of missing data per metabolite and the right-most column displays the amount of complete datapoints available for each reaction. For reactions labeled with *, regression was not able to produce any result.

	Metabolite Enzyme	Glc	PEP	G6P	Pyr	F6P	FBP	DHAP	3PG	Ac-coA	6PG	Ru5P	R5P	S7P	2KG	Suc	Fum	Mal	ATP	Cit	NADPH	NADH	FAD	Ace	# complete
										coA									ADP		NADP	NAD			datapoints
1	PtsG	0.29	-0.89	0.79	1.87	0	0	0	0	0	0	0	0	0	0	0	0	0	0	0	0	0	0	0	14
2	Pgi	0	0	-0.33	0	0.23	0	0	0	0	0	0	0	0	0	0	0	0	0	0	0	0	0	0	27
3	PfkA,PfkB	0	-0.16	0	0	0.04	-0.28	0	0	0	0	0	0	0	0	0	0	0	0.09	0	0	0	0	0	18
4	FbaA,FbaB	0	0	0	0	0	-0.3	0.06	0	0	0	0	0	0	0	0	0	0	0	0	0	0	0	0	8
5	TpiA	0	0	0	0	0	0	-0.07	0.22	0	0	0	0	0	0	0	0	0	0	0	0	0	0	0	12
6	GapA;Pgk	0	0	0	0	0	-0.18	0	-0.05	0	0	0	0	0	0	0	0	0	0.32	0	0	-0.17	0	0	5
7	GpmA,GpmB;Eno	0	0.26	0	0	0	0	0	-0.12	0	0	0	0	0	0	0	0	0	0	0	0	0	0	0	24
8	PykA,PykF	0	0.12	0	0.49	0	-0.19	0	0	0	0	0	0	0	0	0	0	0	0.16	0	0	0	0	0	11
9	AceE:AceF:LpdA	0	0	0	0.64	0	0	0	0	0.05	0	0	0	0	0	0	0	0	0	0	0	-0.21	0	0	6
10	Zwf;Pgl	0	0	-0.22	0	0	0	0	0	0	-0.24	0	0	0	0	0	0	0	0	0	-0.01	0	0	0	2
11	Gnd	0	0	0	0	0	0	0	0	0	0.48	-0.09	0	0	0	0	0	0	0	0	-0.01	0	0	0	2*
12	Rpe	0	0	0	0	0	0	0	0	0	0	0.46	0	-0.39	0	0	0	0	0	0	0	0	0	0	28
13	RpiA,RpiB	0	0	-0.74	0	0	0	0	0	0	0	0.3	-0.16	0	0	0	0	0	0	0	0	0	0	0	18
14	TktA	0	0	0	0	0	0	0	0	0	0	0	0.01	-0.1	0	0	0	0	0	0	0	0	0	0	18
15	TalA,TalB	0	0	0	0	-0.32	0	0	0	0	0	0	0	0.51	0	0	0	0	0	0	0	0	0	0	27
16	TktB	0	0	0	0	-0.58	0	0	0	0	0	0.35	0	0	0	0	0	0	0	0	0	0	0	0	27
17	GltA,PrpC	0	0	0	0	0	0	0	0	0.22	0	0	0	0	-0.001	0	0	0	0	0.49	0	-0.01	0	0	1*
18	AcnA,AcnB	0	0	0	0	0	0	0	0	0	0	0	0	0	0.99	0	0	0	0	0.55	0	0	0	0	5
19	IcdA	0	0	0	0	0	0	0	0	0.08	0	0	0	0	-0.09	0	0	0	0	0	-0.59	0	0	0	4
20	SucA:SucB:LpdA;SucC:SucD	0	0	0	0	0	0	0	0	0	0	0	0	0	1.26	0.3	0	0	0	0	0	-0.48	0	0	2*
21	SdhA:SdhB:SdhC:SdhD	0	0	0	0	0	0	0	0	0	0	0	0	0	0	1.08	-0.44	0	0	0	0	0	0.4	0	21
22	FumA,FumB,FumC	0	0	0	0	0	0	0	0	0	0	0	0	0	0	0	0.46	0.1	0	0	0	0	0	0	25
23	Mdh	0	0.15	0	0	0	0	0	0	0	0	0	0	0	0	0	0	-0.01	0	0.31	0	-0.12	0	0	3*
24	Ppc;PckA	0	0.29	0	0	0	-0.13	0	0	0	0	0	0	0	0	0	0	0.1	-1.15	0.21	0	0	0	0	9
25	MaeB,SfcA	0	0	0	-0.31	0	0	0	0	-0.21	0	0	0	0	0	0	0	0.38	0	0	0.36	-0.05	0	0	2*
26	AceA;AceB	0	0	0	0	0	0	0	0	-0.11	0	0	0	0	0	0.26	0	-0.18	0	0	0	0	0	0	25
27	μ	0	0.1	-0.09	0.04	-0.06	0	0	0.17	0.1	0	0	0.09	0	-0.01	0	0	0	-0.46	0	-0.003	0.01	0	0	0*
28	Edd;Eda	0	0	0	-0.03	0	0	0	0	0	-0.93	0	0	0	0	0	0	0	0	0	0	0	0	0	5
29	Pta;AckA,AckB	0	0	0	-0.06	0	0	0	0	-0.01	0	0	0	0	0	0	0	0	0.21	0	-0.25	-2.03	0	2.19	2*
30	LdhA	0	0	0	2.67	0	0	0	0	0	0	0	0	0	0	0	0	0	0	0	0	-0.11	0	0	6
31	AdhE	0	0	0	0	0	0	0	0	0.91	0	0	0	0	0	0	0	0	0	0	0	0	0	0	28
	% Missing Data	3	17	0	48	7	34	59	10	3	72	3	38	3	59	3	14	14	0	62	79	79	17	17	

a-priori.

We first note that for 3 of these 9 reactions (GapA;Pgk, Mdh and Edd;Eda, see Table 3.3), only very few complete datapoints are available (between 3 and 5) and regression mostly fails in these cases. In addition, all of these reactions involve at least one metabolite missing in more than 70% of the experimental conditions. The combination of very few complete datapoints and a high percentage of missing metabolite measurements obviously makes model identification extremely difficult and it is fair to say that here we reach the limit of the applicability of our method, or of any method for that matter, due to the lack of data.

Second, 4 reactions are known to operate close to equilibrium: Pgi, FbaA,FbaB, TpiA and GpmA,GpmB;Eno [Visser et al., 2004]. Theoretically, these reactions are not identifiable, as their elasticities are not independent [Visser et al., 2004], but PCA did not detect this. Most likely, this is due to the above-mentioned noise in metabolite concentrations, which decreases their correlations. A cautious, preemptive strategy would be to reduce the model for any reaction known to be close to equilibrium and eliminate the corresponding dependent variables.

The errors in the signs of some elasticities in the remaining 2 reactions (PtsG and PykA,PykF) are less straightforward to explain. It is unlikely that they can be attributed to the EM method, given that regression is applicable here with a relatively large number of complete datapoints available (14 and 11, respectively) and gives the same results. Alternatively, they may be explained by a modeling error or a hidden variable, for instance an unknown cofactor, biasing the estimation results. It is also possible that the approximations of the linlog model are not suitable for these reactions, for instance because there are large variations in metabolite concentrations between conditions, driving the system far from the reference state.

In summary, EM gives reasonable results for a fairly complicated model on a challenging dataset. Even though some puzzling issues remain, we believe that these can be safely attributed to the inherent difficulty of the identification problem.

3.5 Discussion

In this chapter we have addressed the problem of estimating parameters of approximate models of metabolic networks from incomplete datasets. Even with the largest datasets available at present, such as those reported in [Ishii et al., 2007], the absence or corruption of a large number of measurements may reduce the effective number of datapoints to a handful of experimental conditions, thus making simple regression techniques ineffective or even inapplicable. Making full use of all the available data is therefore essential to render identification well-posed and improve the quality of the estimated models.

To this aim, we have proposed a maximum-likelihood method for the identification of linlog metabolic network models that compensates for the missing data by the use of statistical priors. We developed an algorithm that attains maximization of the likelihood based on Expectation Maximization, a well accepted paradigm for the numerical optimization of likelihood functions in the presence of unobserved variables. A simpler implementation based on direct likelihood maximization via general-purpose numerical optimization algorithms was also considered and found slightly less powerful. The performance of EM was compared to that of an existing method of reference, namely multiple imputation, and to worst-case and best-case scenarios given by least-squares regression on the sole complete datapoints and on complete datasets, respectively. We showed that EM outperforms multiple imputation by a wide margin. In comparison with worst-case regression, it reduces the estimation variability and is able to produce reasonable estimation results even when regression on incomplete datasets is inapplicable. It also approaches the ideal performance of regression on complete datasets for low rates of missing data, regardless of noise.

Based on these findings, we applied EM to the identification of a linlog model for the central carbon metabolism in *E. coli* from the experimental data presented by Ishii et al. [2007]. Even with the large amount of incomplete datapoints, due to the difficulty of experimentally measuring metabolite concentrations, EM was able to estimate many of the model parameters (elasticities) in agreement with the current understanding of the system. This is even true for reactions where the reduced number of complete datapoints impairs the applicability of least squares regression. On the other hand, the challenging quality of the data sheds light on the performance limits of the method, which tends to fail when large measurement noise makes the estimation of small parameters statistically unreliable, when the same variable cannot be measured in most conditions, or when reactions operate near equilibrium.

Overall, results from the simulations and the application on real data showed that our EM approach is able to make the most of incomplete, noisy high-throughput datasets for the estimation of parameters in approximate kinetic models. In the future, we expect to improve performance by developing a number of technical points, including approximate analytical/dedicated numerical solutions for the EM maximization steps and a more detailed modeling of measurement noise. It is worth noting that, while the method has been developed for linlog models, it is more generally applicable to any other metabolic network model that can be put in a form linear in the parameters by straightforward manipulations, such as generalized mass action models that provide advantages when some metabolite concentrations approach 0 [Savageau, 1976, del Rosario et al., 2008]. In addition, estimated parameters of approximate metabolic models, such as elasticities of linlog models, provide useful hints for the identification of more detailed nonlinear kinetic models.

From a broader perspective, the application of the EM method to the unique multi-omics dataset for *E. coli* carbon metabolism allowed us to isolate issues that are critical for the appropriate exploitation of the data for parameter estimation. These issues may need to be taken into account during the design of the experiments. One such issue is that a high percentage of missing data for some of the individual variables, even at a relatively low average percentage over the entire dataset, was found to be much detrimental to the identification results. This may influence sampling strategies, especially for metabolites that are difficult to measure.

Another issue is the identifiability problems caused by steady-state measurements, which cannot always be resolved by genetic mutation or by varying physiological conditions. From this perspective time-resolved observations of the network dynamics, although much more demanding experimentally, carry great promise [Hardiman et al., 2007]. We discuss these identifiability issues in detail in the next chapter.

Chapter 4

Identifiability of linlog metabolic models

A major and often overlooked problem in parameter estimation is the identifiability of the model, that is, the problem of unambiguously reconstructing the unknown parameter values from the observed network behavior. In the context of approximate kinetic models, we address the key problem of the identifiability of biochemical networks in a principled and scalable way. We focus on the case where the structure of the model is fixed by *a-priori* knowledge on the network (*i.e.*, the chemical species considered, the reactions among them and the eventual regulatory interactions), and discuss the identifiability of the model parameters. That is, we are interested in the problem of unambiguously reconstructing the unknown parameter values from the observed network behavior.

A distinction is usually made between structural (or *a-priori*) and practical (or *a-posteriori*) identifiability [Ljung, 1999, Walter and Pronzato, 1997]. Structural identifiability is an intrinsic property of the model family, guaranteeing that unique parameter reconstruction would be possible from perfect observations of the system response to an arbitrarily rich set of inputs. Practical identifiability refers to the ability of estimating unknown parameter values from the available experimental data within a prespecified degree of accuracy. In classical control theory, this concept is essentially related to the notion of persistence of excitation [Ljung, 1999]. Unfortunately, limitations in the variety and quality of the observed inputs and outputs that can be obtained make this notion inapplicable to biological applications. In recent years, the topic of identifiability has gained considerable interest in the field of systems biology [Ashyraliyev et al., 2009, Nikerel et al., 2009, Chis et al., 2011b, Chen et al., 2010, Raue et al., 2009, 2011, Srinath and Gunawan, 2010, Jaqaman and Danuser, 2006, Gutenkunst et al., 2007, Nemcova, 2010, Voit et al., 2006a] and several specialized software packages have been developed to support the modeler [Chis et al., 2011a, Maiwald and Timmer, 2008]. Despite these efforts, however, no common agreement on definitions and links between structural and practical identifiability exist to date.

The aim of this chapter is to develop methods for the analysis of the (parameter) identifiability of kinetic models of metabolism, and for the reduction of non-identifiable models to identifiable approximations. These methods should have a solid mathematical foundation, but at the same time be applicable to practical problems and currently available data sets, such as those obtained by means of recent high-throughput methods in biology [Ishii et al., 2007]. While many of our definitions are of general applicability, identifiability results will be developed primarily for linlog models, whose pseudo-linear form enables us to apply tools from linear algebra and estimation theory in a straightforward manner. Similar results can be derived easily for many other approximate kinetic modeling formalisms in pseudo-linear form, such as the linear, loglin and generalized mass-action kinetic formats [Delgado and Liao, 1992, Hatzimanikatis and Bailey, 1997, Savageau, 1976].

The main contributions of the chapter are threefold. First, we precisely define the notions of structural and practical identifiability of approximate kinetic models, drawing upon the systems identification literature. This conceptual clarification allows us to develop the relations between structural and practical identifiability in a fundamental way. Second, we show how model reduction using singular value decomposition (SVD) [Jolliffe, 1986] provides a suitable theoretical framework for addressing identifiability problems. We discuss several different criteria for model reduction, based on the singular values returned by the SVD analysis, and we show to which extent these criteria are appropriate for dealing with actual biological data sets, which are typically scarce, noisy and incomplete. Third, we apply the methods for identifiability analysis and model reduction to both simulated data and the dataset of Ishii et al. [2007] concerning central metabolism in *E. coli.* These examples show that the mathematical tools developed in this chapter are of practical utility for the estimation of parameters in models of metabolic networks and beyond, from current high-throughput data sets. In order to simplify the reading of the main text, the proofs of all theoretical results are reported in Appendix B.1.

4.1 Parameter estimation in linlog and other approximate kinetic modeling formalisms

We recall the general ODE form of kinetic models of biochemical networks and the linlog formulation for metabolic models:

$$\dot{x} = N \cdot v(x, u, e), \tag{4.1}$$

$$v(x, u, e) = \mathrm{diag}(e) \cdot \big(a + B^x \cdot \ln x + B^u \cdot \ln u\big) \tag{4.2}$$

where $x \in X \subseteq \mathbb{R}^{n_x}_{>0}$ denotes the vector of (nonnegative) internal metabolite concentrations, $u \in U \subseteq \mathbb{R}^{n_u}_{>0}$ the vector of external metabolite concentrations, $e \in E \subseteq \mathbb{R}^{m}_{>0}$ the vector of enzyme concentrations, and $v : \mathbb{R}^{n_x+n_u+m}_{>0} \to V$, with $V \subseteq \mathbb{R}^m$, the vector of reaction rate

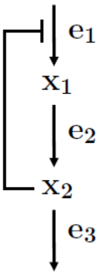

(a)

$$
\begin{aligned}
v_1 &= e_1 \cdot (a_1 + B^x_{1,1} \ln x_1 + B^x_{1,2} \ln x_2)\\
v_2 &= e_2 \cdot (a_2 + B^x_{2,1} \ln x_1 + B^x_{2,2} \ln x_2)\\
v_3 &= e_3 \cdot (a_3 \qquad\qquad\quad + B^x_{3,2} \ln x_2)
\end{aligned}
$$

(b)

Figure 4.1: (a) Structure of a small metabolic network with negative feedback. (b) Equation system of the linlog model of the network

functions. $N \in \mathbb{Z}^{n_x \times m}$ is a stoichiometry matrix. $a \in \mathbb{R}^m$, $B^x \in \mathbb{R}^{m \times n_x}$ and $B^u \in \mathbb{R}^{m \times n_u}$ represent the parameters of the model.

Example 1. *Figure 4.1(a) illustrates a prototype of a metabolic reaction network with negative feedback regulation. In terms of Eq.* (4.1)*, we have* $x = [x_1\ x_2]^T$*,* $e = [e_1\ e_2\ e_3]^T$*,* $v = [v_1\ v_2\ v_3]^T$*, and*

$$N = \begin{bmatrix} 1 & -1 & 0 \\ 0 & 1 & -1 \end{bmatrix}$$

The linlog rate equations for this system are shown in Figure 4.1(b). We will refer to this network as a running example illustrating the concepts introduced in the chapter.

As we have seen before, the identification of linlog models amounts to the estimation of parameters $a \in \mathbb{R}^m$, $B^x \in \mathbb{R}^{m \times n_x}$ and $B^u \in \mathbb{R}^{m \times n_u}$ from experimental data. In most experiments, concentrations of enzymes and external metabolites are under partial control of the experimentalist, and the concentrations of internal metabolites and metabolic fluxes are measured after the system has relaxed to the steady-state

$$N \cdot v(x, u, e) = 0. \tag{4.3}$$

In accordance with this, we shall assume that, from each of $q \in \mathbb{N}$ experiments, the data are noisy measurements $(\tilde{v}^k, \tilde{x}^k, \tilde{u}^k, \tilde{e}^k)$ of (v^k, x^k, u^k, e^k), where the latter satisfy $v^k = v(x^k, u^k, e^k)$ and (4.3), with $k = 1, \ldots, q$. Clearly the restriction to steady-state measurements limits the informativeness of the data and may affect the identifiability of the models, as will be apparent in later sections.

We now reformulate the general estimation problem defined in Problem 1 in the case of noisy experimental data:

Problem 3. *Given the data matrices*

$$\underbrace{\begin{bmatrix} \left(\frac{\tilde{v}^1}{\tilde{e}^1} - \overline{\left(\frac{\tilde{v}}{\tilde{e}}\right)}\right)^T \\ \vdots \\ \left(\frac{\tilde{v}^q}{\tilde{e}^q} - \overline{\left(\frac{\tilde{v}}{\tilde{e}}\right)}\right)^T \end{bmatrix}}_{\triangleq \widetilde{W}}, \quad \underbrace{\begin{bmatrix} \left(\ln \tilde{x}^1 - \overline{\ln \tilde{x}}\right)^T & \left(\ln \tilde{u}^1 - \overline{\ln \tilde{u}}\right)^T \\ \vdots & \vdots \\ \left(\ln \tilde{x}^q - \overline{\ln \tilde{x}}\right)^T & \left(\ln \tilde{u}^q - \overline{\ln \tilde{u}}\right)^T \end{bmatrix}}_{\triangleq \widetilde{Y}}$$

find parameters $B \triangleq \begin{bmatrix} B^x & B^u \end{bmatrix}^T$ *minimizing* $|||\widetilde{W} - \widetilde{Y} \cdot B|||$, *where* $|||\cdot|||$ *is a convenient matrix norm on* $\mathbb{R}^{q\times m}$.

To this avail we consider the probabilistic measurement error model:

$$\widetilde{W} = W + \varepsilon \qquad \varepsilon = \begin{bmatrix} \varepsilon_1, \ldots, \varepsilon_m \end{bmatrix} \qquad \varepsilon_i \sim \mathscr{N}(0, \Sigma_{\varepsilon_i}) \tag{4.4}$$

with $\Sigma_{\varepsilon_i} = \sigma_i^2 I > 0$ and ε_i mutually independent for all $i = 1, \ldots, m$.

Notice that, as in Sec. 3.1, the parameter vector a can be estimated from experimental data and estimates of $B = \begin{bmatrix} B^x & B^u \end{bmatrix}^T$. Assuming that the measurement noise is independent across different reactions, it makes sense to separate the problem into the independent estimation of the parameter vector B_i of each reaction i, with $i = 1, \ldots, m$.

Example 2. *Let* W *and* Y *denote the noiseless versions of* $\widetilde{W}$ *and* $\widetilde{Y}$, *respectively. Consider the case where* $\widetilde{W} = W + \varepsilon = Y \cdot B + \varepsilon$, *i.e., the measurement error for the metabolite concentrations is negligible. This corresponds to the case described in Sec. 3.1. Maximum likelihood estimation of* B *amounts to minimizing the negative logarithm of the likelihood of* W *given* Y. *After simple computations and thanks to the independence assumptions on* ε, *one finds that the maximum likelihood estimate of* B *is any solution of*

$$\min_B \ \frac{1}{2} \sum_{i=1}^{m} (\widetilde{W}_i - YB_i)^T \Sigma_{\varepsilon_i}^{-1} (\widetilde{W}_i - YB_i),$$

which can be solved separately for every column of B *by solving, for* $i = 1, \ldots, m$,

$$\min_{B_i} \ (\widetilde{W}_i - YB_i)^T \Sigma_{\varepsilon_i}^{-1} (\widetilde{W}_i - YB_i) = ||\widetilde{W}_i - YB_i||^2_{\Sigma_{\varepsilon_i}^{-1}}.$$

Thus, defining $||\cdot||_i = ||\cdot||_{\Sigma_{\varepsilon_i}^{-1}}$ *and*

$$|||\cdot||| : \mathbb{R}^{q\times m} \to \mathbb{R}_+ : M \mapsto \sqrt{\begin{bmatrix} M_1 \\ \vdots \\ M_m \end{bmatrix}^T \begin{bmatrix} \Sigma_{\varepsilon_1}^{-1} & & \\ & \ddots & \\ & & \Sigma_{\varepsilon_m}^{-1} \end{bmatrix} \begin{bmatrix} M_1 \\ \vdots \\ M_m \end{bmatrix}},$$

we see that Problem 3 is equivalent to the maximum likelihood estimation of B, *which is in turn equivalent to separate maximum likelihood estimation of the parameters* B_i *of each reaction* i.

Similar to, but in more generality than Example 2, from now on we consider the probabilistic measurement error model

$$\widetilde{W} = W + \varepsilon, \qquad \varepsilon = \left[\varepsilon_1, \dots, \varepsilon_m\right], \qquad \varepsilon_i \sim \mathscr{N}(0, \Sigma_{\varepsilon_i}), \tag{4.5}$$

$$\widetilde{Y} = Y + \eta, \qquad \eta = \left[\eta_1, \dots, \eta_m\right], \qquad \eta_i \sim \mathscr{N}(0, \Sigma_{\eta_i}), \tag{4.6}$$

with $\Sigma_{\varepsilon_i} = \sigma^2 I > 0$, $\Sigma_{\eta_i} = \nu^2 I \geq 0$, and ε_i, $\eta_{i'}$ mutually independent for all $i = 1, \dots, m$ and $i' = 1, \dots, m$.

We can now fully detail Problem 3 and express it as a series of estimation problems on individual reactions. In doing so we note that each reaction i depends only on a (known) subset of metabolites $C(i) \subseteq \{1, \dots, n_x + n_u\}$. Therefore, the entries of B_i corresponding to metabolites that do not participate in reaction i can be set to zero, and the least-squares problem can be reduced accordingly. We will address two cases, formalized by two alternative problem statements. The first we consider is a standard regression problem [Nikerel et al., 2009, Sands and Voit, 1996]. In analogy with Sec. 3.1 and Example 2, it amounts to assuming negligible metabolite measurement noise.

Problem 4. *Given Y and $\widetilde{W}$ as in* (4.5)*,*

$$\min_{B_{C(i),i}} ||\widetilde{W}_i - Y_{C(i)} \cdot B_{C(i),i}||_i, \quad i = 1, \dots, m. \tag{4.7}$$

The second case is more challenging and less commonly addressed in the literature. It corresponds to an errors-in-variables regression model [van Huffel and Vandewalle, 1991] and accounts explicitly for noise on the relative fluxes as well as on metabolite concentrations.

Problem 5. *Given $\widetilde{Y}$ as in* (4.6) *and $\widetilde{W}$ as in* (4.5)*, solve*

$$\min_{B_{C(i),i}} ||\widetilde{W}_i - \widetilde{Y}_{C(i)} \cdot B_{C(i),i}||_i, \quad i = 1, \dots, m. \tag{4.8}$$

From now on we will drop subscript i from $|| \cdot ||_i$, the meaning being clear from the argument of the norm.

Remark 1. *A similar parameter estimation problem can be formulated for other pseudo-linear modeling formalisms. Models linear in metabolite concentrations [Delgado and Liao, 1992], loglin models [Hatzimanikatis and Bailey, 1997], and generalized mass-action models [Savageau, 1976] can be defined analogously to Eq. (3.3). This gives rise to, respectively,*

$$\left(\frac{v}{e}\right)^T = [1\ x^T\ u^T] \cdot \begin{bmatrix} a^T \\ (B^x)^T \\ (B^u)^T \end{bmatrix} \tag{4.9}$$

$$(v)^T - \ln e^T = [1\ \ln x^T\ \ln u^T] \cdot \begin{bmatrix} a^T \\ (B^x)^T \\ (B^u)^T \end{bmatrix} \tag{4.10}$$

$$\ln\left(\frac{v}{e}\right)^T = [1\ \ln x^T\ \ln u^T] \cdot \begin{bmatrix} a^T \\ (B^x)^T \\ (B^u)^T \end{bmatrix} \tag{4.11}$$

Notice that the modifications concern the way in which reaction rates and concentrations enter into the linear equations. The translation of these equations into variants of Problem 5, by removing the mean, is straightforward. In each case, we obtain a linear regression problem.

Although below we illustrate the identifiability issues and reduction methods for the case of linlog models, it should be borne in mind that analogous results also apply to the other approximate kinetic modeling formalisms defined in Eq. (4.9) to Eq. (4.11). However, they are not applicable to formalisms for which parameter estimation cannot be turned into linear regression, such as reversible Michaelis-Menten kinetics and convenience kinetics [Liebermeister and Klipp, 2006].

4.2 Identifiability of linlog and related models

The problem of identifiability refers to the ability to unambiguously extract parameter values of a model structure from experimental data. Here we focus on linlog models and investigate the identifiability of this model class. We shall first discuss the problem from the perspective of structural identifiability. For practical purposes, this is equivalent to answering the question whether each parameter can be uniquely reconstructed from an arbitrarily rich and errorless dataset. Structural identifiability forms the basis for studying practical identifiability, *i.e.*, the ability to estimate parameter values from real datasets, which will be discussed further below.

The system, described by Equations (4.1)–(4.3), is parametrized by the parameter matrix $p = [a\ B^x\ B^u]^T \in P \subseteq \mathbb{R}^{(n_x+n_u+1)\times m}$. Let e, u, x and v take values in the sets $E \subseteq \mathbb{R}^m_{>0}$, $U \subseteq \mathbb{R}^{n_u}_{>0}$, $X \subseteq \mathbb{R}^{n_x}_{>0}$ and $V \subseteq \mathbb{R}^m$ respectively. We assume that e and u are system inputs, i.e. independent variables whose value can be fixed at will. We make the following standing assumption.

Assumption 1. *For every $p \in P$, $e \in E$ and $u \in U$, the solution to the system of equations*

$$\begin{cases} 0 = Nv & (4.12a) \\ v = \operatorname{diag}(e) \cdot (a + B^x \cdot \ln x + B^u \cdot \ln u) & (4.12b) \end{cases}$$

is unique in $x \in X$ and $v \in V$.

This guarantees that, for every admissible parametrization and system input, a steady-state exists and is unique. In order for this steady-state to be observable experimentally, we also make the assumption that it is locally asymptotically stable. In accordance with the metabolic control theory literature [Heinrich and Schuster, 1996], fluxes v at steady-state are denoted by J. We write $J_p(e,u)$ to emphasize dependence on inputs and model parameters.

For varying values of p, Assumption 1 enables us to express the linlog model with parameters p as a map

$$\mathscr{M}_p : \; E \times U \to V \times X : \; (e,u) \mapsto \big(J_p(e,u), x_p(e,u)\big). \tag{4.13}$$

Assumption 1 is met, in particular, when matrix $N\,\mathrm{diag}(e)B^x$ is invertible. In this case, one may write the output $(J_p, x_p) = \mathscr{M}_p(e,u)$ as an explicit function of the input (e,u),

$$\begin{cases} J_p(e,u) = \mathrm{diag}(e) \cdot (a + B^x \cdot \ln x_p(e,u) + B^u \cdot \ln u), & \text{(4.14a)} \\ \ln x_p(e,u) = -(N\,\mathrm{diag}(e)B^x)^{-1} \cdot N\,\mathrm{diag}(e) \cdot (a + B^u \cdot \ln u). & \text{(4.14b)} \end{cases}$$

As can be easily verified, this requires that the stoichiometry matrix N is full row rank, which is the case for systems with no mass conservation constraints [Heinrich and Schuster, 1996].

In agreement with Sec. 4.1, where the identification problem is split into the identification of each reaction separately, we look at the identifiability of the parameters of the generic ith reaction, and say that a model is identifiable if all its reactions are.

4.2.1 Identifiability from a theoretical perspective

We adapt the definition from Ljung [1999] to our context as follows. Recall that p_i is the ith column of p, *i.e.*, the parameter vector for reaction i.

Definition 1. *A reaction i of model $\mathscr{M}_p$ is identifiable at p^* if there exists $D \subseteq E \times U$ such that, for all $p \in P$,*

$$\big((J_p)_i, x_p\big)|_D = \big((J_{p^*})_i, x_{p^*}\big)|_D \Rightarrow p_i = p_i^*. \tag{4.15}$$

Here (J_p, x_p) is seen as a function from $E \times U$ to $X \times V$, and "$|_D$" is its restriction to a specific input set. In words, a reaction i is considered identifiable for a particular model parametrization p^* if no $p \in P$ with $p_i \neq p_i^*$ exists such that the predictions of $\mathscr{M}_p$ and $\mathscr{M}_{p^*}$ are identical over all possible input sets D. Note that this definition is applicable to any metabolic reaction model, provided suitable definition of the parameters of the model class. In particular, it applies to the linlog form of the reaction rates as well as to any other pseudo-linear form reviewed in Sec. 4.1.

How can we apply Def. 1 to the analysis of identifiability of linlog models? The following proposition establishes the link between this definition and the uniqueness of the solution to Problems 4–1. Given the input set $D = \{(e^1, u^1), \cdots, (e^q, u^q)\}$ and a "true" parameter vector p^*, let J_*^k and x_*^k denote the outputs $J_{p^*}(e^k, u^k)$ and $x_{p^*}(e^k, u^k)$, respectively, with $k = 1, \ldots, q$.

Proposition 1. *A reaction i of $\mathscr{M}_p$ is structurally identifiable at p^* if and only if there exists $D = \{(e^1, u^1), \cdots, (e^q, u^q)\} \subseteq E \times U$ such that the solution of the equation $W_i^* = Y^* B_i^*$, with*

$$W_i^* = \left[\left(\frac{J_*^1}{e^1} - \overline{\left(\frac{J_*}{e}\right)} \right)_i \quad \cdots \quad \left(\frac{J_*^q}{e^q} - \overline{\left(\frac{J_*}{e}\right)} \right)_i \right]^T,$$
$$Y^* = \begin{bmatrix} \ln x_*^1 - \overline{\ln x_*} & \cdots & \ln x_*^q - \overline{\ln x_*} \\ \ln u^1 - \overline{\ln u} & \cdots & \ln u^q - \overline{\ln u} \end{bmatrix}^T,$$

is unique in the parameters $B_i^* = \left([B^{x*}\ B^{u*}]^T\right)_i$.

Corollary 1. *A reaction i of $\mathscr{M}_p$ is structurally identifiable at p^* if and only if there exists $D = \{(e^1, u^1), \cdots, (e^q, u^q)\} \subseteq E \times U$ such that $Y_{C(i)}^*$ is full column-rank.*

It is clear that the rank condition of Corollary 1 can be fulfilled only for a number of experiments $q = |D|$ greater than or equal to the number of unknown parameters $n_b = |C(i)|$ of reaction i. The possibility to find $q \geq |C(i)|$ experiments making $Y_{C(i)}^*$ full column rank depends on the network model and parameters themselves. Indeed, in our framework, the experimentalist can impose different enzyme concentrations e and inputs u, but the resulting metabolite concentrations are determined by the network. In other words, there is no full control of the regression matrix Y, which impairs the design of optimal experiments for parameter regression. Let us show this by a simple example.

Example 3. *Consider the negative feedback network structure shown in Figure 4.1. Let us define the network parameter values*

$$a = \begin{bmatrix} a_1 \\ 0.0297 \\ 0.0296 \end{bmatrix}, \quad B^x = B^T = \begin{bmatrix} -0.0938 & B_{2,1} \\ 0.0286 & -0.0073 \\ 0 & 0.0287 \end{bmatrix},$$

where different values of $a_1 \in \mathbb{R}$ and $B_{2,1} \in \mathbb{R}_{<0}$ (the coefficient that determines the strength of the feedback regulation) will be considered. For all values of the enzyme concentrations $e_i > 0$, with $i = 1, 2, 3$, and all $a_1, B_{2,1}$, the equation $Nv(x, e) = N \operatorname{diag}(e)(a + B^x \ln x) = 0$ yields a unique solution $\ln x = -(N \operatorname{diag}(e) B^x)^{-1} N \operatorname{diag}(e) a$. This defines the unique steady-state of the system. Provided it is asymptotically stable, this gives us a steady state of the system that can be observed experimentally. One first consideration is that different values of a_1 and $B_{2,1}$ may lead to very different properties of the matrix Y^* even when this remains full rank, i.e. the system is structurally identifiable. For $a_1 = 0.0297$ and values of $B_{2,1}$ equal to 0.0073 (weaker feedback action) and -7.2961 (stronger feedback action), respectively, scatter plots of the steady state solutions $\ln x$ from 1000 randomly generated samples of e are reported

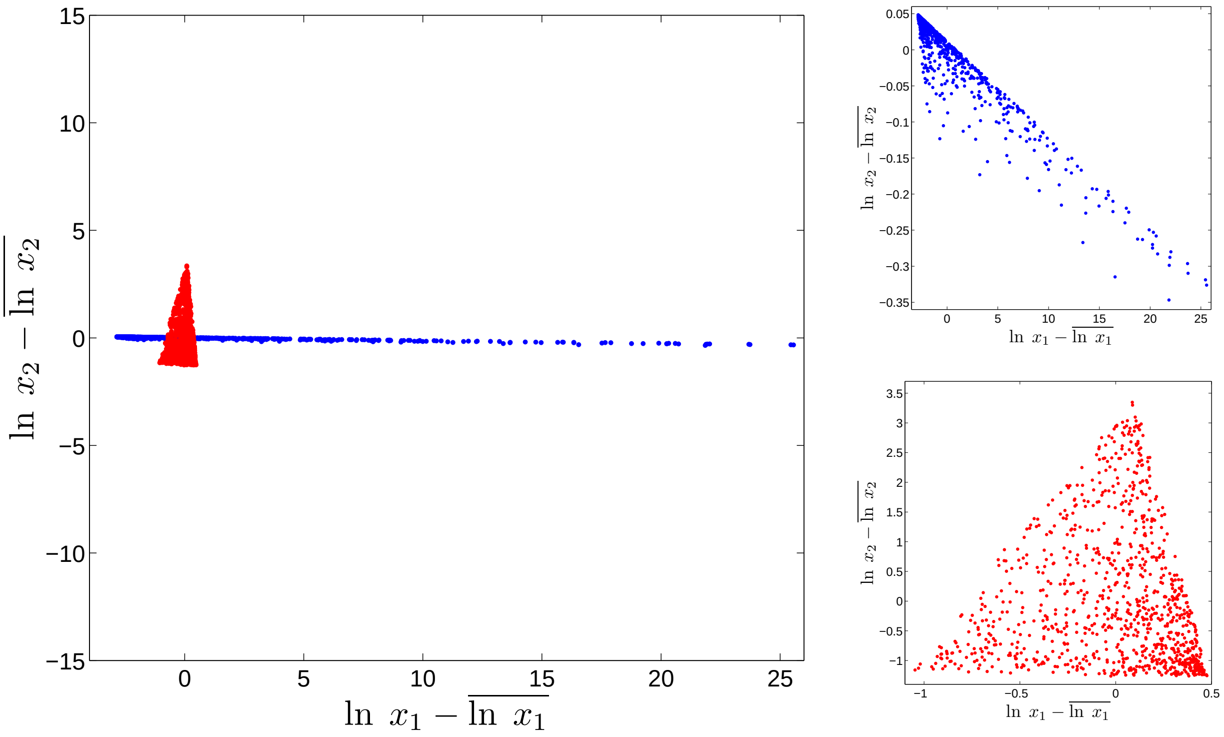

Figure 4.2: Left: Scatter plot of steady-state metabolite concentrations for 1000 randomly generated enzyme concentrations, for two different model parameterizations of the model of Fig. 4.1 (see the text of Example 3 for more details); Red: Simulation for $a_1 = 0.0297$ and $B_{2,1} = -0.0073$ (weak feedback); Blue: Simulation for $a_1 = 0.0297$ and $B_{2,1} = -7.2961$ (strong feedback). Right: Individual zooms of the two datasets, with consistent coloring.

in Figure 4.2. Steady-state metabolite concentrations in the case of weak feedback are spread similarly in all directions, while with stronger feedback they are essentially aligned along a one-dimensional line.Here the strong feedback exerted by metabolite X_2 on the production of X_1 induces a negative correlation between their concentrations, which may result in an ill-conditioned estimation problem. In addition this strong feedback results in a near homeostasis of X_2 that may also impede identification. These points will be further developed in the next example. Second, some pathological parameterizations may give rise to a nonidentifiable model. Indeed, if a is in the span of B^x, then the unique solution of $N\,\mathrm{diag}(e)(a+B^x \ln x) = 0$ always corresponds to the value of $\ln x$ satisfying $B^x \ln x = -a$, independently of the value of e. Thus, no matter the number of experiments q, the rank of Y^* is at most 1 and the model is not identifiable. In our example, this is the case for $a_1 = -7.5491$ and $B_{2,1} = -7.2961$.

From the example above it is clear that a reaction may be nonidentifiable for specific values of the parameters even if it is identifiable for other parameterizations. In the light of this, a generalization of Def. 1 from reaction identifiability *at a parameter* p^* to reaction identifiability *tout court* can be obtained following Walter and Pronzato [1997]. Namely, we stipulate that a model in $\mathscr{M}_p$ is identifiable if it is identifiable at almost every $p^* \in P$ or almost everywhere in P, where 'almost every' and 'almost everywhere' are interpreted in terms of a suitable (*e.g.*, the Lebesgue) measure on P. Hence, the negative feedback network structure of Example 3 is identifiable in the sense of Walter and Pronzato. The identifiability criterion of Def. 1 holds except for the "rare" parameter combinations p^* such that $a \in \mathrm{span}(B^x)$.

A second observation, following from the example above, is that the mathematical conditions that the system must fulfill to be declared nonidentifiable are too strong to be useful in practice. If we look at Figure 4.2, we see that strong collinearities exist between the metabolite concentrations x_1 and x_2. As a result, an unreasonably large number of experiments would be needed to resolve the effects of the two. Moreover, the definition of identifiability assumes that the measurements are not corrupted by noise, which is even less realistic. We therefore need to weaken our definition of identifiability in order to make it more suitable for applications to actual data on metabolism. While taking into account realistic assumptions on the experimental datasets, *i.e.*, measurements available in a limited amount and affected by experimental error, this notion of identifiability should draw upon the theoretical notion of model identifiability discussed above.

4.2.2 Identifiability from a practical perspective

Let D be a fixed set of q inputs (external metabolites and enzyme concentrations), and let O be the set of the corresponding system outputs (fluxes and steady-state concentrations of internal metabolites determined by $\mathscr{M}_{p^*}$). Consider the problem of estimating the parameters B_i of reaction i given observations of D and O affected by measurement error. An *estimator* $\hat{B}_i$ of B_i is a function of the observations of D and O, well-defined for every possible (*a-priori* unknown) value of $p^* \in \mathbb{R}^{n_b}$ (compare [Ljung, 1999, §7.4]). Since, due to noise, the observations are stochastic variables, $\hat{B}_i$ is itself a stochastic variable. Therefore, one cannot hope to estimate B_i exactly, but only within a certain degree of approximation. In this spirit, we define identifiability in terms of the existence of an estimator satisfying prespecified statistical requirements. In doing this, we restrict attention to the nonzero entries of B_i, *i.e.*, $B_{C(i)i}$. Let $\mathscr{B}_i \subset \mathbb{R}^{n_b}$ be a *bounded* neighbourhood of the origin, and let $\alpha \in (0, 1)$.

Definition 2. *For a given $D \subseteq E \times U$, reaction i of $\mathscr{M}_p$ is identifiable at p^* with uncertainty region $\mathscr{B}_i$ and confidence level $1 - \alpha$ if there exists an estimator $\hat{B}_{C(i),i}$ such that*

$$\mathbb{P}_{p^*}[\hat{B}_{C(i),i} - B_{C(i),i} \in \mathscr{B}_i] \geq 1 - \alpha, \tag{4.16}$$

where $\mathbb{P}_{p^*}$ is the probability measure induced by $\mathscr{M}_{p^*}$. [1]

Note that this definition is conceptually different from the one suggested by Raue et al. [2009], where the definition of practical identifiability requires that the uncertainty on the parameter estimates (as defined via the profile likelihood) is bounded, but, contrary to our definition, can be arbitrarily large. In addition, the definition in [Raue et al., 2009] is given in terms of a specific, not necessarily optimal choice of the estimator.

The point of view expressed by Def. 2 is that the experimentalist, or the modeler, sets the requirements (estimation accuracy and confidence level) that the estimates must fulfill in order to be useful, via the *a-priori* specification of $\mathscr{B}_i$ and α. Then, the possibility of fulfilling (4.16), i.e. the practical identifiability of the model, depends on the system itself and on the richness of the input set D. In general, the larger the D, the tighter the requirements that one can fulfill (*i.e.*, the smaller the values of $\mathscr{B}_i$ and α for which practical identifiability in the sense of Def. 2 holds).

From an alternative viewpoint, one may start from a given input set D, and look for the choices of α and $\mathscr{B}_i$ that ensure satisfaction of Eq. (4.16). Here in turn, one may fix α and look for the $\mathscr{B}_i$ that makes Eq. (4.16) achievable, or fix the acceptable estimation uncertainty $\mathscr{B}_i$ and establish at what confidence level α this performance can be attained.

In all of the above cases, the natural questions that arise are how Def. 2 can be verified in practice, how this notion of identifiability depends on the structural system identifiability discussed in the previous section, and what $\mathscr{B}_i$ may look like. To answer these questions, the relation between observations and observed quantities must be specified further. We refer to the measurement model introduced in Sec. 4.1. For the sake of simplicity, we assume for this section that $\nu = 0$, *i.e.*, we address Problem 4. Problem 1 can be addressed with the same tools, but at the price of technical complications.

For the case into question, the following proposition answers the questions above.

[1] Strictly speaking, a better version of Def. 2 would require that condition (4.16) holds for all p^* within a sufficiently large subset of P. This would automatically rule out trivial definitions of $\hat{B}_{C(i),i}$ such as $\hat{B}_{C(i),i} \triangleq B_{C(i),i}$ (which makes the reaction identifiable for any α and $\mathscr{B}_i$ but cannot be built without the knowledge of $B_{C(i),i}$ itself). Unfortunately, this is not a good choice in general, in that the uncertainty set $\mathscr{B}_i$ may severely depend on p^*, as we shall see later on in Example 4. Hence we stick to Def. 2 with the understanding that any such triviality is avoided.

Proposition 2. *If a reaction i of $\mathscr{M}_p$ is structurally identifiable at p^* in the sense of Def. 1 then, for every $\alpha \in (0,1)$, it is practically identifiable in the sense of Def. 2 with confidence level at least $1-\alpha$ for any uncertainty set $\mathscr{B}_i \supseteq \mathcal{E}_{\widehat{\Sigma}}(\alpha)$, where $\mathcal{E}_{\widehat{\Sigma}}(\alpha)$ denotes the $(1-\alpha)$-confidence ellipsoid of a zero-mean Gaussian distribution with variance $\widehat{\Sigma} = (Y_{C(i)}^T \Sigma_{\varepsilon_i}^{-1} Y_{C(i)})^{-1}$.*

The proof relies on the use of minimum variance estimators, as dictated by standard results in linear estimation theory ([Ljung, 1999, Appendix II], see also Appendix B.1). From now on, estimation will be performed based on this type of estimator.

Observe that $\mathcal{E}_{\widehat{\Sigma}}(\alpha)$, and hence the shape and size of the uncertainty regions $\mathscr{B}_i$ for which the model is practically identifiable, depends on the choice of inputs D. In particular, the noise on W_i affects the covariance matrix $\widehat{\Sigma}$ by its statistics Σ_{ε_i}, while the contribution of the data $Y_{C(i)}$ is apparent. The number of data points q enters the picture in terms of the size of the matrix Σ_{ε_i} and the number of rows of $Y_{C(i)}$. Typically, the larger q, the smaller $\mathscr{B}_i$ for a fixed α. We argue that similar identifiability results can be derived even in cases where the noise is not Gaussian and metabolite measurements are affected by stochastic error, at the price of a much more complicated characterization of $\mathscr{B}_i$. Finally, one may speak about identifiability of the whole model, *e.g.*, by requiring that each reaction i is individually identifiable with a given confidence level α and uncertainty set $\mathscr{B}_i \in \mathbb{R}^{n_b}$. Alternatively, one may require that all reactions be simultaneously identifiable with confidence level $1-\alpha$ and a suitably defined joint uncertainty set.

A discussion of practical identifiability in terms of covariance matrix of a (linearized) parameter estimation problem also appears in [Srinath and Gunawan, 2010], in the context of power-law models. However, the discussion in Srinath and Gunawan [2010] is essentially limited to one particular choice of the admissible estimation uncertainty $\mathscr{B}_i$, namely the one ensuring that the sign of the parameter values is estimated correctly with probability $1-\alpha$.

A useful tool for better understanding Proposition 2 and the links between the data and practical identifiability is the Singular Value Decomposition (SVD) of a matrix [Jolliffe, 1986]. The SVD of $Y_{C(i)}$ is given by

$$Y_{C(i)} = USV^T, \qquad S = \mathrm{diag}(s_1, s_2, ..., s_{n_b}), \tag{4.17}$$

with $U \in \mathbb{R}^{q\times n_b}$ and $V \in \mathbb{R}^{n_b \times n_b}$ orthonormal matrices and $s_1 \geq \cdots \geq s_{n_b} \geq 0$ the singular values of $Y_{C(i)}$. In the presence of dependencies between the columns, there exists an index r with $1 \leq r < n_b$ such that $s_{r+1} = \ldots = s_{n_b} = 0$, and $Y_{C(i)}$ is of rank r. Based on this, the covariance matrix of Proposition 2 can be written as $(Y_{C(i)}^T \Sigma_{\varepsilon_i}^{-1} Y_{C(i)})^{-1} = VS^{-1}U^T \Sigma_{\varepsilon_i} US^{-1}V^T$. Because of the independence assumption for ε_i, $\Sigma_{\varepsilon_i} = \sigma_i^2 I$ and the previous formula simplifies to

$$(Y_{C(i)}^T \Sigma_{\varepsilon_i}^{-1} Y_{C(i)})^{-1} = V\sigma_i^2 S^{-2} V^T, \tag{4.18}$$

which is (up to resorting of the entries) the SVD of the covariance matrix with singular values given by $\sigma_i^2 s_1^{-2}, \ldots, \sigma_i^2 s_{n_b}^{-2}$. Multiplied by a factor $\lambda(\alpha)$ fixed by α, these values define the length of the axes of the confidence ellipsoid of Proposition 2. Now suppose that we seek parameter estimates that, with confidence $1-\alpha$, fall within a ball $\mathscr{B}_\delta = \{p : \ |p| < \delta\}$, for some $\delta > 0$. That is, all the entries of the parameter vector must be estimated with accuracy at least δ. From Proposition 2 and Def. 2, reaction i is practically identifiable if it is structurally identifiable and the ellipsoid associated with (4.18) fits into $\mathscr{B}_\delta$, i.e. if $\lambda(\alpha)\sigma_i/s_\ell < \delta$ for $\ell = 1, \dots, n_b$. Since $s_1 \geq \dots \geq s_{n_b}$, this holds whenever $\lambda(\alpha)\sigma_i/s_{n_b} \leq \delta$, *i.e.*, the smallest singular value of $Y_{C(i)}$ dictates the overall estimation performance.

If $Y_{C(i)}$ is ill-conditioned, *i.e.*, some data vectors are nearly collinear, large discrepancies exist between its largest and its smallest singular values. Then, the condition $s_1 \gg s_{n_b}$ implies that, for practical identifiability, it must hold that $\lambda(\alpha)\sigma_i/s_1 \ll \delta$, which sets the accuracy in the estimation of the components of p along direction V_1. Achieving the required accuracy $\lambda(\alpha)\sigma_i/s_{n_b} \leq \delta$ along direction V_{n_b} would generally require an unreasonable amount of experimental effort in terms of experimental replicas and/or measurement accuracy (see also Gutenkunst et al. [2007]). Note, however, that such high accuracy is solely needed to ensure that the less accurate estimates of the components of p in direction V_{n_b} be acceptably good. In a sense, this hard requirement is an artifact of the problem statement: If we accept that certain components are just not relevant, the remaining part of the model is identifiable in practice with good accuracy and much less experimental effort. To quantify our discussion, let us look at a numerical example.

Example 4. *To illustrate the implications for parameter identifiability of a poorly conditioned data matrix, consider the estimation results from noisy and finite datasets for the two different identifiable parameterizations of the model of Example 3. As in the latter example, data-points were simulated from random values of enzyme concentrations. Noise was added to W by drawing values from normal distributions with standard deviations proportional to the corresponding elements of W. Two different dataset sizes ($q = 20$ and $q = 100$) and two different noise levels (20% and 50%) were tested, resulting in a total of 4 experimental scenarios for each model parameterization. For each scenario, 100 datasets were simulated and the corresponding estimates for reaction 2 are reported in the scatter plots of Figure 4.3(a) ($a_1 = 0.0297$ and $B_{2,1} = -0.0073$) and 4.3(b) ($a_1 = 0.0297$ and $B_{2,1} = -7.2961$).*

An immediate observation is that the shape of the 95%-confidence ellipse of the parameter estimates is different for the two model parameterizations. While estimation accuracy for $B_{1,1}$ and $B_{2,1}$ is comparable in the case of weaker feedback ($B_{2,1} = -0.0073$), the shape of the uncertainty ellipse becomes very skewed in the case of stronger feedback ($B_{2,1} = -7.2961$).

In particular, in the latter case estimation accuracy is much higher for $B_{1,1}$ than for $B_{2,1}$ regardless of the features of the dataset because of the strong homeostasis on x_2 (note the change in scale of the vertical axes of the plots in Figure 4.3(a) and Figure 4.3(b)). The plots also show that larger and/or less noisy datasets improve estimation performance, as expected. However, in the case of $B_{2,1}$ in Figure 4.3(b), this improvement is seen to require

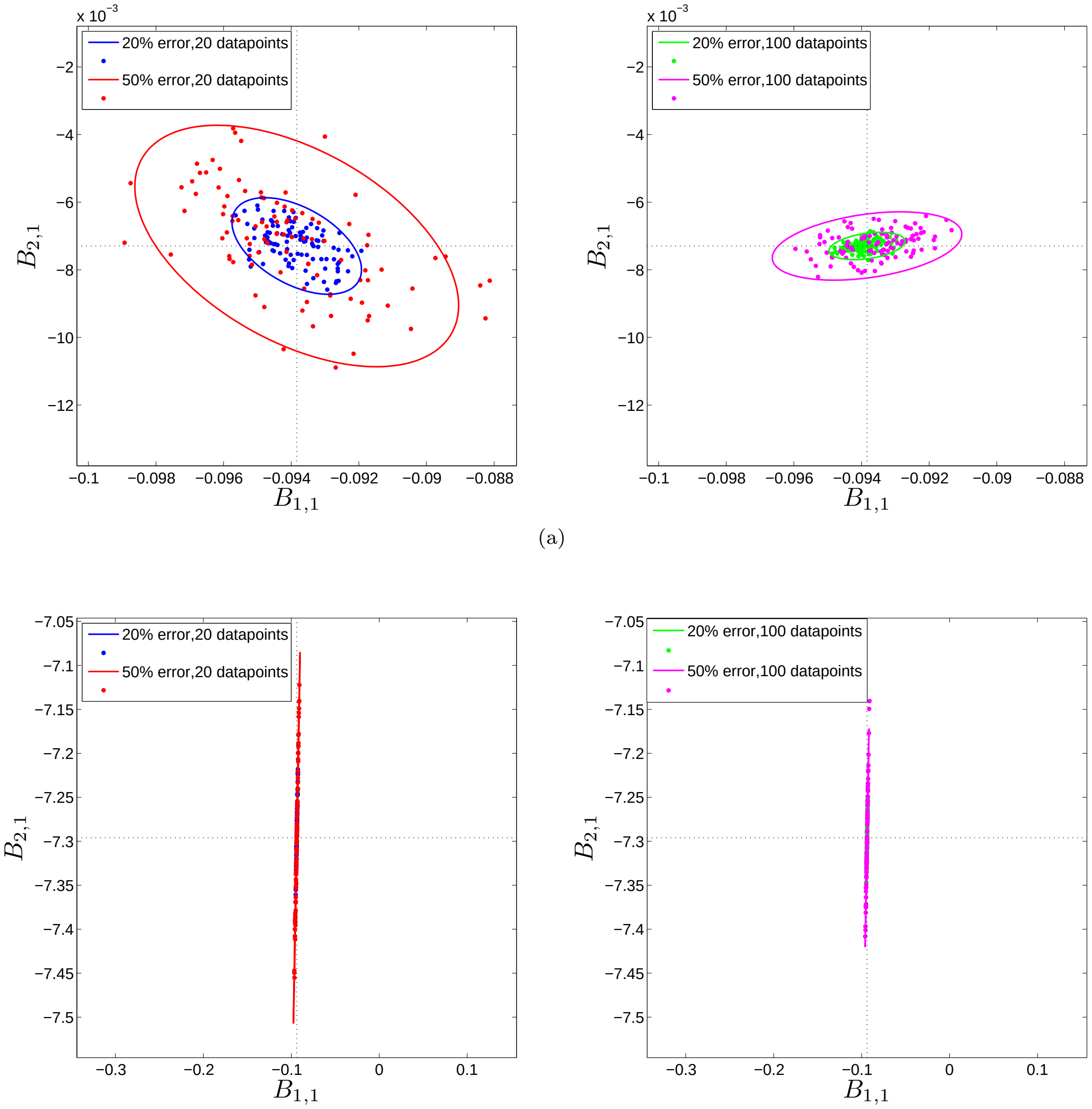

(a)

(b)

Figure 4.3: Estimates of parameters $B_{1,1}, B_{2,1}$ (first row of B^x) from metabolite concentration, enzyme concentration and flux measurements in steady state, for a linlog model of the negative feedback network in Figure 4.1. These coefficients mediate the effect of the metabolite log-concentrations $\ln x_1$ and $\ln x_2$ in reaction 2. In each panel, scatter plots are reported for four different experimental scenarios: 20% noise and $q = 20$ datapoints (blue); 20% noise and $q = 100$ datapoints (green); 50% noise and $q = 20$ datapoints (red); 50% noise level and $q = 100$ datapoints (magenta). 95%-confidence ellipses are drawn for each scenario (solid lines). Reference parameter values are indicated by the intersection of horizontal and vertical dotted lines. Refer to the text of Example 4 for additional details. True parameter values are given in Example 3. **(a)** Case $a_1 = 0.0297$ and $B_{2,1} = -0.0073$. **(b)** Case $a_1 = 0.0297$ and $B_{2,1} = -7.2961$.

extremely large and high-quality datasets. In other words, accurately estimating all parameters of the model demands a significant increase in experimental effort, even when most individual parameters are easy to estimate.

It is apparent that the skewed estimation uncertainty in Fig. 4.3(b) is related to the poor conditioning of the data matrix Y in the case of stronger feedback (the shape of the ellipsoid is determined by the ratio of the singular values of Y). In terms of practical identifiability, assuming a modeler has set a maximum allowable uncertainty $\mathscr{B}_1$ for some confidence level α, it is clear that in this case the system will not be practically identifiable (even if the model is structurally identifiable at the given p^*), unless $\mathscr{B}_1$ is large enough, i.e., rather sloppy estimates are deemed acceptable.

To summarize the main points of the section, we have discussed practical identifiability as a relative concept that depends on the parameter estimation uncertainty that is deemed acceptable. If this is compatible with the quality of the data (dataset size, amount of noise) and the dataset is sufficiently diverse (more independent components than unknown parameters), then practical identifiability follows from structural identifiability. On the other hand, if the experiments are not informative enough or the network itself implies heavy correlations among the data, we detect lack of practical identifiability from the existence of nearly zero singular values in the decomposition of the regression matrix. For metabolic systems this will occur when feedback regulation results in strong homeostasis or when metabolite concentrations are correlated, which could be due in general to steady-state constraints. A particularly relevant situation concerns reactions that operate close to equilibrium. Indeed, in this situation, mass-action law relates metabolite concentrations as follows:

$$\sum_j N_{ji} \ln x_j \approx \ln K_i \tag{4.19}$$

where K_i is the equilibrium constant of reaction i. This results in a quasi-dependency between $\ln x_j$ that makes the reaction nonidentifiable in practice.

In addition to providing little information for the estimation of the model parameters, the smallest components of $Y_{C(i)}$ have negligible effect on the solution of the steady-state equation (4.3), *i.e.*, in the determination of the system steady-state. In the next section, we will build upon this analysis to define a criterion for eliminating the components of $Y_{C(i)}$ associated to the smallest singular values and reduce the network model accordingly. This will make parameter estimation (regression) a well-conditioned problem for every single reaction while minimally affecting the quality of the model.

4.3 Reduction to identifiable models

It was shown in Example 4 that attempting to identify the parameters of a reaction that is not practically identifiable leads to an ill-posed estimation problem. That is, certain parameter combinations are practically indistinguishable from the data. Eliminating redundant components of the model parameters by Principal Component Analysis (PCA, see Jolliffe [1986]) is a way to ensure well-posedness of parameter estimation (*i.e.*, practical identifiability) by a "minimal" approximation of the model.

The method applies as usual reaction by reaction. For any given reaction i, with $i = 1, \dots, m$, we compute and manipulate the SVD of the matrix $\widetilde{Y}_{C(i)}$, so as to get transformed data and a corresponding model with a reduced number of parameters that can be estimated reliably.

4.3.1 Model reduction by PCA

We start by considering the case where the regression matrix is noiseless, *i.e.*, $\widetilde{Y}_{C(i)} = Y^*_{C(i)}$, and $\mathrm{rank}(Y^*_{C(i)}) = r$, with $r < n_b$. Notice that the latter is always the case for structurally nonidentifiable models. The extension of the method to practical identifiability (where $Y_{C(i)}$ is full column rank but ill-conditioned) and to noisy and incomplete data $\widetilde{Y}$ will be discussed in the next sections.

Consider again the SVD $Y_{C(i)} = U \cdot \mathrm{diag}(s_1, s_2, ..., s_{n_b}) \cdot V^T$, with $s_1 \geq s_2 \geq \dots \geq s_{n_b} \geq 0$. Since $r < n_b$, it holds that $s_1 \geq \dots \geq s_r > 0$ and $s_{r+1} = \dots = s_{n_b} = 0$. Then, $Y_{C(i)}$ has an $(n_b - r)$-dimensional kernel K_Y, given by $K_Y = \mathrm{range}(V_{r+1:n_b})$. For any $B_{C(i)}$ and any $k_Y \in K_Y$, it holds that $Y_{C(i)} \cdot B_{C(i),i} = Y_{C(i)} \cdot (B_{C(i),i} + k_Y)$. For the purpose of identification, this means that $B_{C(i),i}$ cannot be uniquely reconstructed from the data. On the other hand, $\mathrm{span}(Y_{C(i)}) = \mathrm{span}(Y_{C(i)} V_{1:r})$, where $Y_{C(i)} V_{1:r}$ is full column rank. Then, for every $B_{C(i),i}$ there exists a unique $\breve{B}_i \in \mathbb{R}^{r \times 1}$ such that $Y_{C(i)} \cdot B_{C(i),i} = Y_{C(i)} V_{1:r} \cdot \breve{B}_i$. This suggests to modify the regression problem $W_i = Y_{C(i)} \cdot B_{C(i),i} + \varepsilon_i$ into

$$\begin{cases} W_i = \breve{Y}_i \cdot \breve{B}_i + \varepsilon_i \\ \breve{Y}_i = Y_{C(i)} V_{1:r} \end{cases} \tag{4.20}$$

which has a unique solution in $\breve{B}_i$, i.e. $\breve{B}_i$ is identifiable. We call (4.20) the reduced model and $\breve{B}_i$ the reduced parameter vector.

For a fixed outcome of the noise ε_i, from the unique solution $\breve{B}$ in the reduced parameter space one can infer a whole subspace of equivalent solutions in the original parameter space as $\{B_{C(i),i} = V_{1:r} \cdot \breve{B}_i + k_Y, \quad k_Y \in K_Y\}$. Thus, in general, a fixed solution $\breve{B}$ does not determine uniquely any of the parameters B_{ji} (j being an element of $C(i)$). However, depending on the structure of V, we may be able to isolate some parameters B_{ji} that can be reconstructed without ambiguity.

Proposition 3. *Suppose that, for an index j with $1 \leq j \leq n_b$, the entries of $V_{j,r+1:n_b}$ are all zero. If $\breve{B}_i$ is the (unique) solution to Eq.* (4.20)*, then $B_{ji} = V_{j,1:r}\breve{B}_i$ is uniquely determined.*

A similar, but less general approach to separate identifiable from nonidentifiable parameters has been considered by [Nikerel et al., 2009].

4.3.2 Model reduction put in practice

In a real setting, as shown in Example 4, small nonzero values of $s_{r+1}, \ldots, s_{n_b}$ can also make the problem of estimating $B_{C(i)}$ ill-conditioned, thus preventing practical identifiability. In addition, measurement error can make certain components of the data indistinguishable from noise. The idea here is to remove the components of the parameters that are poorly determined from the data, thus ensuring smaller estimation uncertainty and hence practical identifiability in a reduced parameter space. In order to develop and explain the rationale of our method, we will first reconsider model reduction in the setting of Problem 4, where the metabolite data are assumed noiseless, and then move on to the more realistic scenario of Problem 1, where metabolite data are noisy. In the remarks concluding the section, we will briefly discuss the application of the method to datasets with missing or corrupted entries (*e.g.*, outliers) and its biological interpretation. We will then summarize the model reduction procedure in Sec. 4.3.3.

The scenario of Problem 4. Here $\widetilde{Y}_{C(i)} = Y^*_{C(i)}$. One may consider the rank-r approximation of the data matrix

$$Y^*_{C(i)} = U \cdot \operatorname{diag}(s_1, s_2, ..., s_{n_b}) \cdot V^T \simeq U \cdot \operatorname{diag}(s_1, s_2, ..., s_r, \underbrace{0, \ldots, 0}_{n_b - r}) \cdot V^T = \hat{Y}_i.$$

Following the previous section, for $\breve{Y}_i = \hat{Y}_i V_{1:r}$, consider the reduced model

$$\begin{cases} W_i = \breve{Y}_i \cdot \breve{B}_i + \varepsilon_i \\ \breve{Y}_i = \hat{Y}_i V_{1:r} \end{cases} . \tag{4.21}$$

with unique least-squares solution for the reduced parameter $\breve{B}_i$. With the same arguments as in Sec. 4.2.2, for $\Sigma_{\varepsilon_i} = \sigma_i^2 I$, one observes that the confidence ellipsoid associated with the estimate of $\breve{B}_i$ is determined by the matrix $\sigma_i^2 \big(\breve{Y}_i^T \breve{Y}_i\big)^{-1}$. In particular, the largest axis length, corresponding to the largest parameter estimation uncertainty, is proportional to σ_i / s_r, i.e. it has been reduced by a factor s_r / s_{n_b} with respect to the original estimation problem. This analysis suggests a criterion for the choice of r based on our definition of practical identifiability. Suppose that, with a given confidence $100 \cdot (1 - \alpha)\%$, the admissible uncertainty $\mathscr{B}_i$ is a ball of radius δ. Since the radii of the estimation error confidence ellipsoid are given by $\lambda(\alpha)\sigma_i/s_r \geq \ldots, \geq \lambda(\alpha)\sigma_i/s_1$ it suffices to choose r as the minimum value for which $\lambda(\alpha)\sigma_i/s_r \leq \delta$ for the reduced model to be practically identifiable. If this holds for $r = n_b$, the full model is practically identifiable and needs no reduction.

The scenario of Problem 1. Here the noisy versions $\widetilde{Y}$ of Y are the available data. The idea is to remove from the problem not only the components that make estimation ill-conditioned, but also those components that are detrimental in that they are dominated by noise. To do this, let us look at the empirical covariance matrix of the data $\widetilde{Y}^T_{C(i)} \widetilde{Y}_{C(i)} / q$. From the approximation[2]

$$\widetilde{Y}_{C(i)}^T \widetilde{Y}_{C(i)} = Y_{C(i)}^T Y_{C(i)} + \eta_{C(i)}^T \eta_{C(i)} + Y_{C(i)}^T \eta_{C(i)} + \eta_{C(i)}^T Y_{C(i)} \simeq Y_{C(i)}^T Y_{C(i)} + q\Sigma_{\eta_{C(i)}},$$

where $\Sigma_{\eta_{C(i)}} = \nu^2 I$, it follows that

$$\begin{aligned}\widetilde{Y}_{C(i)}^T \widetilde{Y}_{C(i)}/q &\simeq \left(U \operatorname{diag}(s_1, \dots, s_{n_b}) V^T\right)^T \left(U \operatorname{diag}(s_1, \dots, s_{n_b}) V^T\right)/q + \nu^2 I \\ &= V\left(\operatorname{diag}(s_1^2, \dots, s_{n_b}^2)/q + \nu^2 I\right) V^T,\end{aligned}$$

where the right-hand side is the SVD of $\widetilde{Y}_{C(i)}^T \widetilde{Y}_{C(i)}/q$, with singular values $\widetilde{s}_\ell^2 = s_\ell^2/q + \nu^2$, $\ell = 1, \dots, n_b$ composed of the signal contribution s_ℓ^2/q and the noise contribution ν^2. In the light of this, to remove the components of the data dominated by noise, we compute the (noisy) singular values $\widetilde{s}_1^2 \geq \widetilde{s}_2^2 \geq \ldots \geq \widetilde{s}_{n_b}^2 \geq 0$ from the SVD of $\widetilde{Y}_{C(i)}^T \widetilde{Y}_{C(i)}/q$, draw estimates $\hat{s}_\ell^2$ of the true (noiseless) singular values s_ℓ^2 by posing $\hat{s}_\ell^2 = \max(0, \tilde{s}_\ell^2 - \nu^2)$ for $\ell = 1, \dots, n_b$, and define what we call the "effective rank" of the data matrix as follows.

Definition 3. *The effective rank of the data matrix is*

$$r = \max\{\ell : \ \hat{s}_\ell^2 \geq \nu^2, \ \ell = 1, \dots, n_b\} \tag{4.22}$$

According to this definition, the effective rank indicates the number of independent components that can be safely distinguished in the data in that not blurred by noise. Notice that noise, by its very nature, tends to decorrelate all matrix entries. Following on the discussion for the scenario of Problem 4, this criterion may also be seen as implementing model reduction for practical identifiability, with a choice of the uncertainty region $\mathscr{B}_i$ depending on ν, *i.e.*, adapted to the presence of noise on metabolite data.

An alternative approach to determine the effective rank of a data matrix, useful when ν is assumed small but is not known with certainty, is to remove the components associated with the smallest singular values by setting r so that a suitable proportion $\theta \in (0, 1)$ of the total variance $\sum_{\ell=1}^{n_b} \tilde{s}_\ell^2$ of the data is retained, as used in Chap. 3. This gives rise to the following definition of effective rank.

Definition 4. *The* $100 \cdot \theta$*%-variance effective rank of the data matrix is*

$$r = \min\left\{ r' : \ \sum_{\ell=1}^{r'} \tilde{s}_\ell^2 \geq \theta \cdot \sum_{\ell=1}^{n_b} \tilde{s}_\ell^2, \ r' = 1, \dots, n_b \right\}. \tag{4.23}$$

Different from the previous definition, effective rank is intended here simply as the number of components needed to express most of the data information content. When applied to data with small noise, data components dominated by noise are also small and are hence excluded from the count. For large noise levels, this reasoning no longer applies. Note that precise

[2] This holds as an equality in the sense of expectation, and can also be motivated by asymptotic arguments as $q \to +\infty$.

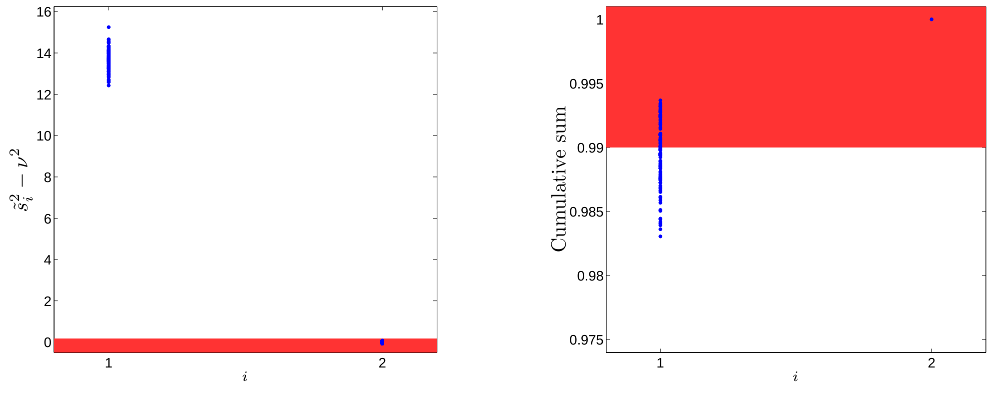

(a)

(b)

Figure 4.4: Identifiability analysis for the feedback model in Fig. 4.1, with $a_1 = 0.0297$ and $B_{2,1} = -7.2961$. (a) Squared singular values for 100 data matrices Y (see text of Example 5). The blue dots are the estimates of the squared singular values $\tilde{s}_\ell^2 - \nu^2$ for each dataset and the red box covers the area below the cutoff of ν^2 (Def. 3). (b) Normalized cumulative sum of squared singular values for 100 data matrices Y. The red box display the area below the cutoff $\theta = 0.99$ (Def. 4).

knowledge of the noise variance ν^2 is not required here, at the price of a rather uninformed choice of parameter θ.

In both cases, after computing the effective rank r, the original model can be replaced by the reduced model (4.21), providing us with a well-behaved model for the subsequent identification of the system.

Example 5. *We have seen in Example 4 that the first reaction of the feedback model with* $a_1 = 0.0297$ *and* $B_{2,1} = -7.2961$ *is not practically identifiable and we want to see which definition of* r *enables PCA to detect this property on a limited noisy dataset. In order to mimic available experimental data [Ishii et al., 2007], noise was added to the data matrix* Y *by drawing* $q = 30$ *values from a normal distribution with standard deviation of* 0.4*, corresponding approximately to 40% noise for metabolite concentrations (hereafter called "40% noise level"). 100 datasets were generated in this way and PCA was performed on each of them. Two different definitions of* r *were tested for model reduction, based on the criteria in Defs. 3 and 4. Fig. 4.4(a) shows the estimates of the squared singular values and the cutoff of* ν^2 *while Fig. 4.4(b) shows the normalized cumulative sums of the squared singular values and the cutoff of* 0.99*. The second squared singular value is always smaller than* $2\nu^2$*, so that the model is correctly found not identifiable with the first definition, contrary to what is found with the second definition 57 times out of 100.*

The above example thus illustrates that the criterion for model reduction taking into account the noise level, when applicable, is more relevant.

Remark 2. *The data matrix $\widetilde{Y}_{C(i)}$ may suffer from the lack of certain data entries, typically due to the removal of outliers or faults of the experimental machinery. A simple but wasteful option to recover a full data matrix for later use in a well-defined model reduction/parameter estimation problem is to discard those data points $\widetilde{Y}_{jC(i)}$, and the corresponding flux information $\widetilde{W}_{ji}$, suffering from the absence of some entry. In Chap. 3, in the context of parameter estimation, we have proposed methods compensating for the missing entries by the use of statistical priors inferred from the available data. For the sake of model reduction, which requires in our approach the SVD of the data matrix, completion of the data matrix by a suitable imputation method was suggested. Several imputation methods can be considered, still relying on statistics from the available data, such as multiple imputation, completion by the mean of the available metabolite data, and so on (see Chap. 3 and references therein). As an appealing alternative we cite minimal rank SVD, which has been developed and applied in Brand [2002] for reduced-order modelling in computer vision.*

Remark 3. *The reduction of the model to Eq.* (4.21) *introduces new parameters that are linear combinations of the original parameters. As a consequence, the results of the identification may be difficult to interpret from a biological point of view. Proposition 3 suggests a way to isolate identifiable parameters in nonidentifiable reactions, and thus extract partial, but unambiguous information from the dataset. Unfortunately, the condition of the proposition is not usually verified in practice, since due to noise the entries of the kernel of Y, given by the vectors $V_{j,r+1:n_b}$, $j = 1, \cdots, n_b$, will never be exactly 0. In order to ease the interpretation of the results, one may relax this condition as follows. Bearing in mind that $V_{j,r+1:n_b}$ is composed of unit-$\mathscr{L}^2$-norm vectors, we consider negligible all entries of $V_{j,r+1:n_b}$ whose square is below a threshold ρ^2 significantly smaller than 1. Further study of the kernel-generating matrix $V_{r+1:n_b}$ would yield a theoretically more sophisticated criterion, but we will not pursue this discussion here.*

Remark 4. *In general, data from repeated experiments may happen to be more densely concentrated in some regions than in others. In the extreme case, homeostatic control of metabolite concentrations may cluster most datapoints around a single value. Thus, the variance will be dominated by the variance of experimental error, strongly distorting the analysis of practical identifiability as outlined above. To compensate for this bias, we modify the estimation problem by introducing a weighting scheme to rebalance the importance of the datapoints, that we develop in Appendix B.2. However, application of this data weighting to Example 3 with a weak feedback showed no significant improvement of the model reduction method (see Appendix B.2).*

4.3.3 The overall model reduction procedure

Based on the discussion of the previous sections, here we summarize the procedure for obtaining a practically identifiable approximate kinetic model from noisy and incomplete datasets. The procedure is also summarized in Figure 4.5.

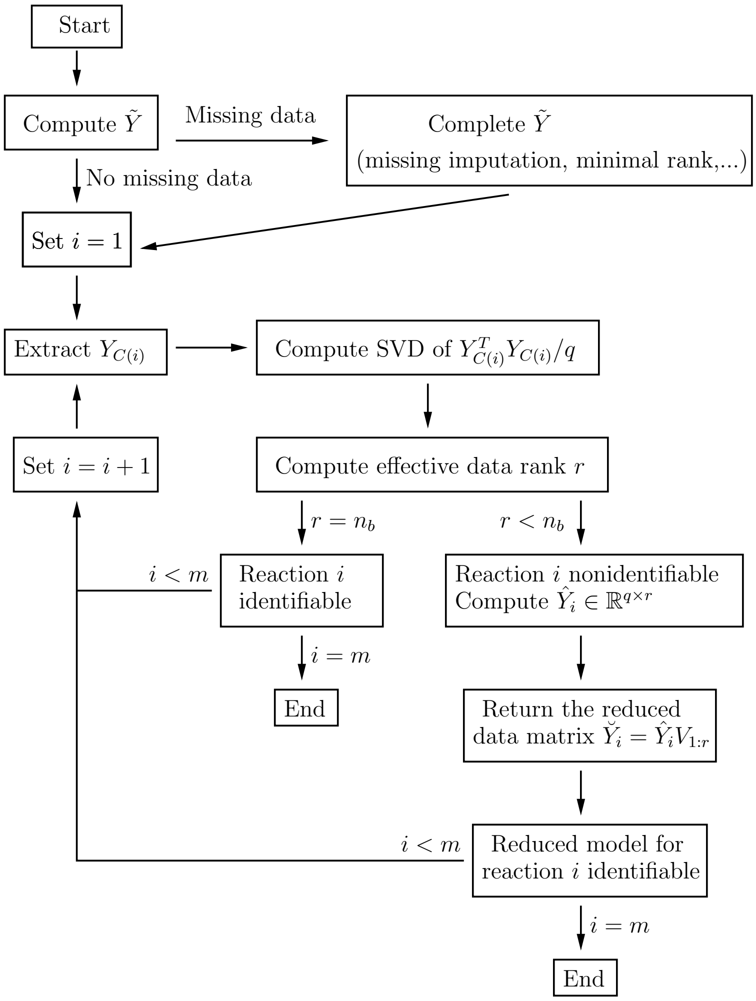
Start
Compute $\tilde{Y}$
Missing data
Complete $\tilde{Y}$
(missing imputation, minimal rank,...)
No missing data
Set $i = 1$
Extract $Y_{C(i)}$
Compute SVD of $Y_{C(i)}^T Y_{C(i)}/q$
Set $i = i + 1$
Compute effective data rank r
$r = n_b$
$r < n_b$
$i < m$
Reaction i identifiable
Reaction i nonidentifiable
Compute $\hat{Y}_i \in \mathbb{R}^{q \times r}$
$i = m$
End
Return the reduced data matrix $\breve{Y}_i = \hat{Y}_i V_{1:r}$
$i < m$
Reduced model for reaction i identifiable
$i = m$
End

Figure 4.5: Overall procedure for identifiability analysis and model reduction

Given noisy steady-state metabolite data $\ln \tilde{x}^1, \dots, \ln \tilde{x}^q$:

- Compute the data matrix $\widetilde{Y}$.
- In case of missing entries, complete the matrix by a method of choice (multiple imputation, minimum rank completion, ...)
- For every reaction $i = 1, \dots, m$
  1. Extract from $\widetilde{Y}$ the data submatrix $\widetilde{Y}_{C(i)}$
  2. Compute the SVD of the empirical data covariance matrix $Y^T_{C(i)} Y_{C(i)}/q = V \operatorname{diag}\{s_1^2, \dots, s_{n_b}^2\} V^T$
  3. Compute the effective data rank $r = \max\{\ell : \; \tilde{s}_\ell^2 - \nu^2 \geq \nu^2\}$
  4. Compute $\hat{Y}_i$, the data matrix obtained by discarding the $n_b - r$ smallest components, as $\hat{Y}_i = Y_{C(i)} \cdot \begin{bmatrix} V_{1:r} & 0_{n_b \times (n_b - r)} \end{bmatrix} V^T$, $0_{n_b \times (n_b - r)}$ being the $n_b \times (n_b - r)$ null matrix.
  5. Return the reduced model $W_i = \breve{Y}_i \cdot \breve{B}_i + \varepsilon_i$, with $\breve{Y}_i = \hat{Y}_i V_{1:r}$

4.4 Applications of the model identifiability and reduction approach

4.4.1 Application to a network with simulated data

In order to evaluate performance of our identifiability and model reduction procedure, we now discuss its application to a more realistic simulated network originally presented in [Visser and Heijnen, 2003] (Fig. 4.6(a)). The network involves $n_x = 8$ internal and $n_u = 3$ external metabolites, participating in a total of $m = 8$ reactions.

The linlog model of the network is based on the state and input vectors x and u whose entries are listed in Fig. 4.6(b). The parameter matrices of the model include 33 nonzero entries and are given by $a = \begin{bmatrix} -31.4 & 4.41 & 0.13 & 0.31 & 0.31 & 0.13 & -0.42 & 0.97 \end{bmatrix}^T$,

$$B^x = \begin{bmatrix} -2.470 & -17.40 & 0 & 0 & 0 & 0 & 0 & 0 \\ 0.061 & -0.219 & 0 & 0 & 0 & 0.351 & 0 & -1.040 \\ 0 & 0.083 & -0.015 & 0 & 0 & 0 & 0 & -0.029 \\ 0 & 0 & 0.027 & -0.003 & 0 & -0.001 & 0 & 0.086 \\ 0 & 0 & 0 & 0.848 & 0 & 0 & 0 & 0 \\ 0 & 0.093 & 0 & 0 & 0 & 0 & -0.004 & -0.017 \\ 0 & 0 & 0 & 0 & -0.486 & -0.039 & 0.090 & 0.099 \\ 0 & 0 & 0 & 0 & 2.160 & 0 & 0 & 0 \end{bmatrix}, \quad B^u = \begin{bmatrix} 3.880 & 0 & 0 \\ 0 & 0 & 0 \\ 0 & 0 & 0 \\ 0 & 0 & 0 \\ 0 & -0.713 & 0 \\ 0 & 0 & 0 \\ 0 & 0 & 0 \\ 0 & 0 & -1.560 \end{bmatrix},$$

The values of B^u were taken directly from [Visser and Heijnen, 2003], while the values of a and B^x were adapted from the same paper. The stoichiometry matrix N, given in Eq. (4.24) below, is fixed by the ordering of the input and state vector entries and the scheme in Fig. 4.6(a). The row rank of this matrix is equal to 6, corresponding 2 mass conservation

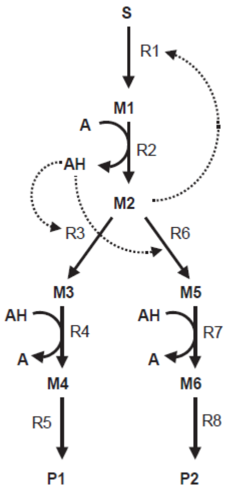

(a)

Internal metabolites		External metabolites	
Variable	Metabolite	Input	Metabolite
x_1	M1	u_1	S
x_2	M2	u_2	P1
x_3	M3	u_3	P2
x_4	M4		
x_5	M6		
x_6	A		
x_7	M5		
x_8	AH		

(b)

Figure 4.6: (a) A branched metabolic pathway with feedback from [Visser and Heijnen, 2003]. All reactions are chemically reversible, the arrows represent the positive flux directions. Dashed lines represent allosteric interactions. (b) Model variables and external metabolites

constraints given in Eq. (4.25). Following the analysis of Reder [1988], it is possible to factor the matrix into a link matrix L expressing dependencies between concentrations and a reduced-order full-row rank matrix $\breve{N}$ corresponding to stoichiometries of independent metabolites. Factorization is non-unique. In our case, one such factorization gives

$$
\begin{aligned}
N = \begin{bmatrix} 1 & -1 & 0 & 0 & 0 & 0 & 0 & 0 \\ 0 & 1 & -1 & 0 & 0 & -1 & 0 & 0 \\ 0 & 0 & 1 & -1 & 0 & 0 & 0 & 0 \\ 0 & 0 & 0 & 1 & -1 & 0 & 0 & 0 \\ 0 & 0 & 0 & 0 & 0 & 0 & 1 & -1 \\ 0 & -1 & 0 & 1 & 0 & 0 & 1 & 0 \\ 0 & 0 & 0 & 0 & 0 & 1 & -1 & 0 \\ 0 & 1 & 0 & -1 & 0 & 0 & -1 & 0 \end{bmatrix} &= \begin{bmatrix} 1 & 0 & 0 & 0 & 0 & 0 \\ 0 & 1 & 0 & 0 & 0 & 0 \\ 0 & 0 & 1 & 0 & 0 & 0 \\ 0 & 0 & 0 & 1 & 0 & 0 \\ 0 & 0 & 0 & 0 & 1 & 0 \\ 0 & 0 & 0 & 0 & 0 & 1 \\ 0 & -1 & -1 & 0 & 0 & -1 \\ 0 & 0 & 0 & 0 & 0 & -1 \end{bmatrix} \cdot \begin{bmatrix} 1 & -1 & 0 & 0 & 0 & 0 & 0 & 0 \\ 0 & 1 & -1 & 0 & 0 & -1 & 0 & 0 \\ 0 & 0 & 1 & -1 & 0 & 0 & 0 & 0 \\ 0 & 0 & 0 & 1 & -1 & 0 & 0 & 0 \\ 0 & 0 & 0 & 0 & 0 & 0 & 1 & -1 \\ 0 & -1 & 0 & 1 & 0 & 0 & 1 & 0 \end{bmatrix} \\
&= L \cdot \breve{N}.
\end{aligned}
\tag{4.24}
$$

With this factorization, the entries of $x_{1:6}$ (M1, M2, M3, M4, M6 and A) are treated as independent quantities, and determine the values of x_7 (M5) and x_8 (AH) via conservation of mass. That is, for some fixed constants $T_1, T_2 \in \mathbb{R}_{>0}$,

$$
\begin{cases} \dot{x}_{1:6} = \breve{N} \operatorname{diag} e(a + B^x \cdot \ln x + B^u \cdot \ln u) \\ T_1 = x_2 + x_3 + x_6 + x_7 \\ T_2 = x_6 + x_8 \end{cases} \tag{4.25}
$$

In addition to analysis purposes, this reformulation allows one to compute the steady-

Reaction	**Number of**	**Average effective rank**	
number	**parameters**	**Def. 3**	**Def. 4**
R1	2	1	1.98
R2	4	2	3.51
R3	3	1.05	3
R4	4	2.11	4
R5	1	0.21	1
R6	3	1.3	2.99
R7	4	2.02	3.96
R8	1	0.03	1

Table 4.1: Average effective rank computed for each reaction and with different definitions of r over 100 datasets of the model of Fig. 4.6. The criterion of Def. 4 was computed choosing $\theta = 0.99$.

state values of all system variables by setting the differential part to zero. In our case, the method is used to simulate steady-state data as a function of enzyme and external metabolite concentrations.

To assess identification performance, we considered the scenario of [Visser and Heijnen, 2003], where the external metabolite concentrations are fixed to $u = [1\ 0.1\ 0.2]^T$, $T_1 = 0.3$ and $T_2 = 0.1$. Since u is fixed, the parameter matrix B^u is obviously nonidentifiable, and the contributions of a and $B^u \ln u$ are indistinguishable. To circumvent this issue, we define the lumped constant term $a' = a + B^u \ln u$ so as to obtain the modified linlog reaction velocity model $v = \operatorname{diag} e \cdot (a' + B^x \ln x)$, and study the identifiability and reduction of the latter in terms of a' and B^x.

We first generate a large noiseless dataset Y^{ref} corresponding to 1000 different values of enzyme concentrations generated at random as in Example 3. This allows us to investigate the properties of the data due solely to the network model (structure and parameters), and will serve as a reference in the analysis of identification performance.

Then, identifiability analysis and model reduction are performed identically in accordance with Sec. 4.3.3 on $R = 100$ realistic randomly generated datasets $\widetilde{Y}$ and $\widetilde{W}$. Each dataset shares the same steady-state values Y and W computed for $q = 30$ different values of enzyme concentrations, generated once as in Example 5, and differs in the randomly generated 40% noise corrupting the measurements. The results from the application of both Def. 3 and Def. 4, with $\theta = 0.99$, were collected. The results are depicted in Figure 4.7 and are reported in the form of statistics in Table 4.1.

First, we notice that for every reaction, the effective rank computed with the criterion of Def. 4 is higher than the one computed with the criterion of Def. 3. Thus, the latter criterion gives more conservative results, in the sense that, on average, fewer reactions are deemed identifiable. Except for reaction 2, application of Def. 4 returns the full size of the reaction for at least 96 out of 100 datasets. That is, in this case, the ability of the criterion to detect dependencies among data is very limited. This can be explained by the presence of a significant amount of noise on metabolite data, which tends to decorrelate the observations.

The criterion based on Def. 3 detects dependencies among the data of all reactions. The effective rank determined by this criterion is consistently smaller and differs from the results of Def. 4 by an average of about 1 for reactions 1, 5 and 8, and of about 2 for the other reactions. This can be attributed to the compensation of noise in the computation of the singular value estimates $\hat{s}_\ell$ in Eq. (4.22), which relies upon and exploits the knowledge of the noise level ν. This is apparent in Fig. 4.7, where the blue dots representing the singular value estimates drawn from each of the 100 datasets $\widetilde{Y}$ are correctly concentrated around the true singular values of Y. The appropriateness of rank estimation based on Eq. (4.22) is also confirmed by the comparison of Figs. 4.7 and 4.8, showing that the singular values buried in the red cutoff regions of Fig. (4.22) correspond to the strongest dependencies among metabolites revealed by the analysis of Y^{ref}, reported as red bars in Fig. 4.8. Fig. 4.7 also clarifies the non-integer average rank values of Table 4.1 (notably for reactions 4, 5 and 6), depending on the fact that the singular values of Y lying close to the significance cutoff value ν^2 are estimated above or below this threshold depending on the simulation run. For instance, the estimates of the second singular value of reaction 6 were smaller than ν^2 in 70 of the 100 runs.

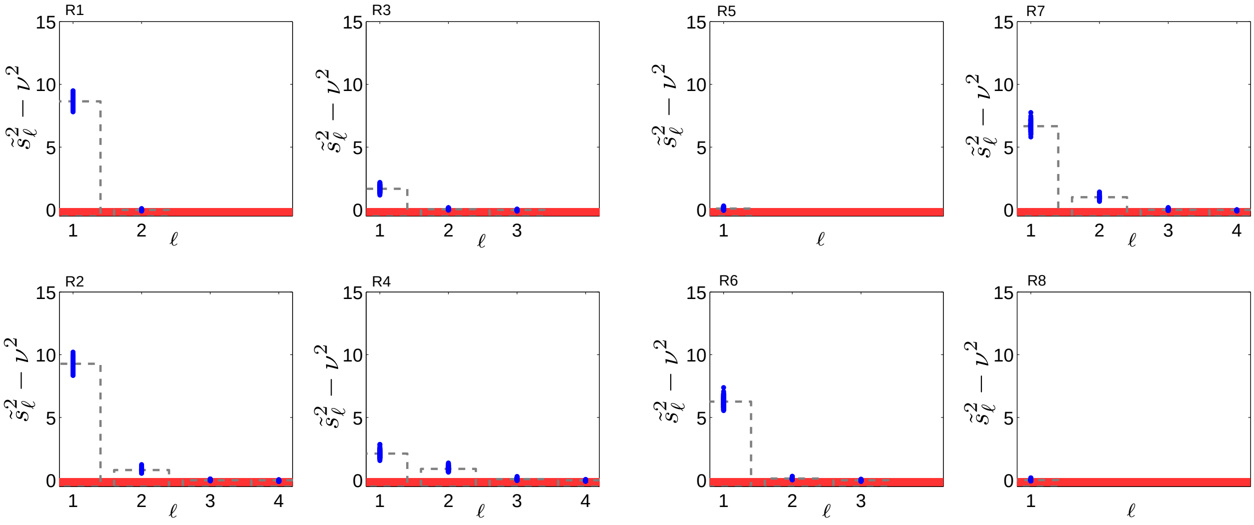

Figure 4.7: Singular value estimates $\tilde{s}_\ell^2 - \nu^2$ computed from 100 noisy datasets $\widetilde{Y}$ of size $q = 30$ (blue dots) of the model of Fig. 4.6. The bars in gray correspond to singular values s_ℓ^2 of the noiseless dataset Y of size $q = 30$. In red is the area below ν^2; all singular values in this area are considered negligible.

Finally, the results for reactions 5 and 8 reveal a fundamental difference between Defs. 3 and 4. The former method leads to conclude that no modeling is possible (the effective rank is estimated to be zero in most runs) in that the corresponding metabolite data is dominated by noise, whereas Def. 4 provides effective rank estimates that are by construction lower-bounded by one.

We would like to compare the results from the model reduction criterion of Def. 3 with the reference dataset Y^{ref}. Apart from an arbitrary threshold on the norm, we do not have an objective quantitative criterion to determine rank deficiency on submatrices of noiseless Y^{ref}. For each reaction, the SVD of the corresponding submatrix of Y^{ref} was computed and singular values are shown in Fig. 4.8. In this figure are highlighted in red the reference singular values that would be considered negligible with the rank reductions of last column of Table 4.1. We observe that all singular values that intuitively matter are captured. Thus the method of Def. 3 gives consistent results with the 'ideal' dataset Y^{ref}.

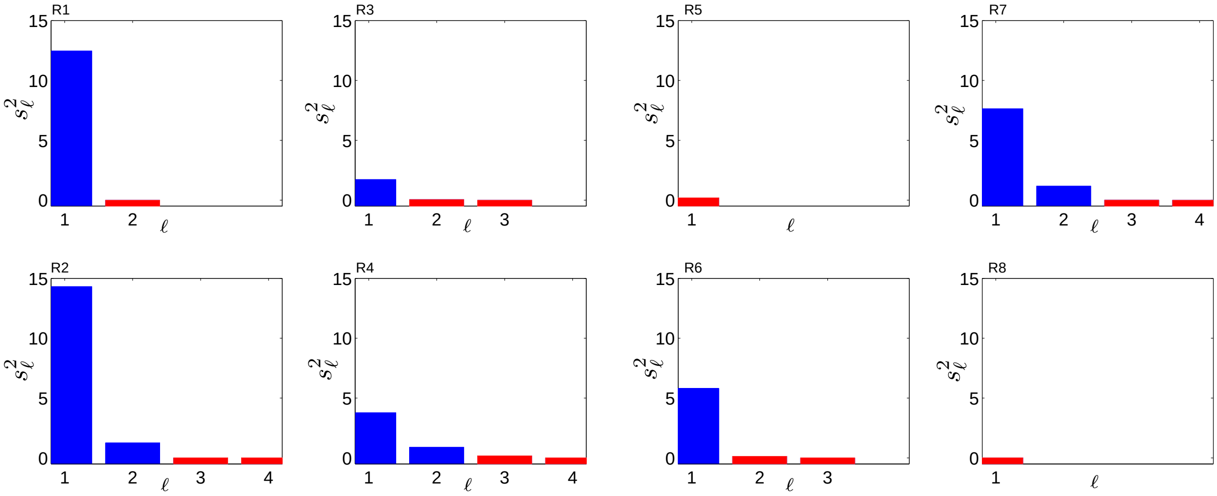

Figure 4.8: Squared singular values of the noiseless dataset Y^{ref} of the model of Fig. 4.6 ($q = 1000$). The bars in red correspond to singular values that are detected as negligible in at least 70% of the cases by Def. 3 on 100 noisy datasets.

From the results of this section, it is clear that identifiability analysis and model reduction in the presence of noise should be performed on the basis of the effective rank of Def. 3, which outperforms Def. 4 to all practical effects and returns consistent results (Table 4.1; compare Fig. 4.7 and 4.8). This makes us select Def. 3 as the basis for identifiability analysis and model reduction of real data. The actual application of the method to a real dataset is discussed in the next section.

A discussion about the application of the model reduction methods discussed in Sec. 4.3.2 in case of a biased dataset can be found in Appendix B.2.

4.4.2 Application to central carbon metabolism of *E. coli*

As a second example, we illustrate the application of our method to a complex network of biochemical reactions involved in carbon assimilation in the enterobacterium *Escherichia coli*.

The network we consider gathers enzymes, metabolites and reactions that make up the bulk of central metabolism, including glycolysis, the pentose-phosphate pathway, the tricarboxylic acid cycle and anaplerotic reactions such as glyoxylate shunt and PEP-carboxylase (Fig. 4.9). The network has been studied for a long time from different perspectives, which makes it an ideal model system for our purpose. The structure of the *E. coli* carbon metabolism network is known in a rather precise way, its dynamics have been modeled by means of a variety of formalisms ([Bettenbrock et al., 2006, Kotte et al., 2010] and references therein), and recently a high-throughput dataset containing the required information for solving Problem 1 has been published [Ishii et al., 2007].

We now investigate which reactions are identifiable following the criteria of Sec. 4.3, given the available experimental data and a linlog model of the network. In particular, from a methodological point of view, we are interested in analyzing the differences between results obtained with Def. 3 and Def. 4. The latter criterion was used in Chap. 3, but as discussed above, it underestimates the effect of noise on the identifiability of reactions. In addition, from a biological point of view, the results of the application will improve our understanding of how much information is actually contained in a state-of-the-art dataset for the purpose of parameter estimation.

The dataset used for identification of the network in Figure 4.9 was obtained by experiments with 24 single-gene deletions that were grown at a fixed dilution rate of 0.2 h^{-1} in a glucose-limited chemostat, and with wild-type cells at 5 different dilution rates [Ishii et al., 2007]. The authors collected data using multiple high-throughput techniques, in particular DNA microarray analysis and two-dimensional differential gel electrophoresis (2D-DIGE) for genes and proteins, capillary electrophoresis time-of-flight mass spectrometry (CE-TOFMS) for metabolites, and metabolic flux analysis. They thus obtained a steady-state dataset consisting of metabolite concentrations, mRNA and protein concentrations for the enzymes, and metabolic fluxes under 29 different experimental conditions. The dataset contains the information for setting up a parameter estimation problem as defined in Sec. 4.1.

We carried out the identifiability analysis for the linlog model developed in Chap. 3. This model is a translation of the reaction scheme of Figure 4.9 into linlog rate equations (3.2). When certain metabolites could not be measured, preventing their inclusion in the model, we lumped together the reactions in which they are involved. In addition to the above model simplification, imposed by the available data, we added a phenomenological reaction to model biomass production. The resulting model has $n_x = 16$ internal metabolites, $n_u = 7$ external metabolites and measured cofactors, and $m = 31$ reactions (see Sec. 3.4).

A complication for determining the identifiability of the reactions and finding a suitable model reduction is that the dataset contains a large amount of missing data. In particular, certain metabolites could not be measured in up to 80% of the experimental conditions (28% on average for all metabolites). Following Remark 2 of Sec. 4.3, we therefore completed the dataset by means of multiple imputation, generating 100 datasets to allow the computation

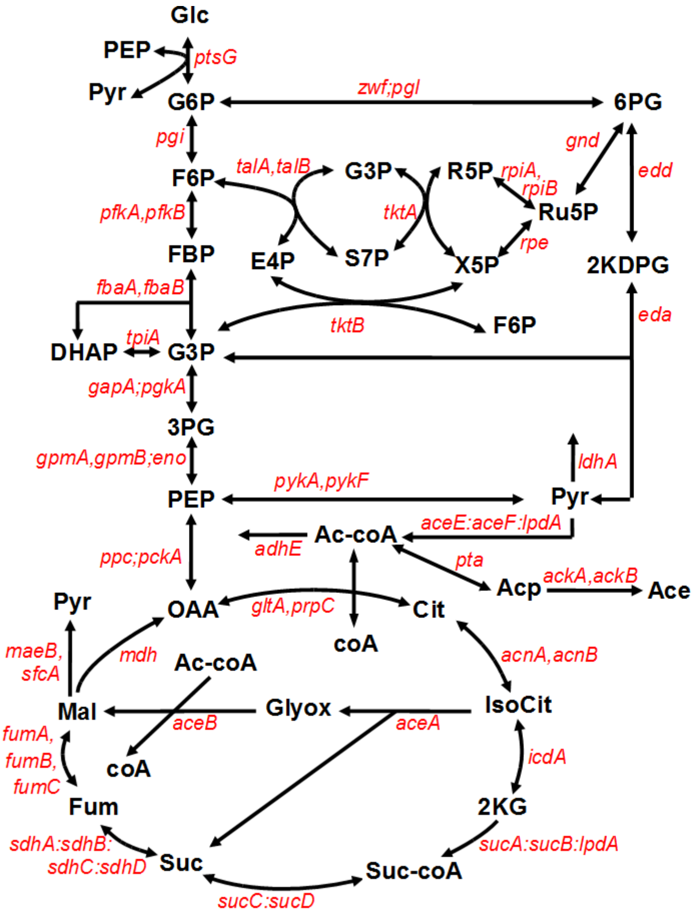

Figure 4.9: Scheme of *Escherichia coli* central carbon metabolism. The map shows metabolites (bold fonts) and genes (italic). Abbreviations of metabolites are glucose (Glc), glucose 6-phosphate (G6P), fructose 6-phosphate (F6P), fructose 1-6-biphosphate (FBP), dihydroxyacetone phosphate (DHAP), glyceraldehyde 3-phosphate (G3P), 3-phosphoglycerate (3PG), phosphoenolpyruvate (PEP), pyruvate (Pyr), 6-phosphogluconate (6PG), 2-keto-3-deoxy-6-phospho-gluconate (2KDPG), ribulose 5-phosphate (Ru5P), ribose 5-phosphate (R5P), xylulose 5-phosphate (X5P), sedoheptulose 7-phosphate (S7P), erythrose 4-phosphate (E4P), oxaloacetate (OAA), citrate (Cit), isocitrate (IsoCit), 2-keto-glutarate (2KG), succinate-CoA (Suc-coA), succinate (Suc), fumarate (Fum), malate (Mal), glyoxylate (Glyox), acetyl-CoA (Ac-coA), acetylphosphate (Acp) and acetate (Ace). Cofactors impacting the reactions are not shown: adenosine triphosphate (ATP), adenosine diphosphate (ADP), nicotinamide adenine dinucleotide phosphate (NADP) and its reduced form (NADPH), nicotinamide adenine dinucleotide (NAD) and its reduced form (NADH) and flavin adenine dinucleotide (FAD). The gene names are separated by a comma in the case of isoenzymes, by a colon for enzyme complexes, and by a semicolon when the enzymes catalyze reactions that have been lumped together in the model.

of statistics and test the robustness of the results.

Table 4.2 summarizes the results of applying the reduction method of Sec. 4.3.3 to the model and the data. For each of the reactions in the model, we computed the average of the effective rank of the 100 datasets. The effective rank for the individual datasets was usually found to be the same (in at least 82 of the 100 datasets), which explains that the computed average values are close to integers. Remarkably, out of the 31 reactions in the model, only 4 were found to be identifiable: reactions 4, 5, 14, and 31. The first three reactions involve two metabolites: fructose 1-6-biphosphate (FBP) and dihydroxyacetone phosphate (DHAP) (reaction 4), dihydroxyacetone phosphate (DHAP) and 3-phosphoglycerate (3PG) (reaction 5) and ribose 5-phosphate (R5P) and sedoheptulose 7-phosphate (S7P) (reaction 14). The identifiability of these reactions means that the method did not detect any dependencies between these pairs of metabolite concentrations. Reaction 31 involves a single metabolic variable acetyl-CoA (Ac-coA). In the remaining 27 nonidentifiable reactions, the effective rank is reduced by 1 (in the case of 18 reactions), 2 (6 reactions), 3 (2 reactions), and 6 (1 reaction). The latter case concerns the growth-rate reaction, which has 11 variables. A striking observation on Tables 4.2 and 4.3 is therefore the large number of nonidentifiable reactions and parameters.

		Average	**Full**
Reaction	**Enzyme**	**effective rank**	**dimension**
1	PtsG	3	4
2	Pgi	1	2
3	PfkA,PfkB	2.85	4
4	FbaA,FbaB	2	2
5	TpiA	2	2
6	GapA;Pgk	2.99	4
7	GpmA,GpmB;Eno	1	2
8	PykA,PykF	2	4
9	AceE:AceF:LpdA	1.99	3
10	Zwf;Pgl	1.98	3
11	Gnd	2	3
12	Rpe	1	2
13	RpiA,RpiB	1.99	3
14	TktA	1.82	2
15	TalA,TalB	1	2
16	TktB	1.01	2
17	GltA,PrpC	2.97	4
18	AcnA,AcnB	1	2
19	IcdA	1	3
20	SucA:SucB:LpdA;SucC:SucD	1	3
21	SdhA:SdhB:SdhC:SdhD	1	3
22	FumA,FumB,FumC	1	2
23	Mdh	2.97	4
24	Ppc;PckA	3	5
25	MaeB,SfcA	2	5
26	AceA;AceB	1	3
27	μ	4.94	11
28	Edd;Eda	1	2
29	Pta;AckA,AckB	3	6
30	LdhA	1	2
31	AdhE	1	1

Table 4.2: Average effective rank computed for the reactions in the linlog model of *E. coli* central carbon metabolism, using the data of Ishii et al. [2007]. SVD has been applied on $Y_{C(i)}$ for each reaction and singular values were discarded based on Def. 3. Identifiable reactions are shown in green. Reaction 27, labeled μ, is a phenomenological reaction for biomass production.

In order to isolate identifiable parameters in nonidentifiable reactions, Prop. 3 proposes a criterion that has been relaxed in Remark 3 so as to make it applicable to noisy data. The approach is based on the choice of a threshold ρ^2 for neglecting components of the kernel matrix of Y. In what follows, to set a ground for discussion, we set ρ equal to 0.15. We verified that changes of this threshold within the range $\rho \in [0.1, 0.2]$ do not significantly alter the results as reported in Table 4.3. In this table, parameters that were diagnosed as being identifiable in more than 50% of the completed datasets are highlighted in green. From the 27 nonidentifiable reactions, no individual parameter could be unambiguously extracted in 8 cases (reactions 2, 7, 8, 12, 15, 16, 22 and 24). Of the 94 parameters in the remaining 19 reactions, 30 are identifiable in more than half of the datasets. In particular, we observe that all parameters associated to glucose (Glc), DHAP, acetyl-CoA/CoA (Ac-coA/coA), 6-phosphogluconate (6PG), ribose 5-phosphate (R5P), FAD and acetate (Ace) are identifiable, in the sense that no significant dependencies with other metabolites could be detected in the experimental conditions of Ishii et al. [2007].

The results shown in Table 4.3 are different from those obtained in Sec. 3.4, where we used a method based on Def. 4 with $\theta = 0.99$ instead of Def. 3. Indeed, we previously found many more reactions to be identifiable (24 out of 31) although, for most cases, parameter estimates were unreliable because of large confidence intervals. We believe that the results shown in Tables 4.2 and 4.3 more faithfully reflect the noisy character of the data, which is not explicitly taken into account by the criterion of Def. 4. Therefore, the results of the identifiability analysis in Sec. 3.4 appear to be overly optimistic, *i.e.*, overestimating the number of identifiable reactions and parameters because measurement noise on metabolite concentrations are not taken into account. Notwithstanding, the results of both analyses are consistent in the sense that all 7 reactions detected as nonidentifiable by means of Def. 4 remain nonidentifiable according to Def. 3 (reactions 10, 11, 17, 25, 27, 28 and 29).

We verified that taking into account the bias in the data sampling did not significantly change the identifiability analysis of the model (see Appendix B.2 for further details).

4.5 Discussion

A major, but often overlooked problem in the identification of metabolic network models is the identifiability of the parameters, and hence of the model. Informally speaking, the identifiability of a model (parameter) consists in the possibility to unambiguously reconstruct the model (parameter) from the observed behavior of the network. Identifiability problems may reside in the very structure of the model, notably the occurrence of (implicit) dependencies between parameters. These dependencies might be due to an inappropriate model formulation, constraints on the kind of experimental perturbations that can be realized, and unobserved variables. In addition, practical identifiability problems may arise from limitations on the quality and quantity of available data, in particular the fact that experimental data in biology are usually noisy, biased, sparse and incomplete.

We have studied identifiability issues in the context of approximate kinetic modeling formalisms, notably linear-logarithmic (linlog) models. On the theoretical side, following the classical systems identification literature [Ljung, 1999, Walter and Pronzato, 1997], we have

Table 4.3: Parameter matrix $[B^x\ B^u]$ and results of identifiability analysis and model reduction on the data by [Ishii et al., 2007] for the linlog model of *E. coli* central carbon metabolism (the columns of the matrix have been permuted for readability). SVD has been applied on $Y_{C(i)i}$ for each reaction and singular values were discarded based on Def. 3. Nonidentifiable parameters are shown in gray and identifiable ones, as well as identifiable reactions, in green. The percentages of cases for which the parameters were found identifiable out of the 100 imputed datasets are mentioned. Abbreviations are as in Fig. 4.9. To avoid complications deriving from the presence of conserved moieties, some of the metabolites are modeled as ratios of metabolite concentrations, *e.g.* ATP/ADP. Reaction 27, labeled μ, is a phenomenological reaction for biomass production. The last row indicates the percentage of missing data per metabolite.

	Metabolite **Enzyme**	Glc	PEP	G6P	Pyr	F6P	FBP	DHAP	3PG	Ac-coA	6PG	Ru5P	R5P	S7P	2KG	Suc	Fum	Mal	ATP	Cit	NADPH	NADH	FAD	Ace
										coA									ADP		NADP	NAD		
1	PtsG	100%	100%	31%	0 %																			
2	Pgi			0 %		0 %																		
3	PfkA,PfkB		70%			2%	63%												8%					
4	FbaA,FbaB						100%	100%																
5	TpiA							100%	100%															
6	GapA;Pgk						84%		6%										0%			51%		
7	GpmA,GpmB;Eno		0%						0%															
8	PykA,PykF		5%		0%		22%												0%					
9	AceE:AceF:LpdA				1%					99%												94%		
10	Zwf;Pgl			70%							100%										2%			
11	Gnd										100%	100%									0%			
12	Rpe											0%		0%										
13	RpiA,RpiB			0%								0%	66%											
14	TktA												82%	82%										
15	TalA,TalB					0%								0%										
16	TktB					1%						1%												
17	GltA,PrpC									97%					2%					98%		97%		
18	AcnA,AcnB														0%					100%				
19	IcdA									100%					0%						0%			
20	SucA:SucB:LpdA;SucC:SucD														0%	0%						90%		
21	SdhA:SdhB:SdhC:SdhD															0%	0%						62%	
22	FumA,FumB,FumC																0%	0%						
23	Mdh		87%															0%		75%		35%		
24	Ppc;PckA		19%				5%											0%	0%	32%				
25	MaeB,SfcA				0%					99%								0%			0%	30%		
26	AceA;AceB									100%						0%		0%						
27	μ		0%	0%	0%	0%			0%	68%			81%		0%				0%		0%	27%		
28	Edd;Eda				0%						100%													
29	Pta;AckA,AckB				0%					70%									0%		0%	37%		100%
30	LdhA				0%																	95%		
31	AdhE									100%														
	% Missing data	3	17	0	48	7	34	59	10	3	72	3	38	3	59	3	14	14	0	62	79	79	17	17

first precisely defined the notions of structural (*a-priori*) identifiability (Def. 1) and practical (*a-posteriori*) identifiability (Def. 2). The latter notion is obviously related to the former, in the sense that structural nonidentifiability entails practical nonidentifiability. However, Proposition 2 goes beyond this evidence by saying that identifiability in the theoretical sense may also imply identifiability in the practical sense, provided that the uncertainty on the parameters, as determined by the available dataset, remains within the desired accuracy bounds. Notice that practical identifiability is thus not an absolute notion, but rather conditional on the data properties and the required model precision.

A second methodological contribution of this chapter is the development of theoretically sound and practically applicable methods for the detection of identifiability problems and the transformation of a nonidentifiable model to a reduced identifiable model. In particular, we have formulated criteria based on the singular value decomposition (SVD) of the matrix of log-transformed and centered measurements of metabolite concentrations. These criteria define the effective rank of the data matrix, corresponding to the number of parameters that can be safely distinguished from the output. The criterion privileged in this chapter (Def. 3), contrary to a criterion that we proposed in the previous chapter (Def. 4), takes into account the estimated variance of the noise. The flow chart in Fig. 4.5 gives a step-by-step procedure for identifiability analysis and model reduction.

The identifiability of models of biological systems is a topic that has been much studied in mathematical biology, and that has received renewed attention in the context of systems biology in recent years (see Chappell et al. [1990], Chis et al. [2011b], Cobelli and di Stefano 3rd [1980], Raue et al. [2011] for reviews). Systems of biochemical reactions, which have the general form of Eq. (4.3) at steady-state, have a number of peculiarities for identifiability analysis. When reaction rates, enzyme concentrations and metabolite concentrations are measured, the identification problem can be decomposed into subproblems for each of the individual reactions. Determining the identifiability of a model then reduces to checking the identifiability of the reactions. If in addition the reaction rates are expressed in terms of linlog or other pseudo-linear equations, identification becomes a linear or orthogonal regression problem, depending on whether noise on the metabolite concentrations is taken into account or not (Problem 4 and Problem 5, respectively). Identifiability analysis then amounts to checking for linear dependencies in the transformed data matrix, which can be easily done using standard techniques from linear algebra and statistics. Related ideas starting from this general approach can be found in other recent work [Srinath and Gunawan, 2010, Nikerel et al., 2009]. However, as discussed in more detail in previous sections, the development of this approach in this chapter is different in fundamental ways, such as the very definition of structural and practical identifiability, and the application of SVD to detect and resolve identifiability problems.

Although linlog models have been central in this chapter, the results directly carry over to the other approximate formalisms mentioned in Sec. 4.1. In addition, they also bear on more general classes of nonlinear models of metabolic networks.Indeed the parameters in the mean-removed linlog model of Eq. (3.5) are proportional to elasticity coefficients that describe the sensitivities of reaction rates to changes in metabolite concentrations. If a reaction in a linlog model is nonidentifiable, this means that elasticity coefficients are not identifiable, therefore any other class of kinetic models is liable to encounter similar identifiability issues.

The approach for determining the identifiability of linlog models proposed in this chapter has been tested on a network with simulated data (Sec. 4.4.1) and applied to a high-throughput dataset for central carbon metabolism in *E. coli* (Sec. 4.4.2). The use of simulated data has made it possible to demonstrate that, for typical sizes of the dataset and realistic noise levels, our approach is able to correctly identify the principal components of the parameter vector (Fig. 4.7 and Fig. 4.8). Surprisingly, the determination of the effective rank of the datasets for the different reactions in the *E. coli* metabolic network shows that only a small fraction of the reactions (4 out of 31) is fully identifiable from the data of Ishii et al. [2007]. In addition, only 37 out of a total of 100 model parameters are individually identifiable. We note that these results are different from those reported in Sec. 3.4, due to the fact that here we take into account the measurement noise of metabolite concentrations to decide whether a parameter associated with a principal component is negligible. The low numbers of identifiable reactions and parameters agree with those obtained with power-law models on other state-of-the-art datasets Srinath and Gunawan [2010]. This further demonstrates the importance of a preliminary identifiability analysis when estimating parameters in metabolic network models.

The rank analysis carried out to determine the identifiability of a reaction also shows how the model can be reduced if the data does not allow the parameters of the model to be unambiguously determined. This reduction step yields minimal models in the form of Eq. (4.21), that have the advantage of being adapted to the informativeness of the dataset. A disadvantage of this approach, however, is that the parameters of the reduced model may be difficult to interpret from a biological point of view, as they do not generally determine the original parameters in a unique way, but rather define a linear subspace of the parameter space. Nevertheless, in some cases it may still be possible to identify some parameters of the original model (Proposition 3 and Remark 3). This criterion was shown to be useful in practice, as it allowed to uniquely identify 30 out of 93 parameters in the nonidentifiable reactions of the *E.coli* metabolic network model (Table 4.3).

If the parameters of the original, non-reduced model cannot be uniquely determined from the data, then additional experiments are necessary. Generally speaking, experimental conditions that explore the range of possible behaviors of the network as much as possible improve identifiability. Given that experiments are usually carried out at steady-state, especially for metabolic flux measurements, the available datasets have a sampling bias that may complicate parameter estimation. In particular, metabolic systems almost invariably contain highly evolved regulatory loops that may homeostatically buffer the concentrations of some metabolic pools [Bennett et al., 2009, Ishii et al., 2007]. As a consequence, a range of different growth conditions and genetic backgrounds may lead to little variation in steady-state metabolite concentrations. The growing availability of time-series data (*e.g.*, Voit et al. [2006b], Hardiman et al. [2007]), although more demanding from an experimental point of view, promises to relieve this problem.

Chapter 5

Shared control of gene expression in bacteria by transcriptional regulators and global physiological state

Bacterial cells continuously adjust gene expression in response to challenges from their environment. These adjustments involve transcription factors that sense metabolic signals and specifically activate or inhibit target genes. Several hundreds of transcription factors have been identified in *E. coli* [Martinez-Antonio and Collado-Vides, 2003]: while some respond to a particular stress and have only a few targets, others coordinate the expression of hundreds of genes across a variety of cellular functions. Well-known examples of the latter are global regulators of transcription such as Crp, Fis, and RpoS (σ^S) [Hengge-Aronis, 2002, Gosset et al., 2004, Bradley et al., 2007, Cho et al., 2008].

In addition to local regulation by DNA-binding transcription factors, the adjustments of gene expression involve global, regulatory mechanisms responding to the overall physiological state of the cell. More specifically, changes in the environment lead to the adaptation of metabolic pools and the macromolecular composition of the cell, which in turn affect the rate of transcription and translation. In balanced exponential growth, changes in the physiological state are reflected in the growth rate supported by the medium. Classical studies in bacterial physiology, reviewed in [Bremer and Dennis, 1996, Neidhardt et al., 1990, Maaloe and Kjeldgaard, 1966], have demonstrated the variation with the growth rate of a variety of physiological parameters, such as the concentrations of free RNA polymerase, ribosome abundance, gene copy number, and the size of amino acid and nucleotide pools. The dependencies between these parameters and the steady-state growth rate of the cells have been expressed in the form of phenomenological growth laws [Scott et al., 2010].

The joint control of gene expression by both local effects of transcription factors and global effects of the physiological state has received relatively little attention thus far. Among the exceptions, we cite the work of Klumpp et al. [2009], who have shown by a combination of models and experiments that the steady-state concentration of proteins in simple network architectures depends on the combined action of transcription factors and the growth rate. Dennis *et al.* review the huge amount of data on the control of rRNA synthesis in *E. coli* accumulated over several decades [Dennis et al., 2004]. They propose a model that integrates both growth-rate dependent effects on the activity of *rrn* promoters and specific regulatory control exerted by Fis. Notwithstanding the insights gained from these and other studies, they are limited in two respects. First, they consider the control of gene expression at steady-state, not during transitions between physiological states. Second, there is currently no dataset available that allows the contributions of local and global effects to be studied on the level of an entire regulatory network, consisting of several genes and their interactions.

Here we address the above questions in the case of a central regulatory circuit in *Escherichia coli* (Fig. 5.1). The network consists of the two most pleiotropic transcription factors of the cell, Fis and Crp, as well as the gene *acs*, encoding the enzyme acetyl-CoA synthetase (Acs). This enzyme converts acetate to acetyl-CoA, a critical step in acetate metabolism [Wolfe, 2005]. We are notably interested in the question how Fis and Crp share control over *acs* expression with the physiological state of the cell when glucose is used as the sole carbon source. Acetate is excreted during growth on glucose and, after exhaustion of the latter, utilized by the cells to continue growth at a lower rate. Glucose depletion triggers the accumulation of the signaling metabolite cyclic AMP (cAMP), which activates Crp and thus enables it to stimulate the expression of *acs*, an effect counteracted by Fis. At the same time, the redistribution of metabolic fluxes upon glucose depletion affects the series of metabolic pools and other global physiological parameters, thus indirectly affecting the expression of *acs* and other genes.

What are the relative contributions of transcription factors and global physiological parameters to changes in gene expression? In order to answer this question in a quantitative way, we monitored in real time and *in vivo*, by means of GFP reporters, the expression of the genes in the *acs* network in response to glucose depletion. In parallel, a GFP reporter driven by a non-regulated phage promoter was used to assay the time-varying physiological state. We show that a simple, parameterless mathematical model can be used to separate the variation of the promoter activity of the genes into a part due to global physiological control and a part due to local transcription regulation. In order to verify if the latter part can be accounted for by known regulators, in particular Crp, we extended the model and measured the time-varying concentration of cAMP. The above experiments were repeated when the network was submitted to various physiological and genetic perturbations, such as shifting the cell to a low-glucose medium or deleting the genes *fis* and *crp*.

The results of the above analysis reveal two new insights into the functioning of the *acs* network. First of all, despite the fact that the network has a dense pattern of regulatory interactions identified by genetic and biochemical studies, only a fraction of these interactions is predominant in our conditions. More precisely, the effect of Crp·cAMP on the expression of *acs* is the only interaction whose physiological role is evident from our data. Rather, and this is the second finding, we observed an important regulatory role for the time-varying activity of the gene expression machinery and other global factors. The latter dominate the control of the expression of *fis* and *crp*, and are also shown to drive the expression of another major transcription factor, the master stress regulator RpoS.

More generally, our results support a reappraisal of the role of gene regulatory networks in shaping expression profiles during growth transitions. Whereas transcription factors and other local regulators have sometimes been seen as the prime movers of changes in gene expression during growth transitions, it may be more fruitful to see these effects as finetuning global control exerted by the physiological state of the cell. The method we present to quantify the relative contributions of these local and global effects to gene expression control can be easily transposed to other regulatory systems in bacteria and higher organisms.

We also present an ODE model of the *acs* gene network. Parameter estimation was performed using sequentially a genetic algorithm and local-search methods on data obtained in the wild-type strain. We then tested the predictions of the calibrated model by comparing them with experimental data obtained for Δ*fis* and Δ*crp* strains and for wild-type strain after redilution in a low-glucose medium. Preliminary results are presented at the end of this chapter.

5.1 Materials and methods

5.1.1 Strains and growth conditions

The *E. coli* strains used in this study are the wild-type strain BW25113 and the deletion mutants Δ*fis* and Δ*crp* from the Keio collection [Baba et al., 2006] (Table 5.1).

Strains	Characteristics	Reference or source
WT	*E. coli* BW25113	[Baba et al., 2006]
Δ*fis*	*E. coli* BW25113 Δ*fis*	[Baba et al., 2006]
Δ*crp*	*E. coli* BW25113 Δ*crp*	[Baba et al., 2006]

Table 5.1: Strains used in this study.

The wild-type and mutant strains were transformed with low-copy pZE or pUA66 plasmids bearing a *gfp* reporter gene [de Jong et al., 2010] (Table 5.2). The pZE*gfp* plasmids possess a colE1 origin of replication, have the ampicillin resistance marker *bla*, are present at about thirty copies per cell, encode the short-lived GFPmut3 reporter, and do not affect bacterial growth [de Jong et al., 2010]. The pUA66*gfp* plasmids possess a SC101 origin of replication, have the ampicillin resistance marker *bla* or kanamycin resistance marker *kanR*, are present at below five copies per cell, encode the long-lived GFPmut2 reporter, and also do not affect bacterial growth. The pUA66*gfp* plasmids are either directly taken from the Alon plasmid library [Zaslaver et al., 2006] or derived from these plasmids by replacing the resistance marker [Baptist et al.]. The pUA66*gfp* plasmids were used when a pZE*gfp* plasmid could not be obtained (*acs*).

We amplified the promoter region of the genes *crp*, *fis*, *acs*, and *rpoS* by PCR from genomic DNA of *E. coli*, and cloned the DNA fragments into the plasmid backbone. In addition, we used a plasmid carrying the pRM phage promoter [Elowitz and Leibler, 2000]. All plasmids were verified by sequencing. The primers used for the strains constructed in this study are shown in Table 5.3.

Plasmid	Characteristics	Reference or source
pZE1RM*gfp*	Amp^r, colE1 *ori*, p*RM-gfpmut3*	[Elowitz and Leibler, 2000]
pZE*gfp*	Amp^r, colE1 *ori*, *gfpmut3*	[de Jong et al., 2010]
pZE*fis-gfp*	Amp^r, colE1 *ori*, p*fis-gfpmut3*	[de Jong et al., 2010]
pZE*crp-gfp*	Amp^r, colE1 *ori*, p*crp-gfpmut3*	This study
pUA66*acs-gfp*	Kan^r, SC101 *ori*, p*acs-gfpmut2*	[Zaslaver et al., 2006]
pUA66*acs-gfp*	Amp^r, SC101 *ori*, p*acs-gfpmut2*	[Baptist et al.]
pZE*rpoS-gfp*	Amp^r, colE1 *ori*, p*rpoS-gfpmut3*	This study

Table 5.2: Plasmids used in this study.

Plasmid	Primer sequence
pZE*crp-gfp*	crp1: CTG GGA ATT CGC TAT CAA CTG TAC TGC crp2: CAT GCT CGA GCG AGA CAC CAG GAG
pZE*rpoS-gfp*	rpoS1: GCT GGC TCG AGA CGT GAG GAA ATA C rpoS2: CGG AGA ATT CAA GCA AAA GCC TG

Table 5.3: Primers used for construction of strains pZe*crp-gfp* and pZe*rpoS-gfp*. We have amplified the promoter region of *crp* and *rpoS* by PCR from genomic DNA of *E. coli*, with oligonucleotides Crp1/Crp2 and RpoS1/RpoS2, respectively. Oligonucleotides RpoS1 and Crp2 contain an XhoI restriction site, and oligonucleotides RpoS2 and Crp1 an EcoRI restriction site, which allows cloning of the amplified DNA between these two sites on plasmid pZEgfp.

Glycerol stocks, stored at -80°C, of the above-mentioned strains were grown overnight (about 15 h) at 37°C, with shaking at 200 rpm, in M9 minimal medium [Miller, 1972] supplemented with 0.3% glucose and mineral trace elements (Zn, Co, Mn, B, Mo, Fe, Cu). For plasmid-carrying strains, the growth medium was supplemented with 100 μg ml^{-1} ampicillin. The overnight cultures were strongly diluted (1500-7000 fold) into a 96-well microplate, so as to obtain an adjusted initial OD$_{600}$ of 0.001. The wells of the microplate contain M9 minimal medium supplemented with 0.3% glucose, mineral trace elements, and 1.2% of the buffering agent HEPES (4-(2-hydroxyethyl)-1-piperazineethanesulfonic acid) for maintaining physiological pH levels in the growth medium. No antibiotics were added at this stage. The wells were covered with 60 μl of mineral oil to avoid evaporation. The microplate cultures were then grown for about 24 h at 37°C, with agitation at regular intervals, in the Fusion microplate reader (Perkin Elmer).

5.1.2 Real-time monitoring of gene expression

The strains growing in the wells of the microplate express a fluorescent reporter of the genes *crp*, *fis*, *acs*, and *rpoS* in a particular genetic background (wild type, Δ*fis*, and Δ*crp*). During a typical acquisition period of about 10 h, we obtain about 120 readings each of absorbance and fluorescence. Fluorescence excitation was at 485 nm and emission was monitored at 520 nm. Absorbance measurements used a 600 nm filter. In order to correct the primary data for background levels of absorbance and fluorescence, we used wells containing growth medium only and wells with strain carrying a promoterless *gfp* plasmid, respectively. We obtained the promoter activity of the genes from these data using methods and computer tools developed previously ([de Jong et al., 2010, Boyer et al., 2010, Ronen et al., 2002], see Appendix C.1 for details). The growth rate $\mu(t)$ was also computed from the absorbance data.

We determined 95%-confidence intervals for the promoter activities and growth rate by computing standard errors from experimental replicas. In order to correct for any bias introduced by small inoculation differences, the growth curves have been synchronized with respect to the maximum of the absorbance derivative ([Isalan et al., 2008] and Appendix C.1).

5.1.3 Measurement of cAMP concentrations

In order to measure concentrations of cAMP (adenosine 3',5'-cyclic monophosphate), we used a commercially-available immunoassay kit (Upstate). The assay is a competitive ELISA in which cAMP quantification occurs by means of a chemiluminescence signal. We took 100 μL samples at regular intervals from cultures in a microplate, under the growth conditions described above (12 time-points, 3 replicates). Following the manufacturer's instructions, the cAMP concentration at the different time-points was determined from luminescence measurements in the Fusion microplate reader (Perkin Elmer) and a calibration standard relating luminescence intensity to cAMP concentration. From these measurements of the time-varying concentration of extracellular cAMP, exported from the cells into the growth medium, we compute the intracellular cAMP concentration by means of a kinetic model developed for this purpose (see Appendix C.2 for details).

5.2 Results

5.2.1 Monitoring the dynamic response of the acs network

In order to experimentally characterize the dynamic response of the network in Fig. 5.1 to glucose depletion, we systematically measured input signals connecting the network to the

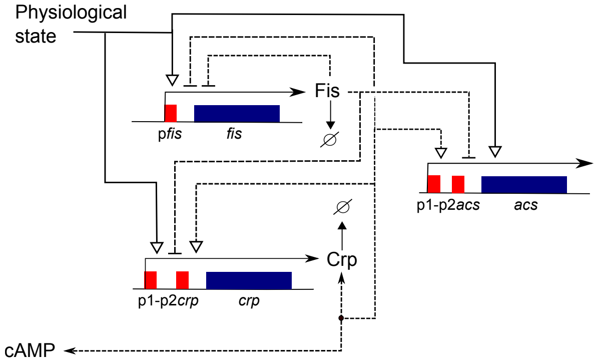

Figure 5.1: Regulatory network controlling expression of *acs* in *E. coli.* Expression of genes (blue) from promoters (red) is regulated by the transcription factors Crp and Fis (broken lines) and by the physiological state (solid lines). Also shown are the activation of Crp by cAMP-binding, and degradation and growth dilution of the proteins. In order not to clutter the figure, the effect of the growth rate on protein dilution has been omitted.

overall physiological state of the cell, including the concentration of cAMP. In parallel, we monitored the outputs of the system, the time-varying expression levels of *acs*, *crp*, and *fis*.

To bring the system into a well-defined initial state, we first grew bacterial cultures in a thermostated microplate to steady-state or balanced growth in minimal medium supplemented with 0.3% glucose. Starting from about 600 min, we monitored the growth rate by measuring the absorbance of the bacterial culture (Fig. 5.2*A*). The shape of the absorbance curves is typical for growth in minimal medium: exponential growth of the bacterial population, followed by a growth arrest due to glucose exhaustion within about 2 h (slightly over one generation). The time-frame of the experiment is too short to observe slow continued growth on acetate after the transition.

At chosen time-points along the growth curve, we determined the concentration of external cAMP using a luminescence-based immunoassay. From these measurement, we derived estimates of internal cAMP concentrations by means of a kinetic model accounting for cAMP import and export, as explained in Appendix C.2. The shape of the intracellular cAMP concentration profile agrees very well with other, direct measurements [Buettner et al., 1973, Kao et al., 2004, Makman and Sutherland, 1965]. cAMP concentrations are low in the presence of glucose, rapidly accumulate at the end of exponential growth, when glucose is exhausted, and return to a lower steady-state level at the end of the transition (Fig. 5.2*B*).

The time-varying physiological state of the cell, such as the free concentration of RNA polymerase, is difficult to measure directly [Klumpp and Hwa, 2008]. We therefore decided to put a fluorescent reporter under the control of a constitutive promoter, not known to be regulated by any transcription factor. In particular, we used a plasmid expressing a GFP reporter for the pRM promoter of phage λ [Oppenheim et al., 2005] (see Methods and

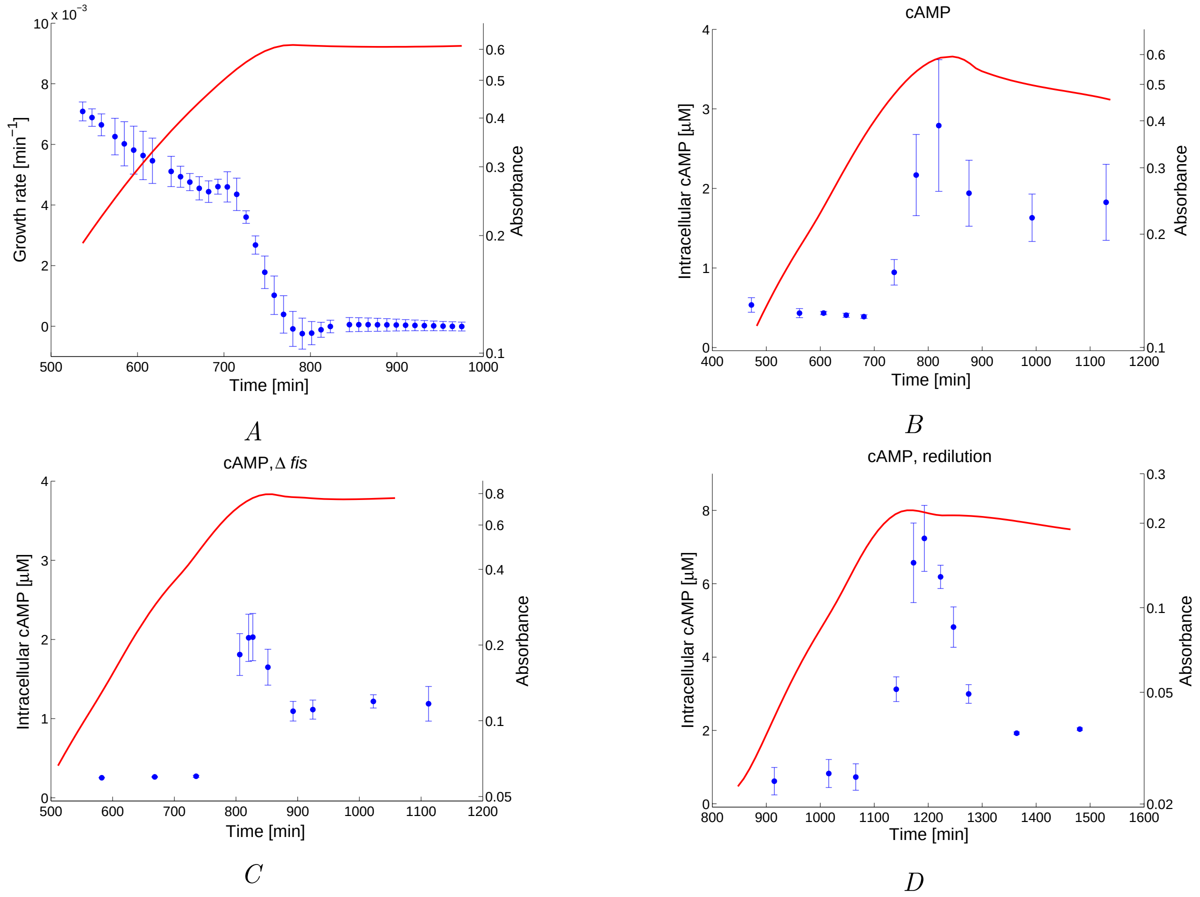

Figure 5.2: Experimental monitoring of physiological parameters. *A:* Growth rate (•, blue) as computed from the measured absorbance of a bacterial culture (-, red). *B:* Intracellular concentration of cAMP in wild-type strain (•, blue) as derived from measured external concentrations of cAMP and a kinetic model of cAMP import/export (Appendix C.2). *C:* Idem for a Δ*fis* strain. *D:* Idem for wild-type strain after down-shift to a low-glucose medium. The data shown in the plots are the mean of 3-4 experimental replicates, with 95%-confidence intervals computed from the standard error of the mean (see Methods and materials).

Materials). The variations in the activity of the constitutive promoter reflect changes in the overall physiological state of the cell, including the gene expression machinery and amino acid and nucleotide metabolism. This approach allows the global state of the cell to be monitored in real-time and *in vivo* during the growth transition. The promoter activity computed from the fluorescence signal is shown in Fig. 5.3D. The activity of the pRM promoter is seen to be approximately stationary in exponential phase, but then decreases to a lower value, slightly preceding the drop of the growth rate.

In parallel, we monitored the promoter activities of the genes in the network using GFP reporter plasmids for the *fis*, *crp*, and *acs* promoters. The results are shown in Fig. 5.3. The promoter activities of *fis* and *crp* gradually decrease at the end of exponential phase, and then remain at a basal level after exhaustion of glucose, with a slight recovery towards the end of the experiment, possibly as a consequence of acetate consumption by the cells. The expression pattern of *acs* in exponential phase seems to be similar, but as the fluorescence signal is close to the background level, the confidence intervals are wide and do not allow an unambiguous conclusion to be drawn. However, contrary to what was observed for *fis* and *crp*, the expression of *acs* is strongly induced when glucose is exhausted at about 700 min. This latter observation is consistent with other reports in the literature [Baptist et al., Wolfe, 2005].

de Jong et al. [2010] have shown that the promoter activities derived from the absorbance and fluorescence data are in good agreement with Northern blot quantifications of mRNA. Here we additionally measured the variation of the plasmid copy number (number of plasmids per chromosomal equivalent of DNA) using qPCR. The number is known to change with the growth rate [Lin-Chao and Bremer, 1986] and may bias the profiles shown in Fig. 5.3. We found that the plasmid copy number increases by a factor of 2 during the growth transition following glucose exhaustion (see Appendix C.3). This does not invalidate the qualitative shape of the profiles, especially the fall in the activity of the constitutive promoter (which is actually underestimated). However, it means that a quantitative bias exists and it requires the development of analysis methods that corrects for this bias.

5.2.2 Dissecting the local and global control of gene expression

In order to analyze the relative contributions of local and global factors to the response of the *acs* network, we developed a simple mathematical model of the measured promoter activity of the genes. Let $p(t)$ denote the promoter activity as a function of time t [min]. We write

$$p(t) = k\, p_1(t)\, p_2(t) \tag{5.1}$$

with k the maximum promoter activity and $p_1(t)$ and $p_2(t)$ the time-varying contributions of the global and local factors to $p(t)$, respectively. For simplicity, without loss of generality, we assume that $p_1(t)$ and $p_2(t)$ vary between 0 and 1. The term $p_1(t)$ quantifies the influence of the global physiological state on the promoter activity, for instance through the availability of

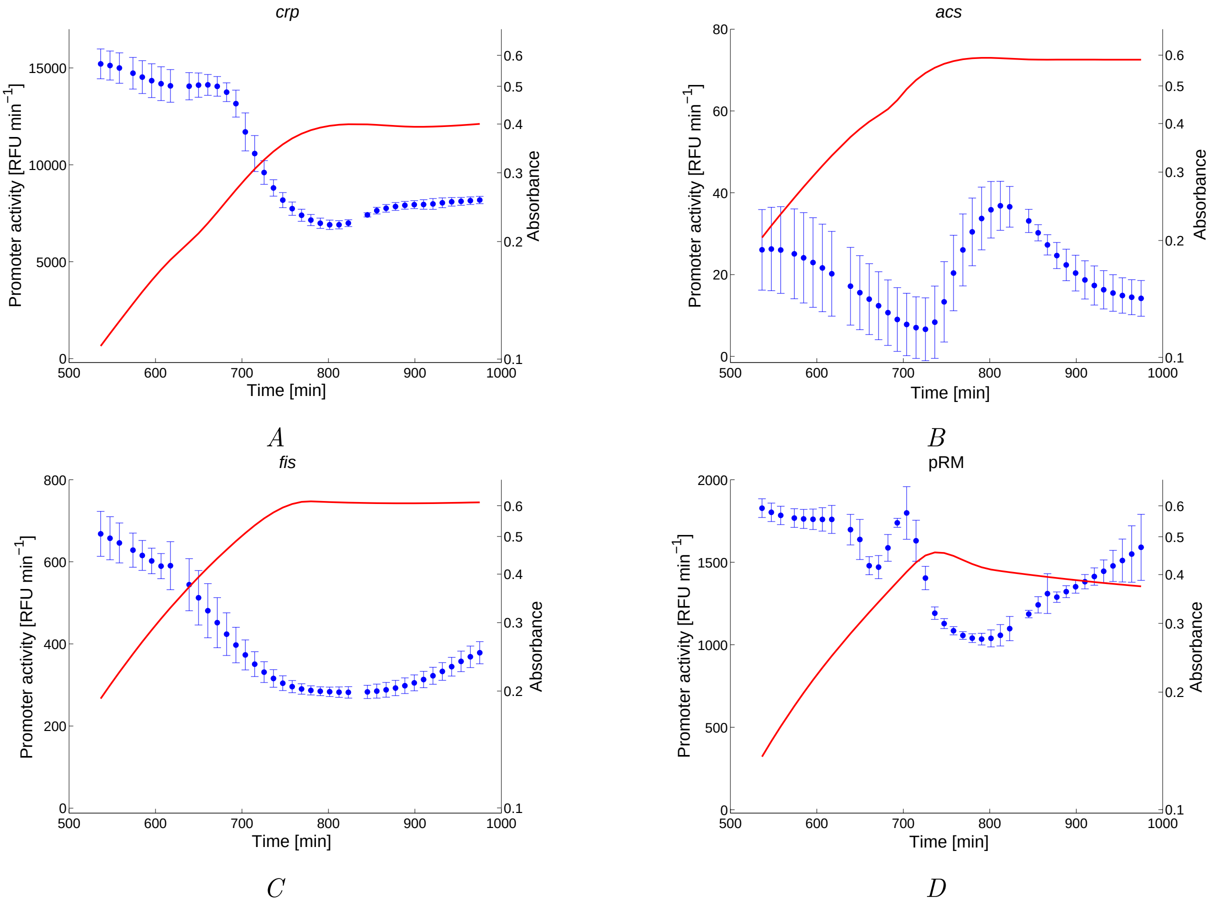

A

B

C

D

Figure 5.3: Experimental monitoring of gene expression. *A:* Time-varying promoter activity of *crp* (●, blue), derived from GFP data with 95%-confidence interval obtained from experimental replicas, and absorbance (solid line, red). Details on the strains and data analysis procedures can be found in Methods and Materials and Appendix C.1. *B-D:* Idem for promoter activities of *fis* and *acs*, as well as the activity of the pRM promoter of phage λ. The latter promoter is constitutive in our conditions and reflects the global physiological state of the cell. The primary fluorescence data for these curves are shown in Appendix C.1.

free RNA polymerase and ribosome. The term $p_2(t)$ accounts for the effect of transcription factors and other local regulators, and may take the form of regulation functions usually found in gene network modeling [Bintu et al., 2005, de Jong, 2002, Bolouri, 2008].

In order to eliminate the usually unknown constant k, we normalize Eq. (5.1) with respect to a reference state at time t^0. At t^0 we have $p(t^0) = k\, p_1(t^0)\, p_2(t^0)$. Writing $p^0 = p(t^0)$, $p_1^0 = p_1(t^0)$, and $p_2^0 = p_2(t^0)$, we divide Eq. (5.1) by the reference promoter activity and after a logarithmic transformation find

$$\log \frac{p(t)}{p^0} = \log \frac{p_1(t)}{p_1^0} + \log \frac{p_2(t)}{p_2^0}. \tag{5.2}$$

Two special cases of this model will be examined in more detail below.

(i) When the global physiological effect is dominant, that is, when the effect of the local regulators is negligible, we have $p_2(t) \approx p_2^0$ and the second terms in Eq. (5.2) approximates 0. Bearing in mind that the global effect is measured by the activity of the constitutive pRM promoter, we can rewrite the model as

$$\log \frac{p(t)}{p^0} = \log \frac{p_{RM}(t)}{p_{RM}^0}, \tag{5.3}$$

with $p_{RM}(t)$ and p_{RM}^0 the time-varying activity of the pRM promoter and its reference value, respectively.

(ii) Figs. 5.2-5.3 show that the expression peak of *acs* at glucose exhaustion seems to correlate with cAMP kinetics. This motivates a model in which the variation of the promoter activity of *acs*, and potentially other Crp·cAMP-regulated genes, is dominated, after subtraction of control by the global physiological state, by the concentration of cAMP. That is, we have

$$\log \frac{p(t)}{p^0} - \log \frac{p_{RM}(t)}{p_{RM}^0} = \log \frac{c(t)}{c^0}, \tag{5.4}$$

where $c(t)$ is the time-varying intracellular concentration of cAMP and c^0 its value in the reference state.

The above models allow us to address a number of questions. To which extent can the observed variation in the promoter activity of the genes be accounted for by the effect of the global physiological state only? And if gene expression control is shared with other, local regulators, how much of the remaining variation is explained by cAMP? Notice that the models of Eqs. (5.3)-(5.4) have a number of advantages for this purpose. First, they are parameterless and therefore do not require preliminary model calibration. Second, the growth-phase-dependent variation of the plasmid copy number equally affects the terms $p(t)$ and $p_{RM}(t)$, and therefore cancels out in the equations.

In order to see this, we make an explicit distinction between $p(t)$, the activity of a promoter on the chromosome, and $\hat{p}(t)$, the activity of the same promoter on a reporter plasmid. Let

$r(t)$ denote the (time-varying) relative plasmid copy number and k the plasmid copy number at t_0 (Appendix C.3). Then we have

$$\hat{p}(t) = k\, r(t)\, p(t). \tag{5.5}$$

In our reporter gene experiments we do not directly measure $p(t)$, but rather $\hat{p}(t)$. As a consequence, Eqs. (5.3)-(5.4) are redefined as

$$\log \frac{\hat{p}(t)}{\hat{p}^0} = \log \frac{\hat{p}_{RM}(t)}{\hat{p}^0_{RM}}, \tag{5.6}$$

$$\log \frac{\hat{p}(t)}{\hat{p}^0} - \log \frac{\hat{p}_{RM}(t)}{\hat{p}^0_{RM}} = \log \frac{c(t)}{c^0}. \tag{5.7}$$

Substituting the expressions for $p(t)$ and $\hat{p}(t)$ into these equations yields

$$\log \frac{r(t)}{r^0} \frac{p(t)}{p^0} = \log \frac{r(t)}{r^0} \frac{p_{RM}(t)}{p^0_{RM}},$$

$$\log \frac{r(t)}{r^0} \frac{p(t)}{p^0} - \log \frac{r(t)}{r^0} \frac{p_{RM}(t)}{p^0_{RM}} = \log \frac{c(t)}{c^0},$$

where $r^0 = r(t^0)$. It is easy to see that by eliminating the terms $r(t)/r^0$ the original Eqs. (5.3)-(5.4) are obtained. That is, the variation of the plasmid copy number equally affects the terms $p(t)$ and $p_{RM}(t)$, and therefore cancels out.

Third, the hypotheses contained in the model can be immediately tested by means of the experimental data, by inserting for $p(t)$ the measured promoter activities of *fis*, *crp*, and *acs* (denoted below by $p_{fis}(t)$, $p_{crp}(t)$, and $p_{acs}(t)$, respectively).

5.2.3 Distributed local and global control of gene expression in *acs* network during growth transition

We first test the hypothesis that the adaptation of gene expression to glucose exhaustion is mainly controlled by the physiological state of the cell, measured by the activity of the pRM promoter. The reference state is chosen to be the state where the growth rate vanishes, that is, after exhaustion of glucose. In this case, Eq. (5.3) predicts a linear relation between $\log(p(t)/p^0)$ and $\log(p_{RM}(t)/p^0_{RM})$, the diagonal in the scatter plots of Fig. 5.4*A*-*C*. If the global effects are dominant, then one would expect the data points to be spread out along the diagonal. This is indeed seen to be the case for *fis* and *crp*. In order to quantify the proportion of the variance explained by the model, we compute the coefficient of determination (R^2), the square of the correlation coefficient [Hamilton, 1992]. For *fis* and *crp*, we have high R^2 values (0.71 and 0.83). However, for *acs* the R^2 value is found to be much lower (0.54).

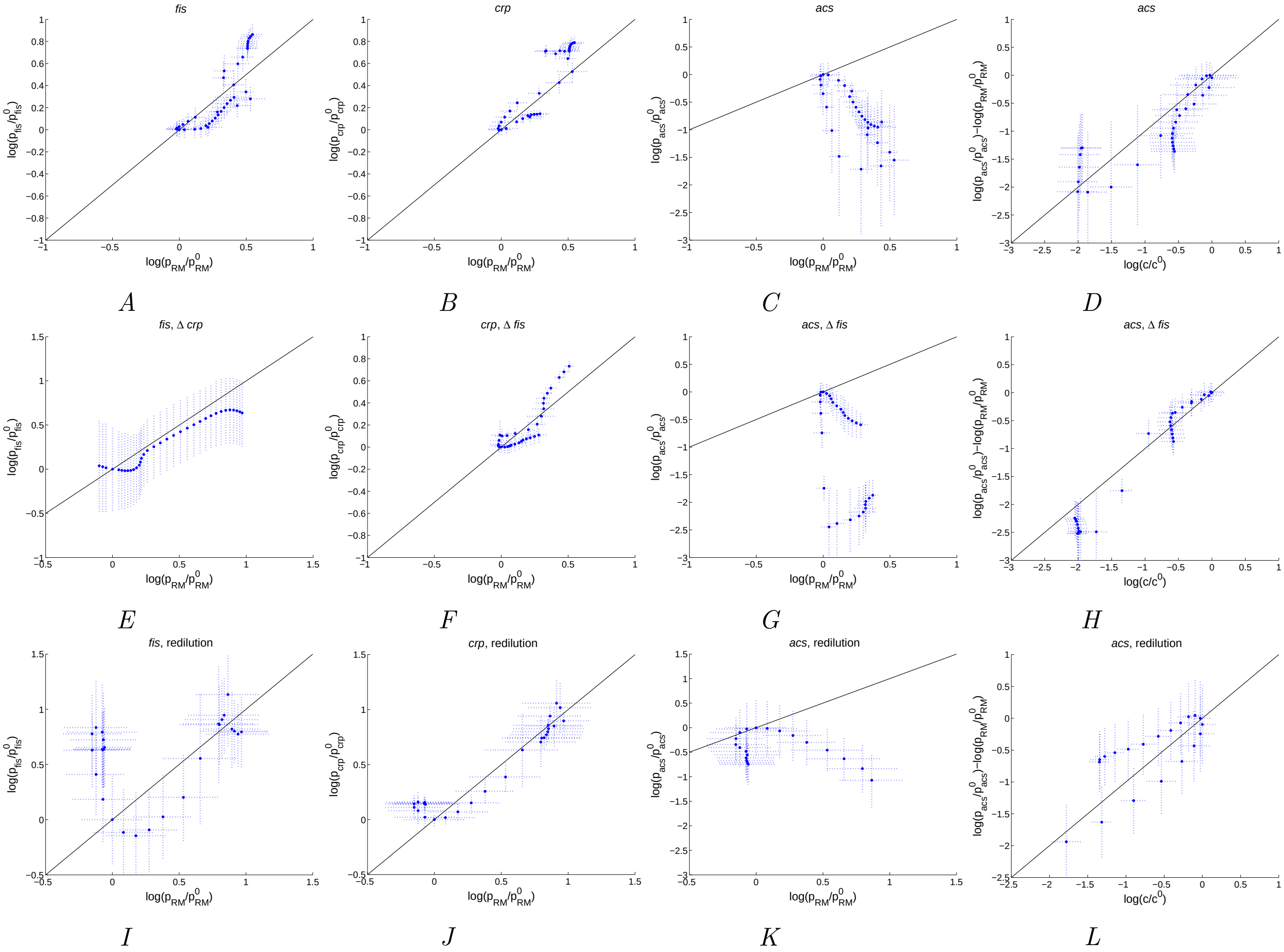

Figure 5.4: Predicted and observed control of *fis*, *crp*, and *acs* expression by Crp·cAMP and the physiological state of the cell, in various experimental conditions and genetic backgrounds. *A:* Predicted (–, black) and measured (●, blue) relative activity of the *fis* promoter $\left(\log(p_{fis}(t)/p^0_{fis})\right)$ as a function of the relative activity of the pRM promoter $\left(\log(p_{RM}(t)/p^0_{RM})\right)$. The 95%-confidence intervals in the plots have been computed from experimental replicas, as described in Materials and methods. *B-C:* Idem for *crp* and *acs*. *D:* Predicted (–, black) and measured (●, blue) remaining relative activity of the *acs* promoter after subtraction of the effect of global physiological parameters $\left(\log(p_{acs}(t)/p^0_{acs}) - \log(p_{RM}(t)/p^0_{RM})\right)$ and as a function of the relative intracellular cAMP concentration $\left(\log(c(t)/c^0)\right)$. In order to facilitate comparison with panel *C*, the measured cAMP concentrations have been interpolated at all time-points using a regression spline (Appendix C.2). *E:* Same as *A*, but in Δ*crp* strain. *F-H:* Same as *B-D*, but in Δ*fis* strain. *I-L:* Same as *A-D*, but after down-shift into a low-glucose medium.

In order to account for the unexplained variation of *acs* expression, we tested the hypothesis that, in addition to the global physiological state, this gene is controlled by Crp·cAMP. Eq. (5.4) predicts a linear relation between the remaining variation of *acs* expression, after subtraction of the global effect, and the effect due to the intracellular concentration of cAMP. This prediction corresponds to the diagonal in Fig. 5.4*D*. We plot the experimental data in the same figure, interpolating the measured intracellular cAMP concentration in Fig. 5.2. Notice that the precision of the measurements is lower than in the previous cases, due to the higher uncertainty of measurements of extracellular cAMP, amplified in the derivation of the concentrations of intracellular cAMP. Moreover, the error in the left-hand side of Eq. (5.4) includes uncertainties for both promoter activities. Nevertheless, the experimental data are in good correspondence with the model prediction ($R^2 = 0.72$).

This confirms that the variation of *fis* and *crp* expression is well accounted for by the effect of the physiological state, whereas for *acs* we need to consider cAMP as well. We tested if further addition of regulatory interactions, notably the effect of Crp·cAMP on *fis* and *crp*, would allow the remaining variance in the data to be explained. This turned out not be the case, in the sense that we obtained lower R^2-values when extending the model with additional regulators (0.31 and 0.60, respectively, see Appendix C.4). We thus conclude that the models of Eq. (5.3)-(5.4) are indeed appropriate descriptions of the data.

The surprising observation that, in our conditions, the global physiological state is the dominant regulator of physiological importance of the transcription factors Crp and Fis was confirmed for another regulator, the master stress regulator RpoS (σ^S). In the same way as for the other genes, we measured the promoter activity of *rpoS*, which is believed to be negatively regulated by Crp·cAMP (although the effect remains somewhat controversial, see [Zgurskaya et al., 1997]). When analyzed by means of Eq. (5.3), the expression of *rpoS* was indeed found to follow the activity of the pRM promoter ($R^2 = 0.73$, see Appendix C.4).

5.2.4 Local and global gene expression control in different physiological conditions and genetic backgrounds

If the control exerted by the physiological state of the cell accounts for the major part of the variation in the expression of *fis* and *crp*, that is, if Fis and Crp·cAMP have a minor effect on the expression of these genes, then one would expect the minimal model of Eq. (5.3) to explain the variation in the promoter activity equally well in Δ*fis* and Δ*crp* backgrounds. In order to test this prediction, we measured the input-output behavior of the *acs* network in mutant strains deleted for *fis* and *crp* [Baba et al., 2006], under the same growth conditions as above. Figs. 5.5-5.6 show the promoter activities of *fis*, *crp* and *acs* as well as the activity of the pRM promoter in Δ*fis* and Δ*crp* mutants, respectively.

The resulting data were used to construct Fig. 5.4*E-F*. The plots confirm the prediction that the global physiological effect is dominant in the control of the expression of *crp* in a

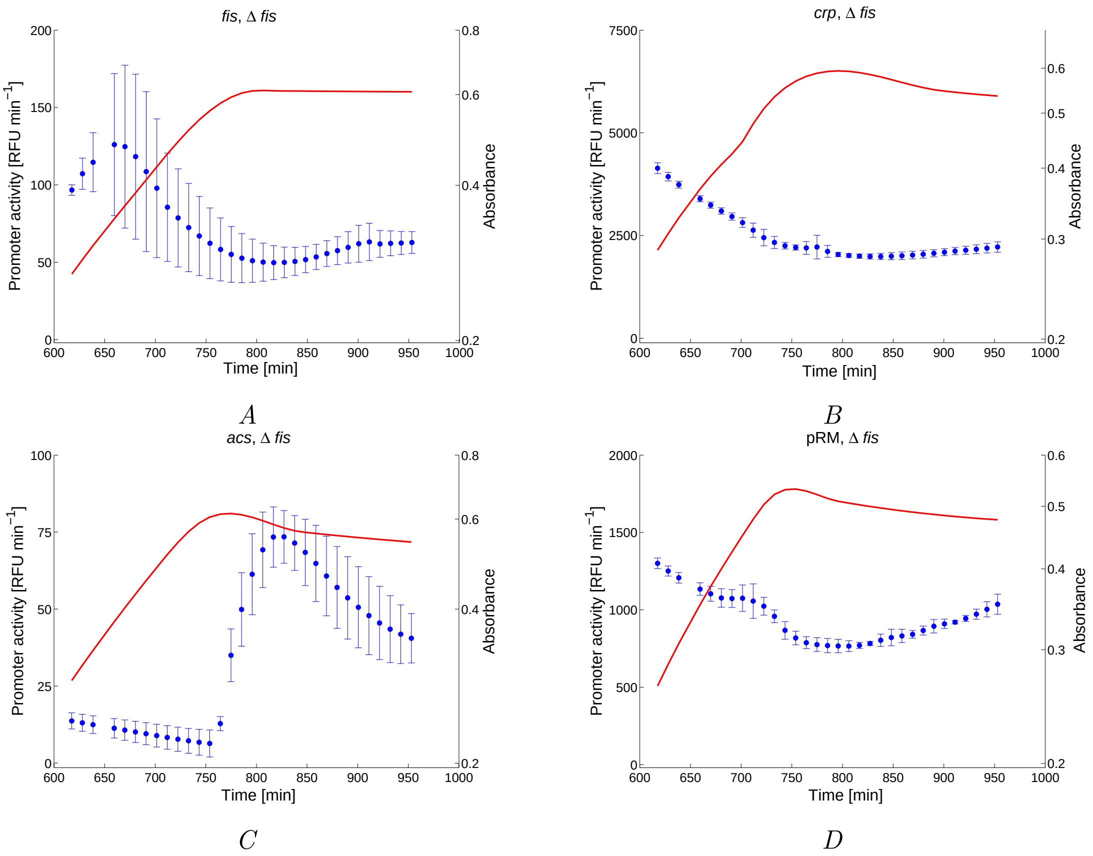

Figure 5.5: Experimental monitoring of gene expression outputs in Δ*fis* strain. *A:* Time-varying promoter activity of *fis* (●, blue), derived from GFP data with 95%-confidence interval obtained from experimental replicas, and absorbance (solid line, red). *B-D:* Idem for promoter activities of *crp* and *acs*, as well as the activity of the pRM promoter of phage λ.

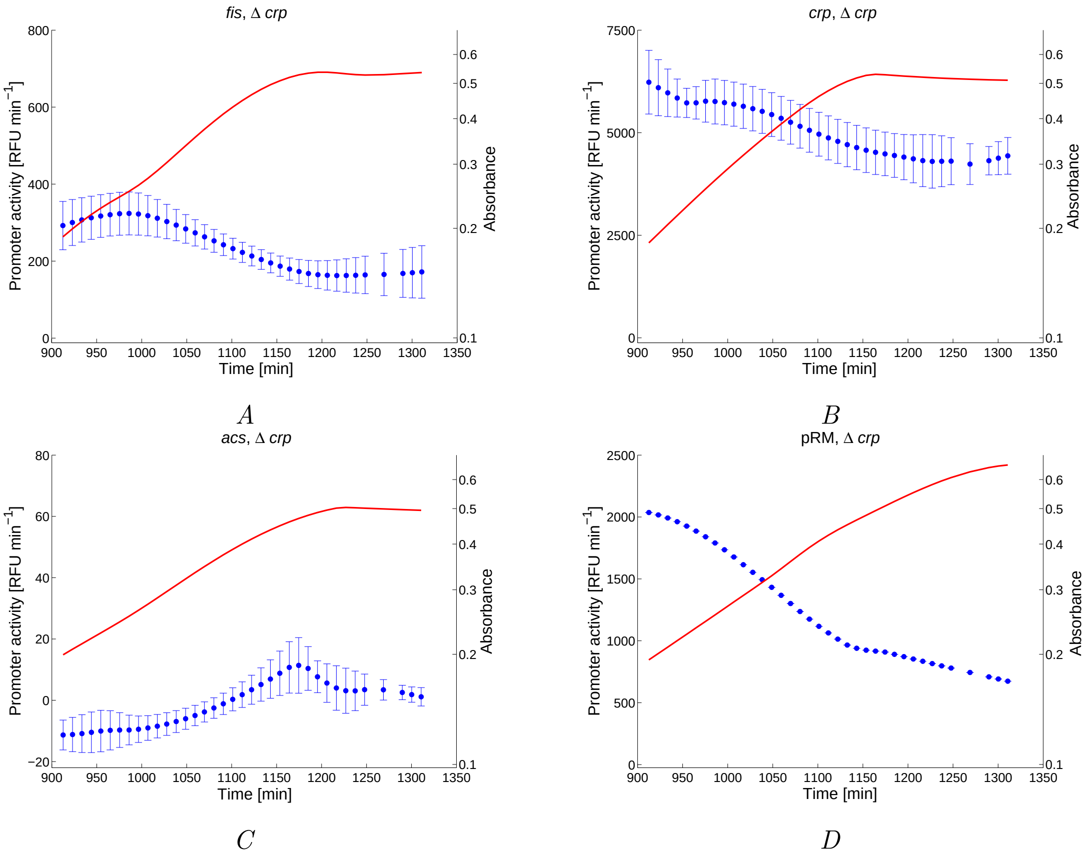

A

B

C

D

Figure 5.6: Experimental monitoring of gene expression outputs in Δcrp strain. *A:* Time-varying promoter activity of *fis* (●, blue), derived from GFP data with 95%-confidence interval obtained from experimental replicas, and absorbance (solid line, red). *B-D:* Idem for promoter activities of *crp* and *acs*, as well as the activity of the pRM promoter of phage λ.

Δ*fis* strain and *fis* in a Δcrp strain (R^2 equal to 0.78 and 0.94, respectively).

Similarly, in the case of *acs*, one would expect little change in a Δ*fis* mutant, given that the overall cellular physiology and cAMP were found to dominate its expression control. This prediction is also confirmed by our data, as shown in Fig. 5.4*G-H.* Together, the local and global effects explain most of the variation of the expression of *acs* (R^2 = 0.97), whereas global effects alone fail to be a good predictor (R^2 = 0.34). The deletion of *crp*, on the other hand, disconnects cAMP from the network and has been shown to prevent the induction of *acs* when glucose is exhausted [Baptist et al., Wolfe, 2005]. This is confirmed in our data in the sense that *acs* is not expressed in a Δcrp background (Fig. 5.6*C*).

The results reported above again suggest that few of the specific interactions in the *acs* network actually contribute to the observed changes in gene expression during the growth transition. It could be argued, however, that the absence of an effect of Crp·cAMP on *fis* and *crp* expression is due to insufficient accumulation of cAMP in our experimental conditions. If this were the case, it might explain why Crp·cAMP had no effect on the activity of the *fis* and *crp* promoters. An observation supporting this argument is that the peak of the intracellular cAMP concentration at 2.3 μM is only six time higher than the steady-state level reached during exponential growth angle (Fig. 5.2*B*).

In order to test this hypothesis, we repeated our experiments in different growth conditions, likely to favor stronger accumulation of cAMP. In particular, once the culture reached a state of balanced growth in minimal medium supplemented with 0.3% glucose, we rediluted the bacteria into the same medium with a low glucose level (0.06%). In parallel, we monitored the expression of the genes in the *acs* network and the activity of the pRM promoter. These data are shown in Fig. 5.7.

The results of the analysis of the data by means of Eq. (5.3)-(5.4) are shown in Fig. 5.4*I-L*. The down-shift is indeed seen to lead to a more abrupt growth arrest and to a higher cAMP peak concentration (7.2 μM, Fig. 5.2*C*). While the expression of *crp* is still largely controlled by the physiological state of the cell (R^2 = 0.91), only half of the variation in the promoter activity of *acs* is explained by the combined local and global effects (R^2 = 0.56). Notice that the data are noisy though, and that the most important deviations from the diagonal, that is, from the model predictions, occur for datapoints with large confidence intervals (Fig. 5.4*L*).

More conspicuous is the low coefficient of determination for *fis* (R^2 = 0.14). When comparing the plot in Fig. 5.4*I* with the expression data in Fig. 5.7*A*, one can observe that the lack of correlation is especially due to the fact that *fis* expression is higher than predicted after glucose exhaustion. The increase of the promoter activity cannot be accounted for by Crp·cAMP, which is known to inhibit *fis* expression [Zheng et al., 2004]. In fact, the explanatory power of the model decreases even further when including the inhibition by Crp·cAMP (R^2 = 0.01). Other regulators may therefore play a role, for instance the level of negative supercoiling in the cell [Travers et al., 2001].

Overall, results in this and the previous sections are consistent with the conclusion that

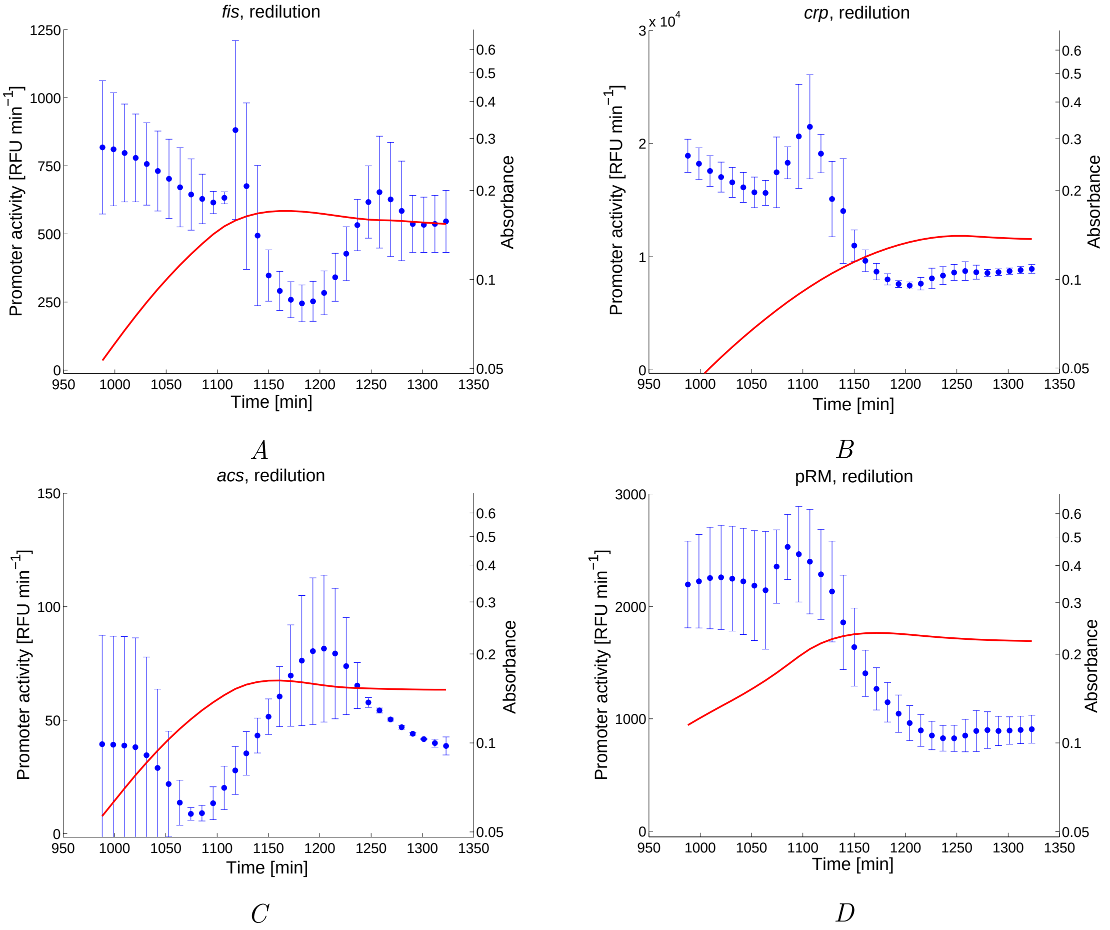

Figure 5.7: Experimental monitoring of gene expression outputs in wild-type strain after redilution into low-glucose medium. *A:* Time-varying promoter activity of *fis* (●, blue), derived from GFP data with 95%-confidence interval obtained from experimental replicas, and absorbance (solid line, red). *B-D:* Idem for promoter activities of *crp* and *acs*, as well as the activity of the pRM promoter of phage λ.

variation in the expression of *fis* and *crp* is mainly controlled by the global physiological state. Interestingly, this is also the case for *rpoS*. In the three variants of our reference conditions, use of Δ*fis* and Δcrp strains and the shift to a low-glucose medium, we find very high R^2-values (0.83, 0.97, and 0.81, respectively, see the plots in Appendix C.4).

5.3 Dynamical model of both global and transcriptional regulation of the *acs* network

After a first analysis based on a static, phenomenological model of transcriptional regulation, we develop more detailed expressions to describe the dynamics of transcriptional regulation of the *acs* network. Both Crp and Acs synthesis are positively regulated by the complex Crp·cAMP and negatively regulated by Fis whereas Fis synthesis is negatively regulated both by Crp·cAMP and Fis (Fig. 5.1) [Zheng et al., 2004, Ninnemann et al., 1992]. Moreover, we also consider the regulation of *rpoS*, which is positively regulated by Crp·cAMP during entry into stationary phase [Hengge-Aronis, 2002]. Thus, using competitive inhibition and Hill kinetics introduced in Sec. 2.1, we can write

$$\begin{cases} p_2^{fis}(x_{Fis}(t), x_{Crp\cdot cAMP}(t)) = \kappa_{fis}^b + \kappa_{fis}^r \cdot \frac{1}{\left(\frac{x_{Fis}(t)}{\theta_{fis_1}}\right)^{n_1} + \left(\frac{x_{Crp\cdot cAMP}(t)}{\theta_{cc_1}}\right)^{n_2} + 1} \\ p_2^{crp}(x_{Fis}(t), x_{Crp\cdot cAMP}(t)) = \kappa_{crp}^b + \kappa_{crp}^r \cdot \frac{x_{Crp\cdot cAMP}(t)^{n_4}}{x_{Crp\cdot cAMP}(t)^{n_4} + \theta_{cc_2}^{n_4} \cdot \left(1 + \left(\frac{x_{Fis}(t)}{\theta_{fis_2}}\right)^{n_3}\right)} \\ p_2^{acs}(x_{Fis}(t), x_{Crp\cdot cAMP}(t)) = \kappa_{acs}^b + \kappa_{acs}^r \cdot \frac{x_{Crp\cdot cAMP}(t)^{n_6}}{x_{Crp\cdot cAMP}(t)^{n_6} + \theta_{cc_3}^{n_6} \cdot \left(1 + \left(\frac{x_{Fis}(t)}{\theta_{fis_3}}\right)^{n_5}\right)} \\ p_2^{rpoS}(x_{Crp\cdot cAMP}(t)) = \kappa_{rpoS}^b + \kappa_{rpoS}^r \cdot \frac{x_{Crp\cdot cAMP}(t)^{n_7}}{x_{Crp\cdot cAMP}(t)^{n_7} + \theta_{cc_4}^{n_7}} \end{cases} \tag{5.8}$$

with κ_{fis}^b, κ_{crp}^b, κ_{acs}^b, $\kappa_{rpoS}^b \in \mathbb{R}_+$ the basal synthesis rates of Fis, Crp, Acs and RpoS, respectively. κ_{fis}^r, κ_{crp}^r, κ_{acs}^r, $\kappa_{rpoS}^r \in \mathbb{R}_+$ represent the regulated synthesis rates of Fis, Crp,Acs and RpoS, respectively. θ_{fis_i}, $\theta_{cc_j} \in \mathbb{R}_+$ represent the Hill thresholds for regulation by Fis and Crp·cAMP, respectively, with $i = 1, 2, 3$ and $j = 1 \cdots 4$. $n_1, \cdots, n_7$ are Hill coefficients.

The promoter activities of these 4 genes depend on the concentration of the two transcription factors of the network, Fis and Crp, and of the complex Crp·cAMP. To investigate the dynamical behaviour of Eq. (5.8), we develop an ODE model taking the concentrations of Fis (x_{Fis}), Crp·cAMP ($x_{Crp\cdot cAMP}$) and Crp (x_{Crp}) as variables and the promoter activities of *acs* (p_{acs}) and *rpoS* (p_{rpoS}) as outputs. The concentration of Crp·cAMP varies as a consequence of complex association and dissociation, as well as degradation and export. The rates of these processes depend on the concentrations of total Crp x_{Crp} and of total intracellular cAMP $c(t)$ (see Sec. 2.1). The dynamics of Fis and Crp concentrations are driven by their synthesis terms $p_{fis}(t)$, $p_{crp}(t)$, respectively, and a decay term accounting for degradation mechanisms and growth dilution. We do not explicitly model the regulation by the global physiological state of the cell. Instead, we treat this term as an input and measure it by setting $k \cdot p_1(t) = p_{RM}(t)$, with $k \in \mathbb{R}_+$. We define γ_{Fis} and γ_{Crp} the degradation rates of Fis and Crp, respectively, and μ the growth rate of the bacterial population. We have

$$\begin{cases} \dot{x}_{Fis}(t) = p_{RM}(t) \cdot p_2^{fis}(x_{Fis}(t), x_{Crp\cdot cAMP}(t)) - (\mu(t) + \gamma_{Fis}) \cdot x_{Fis}(t) \\ \dot{x}_{Crp}(t) = p_{RM}(t) \cdot p_2^{crp}(x_{Fis}(t), x_{Crp\cdot cAMP}(t)) - (\mu(t) + \gamma_{Crp}) \cdot x_{Crp}(t) \\ \dot{x}_{Crp\cdot cAMP}(t) = r_{cc}^{on}(t) - r_{cc}^{off}(t) - (\mu(t) + \gamma_{Crp}) \cdot x_{Crp\cdot cAMP}(t) \\ p_{acs}(t) = p_{RM}(t) \cdot p_2^{acs}(x_{Fis}(t), x_{Crp\cdot cAMP}(t)) \\ p_{rpoS}(t) = p_{RM}(t) \cdot p_2^{rpoS}(x_{Crp\cdot cAMP}(t)) \end{cases} \tag{5.9}$$

with r_{cc}^{on} and r_{cc}^{off} the association and dissociation rates of the Crp·cAMP complex. As extracellular cAMP is not degraded [Epstein et al., 1975], the degradation rate of Crp·cAMP is equal to γ_{Crp}.

As we have seen in Sec. 2.1, r_{cc}^{on} and r_{cc}^{off} can be modeled by the following first-order rate laws

$$\begin{cases} r_{cc}^{on}(t) = k_{on} \cdot (x_{Crp} - x_{Crp\cdot cAMP}) \cdot c(t) \\ r_{cc}^{off}(t) = k_{off} \cdot x_{Crp\cdot cAMP} \end{cases} \tag{5.10}$$

with k_{cc}^{on} and k_{cc}^{off} the association and dissociation constants of the Crp·cAMP complex, respectively.

Using QSSA, introduced in Sec. 2.2.1, we set $\dot{x}_{Crp\cdot cAMP} = 0$ and determine $x_{Crp\cdot cAMP}$ as

$$x_{Crp\cdot cAMP}(t) = \frac{x_{Crp}(t)}{1 + \frac{\gamma_{Crp} + \mu(t) + k_{cc}^{off}}{k_{cc}^{on} \cdot (c(t) - x_{cc}(t))}} \tag{5.11}$$

The dissociation of a complex is much faster than the degradation of a protein or dilution, so that we can assume that $(\gamma_{Crp} + \mu(t)) << k_{cc}^{off}$.

The resulting ODE model is composed of 2 variables ($x(t) = [x_{Fis}(t)\ x_{Crp}(t)]$), takes as inputs the concentration of intracellular cAMP $c(t)$, the growth rate $\mu(t)$ and the promoter activity of pRM $p_{RM}(t)$, returns the promoter activities of *acs* and *rpoS* and follows

$$\begin{cases} \dot{x}_{Fis}(t) = p_{RM}(t) \cdot p_2^{fis}(x_{Fis}(t), x_{Crp\cdot cAMP}(t)) - (\mu(t) + \gamma_{Fis}) \cdot x_{Fis}(t) \\ \dot{x}_{Crp}(t) = p_{RM}(t) \cdot p_2^{crp}(x_{Fis}(t), x_{Crp\cdot cAMP}(t)) - (\mu(t) + \gamma_{Crp}) \cdot x_{Crp}(t) \\ x_{Crp\cdot cAMP}(t) = \frac{x_{Crp}(t)}{1 + K_{cc}/c(t)} \\ p_{acs}(t) = p_{RM}(t) \cdot p_2^{acs}(x_{Fis}(t), x_{Crp\cdot cAMP}(t)) \\ p_{rpoS}(t) = p_{RM}(t) \cdot p_2^{rpoS}(x_{Crp\cdot cAMP}(t)) \end{cases} \tag{5.12}$$

with $K_{cc} = k_{cc}^{off}/k_{cc}^{on}$.

This model contains 21 parameters, listed in Table 5.4. To estimate them, we confronted the model to the data of promoter activities presented in Fig. 5.3 (and Fig. A7*A* of Appendix C.4 for *rpoS* promoter activity). The model was rescaled in order to be consistent with these experimental data (see Appendix C.5 for details).

As mentioned in Sec. 2.4.1, parameter estimation of an ODE model when the vector of observables only contains the outputs of the model has an important computational cost and is performing poorly. Consequently, we divided the parameter estimation procedure in two steps:

Parameters	Description	Units
K_{cc}	equilibrium constant for Crp·cAMP formation reaction	mM
	fis expression	
κ^b_{fis}	basal protein synthesis rate	mM·min^{-1}
κ^r_{fis}	maximal protein synthesis rate	mM·min^{-1}
θ_{fis_1}, θ_{cc_1}	affinity constants	mM
n_1, n_2	Hill coefficients	adimensional
γ_{Fis}	protein degradation constant	min^{-1}
	crp expression	
κ^b_{crp}	basal protein synthesis rate	mM·min^{-1}
κ^r_{crp}	maximal protein synthesis rate	mM·min^{-1}
θ_{fis_2}, θ_{cc_2}	affinity constants	mM
n_3, n_4	Hill coefficients	adimensional
γ_{Crp}	protein degradation constant	min^{-1}
	acs expression	
κ^b_{acs}	basal protein synthesis rate	mM·min^{-1}
κ^r_{acs}	maximal protein synthesis rate	mM·min^{-1}
θ_{fis_3}, θ_{cc_3}	affinity constants	mM
n_5, n_6	Hill coefficients	adimensional
	rpoS expression	
κ^b_{rpoS}	basal protein synthesis rate	mM·min^{-1}
κ^r_{rpoS}	maximal protein synthesis rate	mM·min^{-1}
θ_{cc_4}	affinity constant	mM
n_7	Hill number	adimensional

Table 5.4: Parameters of the ODE model of global and transcriptional regulation of the *acs* network shown in Fig. 5.1 (+ *rpoS*). The model is detailed in Eq. (5.12)

1. We decomposed the ODE model into four different kinetic models of promoter activities using measurements of GFP concentrations as representative of Fis and Crp concentrations (Eq. (5.9)). This way, we face the case where the observable vector of the model contains the variables, which corresponds to the first situation enumerated in Sec. 2.4.1. The parameter estimation problem becomes a set of 4 independent problems of estimating between 5 and 7 parameters with an algebraic objective function (see Appendix C.5).

2. Using the estimates obtained from decomposed estimation problems to form the initial

parameter vector, we performed parameter estimation on the whole ODE model with only the measurements of promoter activities of *fis*, *crp*, *acs* and *rpoS* presented in Fig. 5.3*A*-*C* and Fig. A7*A* as observables. The optimization algorithm used in these two steps is a combination of a genetic algorithm, implemented in the MATLAB function `ga`, and the interior-point algorithm, a local-search method with non-linear constraints implemented in the MATLAB function `fmincon`. Such a combination has been shown to improve optimization performance [Rodriguez-Fernandez et al., 2006].

Following this procedure, we obtained values for the 21 parameters of the model. These values are presented in Appendix C.5.2. To simulate the promoter activities of the model, we used as inputs the data of intracellular cAMP concentration, shown Fig. 5.2*B*, the data of pRM promoter activity, shown Fig. 5.3*D*, and the corresponding growth rate obtained in the experimental conditions described in Sec. 5.1.1. The experimental data of promoter activities of the 4 genes of the model obtained under the same conditions and the corresponding simulated data are shown in Fig. 5.8. The model captures well the increase of *acs* expression after glucose exhaustion and the simulated promoter activity of *acs* is in perfect agreement with the experimental data, as it falls within the data confidence intervals. Moreover, the model is able to reproduce the gradual decrease of promoter activity at the end of exponential phase that was observed experimentally for *fis*, *crp* and *rpoS*. For *rpoS* promoter activity, the simulations, as for *acs*, almost always fall within the confidence interval of experimental data. As for the other genes, the promoter activity levels of *fis* and *crp* observed experimentally during the steady-state of exponential phase are 30% and 20% higher than the levels returned by the model. We conclude that the model returns promoter activity time-courses during glucose exhaustion that are in adequacy with the experimental observations. However, note that the estimated parameter values used for the simulations are preliminary results and parameter estimation deserves to be investigated further.

We now question the behaviour of the outputs of the model in experimental conditions that are different from the ones used for parameter estimation. We simulated promoter activities of *fis*, *crp*, *acs* and *rpoS* in the case of redilution into a low-glucose medium. The inputs taken were the intracellular cAMP concentration, pRM promoter activity and corresponding growth rate data shown in Fig. 5.2*C*, Fig. 5.7*D* and Fig. 5.2.1*D*, respectively. The resulting simulations of promoter activities are presented in Figs. 5.9*I*-*L*. Globally, the qualitative patterns observed experimentally are correctly predicted by the model. Indeed, the model reproduces the steep increase of *acs* expression after glucose exhaustion and the gradual decrease of *fis*, *crp* and *rpoS* expressions at the end of exponential phase. However, we observe experimentally an increase of *fis* expression after glucose exhaustion that is not predicted by the model.

We also tested the model predictions in case of Δ*fis* and Δ*crp* mutant strains. To obtain promoter activity simulations for a Δ*fis* strain, we took for inputs the intracellular cAMP

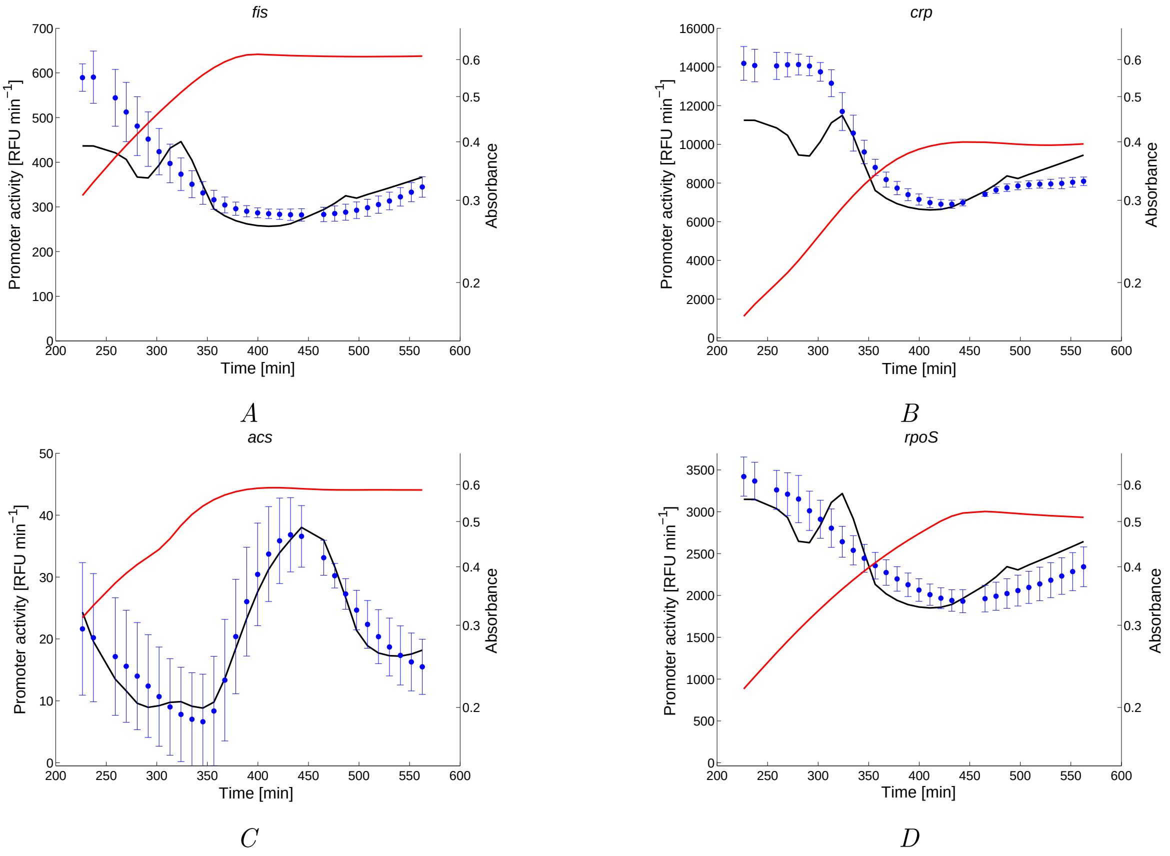

Figure 5.8: Promoter activities of *fis* (*A*), *crp* (*B*), *acs* (*C*) and *rpoS* (*D*) in the wild-type strain. Simulation of time-varying promoter activity (-,black), experimental data (•, blue) derived from GFP data with 95%-confidence interval obtained from experimental replicas, and absorbance (-,red).

concentration, pRM promoter activity and growth rate data measured in a Δ*fis* strain and shown in Fig. 5.2*B*, Fig. 5.5*D* and Fig. 5.2.1*B*, respectively. We fixed $x_{Fis}(t) = 0$ for all t and computed the promoter activities of the 4 genes. The results are shown in Figs. 5.9*A*-*D*. Although the model captures again the decrease of *fis*, *crp* and *rpoS* promoter activities at the end of exponential phase, the simulated data are systematically higher than the experimental data, with a 3-fold and 2-fold difference for *fis* and *crp*, respectively. Moreover, the model predicts a significant increase after glucose exhaustion that we do not observe experimentally in *fis* and *crp* data. More importantly, the increase of *acs* promoter activity observed in the data is not captured by the model. We also computed predictions for a Δcrp strain by fixing $x_{Crp\cdot cAMP}(t) = x_{Crp}(t) = 0$ and taking the corresponding inputs. The resulting simulations are presented in Figs. 5.9*E*-*H*. Although the qualitative patterns of expression are correctly predicted by the model, quantitatively, the differences in promoter activity levels at steady-state of exponential phase are higher than 2-fold for *fis* and *crp*.

The significant differences observed between model simulations and experimental data in the mutant strains suggest that the model can not yet be considered as a predictive tool of the dynamical behaviour of the *acs* network. A possible explanation may come from the change of plasmid copy number in the cell that we observed experimentally (see Appendix C.3). Thus, the model needs to incorporate this bias in order to be compared with experimental data obtained from reporter plasmids. In addition, further investigation into parameter estimation of the model could help improving the predictive performances of this model.

5.4 Discussion

The variation of gene expression across growth phases is controlled both by transcriptional regulators and the global physiological state of the cell. We have presented a method to distinguish between these two effects, based on a simple mathematical model of promoter activity. The approach has several advantages making it easy to put it to work for bacteria but also in higher organisms. The models do not have free parameters that need to be calibrated, hypotheses on the effect of regulators can be readily tested by monitoring the expression of target genes and a constitutive control, and the use of plasmid-borne reporter systems does not bias the analysis. This allows the relative contributions of transcriptional regulators and the global state of the cell to be monitored on the level of a regulatory network and over time.

When applied to the network controlling the expression of the gene *acs*, we obtained a number of surprising results. First, even though the interactions involving the two major pleiotropic transcription factors Fis and Crp have been amply documented in the literature, and are held responsible for the coordination of gene expression changes between growth phases [Bradley et al., 2007, Gosset et al., 2004], we found that they do not play a critical physiological role in our conditions. One explanation for this apparent discrepancy might be that we only considered a single growth condition, minimal medium with glucose as the carbon

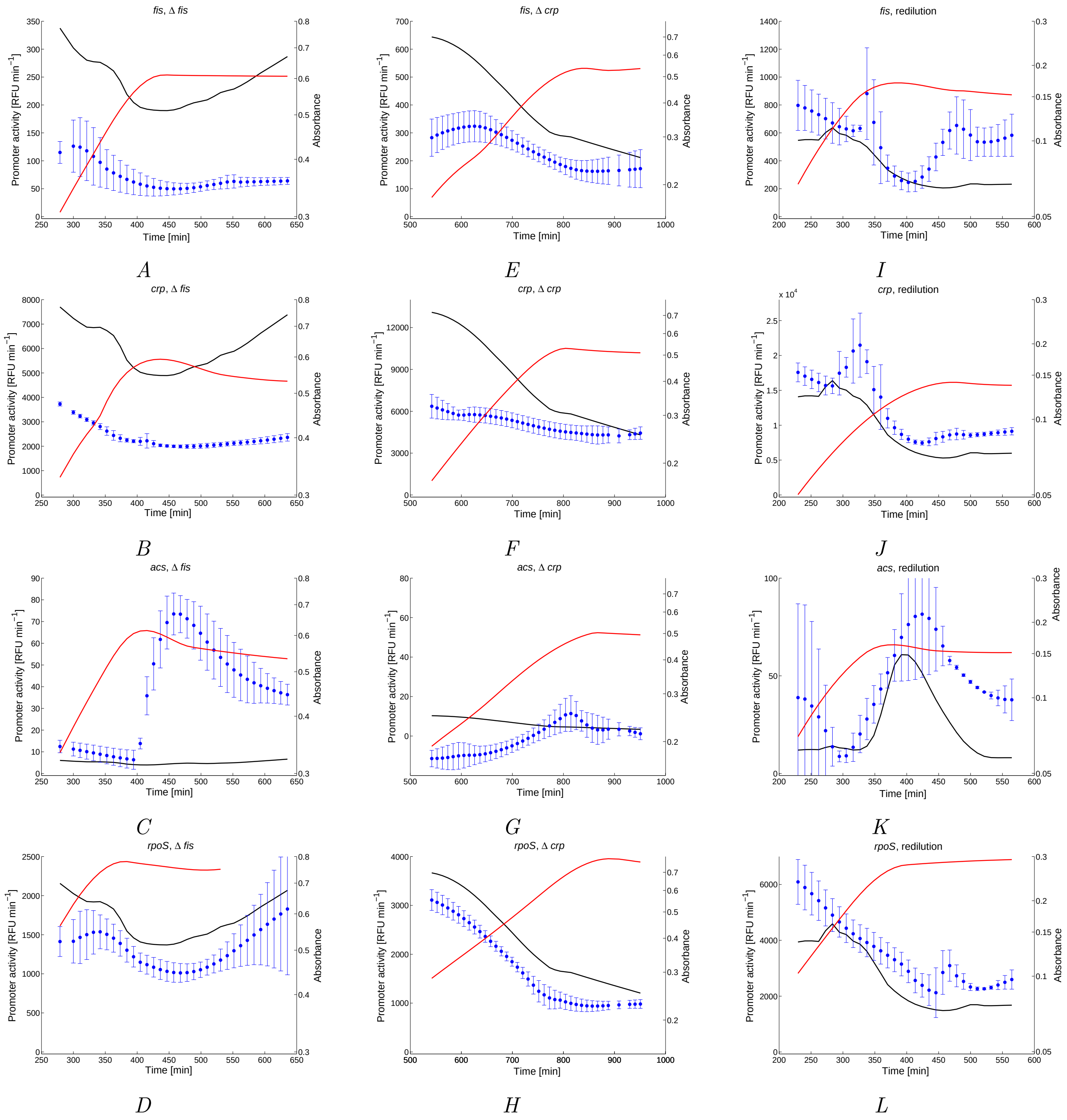

Figure 5.9: Promoter activities obtained by experimental measure and by model simulations for different genes under different conditions. Simulation of time-varying promoter activity (-,black), experimental data (●, blue) derived from GFP data with 95%-confidence interval obtained from experimental replicas, and absorbance (-,red). *A:* Promoter activity of *fis* in a Δ*fis* strain. *B:* Promoter activity of *fis* in a *crp* strain. *C:* Promoter activity of *fis* in a wild-type strain after redilution to a low-glucose medium. *D-F:* Idem but for promoter activity of *crp*. *G-I:* Idem but for promoter activity of *acs*. *J-L:* Idem but for promoter activity of *rpoS*.

source. After all, the interactions that were not found to be important in our experiments may play a role in other physiological conditions. The absence of an effect of Fis and Crp remains puzzling though, as these regulators are believed to be important in glucose-limited growth [Gutierrez-Ríos et al., 2007]. An alternative explanation for the discrepancy might be that many studies do not control for global physiological effects [Dennis et al., 2004].

This brings us to the second surprising finding of this study, namely the dominant role of global physiological control in the case of the expression of the genes encoding the transcription regulators *fis*, *crp*, and *rpoS*. The molecular bases of this global effect are diverse and complex, involving among other things guanosine 3',5'-bispyrophosphate or (p)ppGpp [Potrykus and Cashel, 2008, Traxler et al., 2006], which exerts control on the abundance and activity of the components of the transcription and translation machinery. For the purpose of this study, we have encapsulated these mechanisms into an easy-to-measure variable, the expression of a constitutive gene.

We also developed an ODE model of the network of Fig. 5.1 accounting for regulation both by transcriptional factors and by the global physiological state of the cell. After calibration of the model using a combination of global-search and local-search optimization methods and experimental data presented in this chapter, we computed simulations for all the genes of the network in different experimental conditions. In its current version, the model is not able to correctly predict quantitatively the behaviour of gene expression during glucose exhaustion in the case of Δ*fis* and Δ*crp* strains. In the future, we expect the predictive power of the model to be improved by further investigation of parameter estimation or by correction of the model for the change of plasmid copy number in the cell observed experimentally during glucose exhaustion.

Another interesting extension of the work presented here would be to analyze the global control of the promoter activities in more detail, distinguishing between the contributions from individual physiological parameters, such as ppGpp-dependent reprogramming of RNA polymerase, the variation in gene copy number, and the size of nucleotide pools.

Our results question the dominant role often attributed to gene regulatory networks in controlling genome-wide expression changes during physiological transitions [Regenberg et al., 2006]. The picture that emerges is closer to that advocated in classical studies of bacterial physiology, which focused on global changes in the macromolecular composition of the cell, including the transcription and translation machinery, in response to changes in the growth-supporting ability of the environment [Neidhardt et al., 1990, Maaloe and Kjeldgaard, 1966]. It could indeed be most fruitful to see local regulators as finetuning the global control exerted by the physiological state of the cell.

Chapter 6

Conclusion

We focused on the regulation mechanisms responsible for metabolic and gene expression changes during growth transition in *E. coli.* The analysis of dynamics of such large and embedded systems required the development of quantitative models. This chapter summarizes the contributions of this thesis on two topics: parameter estimation of metabolic network models and regulation undergone by gene expression during growth transition.

We developed a method for estimating parameters of approximated kinetic models called linlog from high-throughput incomplete datasets. We have seen on simulated data that our method outperforms both regression and multiple imputation, a standard method in case of missing data. Moreover, when applied on the largest dataset available, the method was able to estimate many parameters of a linlog model of central carbon metabolism of *E. coli.* Although it has been developed for linlog models, the method is applicable to approximate kinetic models that allow a mathematical formalism linear in the parameters and provides information on network elasticities, which is useful for identification of detailed kinetic models.

It is also important to notice that, even with a simplified formalism, the largest dataset available and a method specifically developed for the case of missing data, the parameter values obtained were not, for most of them, significantly different from 0. We were able, from these results, to highlight critical issues for data exploitation in order to estimate parameters. Indeed, high percentages of missing data for some metabolites tend to critically impact the identification results and the use of steady-state data can prevent the estimation of some parameters, due to identifiability issues.

We investigated this question further and defined a theoretical background for identifiability analysis of linlog models, given steady-state data. We presented precise definitions of structural and practical identifiability and clarified the link between those concepts. We also developed a method to detect nonidentifiability and to reduce the model to an identifiable approximation. Adaptations of the method in case of noisy or incomplete datasets were discussed and their application on simulated data showed improvements on identifiability analysis. Again, the definitions and methods presented are not only applicable to linlog models, but to all kinetic formalisms that allow a linear formulation of the parameter estimation problem.

Moreover, application of our method, taking noise on metabolite measurements into account for identifiability analysis, on experimental data showed that most of the parameters of the linlog model of central carbon metabolism of *E. coli* were actually not identifiable. These results enforce the diagnosis that identification remains very sensitive to noise and missing data, even with the largest high-throughput and steady-state datasets available.

Another important contribution of this thesis is the analysis of regulation of gene expression during growth rate and more specifically, the distribution between the role of the global physiological state of the cell and the role of transcriptional regulation. We developed a method to distinguish between those two effects, based on a simple parameterless model of promoter activity. We applied our method to time-series gene expression data of the network controlling the expression of *acs*, that we measured *in vivo* using reporter plasmids. Surprisingly, we found that the global physiological state of the cell has a dominant regulatory role on gene expression of the transcription factors involved in this network. More generally, our results question the role attributed to gene regulatory networks in the control of gene expression changes during growth transitions, which could be seen as a complement to a global control by the physiological state of the cell.

To explore this role distribution further, we developed a quantitative ODE model of this network that takes the macromolecular composition of the cell into account. After estimating the model parameters on a subset of our experimental data, we tested the model predictions by comparing them to the rest of the dataset. Although the model simulations showed in this thesis are preliminary results, we are confident that, by means of model improvement such as correction for plasmid copy number, we will be able to correctly reproduce gene expression patterns observed for different genetic backgrounds or growth conditions.

Appendices

Appendix A

Additional information on parameter estimation of linlog metabolic models

A.1 Likelihood-based identification of linlog models

We rely on the notation of Sec. 3.2 of the main section, *i.e.,* we focus on a single reaction and drop index i from the notation. The loglikelihood of the model is:

$$\log \mathscr{L}(b) = \log \int f_{W|\check{y},\grave{y},b}(w) f_{\grave{Y}|\check{y},b}(\grave{y}) d\grave{y}. \tag{A1}$$

For convenience, we rewrite (A1) in terms of the random variable $Z = \grave{Y} \cdot b$ introduced in Sec. 3.2 so that it becomes:

$$\log \mathscr{L}(b) = \log \int f_{W|\check{y},z,b}(w) f_{Z|\check{y},b}(z) dz. \tag{A2}$$

Here $f_{W|\check{y},z,b}(\cdot)$ is the Gaussian likelihood function of model (3.7), equivalently rewritten as $W = \check{Y} \cdot b + Z + \varepsilon$, given $\check{Y} = \check{y}$ and $Z = z$, with z varying over all possible values of Z, and $f_{Z|\check{y},b}$ is the Gaussian prior of $Z = \grave{Y} \cdot b$ following from (3.10). The expressions of $f_{W|\check{y},z,b}$ and $f_{Z|\check{y},b}$ are thus

$$\begin{cases} f_{W|\check{y},z,b}(w) = \frac{1}{\sqrt{\det(2\pi\Sigma_\varepsilon)}} \exp(-\frac{1}{2}[w - \check{Y} \cdot b - z]^T \Sigma_\varepsilon^{-1} [w - \check{Y} \cdot b - z]), \\ f_{Z|\check{y},b}(z) = \frac{1}{\sqrt{\det(2\pi\Sigma_{\check{y},b})}} \exp(-\frac{1}{2}[z - \mu_{\check{y},b}]^T \Sigma_{\check{y},b}^{-1} [z - \mu_{\check{y},b}]), \end{cases} \tag{A3}$$

with $\mu_{\check{y},b} = M \cdot b$, where the entry $M_{j,k}$ of matrix M is the mean $\mu_{j,k}$ of the distribution of $\grave{Y}_{j,k}$, and $\Sigma_{\check{y},b}$ is the variance matrix of the random variable Z. By the independence assumptions on $\grave{Y}$, it turns out that

$$\Sigma_{\check{y},b} = diag\left(\sum_{k=1}^{n_b} b_k^2 \cdot [\sigma_{1,k}^2 \cdots \sigma_{q,k}^2]^T\right) \tag{A4}$$

where $\sigma_{j,k}$ is defined in (3.10).

Assume for the moment that $\Sigma_{\check{y},b}$ is invertible. Defining

$$f_{p_b}(z) = f_{W|\check{y},z,b}(w) \cdot f_{Z|\check{y},b}(z), \tag{A5}$$

after simple but tedious calculations, we obtain

$$f_{p_b}(z) = \kappa_{f_b} \cdot f_b(z) \tag{A6}$$

with f_b the density function of a Gaussian distribution $\mathscr{N}(\mu_{f_b}, \Sigma_{f_b})$ and

$$\begin{cases} \Sigma_{f_b} = [\Sigma_\varepsilon^{-1} + \Sigma_{\check{y},b}^{-1}]^{-1}, \\ \mu_{f_b} = \Sigma_{f_b} \cdot [\Sigma_\varepsilon^{-1} \cdot (w - \check{Y} \cdot b) + \Sigma_{\check{y},b}^{-1} \cdot \mu_{\check{y},b}], \\ \kappa_{f_b} = \frac{\exp(-\frac{1}{2}[w-\check{Y}\cdot b-\mu_{\check{y},b}]^T \cdot [\Sigma_\varepsilon+\Sigma_{\check{y},b}]^{-1} \cdot [w-\check{Y}\cdot b-\mu_{\check{y},b}])}{\sqrt{\det(2\pi[\Sigma_\varepsilon+\Sigma_{\check{y},b}])}}. \end{cases} \tag{A7}$$

The proportionality factor κ_{f_b} does not depend on the integration variable z, so it can be taken out of the integral and (A2) can be rewritten as follows:

$$\log \mathscr{L}(b) = \log(\kappa_{f_b}) + \log\left(\int f_b(z)dz\right). \tag{A8}$$

The integral of a normalized Gaussian density function being 1, we finally have an analytical expression for the loglikelihood: $\log \mathscr{L}(b) = \log(\kappa_{f_b})$.

The above results are used in the expectation step of the EM algorithm. Recall the definition

$$Q(b|\hat{b}^{\ell-1}) = \int \log(f_{Z,W|\check{y},b}(z,w)) f_{Z|\check{y},\hat{b}^{\ell-1},w}(z)dz. \tag{A9}$$

The Bayes theorem allows us to rewrite (A9) as follows:

$$Q(b|\hat{b}^{\ell-1}) = \int \log(f_{W|\check{y},z,b}(w) f_{Z|\check{y},b}(z)) \frac{f_{W|\check{y},z,\hat{b}^{\ell-1}}(w) f_{Z|\check{y},\hat{b}^{\ell-1}}(z)}{f_{W|\check{y},\hat{b}^{\ell-1}}(w)} dz. \tag{A10}$$

Function $f_{W|\check{y},\hat{b}^{\ell-1}}(w)$ does not depend on z so it can be taken out of the integral. Moreover, this function does not depend on b so it will have no impact on the maximization step of EM. Thus, we can ignore this function from the computation of the expectation function above.

Using definitions (A5) and (A6), we can rewrite (A10) in the following way:

$$\begin{aligned} Q(b|\hat{b}^{\ell-1}) &\propto \int \kappa_{f_{\hat{b}^{\ell-1}}} f_{\hat{b}^{\ell-1}}(z) \log(\kappa_{f_b} f_b(z))dz \\ &\propto \int f_{\hat{b}^{\ell-1}}(z) \log(\kappa_{f_b} f_b(z))dz. \end{aligned} \tag{A11}$$

We have dropped the constant factor $\kappa_{f_{\hat{b}^{\ell-1}}}$ as it does not depend on b and thus does not influence the maximization step of EM. By replacing $\log(\kappa_{f_b} f_b(z))$ by $\log(\kappa_{f_b} f_b(z) f_{\hat{b}^{\ell-1}}(z) / f_{\hat{b}^{\ell-1}}(z))$ and separating the integrand in a sum of terms, we can rewrite (A11) as

$$-Q(b|\hat{b}^{\ell-1}) \propto \int f_{\hat{b}^{\ell-1}}(z) \log\left(\frac{f_{\hat{b}^{\ell-1}}(z)}{f_b(z)}\right) dz - \int f_{\hat{b}^{\ell-1}}(z) \log(f_{\hat{b}^{\ell-1}}(z)) dz - \log(\kappa_{f_b}). \quad \text{(A12)}$$

We recognize in the first term the definition of the Kullback-Leibler divergence $KL(f_b || f_{\hat{b}^{\ell-1}})$ between the two probability distributions f_b and $f_{\hat{b}^{\ell-1}}$ and in the second term the entropy $H(f_{\hat{b}^{\ell-1}})$ of $f_{\hat{b}^{\ell-1}}$ [Cover and Thomas, 2006, Stoorvogel and van Schuppen, 1996]. For Gaussian distributions, these can be written explicitly as

$$\begin{aligned} KL(f_b || f_{\hat{b}^{\ell-1}}) = \frac{1}{2}(\log\left(\frac{\det(\Sigma_{f_b})}{\det(\Sigma_{f_{\hat{b}^{\ell-1}}})}\right) &+ Tr(\Sigma_{f_b}^{-1} \Sigma_{f_{\hat{b}^{\ell-1}}}) \\ &+ [\mu_{f_b} - \mu_{f_{\hat{b}^{\ell-1}}}]^T \Sigma_{f_b}^{-1} [\mu_{f_b} - \mu_{f_{\hat{b}^{\ell-1}}}]), \end{aligned} \quad \text{(A13)}$$

where $Tr(\ldots)$ stands for trace and

$$H(f_{\hat{b}^{\ell-1}}) = \log\left(\sqrt{\det(2\pi e \Sigma_{f_{\hat{b}^{\ell-1}}})}\right). \quad \text{(A14)}$$

To summarize, together with (A7), this gives us the explicit formula

$$Q(b|\hat{b}^{\ell-1}) \propto -KL(f_b || f_{\hat{b}^{\ell-1}}) - H(f_{\hat{b}^{\ell-1}}) + \log(\kappa_{f_b}), \quad \text{(A15)}$$

which we employ in our implementation of EM.

In more generality, for some values of b, $\Sigma_{\check{y},b}$ may be singular or poorly conditioned. To avoid this circumstance, we can adapt our procedure as follows. We consider a decomposition

$$W = \check{Y} \cdot b + Z + (\varepsilon' + \varepsilon'') = \check{Y} \cdot b + (Z + \varepsilon') + \varepsilon'' \quad \text{(A16)}$$

where ε' and ε'' are independent zero-mean Gaussian random vectors such that $\Sigma_{\varepsilon'} \triangleq Var(\varepsilon') = \alpha \Sigma_\varepsilon$ and $\Sigma_{\varepsilon''} \triangleq Var(\varepsilon'') = (1-\alpha)\Sigma_\varepsilon$, with $\alpha \in (0,1)$ a tunable parameter. Since $\Sigma_\varepsilon > 0$ by assumption, it follows that $\Sigma_{\varepsilon'} > 0$ and $\Sigma_{\varepsilon''} > 0$. Moreover, $\Sigma_\varepsilon = \Sigma_{\varepsilon'} + \Sigma_{\varepsilon''}$, *i.e.*, the statistics of ε and of $\varepsilon' + \varepsilon''$ are identical. Since $Var(Z + \varepsilon') = \Sigma_{\check{y},b} + \Sigma_{\varepsilon'} > 0$, if we interpret $Z + \varepsilon'$ as the unknown observations (in place of Z) and ε'' as the model noise (in place of ε), we ensure that the variance of the 'missing data' is invertible. Thus, in practice, we apply all formulas developed above with $\Sigma_{\check{y},b} + \Sigma_{\varepsilon'}$ in place of $\Sigma_{\check{y},b}$ and $\Sigma_{\varepsilon''}$ in place of Σ_ε.

The effect of the specific choice of α is under investigation. In this work, we took $\alpha = 0.2$, a value that leads to good results in practice.

A.2 Validation of parameter estimation of linlog models on simulated data

The model used for comparing performance of the identification algorithms is a reduced synthetic linlog model of the *E. coli* central carbon metabolism network (Fig. A1 of the main text). This network contains 17 variables, describing internal and external metabolites, and 25 reactions, summarized in Table A1 and Table A2, respectively. The linlog model has the form of Eq. (3.1)-(3.2) of the main text.

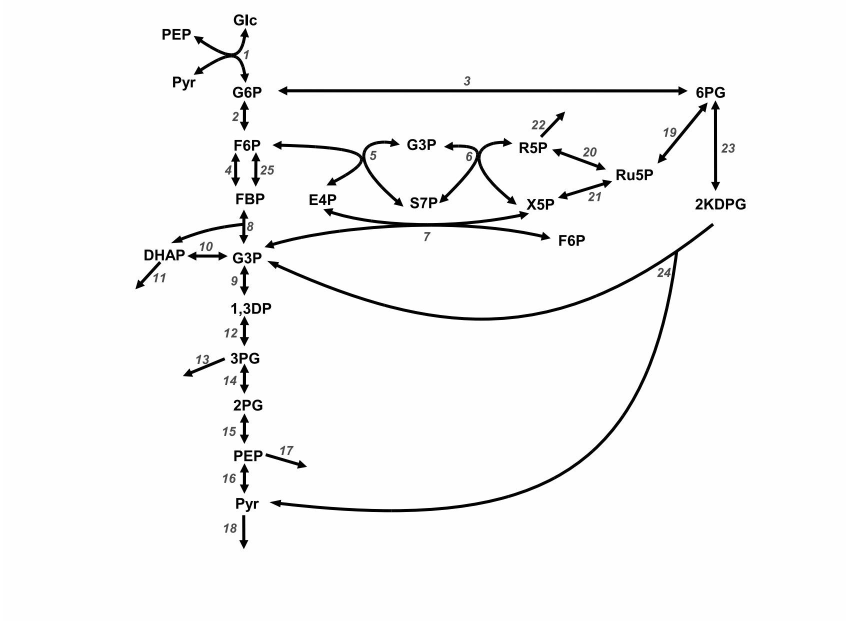

Figure A1: Network for the synthetic model, a reduced version of the *E. coli* central carbon metabolism network.

A dataset was generated from the synthetic linlog model by setting all enzyme concentrations to 1 and choosing plausible values for the parameter vector a and matrices B^x, B^u, that is, values consistent with existing kinetic models of carbon metabolism in *E. coli* [Bettenbrock et al., 2006]. Then $q = 30$ different experimental conditions were simulated by randomly changing enzyme concentrations. For each condition $j \in \{1, ..., q\}$, vectors $\ln(x^j)$, $\ln(u^j)$ and v^j were determined by the equations resulting from the formulation of the linlog model and the (quasi-)steady-state equation $N \cdot v = 0$:

$$\begin{cases} \begin{bmatrix} \ln(x^j) \\ \ln(u^j) \end{bmatrix} = -\left[N \cdot \mathrm{diag}(e^{)}) \cdot [B^x \, B^u]\right]^{-1} N \cdot \mathrm{diag}(e^j) \cdot a, \\ v^j = \mathrm{diag}(e^j) \cdot \big(a + B^x \cdot \ln(x^j) + B^u \cdot \ln(u^j)\big). \end{cases} \tag{A17}$$

For this dataset, four scenarios were considered, corresponding to more or less favorable

Index	Name	Symbol
1	Pyruvate	Pyr
2	Phosphoenol-pyruvate	PEP
3	Glyceraldehyde-3-phosphate	G3P
4	Fructose-6-phosphate	F6P
5	Glucose-6-phosphate	G6P
6	3-phosphoglycerate	3PG
7	Dihydroxyacetonephosphate	DHAP
8	Ribulose-5-phosphate	Ru5P
9	Ribose-5-phosphate	R5P
10	6-phosphogluconate	6PG
11	Erythrose-4-phosphate	E4P
12	Xylulose-5-phosphate	X5P
13	2-phosphoglycerate	2PG
14	1,3-diphosphosphoglycerate	1,3DP
15	Fructose-1,6-bisphosphate	FBP
16	2-keto-3-deoxy-6-phosphogluconate	2KDPG
17	Sedoheptulose-7-phosphate	S7P

Table A1: Metabolites included in the synthetic linlog model.

conditions for identification: 40 % and 75 % missing entries and 10% and 20% noise. For each column of Y, *i.e.,* each metabolite of the model, the 40% or 75% missing data were distributed randomly over the q measurements. Randomly generated noise was added to the same incomplete dataset in each of 100 Monte-Carlo repetitions.

Identifiability analysis was performed following the approach described in Sec. 3.1, with $\lambda = 0.99$. 10 reactions were found to be nonidentifiable (reactions 2, 5, 6, 7, 8, 12, 14, 15, 20 and 21). Among these reactions only 3 identifiable parameters could be isolated (one in reaction 2, one in reaction 7 and one in reaction 12).

Results from all identification methods on identifiable reactions are summarized in Fig. A2 for the most favorable scenario with 40% missing data and 10% noise, and in Fig. A3 for the least favorable scenario with 75% missing data and 20% error. The results for the other scenarios fall between those shown in Fig. A2 and Fig. A3, and are not shown here.

Index	Name
1	Phosphotransferase system
2	Glucose-6-phosphate isomerase
3	Glucose-6-phosphate dehydrogenase
4	Phosphofructokinase
5	Transaldolase
6	Transketolase a
7	Transketolase b
8	Aldolase
9	Glyceraldehyde-3-phosphate dehydrogenase
10	Triosephosphate isomerase
11	Glycerol-3-phosphate dehydrogenase
12	Phosphoglycerate kinase
13	Serine synthesis
14	Phosphoglycerate mutase
15	Enolase
16	Pyruvate kinase
17	PEP carboxylase
18	Pyruvate synthesis
19	6-Phosphogluconate dehydrogenase
20	Ribose-phosphate isomerase
21	Ribulose-phosphate epimerase
22	Ribose-phosphate pyrophosphokinase
23	Phosphogluconate dehydratase
24	KDPG aldolase
25	Fructose bisphosphatase

Table A2: Reactions included in the synthetic linlog model.

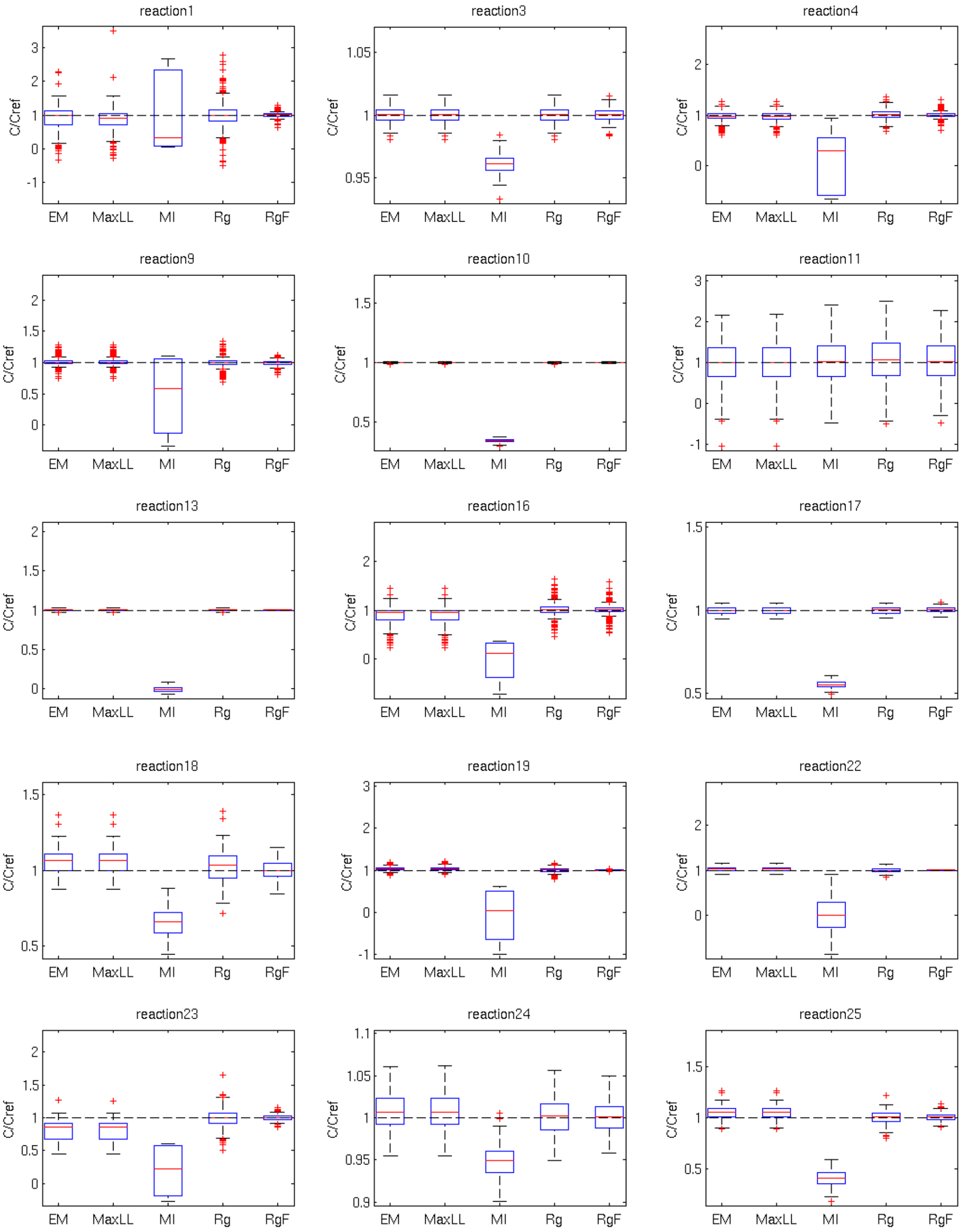

Figure A2: Statistics of estimated parameter values in identifiable reactions for datasets with 40% of missing data and 10% noise. The graphical notations are the same as for Fig. 3.1.

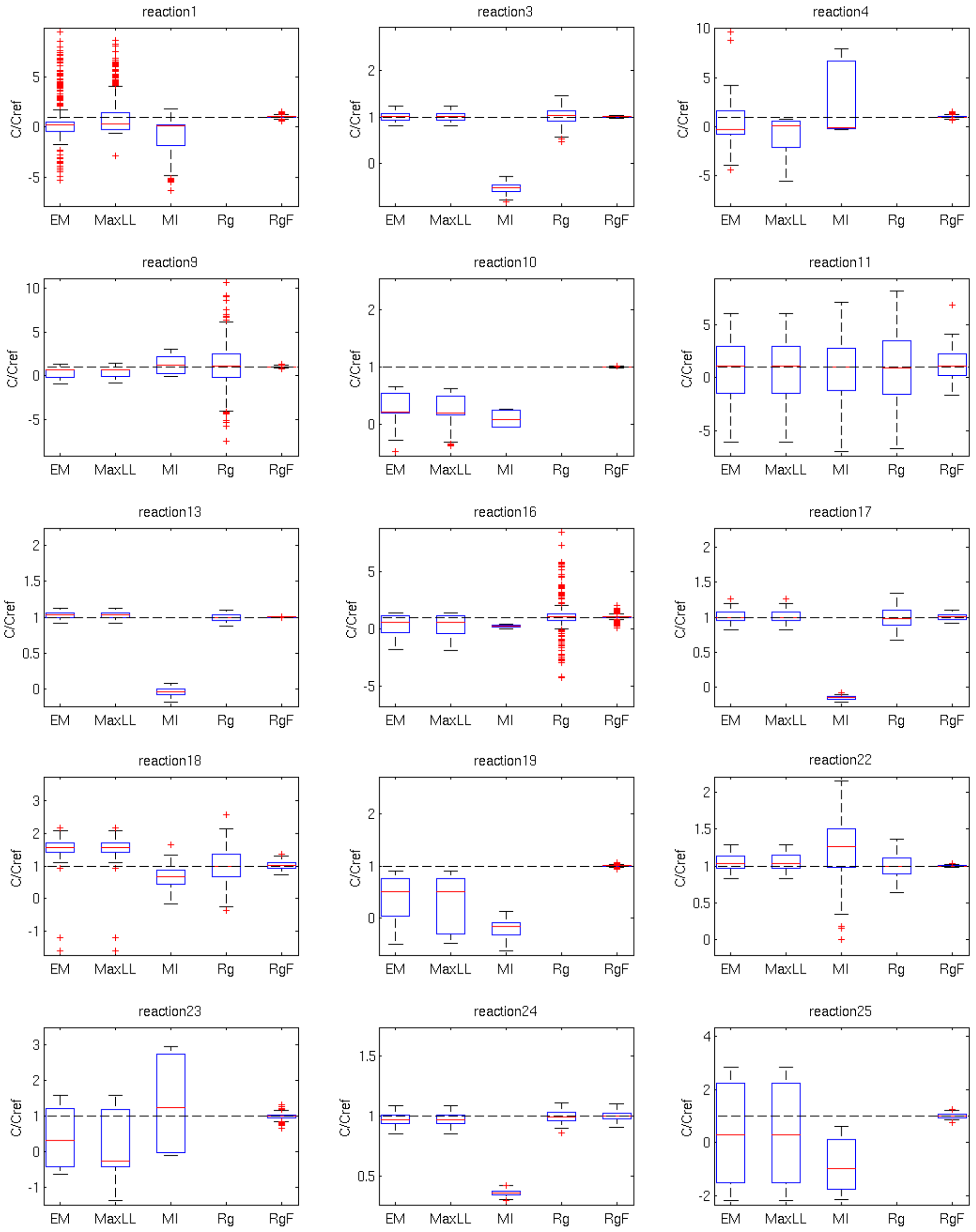

Figure A3: Statistics of estimated parameter values in identifiable reactions for datasets with 75% of missing data and 20% noise. The graphical notations are the same as for Fig. 3.1.

Appendix B

Additional information on identifiability of linlog metabolic models

B.1 Proofs of theorems and propositions concerning identifiability of linlog models

Proposition 1. *A reaction i of $\mathscr{M}_p$ is structurally identifiable at p^* if and only if there exists $D \subseteq E \times U$ such that the solution of the equation $W_i^* = Y^* B_i^*$, with*

$$W_i^* = \left[\left(\tfrac{J_*^1}{e^1} - \overline{\left(\tfrac{J_*}{e}\right)} \right)_i \quad \cdots \quad \left(\tfrac{J_*^q}{e^q} - \overline{\left(\tfrac{J_*}{e}\right)} \right)_i \right]^T,$$

$$Y^* = \begin{bmatrix} \ln x_*^1 - \overline{\ln x_*} & \cdots & \ln x_*^q - \overline{\ln x_*} \\ \ln u^1 - \overline{\ln u} & \cdots & \ln u^q - \overline{\ln u} \end{bmatrix}^T,$$

is unique in the parameters $B_i = \left([B^{x*} \; B^{u*}]^T\right)_i$.

Proof. (If) Assume that, for a given $D \subseteq E \times U$, the solution of $W_i^* = Y^* B_i^*$ is unique. We need to prove that $\big((J_p)_i, x_p\big)|_D = \big((J_{p^*})_i, x_{p^*}\big)|_D$ implies $p_i = p_i^*$. For simplicity, here we drop index i from subscripts.

Given any two parameters $p^* = \begin{bmatrix} a^* & B^{*T} \end{bmatrix}^T$ and $p = \begin{bmatrix} a & B^T \end{bmatrix}^T$, for which $\mathscr{M}_p : (e, u) \mapsto (J_p, x_p)$ and $\mathscr{M}_{p^*} : (e, u) \mapsto (J_{p^*}, x_{p^*})$, it holds by construction that $W = YB$ and $W^* = Y^* B^*$. If $(J_p, x_p)|_D = (J_{p^*}, x_{p^*})|_D$, then it also holds that $Y = Y^*$ and $W = W^*$, therefore we can write $W^* = Y^* B$. Because the solution in B of the latter is unique and one solution is B^*, it follows that $B = B^*$. To conclude that $p = p^*$, we are left with showing that $a = a^*$. This follows from

$$a^* = \overline{\left(\frac{J_*}{e}\right)} - \begin{bmatrix} \overline{\ln x_*} \\ \overline{\ln u} \end{bmatrix}^T \cdot B^* = \overline{\left(\frac{J}{e}\right)} - \begin{bmatrix} \overline{\ln x} \\ \overline{\ln u} \end{bmatrix}^T \cdot B = a.$$

(Only if) Here the hypothesis is that, for a given $D \subseteq E \times U$, $\big((J_p)_i, x_p\big)|_D = \big((J_{p^*})_i, x_{p^*}\big)|_D$ implies $p_i = p_i^*$, and we need to show that the solution in B_i of $W_i^* = Y^* B_i$ is unique. For simplicity, we will again drop i from the subscripts.

For the sake of contradiction, assume that $W^* = Y^* B$ admits distinct solutions. Since B^* is a solution, all solutions are of the form $B = B^* + z$, with z in the nontrivial kernel of Y^*. For any such z we can write $Y^* B^* = Y^*(B^* + z)$, *i.e.*,

$$\left[(\ln x_* - \overline{\ln x_*})^T \quad (\ln u_* - \overline{\ln u_*})^T\right] B^* = \left[(\ln x_* - \overline{\ln x_*})^T \quad (\ln u_* - \overline{\ln u_*})^T\right] (B^* + z). \quad \text{(A1)}$$

Let $p^* = \left[a^* \quad B^{*T}\right]^T$. For any $(e,u) \in D$, $J_* = J_{p^*}(e,u)$ and $x_* = x_{p^*}(e,u)$ are given by the solution of

$$\begin{cases} 0 = N \cdot J_{p^*}, & \text{(A2a)} \\ J_{p^*} = \operatorname{diag}(e) \cdot (a^* + \left[\ln x_*^T \quad \ln u_*^T\right] B^*) & \text{(A2b)} \end{cases}$$

(which is unique by virtue of Assumption 1). Using Eq. (A1), the term $\left[\ln x_*^T \quad \ln u_*^T\right] B^*$ can be rewritten as $\left[\ln x_*^T \quad \ln u_*^T\right](B^* + z) - \left[\overline{\ln x_*^T} \quad \overline{\ln u_*^T}\right] z$. Replacing this into Eq. (A2) yields

$$\begin{cases} 0 = N \cdot J_*, & \text{(A3a)} \\ J_* = \operatorname{diag}(e) \cdot \Big(\underbrace{(a^* - \left[\overline{\ln x_*^T} \quad \overline{\ln u_*^T}\right] z)}_{\triangleq a} + \left[\ln x_*^T \quad \ln u_*^T\right] \underbrace{(B^* + z)}_{=B}\Big), & \text{(A3b)} \end{cases}$$

for all $(e,u) \in D$.

From this we see that $p = [a \ B^T]^T$, with a defined as above, is different from p^* but is such that $\big(J_p(e,u), x_p(e,u)\big) = \big(J_{p^*}(e,u), x_{p^*}(e,u)\big)$ for all $(e,u) \in D$, which contradicts the hypothesis. □

Corollary 1. *A reaction i of $\mathscr{M}_p$ is structurally identifiable at p_i^* if and only if Y^* is full column-rank.*

Proof. From Proposition 1, we know that identifiability is equivalent to the uniqueness of the solution in B_i of $W_i^* = Y^* B_i$. Uniqueness holds if and only if $\ker(Y^*) = \{0\}$, *i.e.*, Y^* is full column-rank or equivalently $\operatorname{rank}(Y^*) = n_b$. □

Proposition 2. *If a reaction i of $\mathscr{M}_p$ is structurally identifiable at p^* in the sense of Def. 1 then, for every $\alpha \in (0,1)$, it is practically identifiable in the sense of Def. 2 with confidence level at least $1-\alpha$ for any uncertainty set $\mathscr{B}_i \supseteq \mathcal{E}_{\widehat{\Sigma}}(\alpha)$, where $\mathcal{E}_{\widehat{\Sigma}}(\alpha)$ denotes the $(1-\alpha)$-confidence ellipsoid of a zero-mean Gaussian distribution with variance $\widehat{\Sigma} = (Y_{C(i)}^T \Sigma_{\varepsilon_i}^{-1} Y_{C(i)})^{-1}$.*

Proof. The definition of $\mathscr{M}_p$ ensures that $W_i^* = Y^* B_i^*$. Hence, given a noisy dataset $\widetilde{W}_i = W_i^* + \varepsilon_i$ and the errorless dataset Y^*, the regression problem becomes

$$\widetilde{W}_i = Y^* \cdot B_i^* + \varepsilon_i. \tag{A4}$$

From Sec. 4.2.1, identifiability of $\mathscr{M}_p$ at p_i^* is equivalent to Y^* being full column rank. Thus, if $\mathscr{M}_p$ is identifiable at p_i^*, Y is full column rank, and the weighted pseudoinverse of Y, $Y^\dagger \triangleq \left(Y^T \Sigma_{\varepsilon_i}^{-1} Y\right)^{-1} Y^T \Sigma_{\varepsilon_i}^{-1}$, is well-defined. This enables us to define the minimum variance estimator of B_i^*, $\hat{B}_i = Y^\dagger W$. From the linearity of the estimator in the Gaussian noise ε_i, after simple calculations of first and second-order moments, one gets $\hat{B}_i \sim \mathscr{N}\left(B_i^*, \widehat{\Sigma}\right)$ (also compare [Ljung, 1999, Appendix II]). Thus, from the definition of $\mathscr{B}_i$, $\mathbb{P}_{p_i^*}[\hat{B}_i - B_i^* \in \mathscr{B}_i] \geq \mathbb{P}_{p_i^*}[\hat{B}_i - B_i^* \in \mathcal{E}_{\widehat{\Sigma}}(\alpha)] = 1 - \alpha$. □

B.2 Reduction to identifiable models in case of sampling bias

In general, data from repeated experiments may happen to be more densely concentrated in some regions than in others. This is particularly true in our case, where the metabolite log-concentrations play the role of regression data but are not controlled directly by the experimenter. In the extreme case, homeostatic control of metabolite concentrations may cluster most datapoints around a single value. Thus, the variance will be dominated by the variance of experimental error, strongly distorting the analysis of practical identifiability as outlined above. To compensate for this bias, we modify the estimation problem by introducing a weighting scheme to rebalance the importance of the datapoints. Following Sander and Schneider [1991], we seek positive coefficients $\alpha = \begin{bmatrix}\alpha_1 & \cdots & \alpha_q\end{bmatrix}^T$, with $\mathscr{L}_1$-norm $||\alpha||_1 = \sum_{k=1}^q \alpha_k = 1$, such that α_k weights the importance of experiment k based on the mean distance of the corresponding datapoint from all other datapoints, where the mean shall be weighted accordingly. Mathematically, consider $\widetilde{Y}_{C(i)}$, where each row $\widetilde{Y}_{k,C(i)}$ corresponds to a different experiment $k = 1, \ldots, q$, and define the Euclidean distance between datapoints k and k' as $D_{k,k'} = ||\widetilde{Y}_{k,C(i)} - \widetilde{Y}_{k',C(i)}||$. Then we want that

$$\alpha_k = \lambda \cdot \sum_{k'=1}^{q} D_{k,k'} \alpha_{k'}, \qquad k = 1, \ldots, q,$$

for some $\lambda > 0$ independent of k. Let $D \in \mathbb{R}_+^{q \times q}$ be the matrix with entries $D_{k,k'}$, $k, k' = 1, \ldots, q$. The above set of q equations is then written compactly as $\alpha = \lambda \cdot D\alpha$, *i.e.*, α must be an eigenvector of D. From the properties of D (nonnegativity and irreducibility, assuming there are no identical datapoints), it can be shown that this set of equations implies that λ is the unique largest real eigenvalue of D and α is the unique eigenvector associated with λ satisfying $||\alpha||_1 = 1$. In practice, α can be computed by efficient numerical algorithms such as the MATLAB routine `eig` or by fast iterative schemes. Once this weighting is found, in view of model reduction, the SVD analysis of Sec. 4.3.2 is performed on reweighted data as follows. Data are centered with respect to their weighted mean and rescaled according to the importance weights $\sqrt{\alpha}$, thus obtaining a new matrix $\mathring{Y}_{C(i)}$ where $\mathring{Y}_{k,C(i)} = \sqrt{\alpha_k}\big(\widetilde{Y}_{k,C(i)} -$

$\alpha^T \widetilde{Y}_{C(i)}\big)$, with $k = 1, \dots, q$. We can apply the SVD analysis of Sec. 4.3.2 to the reweighted empirical covariance matrix of the data,

$$\mathring{Y}^T_{C(i)} \mathring{Y}_{C(i)} = \mathring{V} \operatorname{diag}\{\mathring{s}^2_1, \dots, \mathring{s}^2_{n_b}\} \mathring{V}^T$$

and choose the effective rank of the data r with the criterion (4.22) applied to $\mathring{s}^2_1, \dots, \mathring{s}^2_{n_b}$ instead of $\widetilde{s}^2_1, \dots, \widetilde{s}^2_{n_b}$.

In practice, since $\widetilde{Y}_{k,C(i)}$ is noisy and the largest components are amplified, the reweighting procedure has the effect to systematically amplify the noise. To correct for this, (4.22) is modified so as to compensate for an amplification factor $\beta > 1$, *i.e.*,

$$r = \max\{\ell : \ \mathring{s}^2_\ell - \beta\nu^2 \geq \beta\nu^2\}. \tag{A5}$$

While an appropriate value of β is difficult to compute analytically, suitable values of β for different datasets noise levels can be determined via simulation.

Example 6. *To illustrate the effect of biased datasets on identifiability analysis and the model reduction technique to overcome it, we consider the model of Example 4 with* $a_1 = 0.0297$ *and* $B_{2,1} = -0.0073$ *which has been shown to be practically identifiable on noiseless datasets. We want to see which model reduction method diagnoses well this identifiability property on a limited, noisy and biased dataset. A dataset of* $q = 30$ *datapoints was simulated and sampling bias was introduced by limiting the range of the log-uniform distribution of enzyme values to* $[-\ln 1.05 \ \ \ln 1.05]$ *for 26 conditions and extending it to* $[-\ln 7 \ \ \ln 7]$ *for the remaining 4 conditions. Noise following a normal distribution with a standard deviation of* 0.4 *was added to the data matrix* Y*. We tested two model reduction approaches: the method defined in Sec. 4.3.2 using criteria of Eq.* (4.22) *and the method correcting for sampling bias using criteria of Eq.* (A5) *with* $\beta = 1.2$*. Figs. B.1(a)-B.1(b) show results of both methods on 100 datasets, respectively. Out of 100 datasets, the model reaction was diagnosed identifiable 49 and 55 times with the first and second methods, respectively. Thus, the correction for sampling bias using the weighting scheme defined above produces slightly more relevant results for identifiability analysis and model reduction.*

We apply the model reduction method using Eq. (A5) on the linlog model of the network shown in Fig. 4.6(a). We consider the case when data available are sampled with bias. We computed noisy metabolite concentrations and metabolic flux values from Eq. (4.12) for 30 different conditions with sampling bias, as in Example 6. The metabolite concentrations were computed with 40% noise level and 100 datasets were generated in this way. The same criteria as in Table 4.1 were applied on the 100 data matrices Y and on the corresponding corrected matrices $\mathring{Y}$. Average effective ranks computed from those different criteria are reported in Table A1.

First of all, we notice that, compared to Table 4.1, model reduction of Def. 4 with $\theta = 0.99$ on a biased dataset give the same results as on the dataset of Sec. 4.4.1. Indeed, no

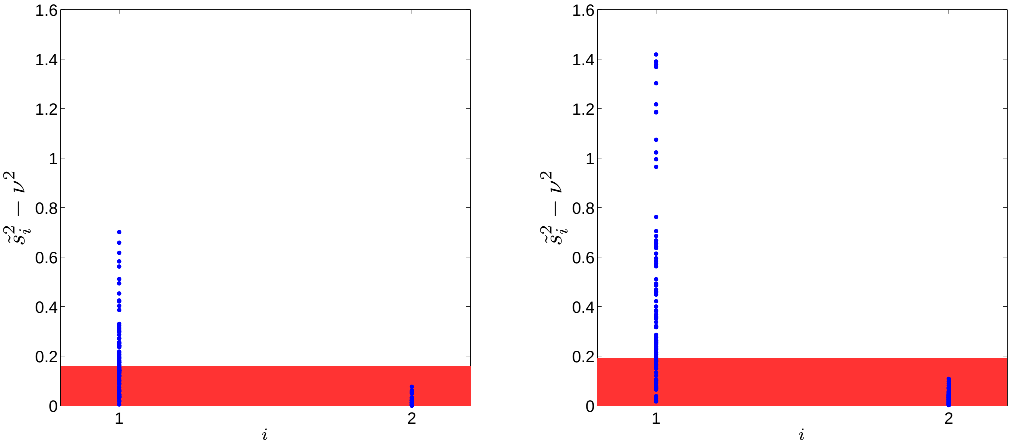

(a)

(b)

Figure A1: Squared singular values for 100 data matrices Y. The data matrices, biased and noisy (40% noise level) were computed from model of Example 3 with $a_1 = 0.0297$ and $B_{2,1} = -0.0073$. **(a)** Singular values and cutoff computed like described in Sec. 4.3.2 with Eq. (4.22). The blue dots are the estimates of the squared singular values $\tilde{s}_\ell^2 - \nu^2$ and the red box covers the area below the cutoff of ν^2. **(b)** Singular values and cutoff computed on data matrices $\mathring{Y}$ corrected for sampling bias with Eq. (A5) and $\beta = 1.2$. The blue dots are the estimates of the squared singular values $\tilde{s}_\ell^2 - \beta\nu^2$ and the red box covers the area below the cutoff of $\beta\nu^2$.

		Average effective rank			
Reaction number	**Number of parameters**	**Def. 4**		**Def. 3**	
		No correction	**Correction**	**No correction**	**Correction**
R1	2	2	2	1	1
R2	4	3.99	3.88	1.3	1.3
R3	3	3	3	0.7	0.74
R4	4	4	4	1.15	1.2
R5	1	1	1	0.01	0.05
R6	3	3	3	0.84	0.88
R7	4	4	3.98	1.21	1.24
R8	1	1	1	0	0.01

Table A1: Average effective rank computed for each reaction and with different definitions of r over 100 noisy and biased datasets (40% noise, 86% sampling bias) of the model of Fig. 4.6(a). The criteria of Def. 4 was computed with $\theta = 0.99$. Method 2 corresponds to model reduction using r as defined in Eq. (4.22). Model reduction was applied both on Y and $\overset{\circ}{Y}$, the data matrix corrected for sampling bias, and the results are shown in the columns titled "No correction" and "Correction", respectively.

dependencies have been detected for any reaction of the network. However, the results of model reduction of Def. 3 on the biased dataset give lower average effective ranks than Def. 3 applied in Table 4.1 for all reactions but the first. Moreover, the average effective rank is reduced by more than 0.7 for reactions 2, 4 and 7. Thus, sampling bias in the data favours the detection of more collinearities in the data when model reduction of Def. 3 is used.

Secondly, the results of Table A1 show that the correction for sampling bias does not significantly affect the results of model reduction. Indeed, the biggest changes in the results for model reduction with and without correction for sampling bias are 0.11 and 0.05 for model reduction methods of Def. 4 with $\theta = 0.99$ and Def. 3, respectively. Finally, the correction for sampling bias does not change the results of identifiability analysis.

We then apply the model reduction method accounting for sampling bias in the data on the linlog model of central carbon metabolism shown Fig. 4.9 to verify that we do not find different results than the ones obtained using Def. 3, presented in Sec. 4.4.2. The results are reported in Table A2. Globally, the identifiability analysis, whether using correction for sampling bias or not, returns similar results. The only exception is reaction 1, for which 1 or 2 singular values were found negligible depending on the method in Tables 4.2 and A2, respectively.

The same method as in Sec. 4.4.2 has been applied to the dataset to detect identifiable parameters. The results are shown in Table A3.

Reaction	Enzyme	Average effective rank	Full dimension
1	PtsG	2.01	4
2	Pgi	1	2
3	PfkA,PfkB	2.82	4
4	FbaA,FbaB	2	2
5	TpiA	2	2
6	GapA;Pgk	2.97	4
7	GpmA,GpmB;Eno	1	2
8	PykA,PykF	2	4
9	AceE:AceF:LpdA	1.99	3
10	Zwf;Pgl	1.55	3
11	Gnd	2	3
12	Rpe	1.04	2
13	RpiA,RpiB	1.99	3
14	TktA	1.89	2
15	TalA,TalB	1	2
16	TktB	1.01	2
17	GltA,PrpC	2.95	4
18	AcnA,AcnB	1	2
19	IcdA	1	3
20	SucA:SucB:LpdA;SucC:SucD	1	3
21	SdhA:SdhB:SdhC:SdhD	1	3
22	FumA,FumB,FumC	1	2
23	Mdh	2.92	4
24	Ppc;PckA	3	5
25	MaeB,SfcA	2	5
26	AceA;AceB	1	3
27	μ	4.76	11
28	Edd;Eda	1	2
29	Pta;AckA,AckB	2.97	6
30	LdhA	1	2
31	AdhE	1	1

Table A2: Average effective rank computed for the reactions in the linlog model of *E. coli* central carbon metabolism, using the data of Ishii et al. [2007]. SVD has been applied on $\mathring{Y}_{C(i)}$ for each reaction and singular values were discarded based on Eq. (A5). Identifiable reactions are shown in green. Reaction 27, labeled μ, is a phenomenological reaction for biomass production.

Table A3: Parameter matrix $[B^x\ B^u]$ and results of identifiability and model reduction on the data of [Ishii et al., 2007] for the linlog model of *E. coli* central carbon metabolism (the columns of the matrix have been permuted for readability). SVD has been applied on the corrected matrix $\mathring{Y}$ and using Eq. (A5). Nonidentifiable parameters are shown in gray and identifiable parameters are shown in green. When PCA on all 100 imputed datasets did not give the same results, the percentages of cases for which the parameters or reactions were found identifiable are mentioned. Abbreviations are as in Fig. 4.9. Some of the cofactors are modeled as ratios of metabolite concentrations, *e.g.* ATP/ADP. Reaction 27, labeled μ, is a phenomenological reaction for biomass production. The last row indicates the percentage of missing data per metabolite and the right-most column displays the average effective rank.

	Metabolite Enzyme	Glc	PEP	G6P	Pyr	F6P	FBP	DHAP	3PG	Ac-coA	6PG	Ru5P	R5P	S7P	2KG	Suc	Fum	Mal	ATP	Cit	NADPH	NADH	FAD	Ace
										coA									ADP		NADP	NAD		
1	PtsG	🟩 59%	🟩 53%	▨ 0%	🟩 82%																			
2	Pgi			▨ 0%		▨ 0%																		
3	PfkA,PfkB		🟩 70%			▨ 13%	🟩 65%												▨ 16%					
4	FbaA,FbaB						🟩 100%	🟩 100%																
5	TpiA							🟩 100%	🟩 100%															
6	GapA;Pgk						🟩 91%		▨ 14%										▨ 1%			🟩 70%		
7	GpmA,GpmB;Eno		▨ 0%						▨ 0%															
8	PykA,PykF		▨ 8%		▨ 0%		▨ 15%												▨ 0%					
9	AceE:AceF:LpdA				▨ 1%					🟩 99%												🟩 99%		
10	Zwf;Pgl			▨ 46%							🟩 100%										▨ 41%			
11	Gnd										🟩 100%	🟩 99 %									▨ 0%			
12	Rpe											▨ 0%		▨ 0%										
13	RpiA,RpiB			▨ 1%								▨ 1%	🟩 84%											
14	TktA												🟩 89%	🟩 89%										
15	TalA,TalB					▨ 0%								▨ 0%										
16	TktB					▨ 0%						▨ 0%												
17	GltA,PrpC									🟩 96%					▨ 5%					🟩 97%		🟩 95%		
18	AcnA,AcnB														▨ 0%					🟩 100%				
19	IcdA									🟩 100%					▨ 0%						▨ 0%			
20	SucA:SucB:LpdA;SucC:SucD														▨ 0%	▨ 0%						🟩 94%		
21	SdhA:SdhB:SdhC:SdhD															▨ 0%	▨ 0%						▨ 46%	
22	FumA,FumB,FumC																▨ 0%	▨ 0%						
23	Mdh		🟩 87%															▨ 2%		🟩 87%		▨ 42%		
24	Ppc;PckA		▨ 27%				▨ 10%											▨ 0%	▨ 0%	🟩 32%				
25	MaeB,SfcA				▨ 0%					🟩 100%								▨ 0%			▨ 0%	▨ 42%		
26	AceA;AceB									🟩 100%						▨ 0%		▨ 0%						
27	μ		▨ 0%	▨ 0%	▨ 0%	▨ 0%			▨ 0%	🟩 81%			🟩 81%		▨ 0%				▨ 0%		▨ 0%	▨ 45%		
28	Edd;Eda				▨ 0%						🟩 100%													
29	Pta;AckA,AckB				▨ 0%					🟩 94%									▨ 0%		▨ 0%	🟩 63%		🟩 100%
30	LdhA				▨ 0%																	🟩 100%		
31	AdhE									🟩 100%														
	% Missing Data	3	17	0	48	7	34	59	10	3	72	3	38	3	59	3	14	14	0	62	79	79	17	17

Appendix C

Additional information on analysis of gene expression regulation of *E. coli*

C.1 Analysis of reporter gene data

In order to monitor gene expression *in vivo* and in real time, we used fluorescent reporter genes in combination with automated microplate readers. The reporter gene experiments result in up to 120 measurements of absorbance and fluorescence during a typical acquisition period (about 10 h). The absorbance or optical density is a measure of the biomass of a bacterial population. It can be used to estimate the total volume of bacterial cells in a well over a large range of growth rates [Volkmer and Heinemann, 2011]. The fluorescence emitted is proportional to the quantity of GFP in the cell population. The absorbance is expressed in dimensionless units, whereas fluorescence intensities are reported in relative fluorescence units (RFU).

The primary data are corrected for background levels of absorbance and fluorescence. For the absorbance background, we use wells in the microplate containing growth medium only, that is, without bacterial cells. Denoting by $a_u(t)$ the uncorrected absorbance at time t and by $a_b(t)$ the background absorbance, the corrected absorbance $a(t)$ is given by

$$a(t) = a_u(t) - a_b(t) \tag{A1}$$

The fluorescence background is usually determined by performing measurements on a strain carrying the promoterless vector pZE*gfp*, that is, a strain with a nonfunctional reporter system. Contrary to the absorbance, the fluorescence background is not constant, but varies with the population size due to the autofluorescence of cells. Since the growth curves of the reporter strain and the strain with the nonfunctional reporter system are not necessarily identical, we cannot straightforwardly subtract the background readings at each time-point.

Instead, we develop a calibration curve relating absorbance readings to background fluorescence levels.

Let $a_u(t)$ and $f_u(t)$ denote the uncorrected absorbance and fluorescence at time t, respectively, for bacteria carrying the functional reporter plasmid. Similarly, let $b_u(t)$ and $g_u(t)$ denote the uncorrected absorbance and fluorescence, respectively, for bacteria carrying the promoterless plasmid pZE*gfp*. We call β the empirical function relating $b_u(t)$ to $g_u(t)$, that is, $g_u = \beta(b_u(t))$. The function β is obtained in our case by non-parametric regression using smoothing splines (Matlab) [de Jong et al., 2010]. By means of this calibration curve, the corrected absorbance is defined as

$$f(t) = f_u(t) - \beta(a(t)) \tag{A2}$$

Fig. A1*A-D* shows an example of background correction, applied to fluorescence data acquired for the gene *fis* in a wild-type strain. The corrected data are included in Fig. 3 of the main text. The fluorescence background correction procedure described above was slightly modified from the one described in [de Jong et al., 2010, Boyer et al., 2010]. The modifications notably take into account that part of the fluorescence background is contributed by the growth medium, that is, the fluorescence background does not approach 0 for small absorbance values.

In the remainder of this section, we explain how the absorbance and fluorescence measurements can be related to biologically relevant quantities, notably promoter activities. Following [de Jong et al., 2010, Boyer et al., 2010], we develop a simple kinetic model describing the expression of the reporter gene. Let $x_g(t)$ [μM] denote the time-varying concentration of GFP in the cells in the population. The dynamics of $x_g(t)$ is defined by the differential equation

$$\frac{dx_g(t)}{dt} = p(t) - (\mu(t) + \gamma_g)\, x_g(t) \tag{A3}$$

where $p(t)$ [μM min^{-1}] represents the synthesis rate of the reporter protein, γ_g [min^{-1}] its degradation constant, and $\mu(t)$ [min^{-1}] the growth rate. In the absence of post-transcriptional regulation, $p(t)$ varies with the rate of transcription of the reporter gene, and is therefore often called promoter activity [Ronen et al., 2002]. In the case of transcriptional fusions, the promoter activity of the reporter is a good indicator of the promoter activity of the host gene. We recall that $\ln 2/\gamma_g$ equals the half-life of the reporter protein.

Given that the fluorescence is a measure of the quantity of GFP and the absorbance a measure of the total cell volume, we infer that

$$x_g(t) = \delta \, \frac{f(t)}{a(t)} \tag{A4}$$

for some positive constant δ [μM RFU^{-1}]. The growth rate is conveniently defined in terms of the absorbance, that is,

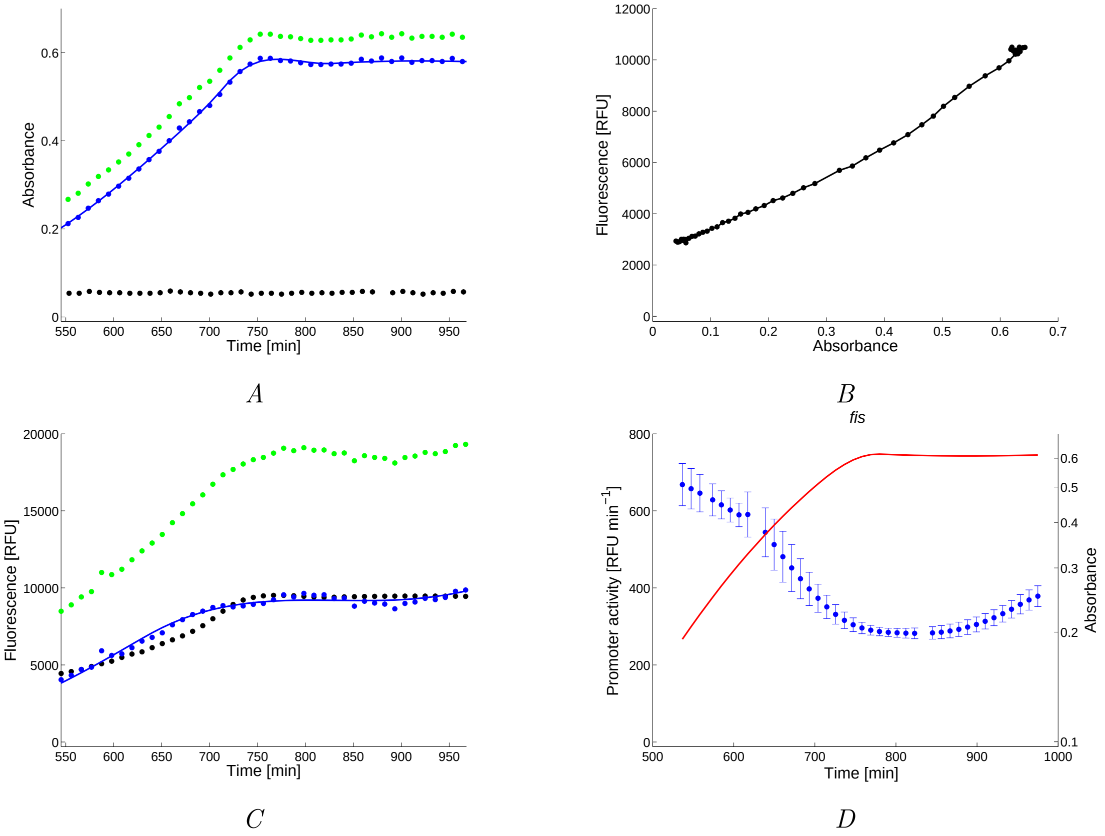

Figure A1: Example of the analysis of fluorescence reporter gene data. *A:* Primary (uncorrected) absorbance (●, green), background absorbance (●, black), and the corrected absorbance (●, blue) following Eq. (A1). The plot also shows the spline fits of the data (-,blue). *B:* Calibration curve for background correction obtained by means of the strain carrying the promoterless vector pZE*gfp*, plotting primary fluorescence data against primary absorbance data. The curve is obtained by interpolation of the data points. *C:* Primary fluorescence (●, green) data for the pZE*fis-gfp* strain. The plot also shows the background fluorescence (●, black), and the corrected fluorescence (●,blue) obtained after subtracting the two (Eq. (A2)). *D:* Promoter activity of *fis* and 95%-confidence intervals computed from the corrected absorbance and fluorescence data of 4 replicates by means of Eq. (A6). This plot is the same as Fig. 3*C* of the main text.

$$\mu(t) = \frac{da(t)}{dt}\frac{1}{a(t)} = \frac{d\ln(a(t))}{dt} \tag{A5}$$

This allows Eq. (A3) to be recast, after some basic calculus, into a expression defining the promoter activity in terms of the measured fluorescence and absorbance intensities

$$p(t) = \delta\left(\frac{df(t)}{dt}\frac{1}{a(t)} + \gamma_g\frac{f(t)}{a(t)}\right) \tag{A6}$$

Notice that for $\mu(t) \gg \gamma_y$, the second term in the right-hand side of Eq. (A6) can be neglected, and we obtain the expression for the promoter activity usually found in the literature (*e.g.*, [Ronen et al., 2002]).

In the absence of knowledge of the value of δ, we arbitrarily set this parameter to 1, and thus express the promoter activity and reporter protein concentration in RFU and RFU min^{-1}, respectively. This leads to a relative instead of absolute measure of gene expression, which is usual for this kind of experiments and sufficient for the purpose of Chap. 5. Recent developments in single-molecule measurements of gene expression will make absolute measurements of gene expression feasible in the future [Cai et al., 2006, Itzkovitz and van Oudenaarden, 2011].

In order to actually compute $p(t)$, the corrected absorbance and fluorescence data are fitted using regression splines [de Jong et al., 2010]. For the GFP reporter used in this study, $\gamma = 0.012 \pm 0.001$ min^{-1}, which corresponds to a half-life of about 1 h [de Jong et al., 2010]. We also take into account the maturation time of GFP (25 min for our reporter).

Confidence intervals for $p(t)$ are computed from technical replicas in the same experiment (see [de Jong et al., 2010] for an alternative approach, based on a residual resampling bootstrap). In order to correct for small inoculation differences, the replicates are synchronized with respect to the absorbance curves. In particular, based on the observation in [Isalan et al., 2008] that the absorbance derivative profile provides a reproductive signature of bacterial growth, we synchronize the promoter activities with respect to the time-points t^* at which $da(t^*)/dt = 0$. Fig. A1*D* shows the *fis* promoter activity, as well as the 95%-confidence intervals computed from 4 replicates. Fig. A2 shows the time-varying growth rates computed by means of Eq. (A5) from the absorbance data, for the four experimental conditions considered in Chap. 5.

Fig. A3 shows the primary fluorescence and absorbance data from which the promoter activities of *fis*, *crp* and *acs* as well as the activity of the pRM promoter of phage λ in the reference conditions have been derived (Fig. 3 in main text), following the method outlined in Sec. C.1. The plots in Fig. A3 show the data for a single replicate.

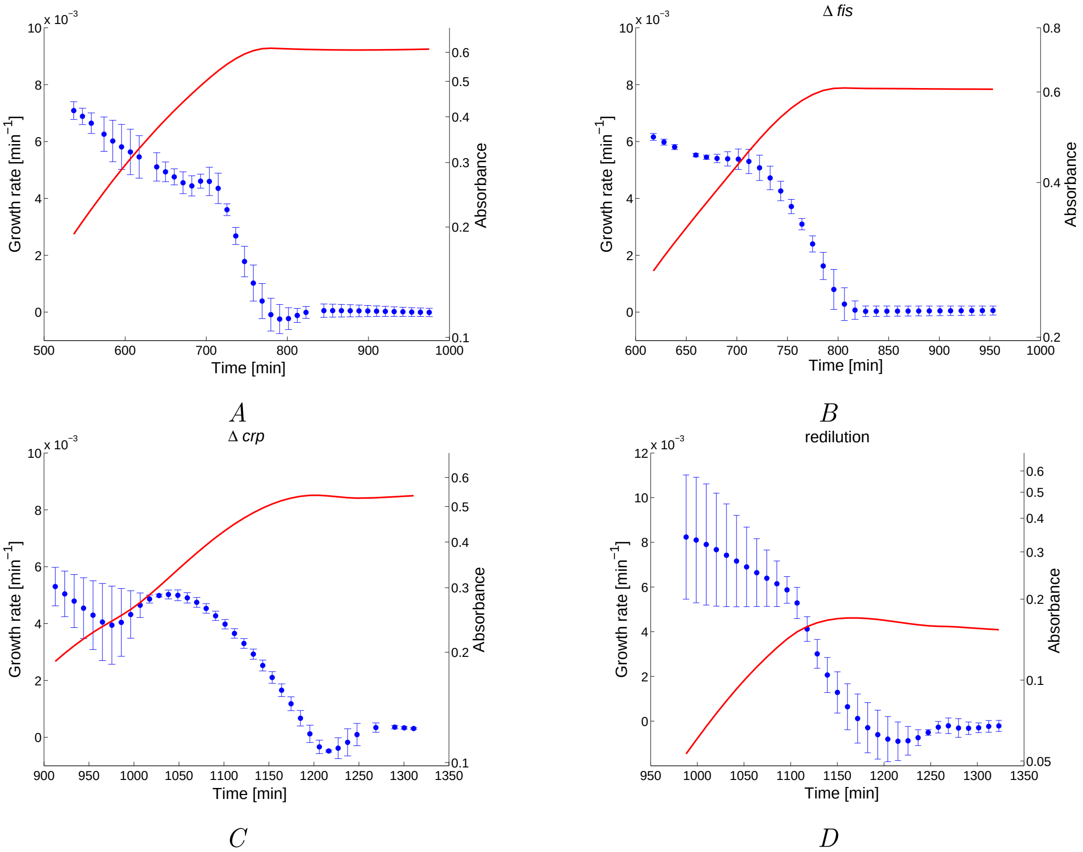

A

B

C

D

Figure A2: Growth rate computed from the corrected absorbance data by means of Eq. (A5). The growth-rate values are the mean of 4 replicates, synchronized with respect to their the absorbance curves as described in the text. The 95%-confidence intervals are computed from the standard error of the mean. *A:* Wild-type strain. *B:* Δ*fis* deletion strain. *C:* Δ*crp* deletion strain. *D:* Wild-type strain after redilution into low-glucose medium.

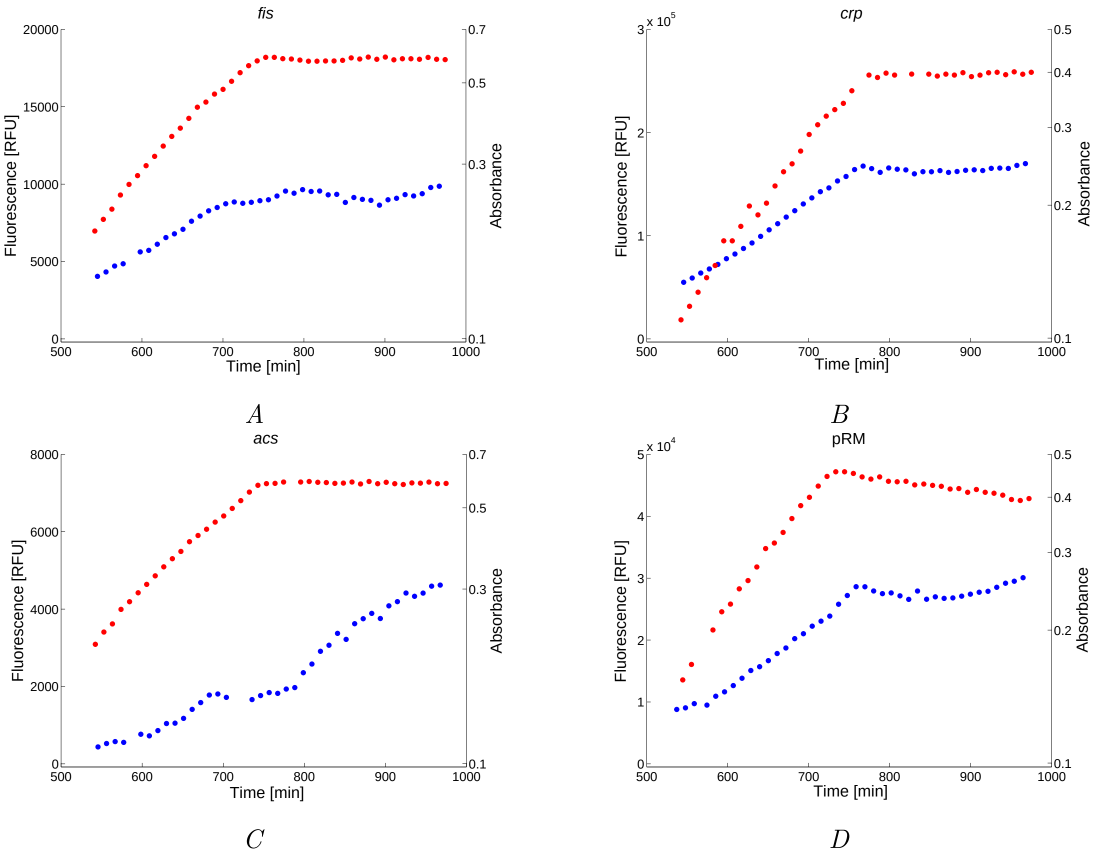

A

B

C

D

Figure A3: Primary data for computation of promoter activities. *A:* Primary (uncorrected) absorbance (+, red) and fluorescence (o, blue) data for the pZE*fis-gfp* strain. *B-D:* Idem for data from pZE*crp-gfp*, pUA66*acs-gfp*, and pZE1RM*gfp*. The primary data in this figure have been used to derive the promoter activities shown in Fig. 3 of the main text.

C.2 Analysis of cAMP measurements

The concentration of cAMP (adenosine 3',5'-cyclic monophosphate) is measured by means of a competitive ELISA. The principle of the assay consists in the quantification of a chemiluminescence signal in a competitive immunoassay using a specific anti-cAMP antibody. By means of a calibration curve, the measured intensities can be related to extracellular cAMP concentrations, that is, the concentration of cAMP exported from the cells into the growth medium. For our purpose, we are interested in the cAMP concentration inside the cells, however, which is much more difficult to measure due to artifacts arising from cell collection and contamination with extracellular cAMP [Pastan and Adhya, 1976]. We explain in this section how the intracellular cAMP concentration can be computed from the measured extracellular cAMP concentration.

The cAMP molecules in the medium are produced inside the cells and exported. Extracellular cAMP is not degraded, that is, it is a metabolic end-product [Epstein et al., 1975]. Therefore, the accumulation of extracellular cAMP is the net sum of cAMP molecules exported from the cells and cAMP molecules imported back from the medium into the cells. Fig. A4 schematically summarizes the relation between intracellular and extracellular cAMP. The concentration of extracellular cAMP is obtained by dividing the molar quantity of cAMP in the sample by the volume of the sample. The concentration of intracellular cAMP is defined as the molar quantity of intracellular cAMP divided by the total volume of the cells in the sample. Whereas the sample volume is constant over the experiment, the total cell volume obviously changes over time.

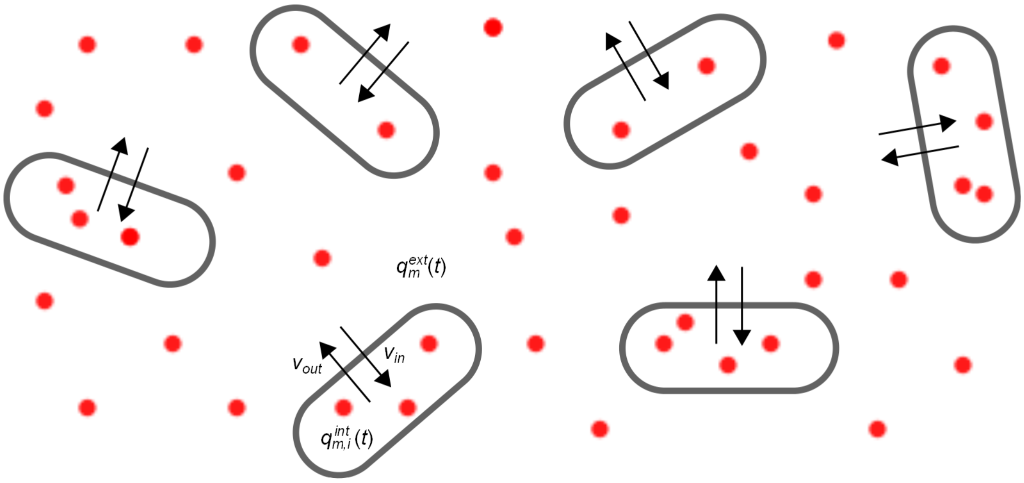

Figure A4: Relation between intracellular and extracellular cAMP in a bacterial culture. $n(t)$ is the number of cells at time t, $q_{m,i}^{int}(t)$ and $q_m^{ext}(t)$ are the quantities of cAMP inside cell i and in the growth medium, respectively, at time t. The rates v_{in} and v_{out} denote the transport into and from the cells.

In order to derive the concentration of cAMP inside the cells from the concentration of cAMP in the medium, we develop a simple kinetic model. We denote by $q_{m,i}^{int}(t)$ and $q_m^{ext}(t)$ the quantities of cAMP inside cell i and in the growth medium [mol], respectively, at time t [min]. At t there are $n(t) \geq 1$ cells in the sample, so $i \in \{1, \dots, n(t)\}$. This gives the following balance equation for the quantity of external cAMP

$$\frac{dq_m^{ext}(t)}{dt} = \sum_{i \in \{1,\dots,n(t)\}} v_{out}(q_{m,i}^{int}(t)) - n(t)\, v_{in}(q_m^{ext}(t)) \tag{A7}$$

The first term in the right-hand side of Eq. (A7) denotes the rate of export of cAMP from the cells into the growth medium, while the second term concerns the rate of import of cAMP from the medium into the cells.

The export and import rates follow simple first-order kinetics [Epstein et al., 1975], so that v_{out} is a linear function of the internal cAMP concentrations with rate constant k_{out} [min^{-1}] and v_{in} a linear function of the external cAMP concentration with rate constant k_{in} [min^{-1}]. This results in

$$v_{out}(q_{m,i}^{int}(t)) = k_{out}\, q_{m,i}^{int}(t) \quad , \quad v_{in}(q_m^{ext}(t)) = n(t)\, k_{in}\, q_m^{ext}(t) \tag{A8}$$

Defining

$$q_m^{int}(t) = \sum_{i \in \{1,\dots,n(t)\}} q_{m,i}^{int}(t) \tag{A9}$$

we rewrite Eq. (A7) as

$$\frac{dq_m^{ext}(t)}{dt} = k_{out}\, q_m^{int}(t) - n(t)\, k_{in}\, q_m^{ext}(t) \tag{A10}$$

In order to obtain concentration variables, we now introduce volume parameters V_{tot} and $V_{cell}(t)$, representing the sample volume and the volume of individual cells, respectively [L]. Notice that the cell volume is a function of time, since the growth rate changes over time and the cell volume varies with the growth rate [Bremer and Dennis, 1996, Volkmer and Heinemann, 2011]. In order to obtain concentrations, the quantity of internal cAMP needs to be weighted by the total cellular volume, given by $n(t)\, V_{cell}(t)$, and the quantity of external cAMP by $V_{tot} - n(t)\, V_{cell}(t)$. Given that the cells occupy only a tiny fraction of the sample volume, the latter term is approximated by V_{tot}.

We multiply the left-hand and right-hand side of the equation with volume terms

$$\frac{dq_m^{ext}(t)}{dt}\, \frac{1}{V_{tot}} = k_{out}\, q_m^{int}(t)\, \frac{1}{V_{tot}}\, \frac{n(t)\, V_{cell}(t)}{n(t)\, V_{cell}(t)} - n(t)\, k_{in}\, \frac{1}{V_{tot}}\, q_m^{ext}(t)$$

which results in

$$\frac{du_m^{ext}(t)}{dt} = n(t)\, V_{cell}(t)\, \frac{k_{out}}{V_{tot}}\, u_m^{int}(t) - n(t)\, k_{in}\, u_m^{ext}(t) \tag{A11}$$

$u_m^{int}(t)$ and $u_m^{ext}(t)$ are the concentrations of intracellular and extracellular cAMP [M], respectively. From Eq. (A11) we obtain the following expression for the concentration of intracellular cAMP

$$u_m^{int}(t) = \frac{1}{n(t)\, V_{cell}(t)} \frac{V_{tot}}{k_{out}} \frac{du_m^{ext}(t)}{dt} + \frac{k_{in}}{k_{out}} \frac{V_{tot}}{V_{cell}(t)}\, u_m^{ext}(t) \tag{A12}$$

The interest of this equation lies in that it allows $u_m^{int}(t)$ to be computed from the measured concentration of extracellular cAMP. For this we need to know the constant k_{out}, the constant V_{tot}, the constant k_{in} and the total cellular volume $n(t)\, V_{cell}(t)$. k_{out} has been measured as 2.1 min^{-1} [Epstein et al., 1975], while the sample volume V_{tot} equals 100 μL. Interestingly, Volkmer and Heinemann [2011] have shown that the ratio $n(t)\, V_{cell}(t)/a(t)$ is constant, where $a(t)$ is the measured absorbance of the culture volume in the microplate at time t. The value of this ratio, which we call α, can be computed for our conditions by means of a calibration curve previously published [de Jong et al., 2010], given that *E. coli* cells growing on glucose have a cell volume of about $3 \cdot 10^{-9}$ μL. We find $\alpha = 0.3$ μL and replace $n(t)\, V_{cell}(t)$ by $\alpha\, a(t)$. When equating the cell volume in the import term to $3 \cdot 10^{-9}$ μL, we obtain the expression used in Chap. 5

$$u_m^{int}(t) = \frac{1}{1.5 \cdot 10^{-3}\, a(t)\, k_{out}} \frac{du_m^{ext}(t)}{dt} + \frac{k_{in}}{3 \cdot 10^{-11}\, k_{out}}\, u_m^{ext}(t) \tag{A13}$$

The concentrations of extracellular cAMP and the absorbance are measured at different time-points. In particular, we took samples from a growing bacterial culture at 12 time-points (3 replicates). In order to obtain $a(t)$, we fit a regression spline to the data (as described above). As for obtaining $u_m^{ext}(t)$, we fitted a cubic spline to the data and took the derivative of the u_m^{ext}-spline to obtain $du_m^{ext}(t)/dt$. The value of k_{in} can then be estimated from Eq. (A13) by using the measured steady-state concentration for intracellular cAMP during exponential growth on glucose, namely 0.4 μM [Epstein et al., 1975, Pastan and Adhya, 1976], as well as the absorbance and the (time-derivative of the) extracellular cAMP concentration measured in our experiments. We thus find a value $k_{in} = 12 \cdot 10^{-10}$ min^{-1}.

With all parameter values known, Eq. (A13) allows the reconstruction of the temporal profile of the concentration of intracellular cAMP from $a(t)$, $u_m^{ext}(t)$, and $du_m^{ext}(t)/dt$. The values for $u_m^{int}(t)$ reported in Chap. 5 are the mean of three replicates. 95%-confidence intervals are computed from the standard error of the mean after synchronization of the absorbance curves, as described in Sec. C.1. One of the advantages of the use of splines is that the intracellular cAMP concentration can easily be calculated at all time-points by spline interpolation.

Fig. A5 shows plots of the measured extracellular and derived intracellular cAMP concentrations over the duration of the experiment. The shape of the intracellular cAMP concentration profile agrees very well with other, direct measurements [Buettner et al., 1973, Kao et al., 2004, Makman and Sutherland, 1965]. cAMP rapidly accumulates at the end of exponential growth, when glucose is exhausted, and returns to a lower level after the growth transition.

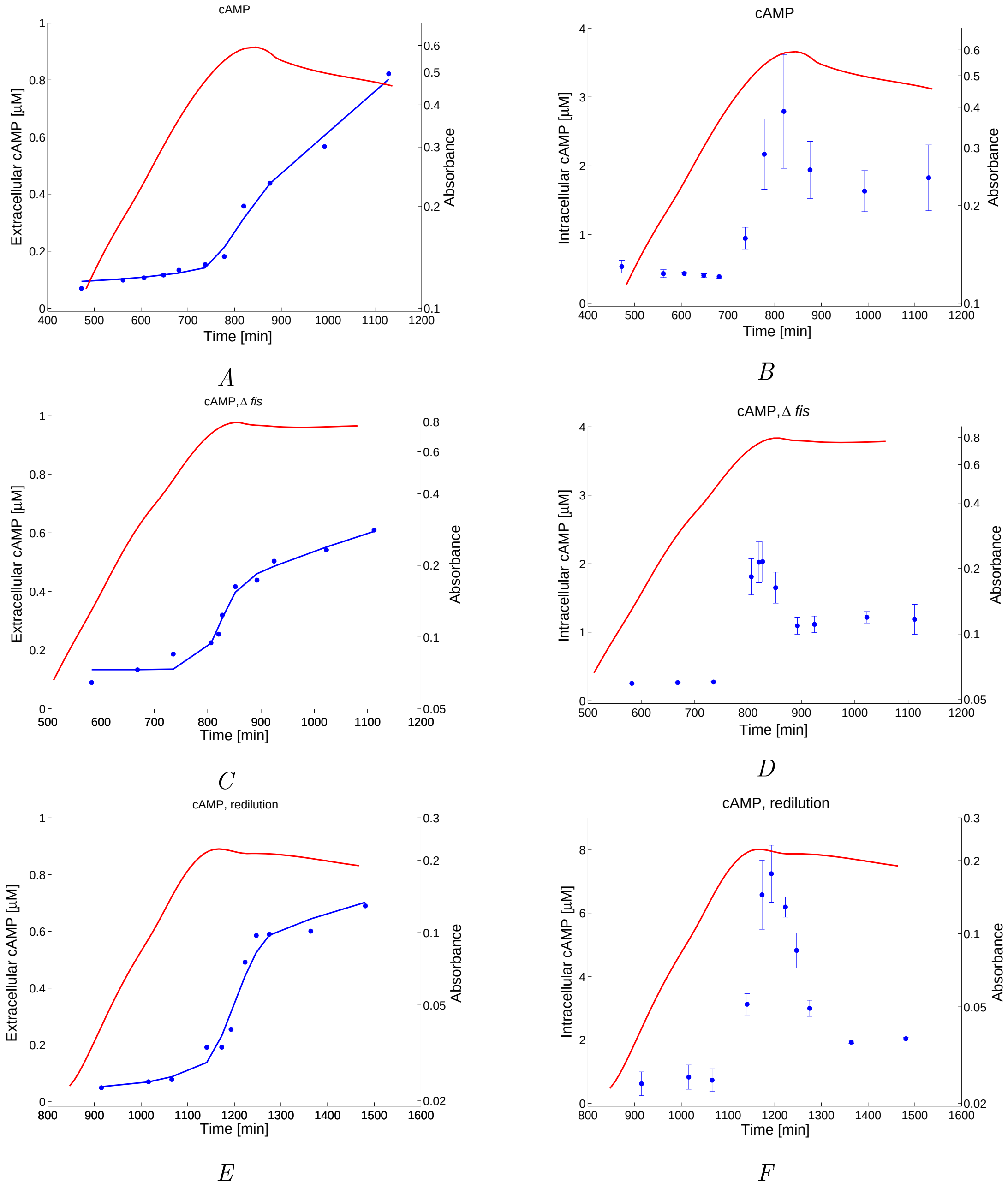

A *B* *C* *D* *E* *F*

Figure A5: Measurements of cAMP concentration in samples taken from a bacterial culture growing in a microplate. *A* Absorbance and measured concentration of extracellular cAMP, with spline fit to cAMP data. *B* Absorbance and derived concentration of intracellular cAMP. The cAMP concentrations are the mean of 3 replicates, synchronized with respect to their the absorbance curves as described in Sec. C.1. The 95%-confidence intervals are computed from the standard error of the mean. This plot corresponds to Fig. 2*B* of the main text. *C-D:* Idem in Δ*fis* strain. *E-F:* Idem in wild-type strain after glucose down-shift.

C.3 Measurement of time-varying plasmid copy number

We used quantitative PCR (qPCR) to determine the time-varying number of plasmids per chromosomal equivalent of DNA (plasmid copy number), following a previously validated protocol [Lee et al., 2004]. We took 5 μL samples at 11 time-points from cultures of strains carrying a reporter plasmid, growing in a microplate under the conditions described in the Materials and methods section of the main text. The samples were diluted 100x into MESA Green qPCR Master Mix (Eurogentec), supplemented with primers for the plasmid β-lactamase gene (*bla*) and for the chromosomal d-1-deoxyxylulose 5-phosphate synthase gene (*dxs*). Quantitative PCR was performed in a StepOnePlus Real-Time PCR System (Applied Biosystems) according to the instructions of the manufacturer. Briefly, 20 μL reaction mixtures were incubated for 10 min at 95°C and 40 PCR cycles (15 s at 95°C, 10 s at 62°C and 10 s at 72°C). PCRs were run in quadruplicate. Raw data were transformed into threshold cycle (C_T) values. PCR amplification efficiencies for *bla* and *dxs* were determined by constructing standard curves from serial dilutions [Lee et al., 2004].

The results were analyzed by means of the following model for computing the relative plasmid copy number $r(t)$ at the different sample time-points t [Reiter et al., 2011]:

$$r(t) = \frac{E_{bla}^{\Delta C_T^{bla}(t)}}{E_{dxs}^{\Delta C_T^{dxs}(t)}} \tag{A14}$$

where C_T^{bla} and C_T^{dxs} are the C_T values for *bla* and *dxs*, respectively, $\Delta C_T^{bla}(t) = C_T^{bla}(t) - C_T^{bla}(t_0)$, $\Delta C_T^{dxs}(t) = C_T^{dxs}(t) - C_T^{dxs}(t_0)$, and t_0 is the reference time-point, corresponding to the time of the first measurement during steady-state exponential growth on glucose. The efficiencies were measured to be nearly 100% for *dxs* ($E_{dxs} = 2$) and 91% for *bla* ($E_{dxs} = 1.91$).

The results of the analysis of data obtained for the pZE*fis-gfp* plasmid are shown in Fig. A6. The plasmid has a colE1 origin of replication (Table 5.2), like most vectors used in this study. The plasmid copy number increases by a factor of 2 during the growth transition following glucose exhaustion, which means that the variation of $r(t)$ introduces a quantitative bias (although this bias does not invalidate the qualitative shape of the reported promoter activities, see Results section of main text). Similar results were found for the pZE*acs-gfp* plasmid, which has an SC101 origin of replication (results not shown).

C.4 Additional gene expression profiles and analysis results during glucose/acetate diauxie for different conditions

Fig. 5.3 shows the gene expression response of the network, for the *fis*, *crp*, *acs*, and pRM promoters in the reference conditions (depletion of glucose by wild-type bacteria in batch culture). Figs. 5.5-5.7 show them in the case of Δ*fis* and Δ*crp* mutants, as well as dilution

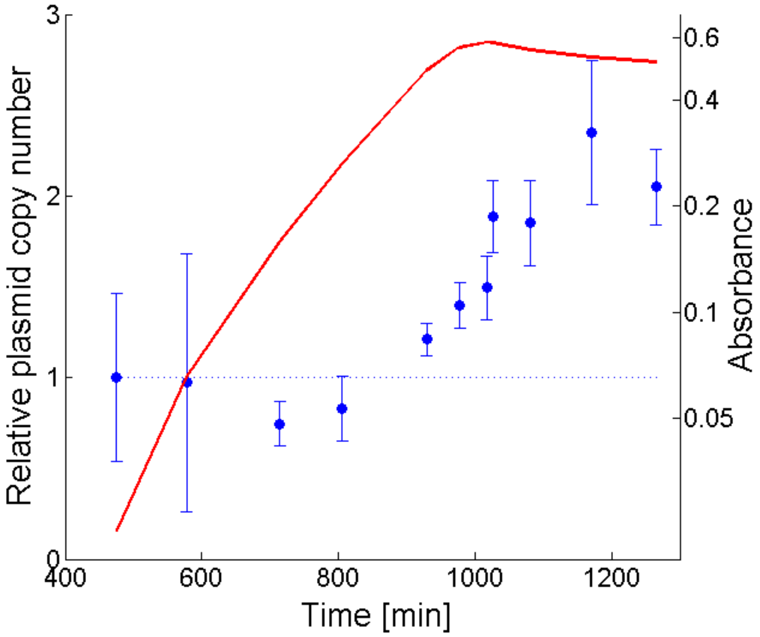

Figure A6: Variation in number of plasmids per chromosomal equivalent of DNA (plasmid copy number) measured by means of qPCR. The quantities have been normalized with respect to the observed plasmid copy number in steady-state exponential growth on glucose, corresponding to the first time-point. The 95%-confidence intervals were computed from the standard error of the mean of 4 replicates, after synchronization of the absorbance curves (Sec. C.1).

into a low-glucose medium. The figures in this section show additional data referred to in Chap. 5.

Fig. A7 shows the promoter activity of the gene *rpoS*, coding for the master stress regulator RpoS (σ^S), in the four conditions considered in Chap. 5 (wild-type, Δ*fis*, Δ*crp*, and redilution into low-glucose medium).

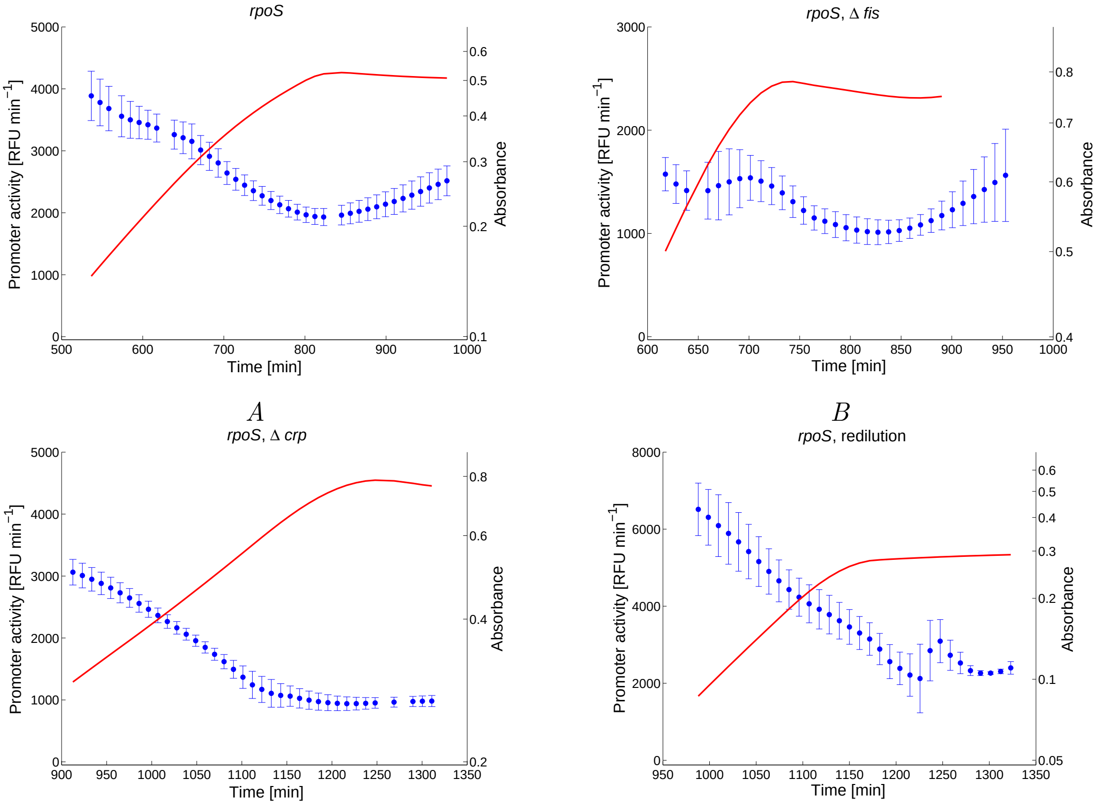

A

B

C

D

Figure A7: Experimental monitoring of the expression of *rpoS*. *A:* Time-varying promoter activity of *rpoS* (●, blue), derived from GFP data with 95%-confidence interval obtained from experimental replicas, and absorbance (solid line, red). *B:* Idem for Δfis mutant. *C:* Idem for Δcrp mutant. *D:* Idem for wild-type strain rediluted into low-glucose medium.

The plots in Fig. 5.4 show the relative contributions of the global physiological state and local transcription regulators to the control of the promoter activities of the genes considered in this study. Fig. A8 shows additional data referred to in Chap. 5. Table A1 summarizes the coefficients of determination obtained by the different models for all genes of the network under different experimental conditions.

Fig. A9 shows results of model calibration on wild-type data and results of model simulation for *rpoS* on data of Δ*fis* and Δ*crp* strains and for wild-type strain after downshift into a low-glucose medium.

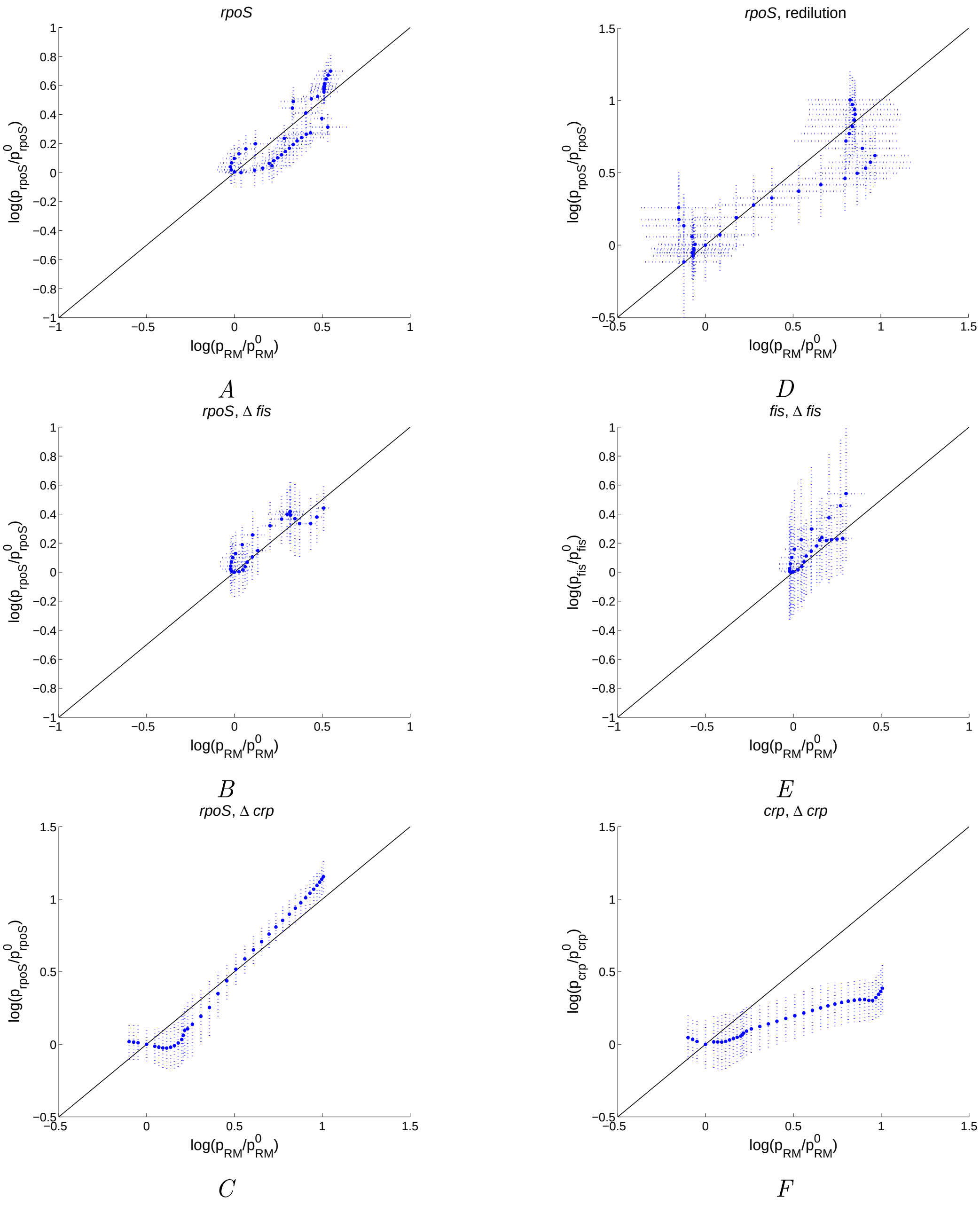

Figure A8: Predicted and observed control of *rpoS*, *fis*, and *crp* expression by the GEM and Crp·cAMP, in various experimental conditions and genetic backgrounds. *A:* Predicted (-, black) and measured (•, blue) relative activity of the *rpoS* promoter ($\log(p_{rpoS}(t)/p^0_{rpoS})$) as a function of the relative activity of the pRM promoter ($\log(p_{RM}(t)/p^0_{RM})$). The 95%-confidence intervals in the plots have been computed from experimental replicas, as described in Sec. C.1. *B-C:* Idem for *rpoS* in Δ*fis* and Δcrp strains. *D:* Idem for *rpoS* in a wild-type strain after a down-shift into a low-glucose medium. *E:* Idem for *fis* in a Δ*fis* strain. *F:* Idem for *crp* in a Δcrp strain.

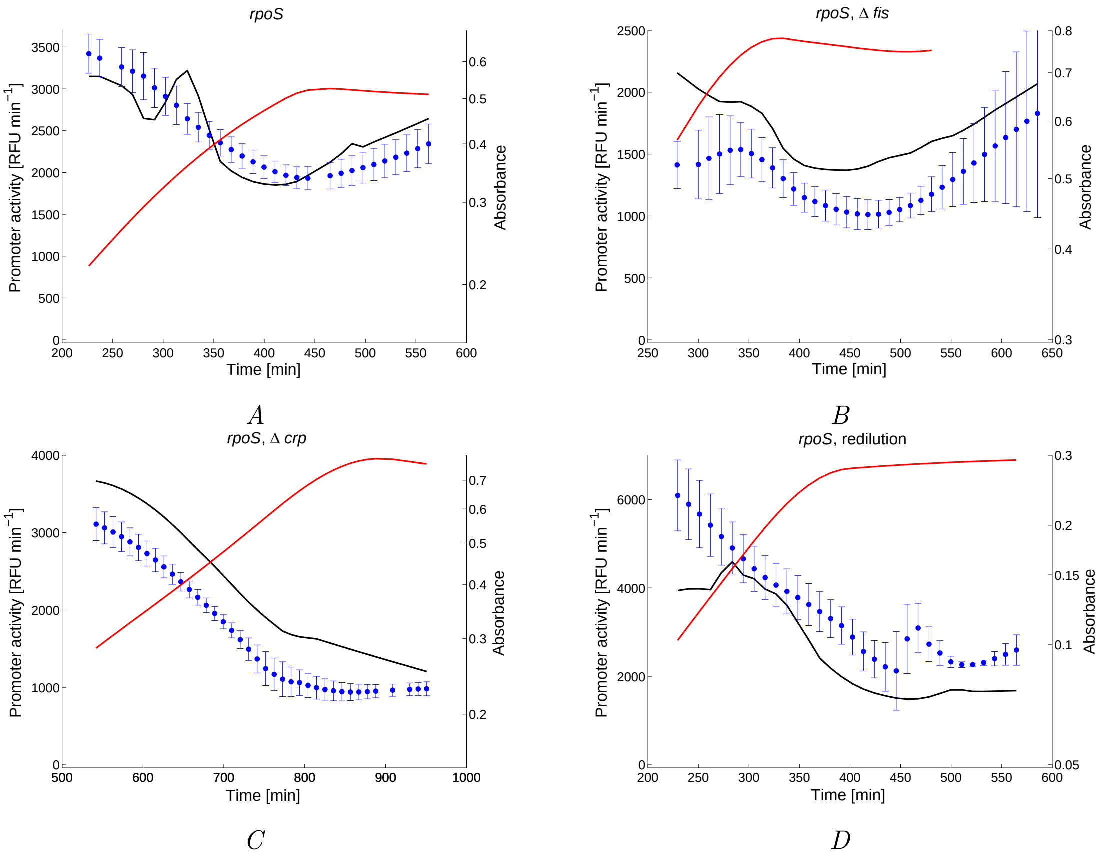

Figure A9: Promoter activity of *rpoS* simulated from the ODE model presented in Chap. 5. *A:* Simulation of time-varying promoter activity of *rpoS* (-,black), experimental data (●, blue) derived from GFP data with 95%-confidence interval obtained from experimental replicas, and absorbance (-,red). *B:* Idem for Δfis mutant. *C:* Idem for Δcrp mutant. *D:* Idem for wild-type strain rediluted into low-glucose medium.

Experimental condition	Model	R^2
WT	p_{fis} vs p_{RM}	0.71
	p_{crp} vs p_{RM}	0.83
	p_{acs} vs p_{RM}	0.54
	p_{rpoS} vs p_{RM}	0.73
	$p_{fis} - p_{RM}$ vs c	0.31
	$p_{crp} - p_{RM}$ vs c	0.6
	$p_{acs} - p_{RM}$ vs c	0.72
Δ*fis*	p_{fis} vs p_{RM}	0.70
	p_{crp} vs p_{RM}	0.78
	p_{acs} vs p_{RM}	0.34
	p_{rpoS} vs p_{RM}	0.83
	$p_{fis} - p_{RM}$ vs c	0.83
	$p_{crp} - p_{RM}$ vs c	0.33
	$p_{acs} - p_{RM}$ vs c	0.97
	$p_{rpoS} - p_{RM}$ vs c	0.04
Δ*crp*	p_{fis} vs p_{RM}	0.94
	p_{crp} vs p_{RM}	0.97
	p_{rpoS} vs p_{RM}	0.97
WT+Redilution	p_{fis} vs p_{RM}	0.14
	p_{crp} vs p_{RM}	0.91
	p_{acs} vs p_{RM}	0.20
	p_{rpoS} vs p_{RM}	0.81
	$p_{fis} - p_{RM}$ vs c	0.01
	$p_{crp} - p_{RM}$ vs c	0.03
	$p_{acs} - p_{RM}$ vs c	0.56
	$p_{rpoS} - p_{RM}$ vs c	0.17

Table A1: Summary of the coefficient of determinations found for the model on different experimental conditions. "p_{fis} vs p_{RM}" corresponds to the coefficient of correlation between $\log(p_{fis}(t)/p^0_{fis})$ and $\log(p_{RM}(t)/p^0_{RM})$ while "$p_{fis} - p_{RM}$ vs c" corresponds to the coefficient of correlation between $\log(p_{fis}(t)/p^0_{fis}) - \log(p_{RM}(t)/p^0_{RM})$ and $\log(c(t)/c^0)$. Idem for *crp*, *acs* and *rpoS*.

C.5 Additional information on parameter estimation of the ODE model of the *acs* network

In Sec. 5.3, we present an ODE model of the dynamics of the *acs* regulatory network presented in Fig. 5.1 and extended to also consider *rpoS* regulation by the complex Crp·cAMP. The model, presented in Eq. (5.8) and Eq. (5.12), contains 21 parameters that need to be estimated in order to obtain quantitative simulations of the behaviours of the promoter activities of these genes during glucose/acetate diauxie. Below we detail the parameter estimation procedure we followed.

C.5.1 Making the model consistent with available experimental data

In order to estimate the model parameters, we compared simulations of promoter activities with promoter activities measured for *fis*, *crp*, *acs* and *rpoS* in the conditions described in the Methods and Materials section in Chap 5. These experimental data, which are shown in Fig. 5.3*A*-*C* and Fig. A7*A*, are measured in fluorescence units per minute (RFU·min^{-1}). However, the model of Eq. (5.12) returns promoter activities in units of mRNA concentration per minute (mM·min^{-1}). In order to confront model simulations with available data, we rescale the model in order to obtain variables and outputs expressed in the same unit as the data.

Let us define $x_{Fis'}$ and $x_{Crp'}$ the rescaled concentrations of Fis and Crp expressed in fluorescence units (RFU) as well as $p_{fis'}$, $p_{crp'}$, $p_{acs'}$ and $p_{rpoS'}$ the rescaled promoter activities of *fis*, *crp*, *acs* and *rpoS* expressed in RFU·min^{-1}, respectively. We have

$$x_{Fis'} = \frac{x_{Fis}}{\alpha_{fis}} \quad , \quad x_{Crp'} = \frac{x_{Crp}}{\alpha_{fis}} \tag{A15}$$
$$p_{fis'} = \frac{p_{fis}}{\alpha_{fis}} \ , \ p_{crp'} = \frac{p_{crp}}{\alpha_{fis}} \ , \ p_{acs'} = \frac{p_{acs}}{\alpha_{acs}} \ , \ p_{rpoS'} = \frac{p_{rpoS}}{\alpha_{rpoS}}$$

with α_{fis}, α_{crp}, α_{acs} and α_{rpoS} the scaling factors for *fis*, *crp*, *acs* and *rpoS*, respectively. We can reformulate the model of Eq. (5.12) with $x_{Fis'}$ and $x_{Crp'}$ as variables and $p_{acs'}$ and $p_{rpoS'}$ as outputs. This gives

$$\begin{cases} \dot{x}_{Fis'}(t) = p_{fis'}(x_{Fis'}(t), x_{Crp\cdot cAMP'}(t)) - (\mu(t) + \gamma_{Fis}) \times x_{Fis'}(t) \\ \dot{x}_{Crp'}(t) = p_{crp'}(x_{Fis'}(t), x_{Crp\cdot cAMP'}(t)) - (\mu(t) + \gamma_{Crp}) \times x_{Crp'}(t) \\ x_{Crp\cdot cAMP'}(t) = \frac{x_{Crp'}(t)}{1+\frac{K_{cc}}{c(t)}} \\ p_{acs'}(t) = p_{acs'}(x_{Fis'}(t), x_{Crp\cdot cAMP'}(t)) \\ p_{rpoS'}(t) = p_{rpoS'}(x_{Crp\cdot cAMP'}(t)) \end{cases} \tag{A16}$$

with $x_{Crp\cdot cAMP'} = x_{Crp\cdot cAMP}/\alpha_{crp}$. This reformulation requires the definition of the following rescaled parameters:

$$\begin{aligned}
\kappa^b_{fis'} = \frac{\kappa^b_{fis}}{\alpha_{fis}}\ ,\ \kappa^b_{crp'} = \frac{\kappa^b_{crp}}{\alpha_{crp}}\ ,\ \kappa^b_{acs'} = \frac{\kappa^b_{acs}}{\alpha_{acs}}\ ,\ \kappa^b_{rpoS'} = \frac{\kappa^b_{rpoS}}{\alpha_{rpoS}} \\
\kappa^r_{fis'} = \frac{\kappa^r_{fis}}{\alpha_{fis}}\ ,\ \kappa^r_{crp'} = \frac{\kappa^r_{crp}}{\alpha_{crp}}\ ,\ \kappa^r_{acs'} = \frac{\kappa^r_{acs}}{\alpha_{acs}}\ ,\ \kappa^r_{rpoS'} = \frac{\kappa^r_{rpoS}}{\alpha_{rpoS}} \\
\theta_{fis'_i} = \frac{\theta_{fis_i}}{\alpha_{fis}}\ \forall i = 1, \cdots, 3\ , \theta_{cc'_j} = \frac{\theta_{cc'_j}}{\alpha_{crp}}\ \forall j = 1, \cdots, 4
\end{aligned} \tag{A17}$$

The kinetic expressions for promoter activities of the 4 genes become

$$\begin{cases}
p_{fis'}(x_{Fis'}(t), x_{Crp\cdot cAMP'}(t)) = p_{RM}(t) \cdot \left(\kappa^b_{fis'} + \kappa^r_{fis'} \cdot \frac{1}{\left(\frac{x_{Fis'}(t)}{\theta_{fis'_1}}\right)^{n_1} + \left(\frac{x^r_{Crp\cdot cAMP}(t)}{\theta_{cc'_1}}\right)^{n_2} + 1} \right) \\
p_{crp'}(x_{Fis'}(t), x_{Crp\cdot cAMP'}(t)) = p_{RM}(t) \cdot \left(\kappa^b_{crp'} + \kappa^r_{crp'} \cdot \frac{x_{Crp\cdot cAMP'}(t)^{n_4}}{x_{Crp\cdot cAMP'}(t)^{n_4} + \theta^{n_4}_{cc'_2} \cdot \left(1 + \left(\frac{x_{Fis'}(t)}{\theta_{fis'_2}}\right)^{n_3}\right)} \right) \\
p_{acs}(x_{Fis'}(t), x_{Crp\cdot cAMP'}(t)) = p_{RM}(t) \cdot \left(\kappa^b_{acs'} + \kappa^r_{acs'} \cdot \frac{x_{Crp\cdot cAMP'}(t)^{n_6}}{x_{Crp\cdot cAMP'}(t)^{n_6} + \theta^{n_6}_{cc'_3} \cdot \left(1 + \left(\frac{x_{Fis'}(t)}{\theta_{fis'_3}}\right)^{n_5}\right)} \right) \\
p_{rpoS}(x_{Crp\cdot cAMP'}(t)) = p_{RM}(t) \cdot \left(\kappa^b_{rpoS'} + \kappa^r_{rpoS'} \cdot \frac{x_{Crp\cdot cAMP'}(t)^{n_7}}{x_{Crp\cdot cAMP'}(t)^{n_7} + \theta^{n_7}_{cc'_4}} \right)
\end{cases} \tag{A18}$$

and the parameters of the rescaled model are listed in Table A2.

In order to obtain simulations of the promoter activities of the genes of the *acs* network and *rpoS*, we need to specify the inputs of the model, *i.e.,* the time-course data of intracellular cAMP concentration $c(t)$, bacterial growth rate $\mu(t)$ and pRM promoter activity $p_{RM}(t)$ during glucose/acetate diauxie. Contrary to the promoter activity data, we were able to compute, from measurements of extracellular cAMP, the intracellular cAMP concentration in units of micromolar (see Appendix C.2). As K_{cc}, the equilibrium constant for Crp·cAMP formation is also in the unit of micromolar (mM), no rescaling is required. As for the growth rate input, we computed it, following the procedure described in Appendix C.1, from the corrected absorbance data measured in the experiment recording pRM promoter activity in the conditions described in Sec. 5.1.1. Finally, the promoter activity of pRM has been measured in the units of RFU·min^{-1}, which is in agreement with Eqs. (A16)-(A18). The time-course data of promoter activities of *fis*, *crp*, *acs* and *rpoS* have been synchronized to the pRM promoter activity data with respect to the maximum of absorbance (see [Isalan et al., 2008] and Appendix C.1).

Eventually, the rescaled model is in agreement with inputs and promoter activity data. Thus, we can confront it with outputs of the system so as to perform parameter estimation.

Parameters	Description	Units
K_{cc}	equilibrium constant for Crp·cAMP formation reaction	mM
	fis expression	
$\kappa^b_{fis'}$	basal protein synthesis rate	RFU·min^{-1}
$\kappa^r_{fis'}$	maximal protein synthesis rate	RFU·min^{-1}
$\theta_{fis'_1}$, $\theta_{cc'_1}$	affinity constants	RFU
n_1, n_2	Hill numbers	adimensional
γ_{Fis}	protein degradation constant	min^{-1}
	crp expression	
$\kappa^b_{crp'}$	basal protein synthesis rate	RFU·min^{-1}
$\kappa^r_{crp'}$	maximal protein synthesis rate	RFU·min^{-1}
$\theta_{fis'_2}$, $\theta_{cc'_2}$	affinity constants	RFU
n_3, n_4	Hill numbers	adimensional
γ_{Crp}	protein degradation constant	min^{-1}
	acs expression	
$\kappa^b_{acs'}$	basal protein synthesis rate	RFU·min^{-1}
$\kappa^r_{acs'}$	maximal protein synthesis rate	RFU·min^{-1}
$\theta_{fis'_3}$, $\theta_{cc'_3}$	affinity constant	RFU
n_5, n_6	Hill number	adimensional
	rpoS expression	
$\kappa^b_{rpoS'}$	basal protein synthesis rate	RFU·min^{-1}
$\kappa^r_{rpoS'}$	maximal protein synthesis rate	RFU·min^{-1}
$\theta_{cc'_4}$	affinity constant	RFU
n_7	Hill number	adimensional

Table A2: List of parameters of the rescaled model of Eqs. A16-A18. Units of the parameters are specified.

C.5.2 Divide estimation problem into subproblems

To perform parameter estimation, we minimize the difference between the promoter activities of *fis*, *crp*, *acs* and *rpoS* simulated by the model and measured experimentally. We define ρ the vector of all 21 parameters, $t_1, \cdots, t_T$ the measurement time-points, with $T \in \mathbb{N}$ and $\check{p}_{fis}$, $\check{p}_{crp}$, $\check{p}_{acs}$ and $\check{p}_{rpoS}$ the simulated promoter activities of *fis*, *crp*, *acs* and *rpoS*, respectively. Thus, the objective function can be defined as

$$\begin{aligned} F(\rho) = & \sum_{i=1}^{T} \frac{(\check{p}_{fis}(t_i,\rho) - p_{fis}(i))^2}{p_{fis}(i)^2} + \sum_{i=1}^{T} \frac{(\check{p}_{crp}(t_i,\rho) - p_{crp}(i))^2}{p_{crp}(i)^2} \\ & + \sum_{i=1}^{T} \frac{(\check{p}_{acs}(t_i,\rho) - p_{acs}(i))^2}{p_{acs}(i)^2} + \sum_{i=1}^{T} \frac{(\check{p}_{rpoS}(t_i,\rho) - p_{rpoS}(i))^2}{p_{rpoS}(i)^2} \end{aligned} \tag{A19}$$

The estimation problem is nonlinear in the parameters and the computation of $F(\rho)$

requires the resolution of the the ODE model presented in Eq. (A16). Thus, at each iteration of the non-linear optimization algorithm, the system needs to be solve, which considerably increases the computational time and worsens the convergence efficiency. Thus, it would be useful to find a decomposition of the estimation problem so as to simplify the optimization process.

One way to decompose the estimation problem, as mentioned in Sec. 2.4, is to obtain measurements for the model variables, here the rescaled concentrations of Fis and Crp. We have seen in Appendix C.1 how to compute promoter activities from fluorescence data obtained from reporter plasmids. In the same section is described how to compute the GFP concentration in the cells $x_g(t)$ from fluorescence and absorbance data. We define $x_{g,fis}$ and $x_{g,crp}$ the GFP concentrations computed from experiments in the wild-type strain with reporter genes having *fis* and *crp* promoters, respectively. $x_{g,fis}$ and $x_{g,crp}$ are expressed in RFU and can be used as proxy measurements of $x_{Fis'}$ and $x_{Crp'}$.

This way, we can uncouple the ODE model of Eq. (A16) and decompose it into 4 algebraic models describing the promoter activities of each gene of the model (Eq. (A18)). Each model now takes as inputs the concentration of intracellular cAMP $c(t)$, the pRM promoter activity p_{RM}, the rescaled concentration of Fis $x_{Fis'}$ and the rescaled concentration of Crp $x_{Crp'}$. We notice that the degradation rates of Fis and Crp are no longer model parameters. Moreover, only K_{cc} appears in all 4 models, the 18 other parameters being only involved in one promoter activity expression. These observations motivate the redefinition of the parameter estimation problem as a two-step procedure, described below.

1. First of all, we performed parameter estimation independently for each of the 4 equations of Eq. (A18) using $x_{Fis'}$ and $x_{Crp'}$ measurements. With

$$\begin{aligned}\rho_{fis} &= [\kappa^b_{fis'}\ \kappa^r_{fis'}\ \theta_{fis'_1}\ \theta_{cc'_1}\ n_1\ n_2\ K_{cc}]\\ \rho_{crp} &= [\kappa^b_{crp'}\ \kappa^r_{crp'}\ \theta_{fis'_2}\ \theta_{cc'_2}\ n_3\ n_4\ K_{cc}]\\ \rho_{acs} &= [\kappa^b_{acs'}\ \kappa^r_{acs'}\ \theta_{fis'_3}\ \theta_{cc'_3}\ n_5\ n_6\ K_{cc}]\\ \rho_{rpoS} &= [\kappa^b_{rpoS'}\ \kappa^r_{rpoS'}\ \theta_{cc'_4}\ n_7\ K_{cc}],\end{aligned} \tag{A20}$$

we defined the following objective functions

$$\begin{aligned}F_{fis}(\rho_{fis}) &= \sum_{i=1}^{T}\frac{(\check{p}_{fis}(t_i,\rho_{fis}) - p_{fis}(i))^2}{p_{fis}(i)^2}\\ F_{crp}(\rho_{crp}) &= \sum_{i=1}^{T}\frac{(\check{p}_{crp}(t_i,\rho_{crp}) - p_{crp}(i))^2}{p_{crp}(i)^2}\\ F_{acs}(\rho_{acs}) &= \sum_{i=1}^{T}\frac{(\check{p}_{acs}(t_i,\rho_{acs}) - p_{fis}(i))^2}{p_{acs}(i)^2}\\ F_{rpoS}(\rho_{rpoS}) &= \sum_{i=1}^{T}\frac{(\check{p}_{rpoS}(t_i,\rho_{rpoS}) - p_{rpoS}(i))^2}{p_{rpoS}(i)^2}.\end{aligned} \tag{A21}$$

Each of these 4 objective functions was minimized using a combination of global-search and local-search methods. The global-search method used is the genetic algorithm implemented in the MATLAB function `ga`, parameterized with 5000 generations. The local-search method used is the sequential quadratic programming algorithm implemented in the MATLAB function `fmincon`. For each parameter estimation problem, the optimization algorithms were launched with 100 different initial parameter vectors, randomly obtained within a specified range, and the parameter vector giving the lowest objective function was chosen. As the parameter K_{cc} appears in all 4 estimation problems, we limited the range of parameter search in order to obtain consistent estimated values.

2. Using the estimated values obtained in the previous step to define the initial vector, we launched optimization algorithms to minimize the objective function of the whole model, defined in Eq. (A19). For K_{cc}, we took the value estimated when minimizing $F_{acs}(\rho_{acs})$. For γ_{Fis} and γ_{Crp}, that were not estimated in the previous step, we defined a range of parameter search and randomly set initial values. The optimization algorithm used is a combination of the genetic algorithm implemented in the MATLAB function `ga`, parameterized with 5000 generations, and the interior-point algorithm, a local-search method with non-linear constraints implemented in the MATLAB function `fmincon`.

   In the preliminary results we present in this section and in Sec. 5.3, γ_{Fis} and γ_{Crp} were not estimated but fixed to values taken from the literature [de Jong et al., 2010]. Moreover, the affinity constants for regulation by Crp·cAMP and the equilibrium constant of Crp·cAMP formation reaction were the only parameters estimated again in this step. All other parameters were fixed to their values estimated in the previous step.

The parameter values obtained in this way are presented in Table A3.

Parameters	Description	Estimated value
K_{cc}	equilibrium constant for Crp·cAMP formation reaction	5.57
fis expression		
$\kappa^b_{fis'}$	basal protein synthesis rate	$2.48 \cdot 10^{-1}$
$\kappa^r_{fis'}$	maximal protein synthesis rate	$6.60 \cdot 10^{-2}$
$\theta_{fis'_1}$	affinity constant for regulation by Fis	$5.23 \cdot 10^3$
$\theta_{cc'_1}$	affinity constant for regulation by Crp·cAMP	$1.04 \cdot 10^2$
n_1	Hill number for regulation by Fis	2.8
n_2	Hill number for regulation by Crp·cAMP	3
γ_{Fis}	protein degradation constant	$6.50 \cdot 10^{-3}$
crp expression		
$\kappa^b_{crp'}$	basal protein synthesis rate	6.39
$\kappa^r_{crp'}$	maximal protein synthesis rate	$2.82 \cdot 10^{-2}$
$\theta_{fis'_2}$	affinity constant for regulation by Fis	$3.04 \cdot 10^3$
$\theta_{cc'_2}$	affinity constant for regulation by Crp·cAMP	$1.31 \cdot 10^4$
n_3	Hill number for regulation by Fis	1
n_4	Hill number for regulation by Crp·cAMP	2.85
γ_{Crp}	protein degradation constant	$6.50 \cdot 10^{-3}$
acs expression		
$\kappa^b_{acs'}$	basal protein synthesis rate	$5 \cdot 10^{-3}$
$\kappa^r_{acs'}$	maximal protein synthesis rate	1.14
$\theta_{fis'_3}$	affinity constant for regulation by Fis	$1.61 \cdot 10^3$
$\theta_{cc'_3}$	affinity constant for regulation by Crp·cAMP	$1.34 \cdot 10^3$
n_5	Hill number for regulation by Fis	3
n_6	Hill number for regulation by Crp·cAMP	3
rpoS expression		
$\kappa^b_{rpoS'}$	basal protein synthesis rate	1.79
$\kappa^r_{rpoS'}$	maximal protein synthesis rate	$1.40 \cdot 10^{-3}$
$\theta_{cc'_4}$	affinity constant for regulation by Crp·cAMP	$8.76 \cdot 10^2$
n_7	Hill number for regulation by Crp·cAMP	1

Table A3: Estimated values of parameters of the model of Eq. (A16).

Bibliography

R. Alves, E. Vilaprinyo, B. Hernandez-Bermejo, and A. Sorribas. Mathematical formalisms based on approximated kinetic representations for modeling genetic and metabolic pathways. *Biotechnol. Genet. Eng. Rev.*, 25:1–40, 2008.

M. Ashyraliyev, Y. Fomekong-Nanfack, J.A. Kaandorp, and J.G. Blom. Systems biology: Parameter estimation for biochemical models. *FEBS J.*, 276(4):886–902, 2009.

T. Baba, T. Ara, M. Hasegawa, Y. Takai, Y. Okumura, M. Baba, K.A. Datsenko, M. Tomita, B.L. Wanner, and H. Mori. Construction of *Escherichia coli* K-12 in-frame, single-gene knockout mutants: the Keio collection. *Mol. Syst. Biol.*, 2:2006.0008, 2006.

V. Baldazzi, D. Ropers, Y. Markowicz, D. Kahn, J. Geiselmann, and H. de Jong. The carbon assimilation network in *Escherichia coli* is densely connected and largely sign-determined by directions of metabolic fluxes. *PLoS Comput. Biol.*, 6(6):e1000812, 2010.

V. Baldazzi, D. Ropers, J. Geiselmann, D. Kahn, and H. de Jong. Importance of metabolic coupling for the dynamics of gene expression following a diauxic shift in *Escherichia coli*. *J. Theor. Biol.*, 296:100–15, 2012.

B.D. Bennett, E.H. Kimball, M. Gao, R. Osterhout, S.J. Van Dien, and J.D. Rabinowitz. Absolute metabolite concentrations and implied enzyme active site occupancy in *Escherichia coli*. *Nat. Chem. Biol.*, 5(8):593–9, 2009.

S. Berthoumieux, M. Brilli, H. de Jong, D. Kahn, and E. Cinquemani. Identification of linlog models of metabolic networks from incomplete high-throughput datasets. *Bioinformatics*, 27(13):i186–i195, 2011.

S. Berthoumieux, M. Brilli, D. Kahn, H. de Jong, and E. Cinquemani. Identifiability analysis of metabolic network models. 2012a. Submitted.

S. Berthoumieux, D. Kahn, H. de Jong, and E. Cinquemani. Structural and practical identifiability of approximate metabolic network models. *Proc. 16th IFAC Symp. System Identif. (SYSID 2012)*, 2012b. To appear.

K. Bettenbrock, S. Fischer, K. Jahreis, T. Sauter, and E.D. Gilles. A quantitative approach to catabolite repression in *Escherichia coli*. *J. Biol. Chem.*, 281(5):2578–84, 2006.

H.G. Beyer and H.P. Schwefel. Evolution strategies, a comprehensive introduction. *Natural Computing*, 1:3–52, 2002.

L. Bintu, N.E. Buchler, H.G. Garcia, U. Gerland, T. Hwa, J. Kondev, T. Kuhlman, and R. Phillips. Transcriptional regulation by the numbers: applications. *Curr. Opin. Genet. Dev.*, 15(2):125–35, 2005.

H. Bolouri. *Computational modeling of gene regulatory networks-a primer*. Imperial College Press, 2008.

F. Boyer, B. Besson, G. Baptist, J. Izard, C. Pinel, D. Ropers, J. Geiselmann, and H. de Jong. WellReader: a MATLAB program for the analysis of fluorescence and luminescence reporter gene data. *Bioinformatics*, 26(9):1262–63, 2010.

M.D. Bradley, M.B. Beach, A.P.J. de Koning, T.S. Pratt, and R. Osuna. Effects of Fis on *Escherichia coli* gene expression during different growth stages. *Microbiology*, 153:2922–40, 2007.

M. Brand. Incremental singular value decomposition of uncertain data with missing values. In A. Heyden, G. Sparr, M. Nielsen, and P. Johansen, editors, *Proc. 7th Eur. Conf. Comput. Vision (ECCV 2002)*, volume 2350 of *LNCS*, pages 707–20. Springer Verlag, 2002.

H. Bremer and P.P. Dennis. Modulation of chemical composition and other parameters of the cell by growth rate. In F.C. Neidhardt, R. Curtiss III, J. Ingraham, E.C.C. Lin, K.B. Low, B. Magasanik, W. Reznikoff, M. Riley, M. Schaechter, and H.E. Umbarger, editors, *Escherichia coli and Salmonella: Cellular and molecular biology, 2nd Ed.*, pages 1553–69. ASM Press, 1996.

M.J. Buettner, E. Spitz, and H.V. Rickenberg. Cyclic adenosine 3',5'-monophosphate in *Escherichia coli*. *J. Bacteriol.*, 14(3):1068–73, 1973.

S. Bulik, S. Grimbs, C. Huthmacher, J. Selbig, and H.G. Holzhütter. Kinetic hybrid models composed of mechanistic and simplified enzymatic rate laws a promising method for speeding up the kinetic modelling of complex metabolic networks. *FEBS J.*, 276(2):410–24, 2009.

S. Bulik, S. Grimbs, C. Huthmacher, J. Selbig, and H.G. Holzhütter. Integration of metabolic reactions and gene regulation. *Mol. Biotechnol.*, 47(1):70–82, 2011.

L. Cai, N. Friedman, and X.S. Xie. Stochastic protein expression in individual cells at the single molecule level. *Nature*, 440(7082):358–62, 2006.

M.J. Chappell, K.R. Godfrey, and S. Vajda. Global identifiability of the parameters of nonlinear systems with specified inputs: A comparison of methods. *Math. Biosci.*, 102(1):41–73, 1990.

C. Chassagnole, N. Noisommit-Rizzi, J.W. Schmid, K. Mauch, and M. Reuss. Dynamic modeling of the central carbon metabolism of *Escherichia coli*. *Biotechnol. Bioeng.*, 79(1):53–73, 2002.

C. Chen, D.A. Ridzon, A.J. Broomer, Z. Zhou, D.H. Lee, J.T. Nguyen, M. Barbisin, N.L. Xu, V.R. Mahuvakar, M.R. Andersen, K.Q. Lao, K.J. Livak, and K.J. Guegler. Real-time quantification of microRNAs by stem-loop RT-PCR. *Nucleid Acids Res.*, 33(20):e179, 2005.

W.W. Chen, M. Nieper, and P.K. Sorger. Classic and contemporary approaches to modeling biochemical reactions. *Genes Dev.*, 24:1861–75, 2010.

O.T. Chis, J.R. Banga, and E. Balsa-Canto. GenSSI: a software toolbox for structural identifiability analysis of biological models. *Bioinformatics*, 27(18):2610–1, 2011a.

O.T. Chis, J.R. Banga, and E. Balsa-Canto. Structural identifiability of systems biology models: a critical comparison of methods. *PLoS One*, 6(11):e27755, 2011b.

B.-K. Cho, E.M. Knight, C.L. Barrett, and B.O. Palsson. Genome-wide analysis of Fis binding in *Escherichia coli* indicates a causative role for A-/AT-tracts. *Genome Res.*, 18(6):900–10, 2008.

I.C. Chou and E.O. Voit. Recent developments in parameter estimation and structure identification of biochemical and genomic systems. *Math. Biosci.*, 219(2):57–83, 2009.

C. Cobelli and J.J. di Stefano 3rd. Parameter and structural identifiability concepts and ambiguities: A critical review and analysis. *Am. J. Physiol.*, 239(1):R7–24, 1980.

A. Cornish-Bowden. *Fundamentals of enzyme kinetics.* Portland Press, 1995.

R.S. Costa, D. Machado, I. Rocha, and E.C. Ferreira. Hybrid dynamic modeling of *Escherichia coli* central metabolic network combining Michaelis-Menten and approximate kinetic equations. *Biosystems*, 100(2):150–8, 2010.

T.M. Cover and J.A. Thomas. *Elements of Information Theory, 2nd edition.* Wiley, 2006.

E.J. Crampin. System identification challenges from systems biology. In *Proc. 14th IFAC Symp. Syst. Identif. (SYSID 2006)*, pages 81–93, Newcastle, Australia, 2006.

H. de Jong. Modeling and simulation of genetic regulatory systems: A literature review. *J. Comput. Biol.*, 9(1):67–103, 2002.

H. de Jong, J-L. Gouzé, C. Hernandez, M. Page, T. Sari, and J. Geiselmann. Qualitative simulation of genetic regulatory networks using piecewise-linear models. *Bull. Math. Biol.*, 66:301–40, 2004.

H. de Jong, C. Ranquet, D. Ropers, C. Pinel, and J. Geiselmann. Experimental and computational validation of models of fluorescent and luminescent reporter genes in bacteria. *BMC Syst. Biol.*, 4:55, 2010.

R.C.H. del Rosario, E. Mendoza, and E.O. Voit. Challenges in lin-log modelling of glycolysis in *Lactococcus lactis. IET Syst. Biol.*, 2(3):136–49, 2008.

X. Delgado and J.C. Liao. Metabolic control analysis using transient metabolite concentrations. *Biochem. J.*, 285: 965–72, 1992.

A.P. Dempster, N.M. Laird, and D.B. Rubin. Maximum likelihood from incomplete data via the EM algorithm. *J. Roy. Stat. Soc. Ser. B*, 39(1):1–38, 1977.

P.P. Dennis, M. Ehrenberg, and H. Bremer. Control of rRNA synthesis in *Escherichia coli*: a systems biology approach. *Microbiol. Mol. Biol. Rev.*, 68(4):639–68, 2004.

Y. Dharmadi and R. Gonzalez. DNA microarrays: Experimental issues, data analysis, and application to bacterial systems. *Biotechnology Progress*, 20(5):1309–24, 2004.

K. Dürrschmid, H. Reischer, W. Schmidt-Heck, T. Hrebicek, R. Guthke, A. Rizzi, and K. Bayer. Monitoring of transcriptome and proteome profiles to investigate the cellular response of *E. coli* towards recombinant protein expression under defined chemostat conditions. *J. Biotechnol.*, 135:34–44, 2008.

T.K. Van Dyk, E.J. Derose, and G.E. Gonye. LuxArray, a high-density, genomewide transcription analysis of *Escherichia coli* using bioluminescent reporter strains. *J. Bacteriol.*, 183(19):5496–505, 2001.

M.B. Elowitz and S. Leibler. A synthetic oscillatory network of transcriptional regulators. *Nature*, 403(6767):335–8, 2000.

W. Epstein, L.B. Rothman-Denes, and J. Hesse. Adenosine 3':5'-cyclic monophosphate as mediator of catabolite repression in *Escherichia coli. Proc. Nat. Acad. Sci. USA*, 72(6):2300–4, 1975.

J.J. Faith, B. Hayete, J.T. Thaden, I. Mogno, J. Wierzbowski, G. Cottarel, S. Kasif, J.J. Collins, and T.S. Gardner. Large-scale mapping and validation of *Escherichia coli* transcriptional regulation from a compendium of expression profiles. *PLoS Biol.*, 5(1):e8, 2007.

L. Glass and S.A. Kauffman. The logical analysis of continuous non-linear biochemical control networks. *J. Theor. Biol.*, 39:103–29, 1973.

B. Görke and J. Stülke. Carbon catabolite repression in bacteria: many ways to make the most out of nutrients. *Nat. Rev. Microbiol.*, 6(8):613–24, 2008.

G. Gosset, Z. Zhang, S. Nayyar, W. Cuevas, and M. Saier Jr. Transcriptome analysis of CRP-dependent catabolite control of gene expression in *Escherichia coli. J. Bacteriol.*, 186(11):3516–24, 2004.

J.W. Graham. Missing data analysis: Making it work in the real world. *Annu. Rev. Psychol.*, 60:549–76, 2009.

M. Gstaiger and R. Aebersold. Applying mass spectrometry-based proteomics to genetics, genomics and network biology. *Nat. Rev. Genet.*, 10(9):617–27, 2009.

R.N. Gutenkunst, J.J. Waterfall, F.P. Casey, K.S. Brown, C.R. Myers, and J.P. Sethna. Universally sloppy parameter sensitivities in systems biology models. *PLoS Comput. Biol.*, 3(10):1871–78, 2007.

R.M. Gutierrez-Ríos, J.A. Freyre-Gonzalez, O. Resendis, J. Collado-Vides, M. Saier, and G. Gosset. Identification of regulatory network topological units coordinating the genome-wide transcriptional response to glucose in *Escherichia coli. BMC Microbiol.*, 7:53, 2007.

F. Hadlich, S. Noack, and W. Wiechert. Translating biochemical network models between different kinetic formats. *Metab. Eng.*, 11(2):87–100, 2009.

J.B.S. Haldane. *Enzymes.* Monographs on biochemistry. Longmans, Green and Co, 1930.

L.C. Hamilton. *Regression with graphics: a second course in applied statistics.* Brooks/Cole Pub. Co., 1992.

T. Hardiman, K. Lemuth, M.A. Kellerand, M. Reuss, and M. Siemann-Herzberg. Topology of the global regulatory network of carbon limitation in *Escherichia coli. J. Biotechnol.*, 132(4):359–74, 2007.

T. Hardiman, K. Lemuth, M. Siemann-Herzberg, and M. Reuss. Dynamic modeling of the central metabolism of *E. coli* linking metabolite and regulatory networks. In S.Y. Lee, editor, *Systems Biology and Biotechnology of Escherichia coli*, pages 209–235. Springer Netherlands, 2009.

V. Hatzimanikatis and J.E. Bailey. Effects of spatiotemporal variations on metabolic control: approximate analysis using (log)linear kinetic models. *Biotechnol. Bioeng.*, 54(2):91–104, 1997.

J.J. Heijnen. Approximative kinetic formats used in metabolic network modeling. *Biotechnol. Bioeng.*, 91(5):534–45, 2005.

R. Heinrich and S. Schuster. *The regulation of cellular systems.* ITP, 1996.

R. Hengge-Aronis. Signal transduction and regulatory mechanisms involved in control of the σ^S (RpoS) subunit of RNA polymerase. *Microbiol. and Mol. Biol. Rev.*, 66(3):373–95, 2002.

A.V. Hill. The possible effects of the aggregation of the molecules of hemoglobin on its dissociation curves. *J. Physiol.*, 40:iv–vii, 1910.

N.J. Horton and K.P. Kleinman. Much ado about nothing: A comparison of missing data methods and software to fit incomplete data regression models. *Am. Stat.*, 61(1):79–90, 2007.

M. Isalan, C. Lemerle, K. Michalodimitrakis, C. Horn, P. Beltrao, E. Raineri, M. Garriga-Canut, and L. Serrano. Evolvability and hierarchy in rewired bacterial gene networks. *Nature*, 452(7189):840–5, 2008.

N. Ishii, K. Nakahigashi, T. Baba, M. Robert, T. Soga, A. Kanai, T. Hirasawa, M. Naba, K. Hirai, A. Hoque, P.Y. Ho, Y. Kakazu, K. Sugawara, S. Igarashi, S. Harada, T. Masuda, N. Sugiyama, T. Togashi, M. Hasegawa, Y. Takai, K. Yugi, K. Arakawa, N. Iwata, Y. Toya, Y. Nakayama, T. Nishioka, K. Shimizu, H. Mori, and M. Tomita. Multiple high-throughput analyses monitor the response of *E. coli* to perturbations. *Science*, 316(5824):593–7, 2007.

S. Itzkovitz and A. van Oudenaarden. Validating transcripts with probes and imaging technology. *Nat. Methods*, 8(4 Supp):S12–9, 2011.

K. Jaqaman and G. Danuser. Linking data to models: data regression. *Nat. Rev. Mol. Cell. Biol.*, 7(11):813–9, 2006.

L. Jia, N. Tanaka, and S. Terabe. Two-dimensional separation system of coupling capillary liquid chromatography to capillary electrophoresis for analysis of *Escherichia coli* metabolites. *Electrophoresis*, 26(18):3468–78, 2005.

I.T. Jolliffe. *Principal Component Analysis.* Springer-Verlag, 1986.

S. Jozefczuk, S. Klie, G. Catchpole, J. Szymanski, A. Cuadros-Inostroza, D. Steinhauser, J. Selbig, and L. Willmitzer. Metabolomic and transcriptomic stress response of *Escherichia coli. Mol. Syst. biol.*, 6:364, 2010.

S. Kalir, S. Mangan, and U. Alon. A coherent feed-forward loop with a sum input function prolongs flagella expression in *Escherichia coli. Mol. Syst. biol.*, 1:2005.0006, 2005.

K.C. Kao, Y.-L. Yang, R. Boscolo, C. Sabatti, V. Roychowdhury, and J.C. Liao. Transcriptome-based determination of multiple transcription regulator activities in *Escherichia coli* by using network component analysis. *Proc. Natl. Acad. Sci.USA*, 101(2):641–6, 2004.

G. Karlebach and R. Shamir. Modelling and analysis of gene regulatory networks. *Nat. Rev. Mol. Cell Biol.*, 9(10): 770–80, 2008.

S. Kirkpatrick, C.D. Gelatt, and M.P. Vecchi. Optimization by simulated annealing. *Science*, 220:671–80, 1983.

S. Klamt and J. Stelling. Two approaches for metabolic pathway analysis? *Trends Biotechnol.*, 21(2):64–9, 2003.

S. Klumpp and T. Hwa. Growth-rate-dependent partitioning of RNA polymerases in bacteria. *Proc. Nat. Acad. Sci. USA*, 105(51):20245–50, 2008.

S. Klumpp, Z. Zhang, and T. Hwa. Growth rate-dependent global effects on gene expression in bacteria. *Cell*, 139(7): 1366–75, 2009.

D.E. Koshland, G. Némethy, and D. Filmer. Comparison of experimental binding data and theoretical models in proteins containing subunits. *Biochemistry*, 5:365–85, 1966.

O. Kotte, J.B. Zaugg, and M. Heinemann. Bacterial adaptation through distributed sensing of metabolic fluxes. *Mol. Syst. Biol.*, 6:355, 2010.

A. Kremling. Comment on mathematical models which describe transcription and calculate the relationship between mRNA and protein expression ratio. *Biotechnol. Bioeng.*, 96(4):815–9, 2007.

A. Kremling, K. Bettenbrock, and E.D. Gilles. Analysis of global control of escherichia coli carbohydrate uptake. *BMC. Syst. Biol.*, 1:1–42, 2007.

A. Kremling, K. Bettenbrock, and E.D. Gilles. A feed-forward loop guarantees robust behavior in *Escherichia coli* carbohydrate uptake. *Bioinformatics*, 24(5):704–10, 2008.

A. Kremling, S. Kremling, and K. Bettenbrock. Catabolite repression in *Escherichia coli* - a comparison of modeling approaches. *FEBS J.*, 276:594–602, 2009.

C. Lee, J. Kim, S.G. Shin, and S. Hwang. Absolute and relative QPCR quantification of plasmid copy number in *Escherichia coli*. *J. Biotechnol.*, 123(3):27380, 2004.

M. Li, P.Y. Ho, S. Yao, and K. Shimizu. Effect of *lpdA* gene knockout on the metabolism in *Escherichia coli* based on enzyme activities, intracellular metabolite concentrations and metabolic flux analysis by ^{13}C-labeling experiments. *Mass Spectrom. Rev.*, 122:254–66, 2006.

W. Liebermeister and E. Klipp. Bringing metabolic networks to life: Convenience rate law and thermodynamic constraints. *Theor. Biol. Med. Model.*, 3:41, 2006.

S. Lin-Chao and H. Bremer. Effect of the bacterial growth rate on replication control of plasmid pBR322 in *Escherichia coli*. *Mol. Gen. Genet.*, 203(1):143–9, 1986.

R.J.A Little and D.B. Rubin. *Statistical Analysis with Missing Data.* Wiley, 2002.

L. Ljung. *System identification, theory for the user.* Prentice Hall PTR, 1999.

D.J. Lockhart, H. Dong, M.C. Byrne, M.T. Follettie, M.V. Gallo, M.S. Chee, M. Mittmann, C. Wang, M. Kobayashi, H. Norton, and E.L. Brown. Expression monitoring by hybridization to high-density oligonucleotide arrays. *Nat. Biotechnol.*, 14(13):1675–80, 1996.

D. Longo and J. Hasty. Dynamics of single-cell gene expression. *Mol. Syst. Biol.*, 2:64, 2006.

G.L. Lorca, A. Ezersky, V.V. Lunin, J.R. Walker, S. Altamentova, E. Evdokimova, M. Vedadi, A. Bochkarev, and A. Savchenko. Glyoxylate and pyruvate are antagonistic effectors of the *Escherichia coli* IclR transcriptional regulator. *J. Biol. Chem.*, 282(22):16476–91, 2007.

G.W. Luli and W.R. Strohl. Comparison of growth, acetate production, and acetate inhibition of *Escherichia coli* strains in batch and fed-batch fermentations. *Appl. Environ. Microbiol.*, 56(4):1004–11, 1990.

O. Maaloe and N.O. Kjeldgaard. *Control of macromolecular synthesis.* W.A. Benjamin, 1966.

T. Maiwald and J. Timmer. Dynamical modeling and multi-experiment fitting with PottersWheel. *Bioinformatics*, 24 (18):2037–43, 2008.

R.S. Makman and E.W. Sutherland. Adenosine 3',5'-phosphate in *Escherichia coli*. *J. Biol. Chem.*, 240(3):1309–14, 1965.

B.F.J. Manly. *Randomization, Bootstrap and Monte-Carlo Methods in Biology.* Chapman and Hall, 1997.

R. Marouga, S. David, and E. Hawkins. The development of the DIGE system: 2D fluorescence difference gel analysis technology. *Anal. Bioanal. Chem.*, 382:669–78, 2005.

A. Martinez-Antonio and J. Collado-Vides. Identifying global regulators in transcriptional regulatory networks in bacteria. *Curr. Opin. Microbiol.*, 6:482–9, 2003.

L. Marucci, S. Santini, M. di Bernardo, and D. di Bernardo. Derivation, identification and validation of a computational model of a novel synthetic regulatory network in yeast. *J. Math. Biol.*, 62(5):685–706, 2011.

G. Baptist et al. A genome-wide screen for identifying all regulators of a target gene. *Under revision.*

D. Del Vecchio, A.J. Ninfa, and E.D. Sontag. Modular cell biology: retroactivity and insulation. *Mol. Syst. Biol.*, 4: 161, 2008.

M.H. Saier Jr, T.M. Ramseier, and J. Reizer. Regulation of carbon utilization. In F.C. Neidhardt, R. Curtiss III, J. Ingraham, E.C.C. Lin, K.B. Low, B. Magasanik, W. Reznikoff, M. Riley, M. Schaechter, and H.E. Umbarger, editors, *Escherichia coli and Salmonella: Cellular and molecular biology, 2nd Ed.*, pages 1325–43. ASM Press, 1996.

R. Meloni, O. Khalfallah, and N.F. Biguet. DNA microarrays and pharmacogenomics. *Pharmacol. Res.*, 49(4):303–8, 2004.

L. Michaelis and M.L. Menten. Die Kinetik der Invertinwirkung. *Biochem. Z.*, 49:333–69, 1913.

L. Michaelis, M.L. Menten, K.A. Johnson, and R.S. Goody. The original Michaelis constant: translation of the 1913 Michaelis-Menten paper. *Biochemistry*, 50(39):8264–9, 2011.

J.H. Miller. *Experiments in molecular genetics.* CSHL, 1972.

C.G. Moles, P. Mendes, and J.R. Banga. Parameter estimation in biochemical pathways: A comparison of global optimization methods. *Genome Res.*, 13:2467–74, 2003.

J. Monod, J. Wyman, and J.P. Changeux. On the nature of allosteric transitions: A plausible model. *J. Mol. Biol.*, 12: 88–118, 1965.

M.R.N. Monton and T. Soga. Metabolome analysis by capillary electrophoresismass spectrometry. *J. Chromatogr. A.*, 1168:237–248, 2007.

F.C. Neidhardt and D.G. Fraenkel. Metabolic regulation of RNA synthesis in bacteria. *Cold Spring Harb. Symp. Quant. Biol.*, 26:63–74, 1961.

F.C. Neidhardt, J.L. Ingraham, and M. Schaechter. *Physiology of the bacterial cell, a molecular approach.* Sinauer Associates, Inc. Sunderland, Mass, 1990.

J.A. Nelder and R. Mead. A simplex method for function minimization. *Computer J.*, 7(4):308–13, 1965.

J. Nemcova. Structural identifiability of polynomial and rational systems. *Math. Biosci.*, 223(2):83–96, 2010.

C. Nicolas, P. Kiefer, F. Letisse, J. Krmer, S. Massou, P. Soucaille, C. Wittmann, N.D. Lindley, and J-C. Portais. Response of the central metabolism of *Escherichia coli* to modified expression of the gene encoding the glucose-6-phosphate dehydrogenase. *FEBS Lett.*, 581(20):3771–6, 2007.

I.E. Nikerel, W.A. van Winden, W.M. van Gulik, and J.J. Heijnen. A method for estimation of elasticities in metabolic networks using steady state and dynamic metabolomics data and linlog kinetics. *BMC Bioinform.*, 7:540, 2006.

I.E. Nikerel, W.A. van Winden, P.J.T. Verheijen, and J.J. Heijnen. Model reduction and *a priori* kinetic parameter identifiability analysis using metabolome time series for metabolic reaction networks with linlog kinetics. *Metab. Eng.*, 11(1):20–30, 2009.

O. Ninnemann, C. Koch, and R. Kahmann. The *E.coli fis* promoter is subject to stringent control and autoregulation. *EMBO J.*, 11(3):1075–83, 1992.

S. Oba, M.A. Sato, I. Takemasa, M. Monden, K. Matsubara, and S. Ishii. A Bayesian missing value estimation method for gene expression profile data. *Bioinformatics*, 19(16):2088–96, 2003.

M.K. Oh, L. Rohlin, K.C. Kao, and J.C. Liao. Global expression profiling of acetate-grown *Escherichia coli*. *J. Biol. Chem.*, 277(15):13175–83, 2002.

M.S. Okino and M.L. Mavrovouniotis. Simplification of mathematical models of chemical reaction systems. *Chem. Rev.*, 98(391-408):685–706, 1998.

A.B. Oppenheim, O. Kobiler, J. Stavans, D.L. Court, and S. Adhya. Switches in bacteriophage lambda development. *Annu. Rev. Genet.*, 39:409–29, 2005.

S.J. Park, S.Y. Lee, J. Cho, T.Y. Kim, J.W. Lee, J.H. Park, and M.J. Han. Global physiological understanding and metabolic engineering of microorganisms based on omics studies. *Appl. Microbiol. Biotechnol.*, 68:567–79, 2005.

I. Pastan and S. Adhya. Cyclic adenosine 5'-monophosphate in *Escherichia coli*. *Bacteriol. Rev.*, 40(3):527–51, 1976.

K. Potrykus and M. Cashel. (p)ppGpp: Still magical? *Ann. Rev. Microbiol.*, 62:35–51, 2008.

M.A. Quail and J.R. Guest. Purification, characterization and mode of action of PdhR, the transcriptional repressor of the pdhR-aceEF-lpd operon of *Escherichia coli*. *Mol. Microbiol.*, 15(3):519–29, 1995.

A. Raue, C. Kreutz, T. Maiwald, J. Bachmann, M. Schilling, U. Klingmüller, and J. Timmer. Structural and practical identifiability analysis of partially observed dynamical models by exploiting the profile likelihood. *Bioinformatics*, 25(15):1923–29, 2009.

A. Raue, C. Kreutz, T. Maiwald, U. Klingmüller, and J. Timmer. Addressing parameter identifiability by model-based experimentation. *IET Syst. Biol.*, 5(2):120–30, 2011.

C. Reder. Metabolic control theory: a structural approach. *J. Theor. Biol.*, 135(2):175–201, 1988.

B. Regenberg, T. Grotkjaer, O. Winther, A. Fausbøll, M. Åkesson, C. Bro, L.K. Hansen, S. Brunak, and J. Nielsen. Growth-rate regulated genes have profound impact on interpretation of transcriptome profiling in *Saccharomyces cerevisiae*. *Genome Biol.*, 7(11):R107, 2006.

M. Reiter, B. Kirchner, H. Müller, C. Holzhauer, W. Mann, and M.W. Pfaffl. Quantification noise in single cell experiments. *Nucleids Acids Res.*, 38(18):e124, 2011.

M. Rodriguez-Fernandez, P. Mendes, and J.R. Banga. A hybrid approach for efficient and robust parameter estimation in biochemical pathways. *BioSystems*, 83:248–65, 2006.

M. Ronen, R. Rosenberg, B.I. Shraiman, and U. Alon. Assigning numbers to the arrows: Parameterizing a gene regulation network by using accurate expression kinetics. *Proc. Natl. Acad. Sci. USA*, 99(16):10555–60, 2002.

D. Ropers, H. de Jong, M. Page, D. Schneider, and J. Geiselmann. Qualitative simulation of the carbon starvation response in *Escherichia coli*. *Biosystems*, 84:124–52, 2006.

M.R. Roussel and S.J. Fraser. Invariant manifold methods for metabolic model reduction. *Chaos*, 11(1):196–206, 2001.

D.B. Rubin. Inference and missing data. *Biometrika*, 63:581–90, 1976.

D.B. Rubin. Multiple imputation after 18+ years. *J. Am. Stat. A.*, 81:473–89, 1996.

J. Saez-Rodriguez, A. Kremling, and E.D. Gilles. Dissecting the puzzle of life: modularization of signal transduction networks. *Comput. Chem. Eng.*, 29:619–29, 2005.

C. Sander and R. Schneider. Database of homology-derived protein structures and the structural meaning of sequence alignment. *Proteins*, 9:56–68, 1991.

P.J. Sands and E.O. Voit. Flux-based estimation of parameters in S-systems. *Ecological Modelling*, 93(1-3):75–88, 1996.

U. Sauer. Metabolic networks in motion: ^{13}C-based flux analysis. *Mol. Syst. biol.*, 2:62, 2006.

M.A. Savageau. *Biochemical Systems Analysis: A Study of Function and Design in Molecular Biology.* Addison-Wesley, 1976.

M. Schaechter, J.L. Ingraham, and F.C. Neidhardt. *Microbe.* ASM Press, 2006.

M. Schena, D. Shalon, R.W. Davis, and P.O. Brown. Quantitative monitoring of gene expression patterns with a complementary DNA microarray. *Science*, 270(5235):467–70, 1995.

M. Scholz, F. Kaplan, C.L. Guy, J. Kopka, and J. Selbig. Non-linear PCA: A missing data approach. *Bioinformatics*, 21(20):3887–95, 2005.

S. Schuster, D. Kahn, and H.V. Westerhoff. Modular analysis of the control of complex metabolic pathways. *Biophys. Chem.*, 48(1):1–17, 1993.

M. Scott, C.W. Gunderson, E.M. Mateescu, Z. Zhang, and T. Hwa. Interdependence of cell growth and gene expression: origins and consequences. *Science*, 330:1099–102, 2010.

K. Smallbone, E. Simeonidis, N. Swainston, and P. Mendes. Towards a genome-scale kinetic model of cellular metabolism. *BMC Syst. Biol.*, 4:6, 2010.

S. Srinath and R. Gunawan. Parameter identifiability of power-law biochemical system models. *J. Biotechnol.*, 149(3): 132–40, 2010.

A. Stoorvogel and J.H. van Schuppen. System identification with information theoretic criteria. In S. Bittanti and G. Picci, editors, *Identification, Adaptation, Learning*, volume 153 of *NATO ASI*, pages 289–338. Springer Verlag, 1996.

A.D. Tadmor and T. Tlusty. A coarse-grained biophysical model of *E. coli* and its application to perturbation of the rRNA operon copy number. *PLoS Comput. Biol.*, 4(5):e1000038, 2008.

N. Tenazinha and S. Vinga. A survey on methods for modeling and analyzing integrated biological networks. *IEEE/ACM Trans. Comput. Biol. Bioinform.*, 8(4):943–58, 2011.

A. Travers, R. Schneider, and G. Muskhelishvili. DNA supercoiling and transcription in *Escherichia coli*: The FIS connection. *Biochimie*, 83(2):213–7, 2001.

M.F. Traxler, D.-E. Chang, and T. Conway. Guanosine 3',5'-bispyrophosphate coordinates global gene expression during glucose-lactose diauxie in *Escherichia coli. Proc. Nat. Acad. Sci. USA*, 103(7):2374–9, 2006.

Y. Usuda, Y. Nishio, S. Iwatani, S.J. Van Dien, A. Imaizumi, K. Shimbo, N. Kageyama, D. Iwahata, H. Miyano, and K. Matsui. Dynamic modeling of *Escherichia coli* metabolic and regulatory systems for amino-acid production. *J. Biotechnol.*, 147(1):17–30, 2010.

S. van Huffel and J. Vandewalle. *The Total Least Squares problems: Computational aspects and analysis.* SIAM, Philadelphia, PA, 1991.

B.R.B. Haverkorn van Rijsewijk, A. Nanchen, S. Nallet, R.J. Kleijn, and U. Sauer. Large-scale ^{13}C-flux analysis reveals distinct transcriptional control of respiratory and fermentative metabolism in *Escherichia coli. Mol. Syst. biol.*, 7: 477, 2011.

G.N. Vemuri and A.A. Aristidou. Metabolic engineering in the -omics era: Elucidating and modulating regulatory networks. *Microbiol. Mol. Biol. Rev.*, 69(2):197–216, 2005.

S.G. Villas-Boas, S. Mas, M. Akesson, J. Smedsgaard, and J. Nielsen. Mass spectrometry in metabolome analysis. *Mass Spectrom. Rev.*, 24(5):613–46, 2005.

D. Visser and J.J. Heijnen. Dynamic simulation and metabolic re-design of a branched pathway using linlog kinetics. *Metab. Eng.*, 5:164–76, 2003.

D. Visser, J.W. Schmid, K. Mauch, M. Reuss, and J.J. Heijnen. Optimal re-design of primary metabolism in *Escherichia coli* using linlog kinetics. *Metab. Eng.*, 6(4):378–90, 2004.

E.O. Voit, J. Almeida, S. Marino, R. Lall, G. Goel, A.R. Neves, and H. Santos. Regulation of glycolysis in *Lactococcus lactis*: an unfinished systems biological case study. *Syst. Biol. (Stevenage)*, 153(4):286–98, 2006a.

E.O. Voit, A.R. Neves, and H. Santos. The intricate side of systems biology. *Proc. Natl. Acad. Sci. USA*, 103(25): 9452–7, 2006b.

B. Volkmer and M. Heinemann. Condition-dependent cell volume and concentration of *Escherichia coli* to facilitate data conversion for systems biology modeling. *PLoS One*, 6(7):e23126, 2011.

E. Walter and L. Pronzato. *Identification of parametric models*. Springer, 1997.

A.K. White, M. VanInsberghe, O.I. Petriv, M. Hamidi, D. Sikorski, M.A. Marra, J. Piret, S. Aparicio, and C.L. Hansen. High-throughput microfluidic single-cell RT-qPCR. *Appl. Microbiol. Biotechnol.*, 108(34):13999–4004, 2011.

A.J. Wolfe. The acetate switch. *Microbiol. Mol. Biol. Rev.*, 69(1):12–50, 2005.

J. Wu and E. Voit. Hybrid modeling in biochemical systems theory by means of functional petri nets. *J. Bioinform. Comput. Biol.*, 7(1):107–34, 2009.

S.H. Yoon, M.J. Han, S.Y. Lee, K.J. Jeong, and J.S. Yoo. Combined transcriptome and proteome analysis of *Escherichia coli* during high cell density culture. *Biotechnol. Bioeng.*, 81:753–67, 2003.

A. Zaslaver, A. Bren, M. Ronen, S. Itzkovitz, I. Kikoin, S. Shavit, W. Liebermeister, M.G. Surette, and U. Alon. A comprehensive library of fluorescent transcriptional reporters for *Escherichia coli*. *Nat. Methods*, 3(8):623–8, 2006.

H.I. Zgurskaya, M. Keyhan, and A. Matin. The σ^s level in starving *Escherichia coli* cells increases solely as a result of its increased stability, despite decreased synthesis. *Mol. Microbiol.*, 24(3):643–51, 1997.

J. Zhao, T. Baba, H. Mori, and K. Shimizu. Effect of *zwf* gene knockout on the metabolism of *Escherichia coli* grown on glucose or acetate. *Metab. Eng.*, 6:164–74, 2004.

D. Zheng, C. Constantinidou, J.L. Hobman, and S.D. Minchin. Identification of the CRP regulon using *in vitro* and *in vivo* transcriptional profiling. *Nucleid Acids Res.*, 32(19):5874–93, 2004.

Notation and terminology

$\mathbb{R}$, $\mathbb{R}_+$, $\mathbb{R}_{>0}$, $\mathbb{Z}$ and $\mathbb{N}$ denote the set of real, nonnegative real and strictly positive real, integer and positive natural numbers, respectively.

For an index $n \in \mathbb{N}$, $\mathbb{R}^n$, $\mathbb{R}^n_+$ and $\mathbb{R}^n_{>0}$ denote the n dimensional versions of $\mathbb{R}$, $\mathbb{R}_+$ and $\mathbb{R}_{>0}$, respectively.

I denotes an identity matrix of dimension fixed by the context.

For a square matrix Σ, $\Sigma > 0$ (resp. $\Sigma \geq 0$) means that Σ is positive definite (resp. semidefinite).

For a vector μ of suitable dimension, $\varepsilon \sim \mathscr{N}(\mu, \Sigma)$ means that ε is a Gaussian random vector with mean μ and covariance matrix Σ.

Let M be any matrix. For two indices i and j and a vector of indices C compatible with the dimensions of M:
M_i denotes the $i-th$ column of M.
M_C denotes the submatrix of M formed by the columns of M with indices C.
$M_{j,i}$ denotes the element of M in row j and column i.
$M_{j,C}$ denotes the row vector formed by the elements of M in row j and columns indexed by C.
$[\Sigma]_{C,C}$ denotes the diagonal minor formed by the rows and columns indexed by C.
When convenient, notation $M_{i:i'}$ with $i' \geq i$ is used instead of M_C with $C = \Big[i, i+1, \ldots, i'\Big]$.

For vectors, a subscript i means the i-th element of the vector.

For two vectors v and e of equal size, both v/e and $\frac{v}{e}$ indicate the vector of equal size obtained by element-wise division.

Given a vector sequence $v^1, \ldots, v^q$, $\bar{v}$ is the mean $(1/q)\sum_{k=1}^{q} v^k$.

For sets, $|\cdot|$ denotes cardinality.